

Universiteit
Leiden
The Netherlands

Synthetic, physical and computational chemistry of propeller-shaped polycyclic aromatic hydrocarbons

Ham, A. van der

Citation

Ham, A. van der. (2022, February 24). *Synthetic, physical and computational chemistry of propeller-shaped polycyclic aromatic hydrocarbons*. Retrieved from https://hdl.handle.net/1887/3276776

Version:	Publisher's Version
License:	Licence agreement concerning inclusion of doctoral thesis in the Institutional Repository of the University of Leiden
Downloaded from:	https://hdl.handle.net/1887/3276776

Note: To cite this publication please use the final published version (if applicable).

Synthetic, Physical and Computational Chemistry of Propeller-shaped Polycyclic Aromatic Hydrocarbons

PROEFSCHRIFT

ter verkrijging van
de graad van doctor aan de Universiteit Leiden,
op gezag van rector magnificus prof.dr.ir. H. Bijl,
volgens besluit van het college voor promoties
te verdedigen op donderdag 24 februari 2022
klokke 15:00 uur

door

Alexander van der Ham
geboren te ’s-Gravenhage in 1993

Promotiecommissie

Promotor:	Prof. dr. H. S. Overkleeft
	Dr. G. F. Schneider
Copromotor:	Dr. D. V. Filippov

Promotiecommissie:	Prof. dr. A. Kros (voorzitter)
	Prof. dr. S. A. Bonnet (secretaris)
Overige commissieleden:	Dr. R. E. Kieltyka
	Dr. F. Buda
	Prof. dr. A. M. Brouwer, UvA
	Prof. dr. X. Feng, TU Dresden

Printed by Ridderprint B.V.
ISBN 978-94-6458-030-3

The Front cover is a photograph shot from the basement of the old LCP building, the place where my scientific career began.
The Back cover refers to the computational aspect of this work, showing how heavily different parts of a propellerene molecule contribute to its conformational preference.

Science has always been stimulated by such important social events as wars, geographical discoveries, epidemics, and so on. On the other hand, I think it is true to say that throughout the whole of history there has always been some scientific activity which has been done "for itself alone" out of pure intellectual curiosity.

Hardie, C.D. (1944)
The Relations between Science and Philosophy. *Philosophy*, *19*(73), p.108

Table of Contents

- Chapter 1 — 7
  General introduction
- Chapter 2 — 23
  Synthesis of a Pyrene-based π-extended Triple Helicene
- Chapter 3 — 51
  Conformational Behavior and Spectroscopic Properties of a Pyrene-based π-extended Triple Helicene
- Chapter 4 — 73
  Understanding the Conformational Preference of Propeller-shaped Polycyclic Aromatic Hydrocarbons
- Chapter 5 — 95
  Freestanding Non-covalent Thin Films of the Propeller-shaped Polycyclic Aromatic Hydrocarbon Decacyclene
- Chapter 6 — 117
  Summary and perspective

Nederlandse samenvatting — 133

List of Publications — 137

Curriculum Vitae — 139

Acknowledgements — 141

Chapter 1

General introduction

The present Thesis revolves around propellerenes – a particular type of polycyclic aromatic hydrocarbon, or PAH for short. PAHs are molecules that consist entirely of carbon and hydrogen atoms, arranged in such a fashion as to make rings, some of which share a number of carbon atoms between them (Fig. 1.1). These rings, in turn, are called aromatic because they adhere to a fixed set of requirements. The most important of these is that the bonds making up the ring have a number of p_z-electrons equal to $4n + 2$ (where n is an integer), which can freely delocalize between any pair of adjacent carbon atoms (Fig. 1.1), and which is known as Hückel's rule.[1-3] It is from this electron delocalization that aromatic rings, and thus aromatic molecules, including propellerenes, acquire their most interesting properties, some of which will be the subject of this thesis. Before discussing propellerenes specifically, the chemistry of aromatic molecules in general will be treated first.

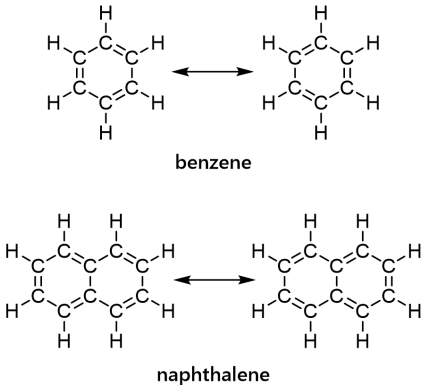


Figure 1.1 Chemical structure of benzene, the base unit of all polycyclic aromatic hydrocarbons, and naphthalene, a bicyclic aromatic molecule. For each, two resonance structures are shown, *both of which contribute to the total structure*. This concept will be further explored when discussing Clar sextets in Chapter 2.

A brief history. Although it is impossible to do justice to all the chemists which have indulged themselves in tackling the chemistry of aromatic molecules, the timeline on the next page aims to highlight some of the most notable names and achievements in this field (Fig. 1.2). The roughly 200-year story on aromatic chemistry starts with August Kekulé who correctly proposed the structure of benzene in 1865, and which is widely recognized as the starting point of aromatic chemistry.[5-9] The chemists Gustav Schultz and Richard Anschütz both became assistant to August Kekulé in 1875, with Francis R. Japp joining the laboratory a year later. This small team of chemists who would go on to identify and characterize a great number of small PAHs, and some of their pioneering work is referenced here in this Thesis. Without a doubt the most instrumental chemist at the beginning of the previous century was Erich Clar, who defended his thesis on condensed (now called polycyclic) aromatic hydrocarbons in 1927 and by the end of his career in 1983 had synthesized the parent structure of over 50 PAHs.[10] His crowning work in terms of synthesis is that of ovalene in 1948, which was the largest PAH known to that date.[11] Following in his footsteps was Ronald Harvey who significantly extended our knowledge on the reactivity of PAHs, not only in chemical but also in biological systems.[12] The last chemist to mention is Klaus Müllen who, together with others, has in the past few decades revived the field of PAH chemistry. His current PAH portfolio numbers over 3000 publications, with the largest PAH among them being C222. Published in 2002, this molecule is expected to remain the largest ever synthesized PAH for a long time to

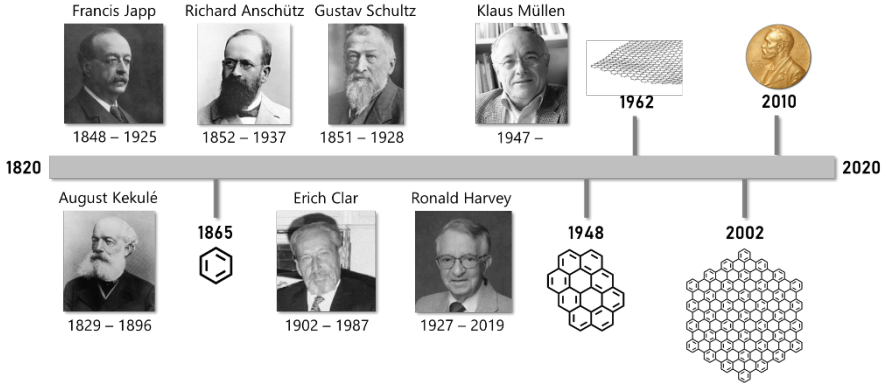


Figure 1.2 Timeline highlighting some of the most influential figures in the field of aromatic chemistry in the past 200 years, and some of their notable achievements.

come.[13] The only PAH conceivably larger than C222 would be graphene, which can be regarded as resulting from the merger of a near infinite number of benzene molecules. The first observation of a single layer of this material was in 1962,[14] although only after its rediscovery and characterization by Andrey Geim and Konstantin Novoselov in 2004 was the full potential of this material recognized.[14] For their work, Geim and Novoselov would receive the Nobel Prize in Physics six years later.

Properties and use. One of the more infamous properties of PAHs is their carcinogenicity. Already in 1775, Percivall Pott reported the anomalously large incidence of cancer in chimney sweeps as a result of their occupational exposure to soot.[15,16] Indeed, with advances in analytical chemistry, it has become apparent that PAHs are being formed even in everyday pyrolysis reactions like the burning of candles[17] and in the preparation of food.[18,19] Not only that, with increasing resolution of spectroscopic measurements we now know PAHs to even be present in outer space.[20-22] With a knowledge of their existence came a desire to make them and study their properties. Where small PAHs are studied for their biological properties, interest in larger PAHs stems from their potential application in organic electronic devices,[23] which are anticipated to one day replace the now commonplace inorganic ones.[24-27] The aforementioned graphene is special in this regard.[28]

Being a 2D material, its electronic properties,[29-31] mechanical flexibility,[32] and chemical inertness make graphene the ideal material for use in electronic devices.[33] Techniques commonly used to produce graphene include the evaporation of silicon from SiC, Chemical and Physical Vapor Deposition (CVD and PVD), diffusion and precipitation, and Molecular Beam Epitaxy (MBE).[34] But despite being able to provide samples on a laboratory scale, they are not able to provide enough material of sufficiently high quality to allow its wide-scale use.[34] For example, the production of 1 cm^2 of single crystal graphene was achieved only relatively recently, and required a 10 hour preparation time.[35] The controlled, chemical synthesis of graphene, starting from PAHs would thus be ideal. Not only would this allow access to large areas of graphene, but

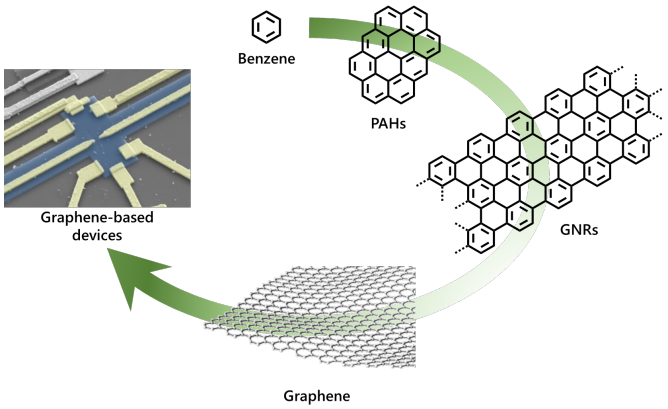


Figure 1.3 Transition from benzene, through polycyclic aromatic hydrocarbons (PAHs) and graphene nanoribbons (GNRs), to graphene and graphene-based devices. Shown on the left is a quantum point contact device on an hBN/Graphene/hBN heterostructure from the Sacépé group.[4]

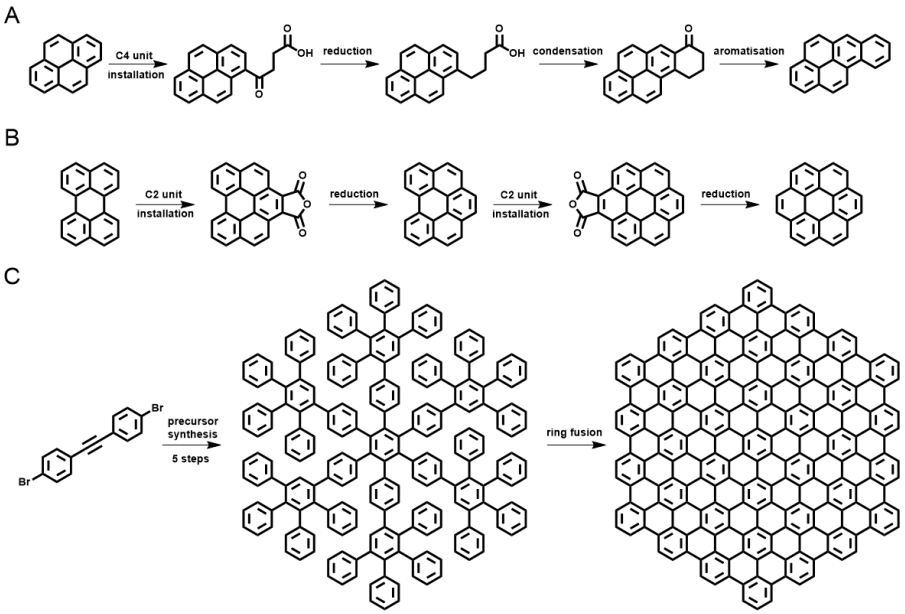


Figure 1.4 Comparison of classical and modern synthetic approaches to obtain PAHs. A) Cook's synthesis of benzo[a]pyrene, an archetypical example of ring attachment *via* condensation type synthesis.[36] B) Clar's conversion of perylene to coronene, illustrating C2 unit installation *via* Diels-Alder type synthesis, using (bromo)maleic anhydride.[37] C) Müllen's synthesis of C222 *via* a soluble precursor strategy.[13]

by use of different aromatic precursors, the properties of the resultant material can be controlled on a molecular level. The bottom-up synthesis of pristine graphene is therefore the holy grail in the PAH field.[34,38,39] As such, the synthesis of graphene nanoribbons (GNRs) is currently actively pursued to obtain graphene sheets in quantities useful for application in electronics.[40] However, poor control over the length of the ribbons and their purity, as well as the lack of a direct way of incorporating the resultant materials in electronic devices mean much work is still to be done before such devices will emerge on the consumer market (Fig. 1.3).[41]

The solubility problem. The drive to make ever-larger PAHs has necessitated a shift away from the old approach whereby new rings are introduced one at a time (Fig. 1.4A-B). The reason for this is that large PAHs pose a significant synthetic challenge, due to their poor solubility. This poor solubility of PAHs is a direct result of the strong intermolecular interactions they can engage in. Due to their planar structure, they can approach each other at very close distances, a process known as stacking. For PAHs incorporating four or more rings, this results in a significant amplification of the van der Waals forces acting on the molecules, an effect known as the π – π stacking effect (PSE).[42] New synthetic approaches were thus needed, to circumvent this solubility problem.

One particularly useful strategy is to first make a precursor molecule which *is* soluble up to the penultimate step, and to then do a single transformation to make the final insoluble material. All that is then needed is to simply filter off the product and wash it. There are several ways in which one can make such a soluble molecule. Within the PAH field, one of the most common approaches is to introduce polar functional groups on a molecule, which enhances its solubility by increasing its affinity with polar solvents. Another common approach is to introduce bulky substituents which hampers the association, *i.e.* stacking, of the molecules. If the presence of functional groups is, however, undesired, it is also possible to make a flexible or non-planar PAH precursor, in which their very structure precludes a proper approach of the molecules, thus enhancing their solubility. Fusion together of different parts of the molecule then results in the desired, planar molecule. It was in this latter way that C222 was synthesized (Fig. 1.4C), and this "non-planar precursor approach" forms the starting point for this Thesis.

Helicenes. "Non-planar PAH" might sound like an oxymoron, as most elementary chemistry books recall that a molecule has to be planar for it to be aromatic. This statement derives from the necessity of the p_z orbitals to overlap, to allow delocalization of the electrons. That the picture here is not all that black-and-white, however, is reflected in the existence of an entire field of non-planar PAHs, collectively known as contorted or geodesic PAHs, which defy this overhasty assertion.[43-45] It is now understood that molecules can have different *degrees of aromaticity* depending on the extent of planarity (and thus orbital overlap and electron localization/delocalization), as long as Hückel's rule is satisfied. Moreover, as Hückel's rule is strictly applicable to single ring systems, for polycyclic aromatic molecules it is more accurate to speak of differences in *local aromaticity* within a single molecule.

By far the most well-known of the non-planar PAHs are the helicenes, which originate from the *ortho*-fusion of benzene rings (Fig. 1.5). Already when the number of rings reaches four, steric clash between the spatially proximal protons on both ends of the molecule forces the adaptation of a twisted geometry. When the number reaches five, the rings at both ends start to overlap and a clearly helical geometry is adopted, explaining the name. Although comprehensive nomenclature for helicene derivatives has not yet been established, the parent structures are named as [*n*]helicene, with *n* being the number of fused benzene rings. As the mirror images of helixes are non-superimposable, they are chiral, and clockwise and counterclockwise rotating helices are denoted as plus (P) and minus (M) respectively (Fig. 1.5).[46]

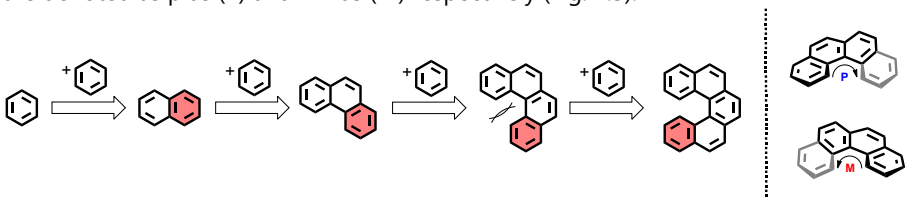


Figure 1.5 Schematic representation of the formation of helicenes from the stepwise *ortho*-fusion of benzene rings. On the right is shown the definition of plus (P) and minus (M) rotation.

A comprehensive review on helicenes, covering 100 years of helicene chemistry, was published in 2012 by Gingras and the interested reader is kindly referred thereto.[47-49] The following section aims to give some of the highlights of helicene chemistry, in particular their application in enantioselective synthesis, as well as photo-optical applications, for which they are most lauded. It then proceeds with the π–extension of helicenes to yield larger constructs, as well as the incorporation of multiple helicene motifs in a single molecule, before finally arriving at propellerenes, which form the main topic of the present Thesis.

Application in synthesis. A first hint that helicenes could be used to achieve enantioselectivity in chemical conversions was gleaned from the fact that a difference in the absorption of polarized light (*i.e.* circular dichroism (CD)) was observed upon the reduction of [6]helicene with potassium metal in (+)-2,3-dimethoxybutane.[50] One of the earliest practical examples showing the actual utility of helicenes was in the form of chiral selectors. In 1986, Ben Hassine *et al.* showed perfect enantiomeric control over the epoxidation product of stilbene derivatives in the presence of 2-cyano-[6]helicenes (Fig. 1.6A-B).[51] It is assumed that the nitrile on the helicene and hydrogen peroxide first combine to form the active agent, and diastereotopic face discrimination is then induced by the helicene skeleton itself; *i.e.* the aromatic rings of the stilbene engage in stacking with the helicene helix in a way which precludes different modes of attack. Additional findings pointing towards this role of the helicene skeleton were found by Kawasaki and co-workers who found that even without specific funcational groups, helicene molecules are able to induce enantioselectivity in the addition of alkylzinc to aldehydes, resulting in enantio-enriched secondary alcohols, tuned by the chirality of the ligand (Fig. 1.6C).[52,53] In this case, it is hypothesized that helicenes act as "chiral initiators", inducing the first enantio-selective conversion of some of the substrate, which itself then becomes the active chirality inducing agent; a concept known as asymmetric autocatalysis. As a final example, Gottard and co-workers were the first to find that a [6]helicene-based biphosphine ligand was capable of affecting some enantioselectivity in the hydrogenation of itaconic acid ester (Fig. 1.6D),[54] further illustrating the breath of chemical conversions that can be enantio-selectively steered using helicene-based auxiliaries.

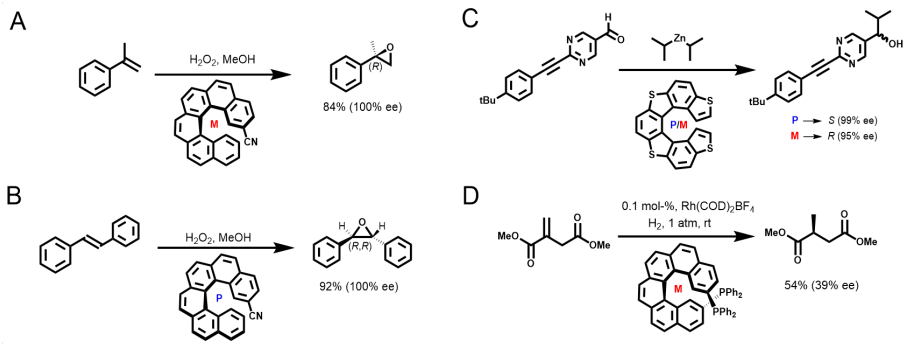


Figure 1.6 Some examples of the use of helicenes to achieve enantioselectivity: (A – B) Epoxidation of deactivated alkenes. (C) Addition of an alkylzinc reagent to aldehydes. (D) Hydrogenation of itaconic acid ester.

Application in electronic devices. Just like the aforementioned graphene and GNRs, a plethora of reports suggest the use of helicenes as organo-electronic components, for example, in the form of molecular switches, polarized organic light-emitting diodes (POLEDs),[55-58] organic thin-film transistors (OTFTs)[59] and others.[60] Their application in functional devices, however, remains in its infancy. Probably the most promising application is in the solar cell field. With an increasing shift towards renewable energy, dye-sensitized solar cells (DSSCs) are heralded as the next-generation in solar cell technology. However, the high costs of conventional ruthenium-based dyes, combined with their environmental toxicity, has warranted a search for dyes that benefit from low processing cost, high performance, and ease of production;[61] and helicenes fit just this description.[62,63] Harima and co-workers have been particularly active in this field and synthesized a series of helicene-based donor-acceptor π-conjugated (DπA) dyes.[64]

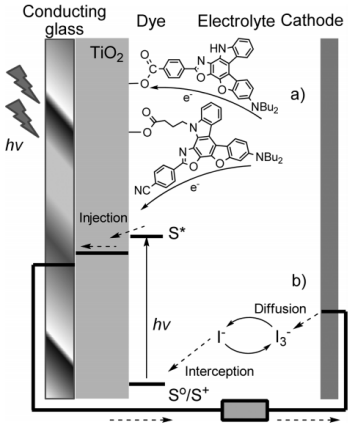


Figure 1.7 Schematic representation of a DSSC employing DπA dyes as sensitizers. Reproduced from Ref. 60. Note that in practice only a single sensitizer will be used in a device.

The working principle of DSSCs is illustrated in Figure 1.7. In short, in DSSCs, a dye (here a heterohelicene based DπA dye) is attached to a semiconducting surface (typically TiO_2), and absorbs incoming light. The dye gets excited and an electron is injected from the excited dye into the conductance band of the TiO_2. Electrons then flow through the device and end up at the cathode, where they are taken up by a redox-couple (here I^-/I_3^-) and transferred back to the dye. Indeed, helicenes are ideal candidates as photosensitizer in DSSCs as their HOMO – LUMO levels can be tuned by altering their chemical structure, they absorb in the entire visible light region, and can be covalently attached to the TiO_2 surface.

Beyond helicenes. One downside to helicenes, however, is their poor photo-stability, prompting researchers to search for molecules which contain these elusive helical motifs, but benefit from greater stability, for example by extension of the π–conjugated system. The unique properties of helicenes originate by and large from the way in which electrons are localized and delocalized within the helical structure. It is therefore not surprising that extension of the π–conjugated system, *i.e.* from the fusion of additional benzene rings to the helical backbone (*cq.* Fig. 1.5), can result in significantly different physicochemical properties (Fig. 1.8). Yet although the use of π–extension to alter the photo-optical response of aromatic molecules is well established, the π–extension of helicenes appears thus far to mostly stem from synthetic ease or arise gratuitously, rather than as a goal in and of itself.[65-69] Indeed, a systematic study investigating the effect of π–extension in helicenes is lacking in the literature and constitutes an interesting field of opportunity.

Much more systematically studied are molecules incorporating more than one helical motive, known as multiple helicenes (Fig. 1.8).[70] Evidently, merger of multiple helicene structures into a single molecule is accompanied by extension of the conjugated system, and comparison of mono,[71] double[72,73] and triple [5]helicene[74] shows them to indeed have completely different physicochemical properties.

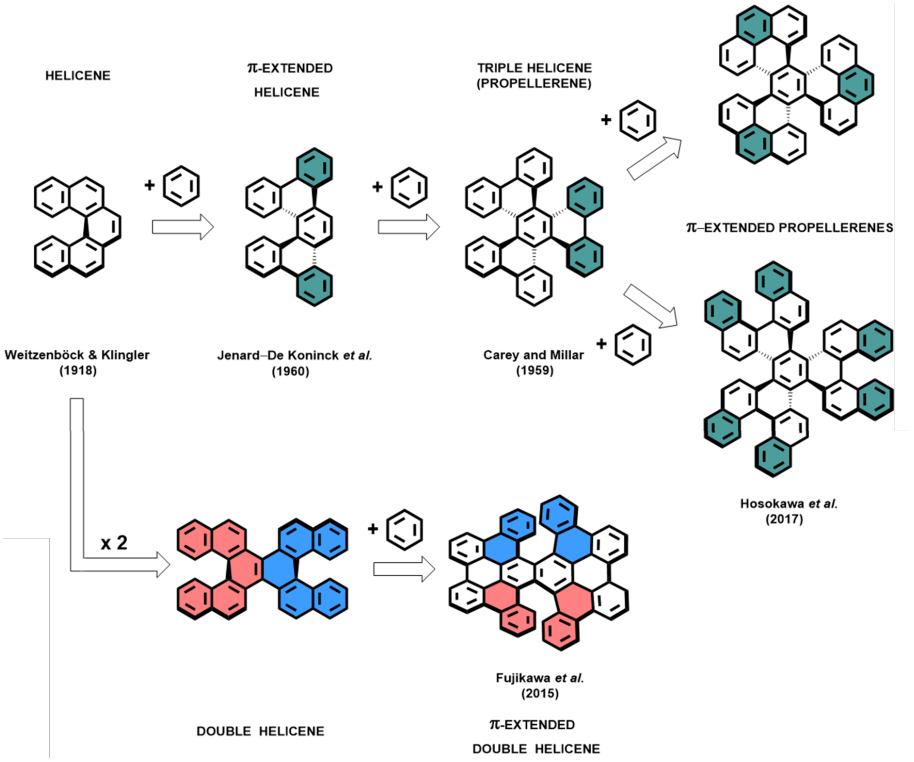


Figure 1.8 Schematic representation of the formation of π-extended helicenes, as well as double and triple helicenes, from the consecutive addition of fused benzene rings. Reported authors and dates relate to the first mention of the corresponding molecule in the literature.

Although the term *triple helicene* is sometimes invoked to describe propeller-shaped PAHs, use of this term in the literature is restricted to π–extended, or benzoid, triphenylenes. A new term was therefore needed to encompass all non-planar PAHs with a single central ring and trifold symmetry, some known examples of which are given in Figure 1.9A. The term *propellerene* is thus coined here. What differentiates propellerenes from helicenes, and justifies coinage of a new, common name to refer to them, is that, apart from a C_2 symmetry typical for helicenes, they can all adopt a structure with a D_3 symmetry. It is from this common conformational space that propellerenes derive their most interesting features. As illustrated in Figure 1.9B, symmetry in both helicenes and propellerenes is defined by the relative orientation of the rings.

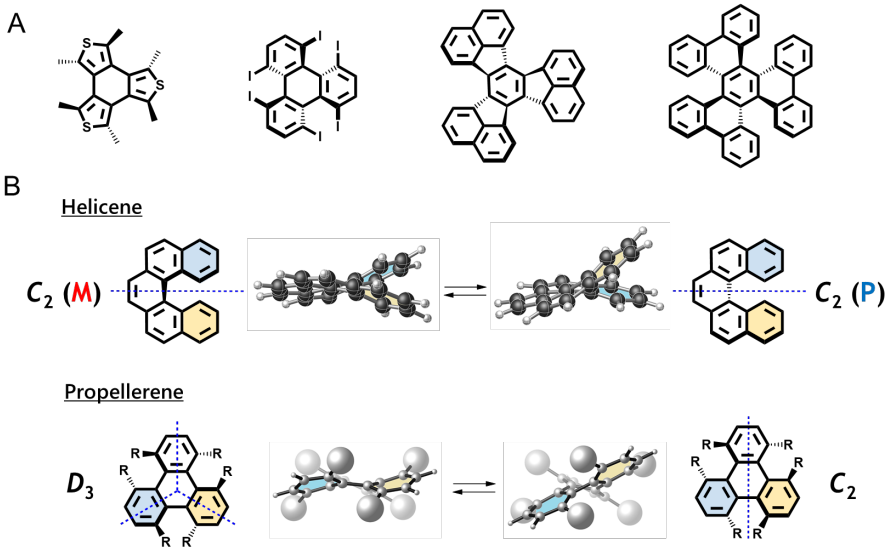


Figure 1.9 (A) Examples of known propellerenes, from left to right: hexamethylbenzotrithiophene, hexaiodotriphenylene, decacyclene, hexabenzotriphenylene. (B) General representation of interconversion of helicenes and propellerenes. The dotted blue lines indicate the axes of rotation. Note that symmetry is defined by the relative orientation of the rings highlighted in blue and yellow. Also note that interconversion between the two C_2 conformers of [5]helicene in (B) is associated with a change in the helical chirality (*cq.* Fig. 1.5).

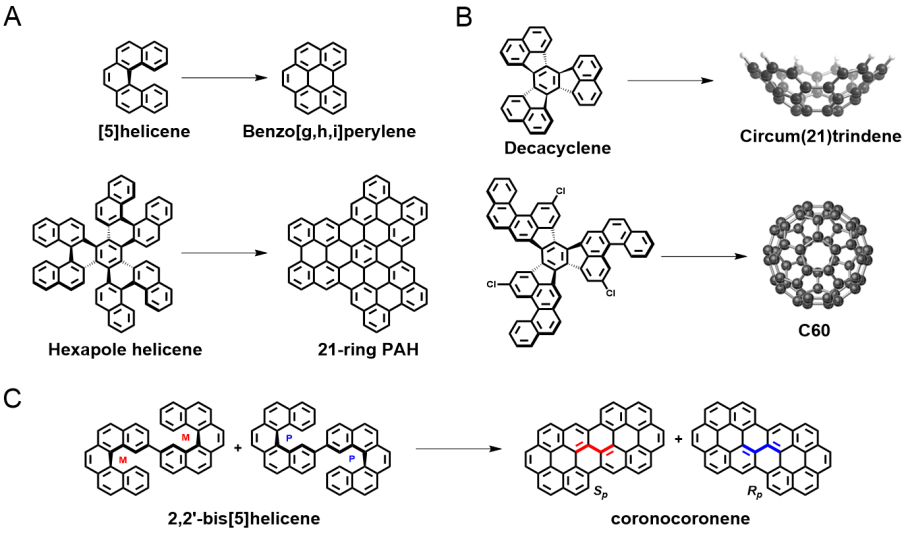


Figure 1.10 Intramolecular ring fusion reactions yielding planar (A) and non-planar (B) products. (C) Example of the retention of handedness in ring fusion of bis[5]helicenes, yielding planar coronocoronenes.

Ring fusion of helicenes and propellerenes. When sterically congested parts of a molecule are properly positioned they can be covalently connected in a process known as intramolecular ring coupling. As a typical example, the ring coupling of [5]helicene results in the formation of benzo[g,h,i]perylene (Fig. 1.10A).[75-77] By extension, planarization of a hexapole helicene gives a planar 22-ring product.[78] Importantly, the symmetry of the starting material is retained in the final product. Thus, helicenes yield products with a C_2 symmetry, whereas propellerenes give products with D_3 symmetry. In addition, the multiplicity of the rings directly attached to the central ring determines whether the resultant product is planar or not. When the rings attached to the central ring are composed of an even number of bonds, a planar structure is obtained after ring fusion (Fig. 1.10A), whereas an odd number of bonds yields a non-planar product (Fig. 1.10B). This is exemplified by the flash vapor pyrolysis (FVP) of decacyclene, which yields the bowl-shaped circum(21)trindene.[79-82] Further illustrating the power of this strategy, Scott *et al.* managed to synthesize Buckminster fullerene C_{60} *via* the same procedure using a slightly more elaborate precursor.[83,84] Lastly, it was recently shown that the on-surface dehydrogenative ring fusion of bis[5]helicenes proceeds with retention of handedness (Fig. 1.10C).[86]

Aim and outline. The target molecule of the research described in this Thesis is circum(30)triphenylene, whose large size and D_{3h} symmetry make interesting molecule in the context of astrochemistry. Two possible synthetic routes were considered, both based on a ''non-planar precursor approach'' (Figure 1.11). Route A was inspired by the work of Müllen *et al.* who reported a derivative of circum(30)triphenylene.[85] However, the unavailability and inaccessibility of the required phenanthrene-4-boronic acid, and reported poor yield of the Suzuki coupling reaction diverted attention to another route. Route B is based on a palladium-catalyzed trimerization protocol, developed and extensively studied by Diego Peña, in which a propellerene precursor is formed, which is then ring fused to the final product. Given that the required 4-hydroxypyrene was known in literature, focus was directed to this route. During the work, it became apparent, however, that literature procedures were unable to provide enough of the required intermediate to synthesize the target molecule on a reasonably large scale.

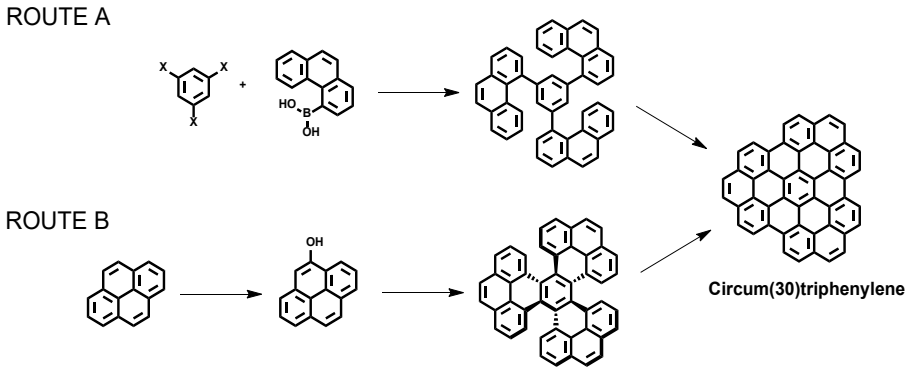


Figure 1.11 Two routes considered for the synthesis of the target circum(30)triphenylene.

Chapter 2 therefore starts by describing the development and optimization of a novel synthetic route to obtain 4-hydroxypyrene from pyrene. The synthesis route described involves a sequence of ring contraction and ring expansion reactions, which ultimately allows introduction of a hydroxyl group on the elusive C4 position of pyrene. The 4-hydroxypyrene was then used to make a pyrene-based π–extended propellerene, that serves as the non-planar precursor to the target molecule.

As mentioned above, the effect π–extension has on the physico-chemical properties of propellerenes is little studied in literature and **Chapter 3** therefore looks at the conformational behavior (C_2 *versus* D_3) of pyrene propellerene, in comparison to other, structurally similar helicenes (*cf*. Fig. 1.8). The impact of the position of π–extension on the physicochemical and chiroptical properties of propellerenes and helicenes is also described.

Propellerenes typically show a strong preference for either a C_2 or D_3 conformation, and previous computational and experimental findings have pointed towards a combination of aromatic, steric, and electrostatic factors to be responsible for this preference. However, a unifying theory that allows one to predict which conformation is preferably adopted, and would allow for the rational design of propellerenes in a particular conformation, remains lacking. Indeed, the origin of the conformational preference of propellerenes is a long standing question in the field. **Chapter 4** provides a thorough computational study addressing the observed conformational preference of the pyrene propellerene and several other propellerenes to try and resolve this issue. This is done by employing a DFT based computational model that dissects propellerenes, investigates the preference of the individual parts of the molecule, and the balance between these.

Practical applications of propellerenes are studied in **Chapter 5**. There the small propellerene decacyclene is used to produce nanometer thin film, which were found capable of spanning up to micrometer distances, held together solely by the collective action of van der Waals forces acting on the molecules. To explain this unexpected observation, a combination of computational studies was performed to study the composition of the thin film on a molecular scale. On a microscopic scale, atomic force microscopy (AFM) and electron microscopy (EM) were used to both qualitatively and quantitatively study the physical properties of the thin film.

Chapter 6 concludes with a summary of the work, and explicates the spectroscopic properties of circum(30)triphenylene in the context of astrochemistry. It shows it to have unique identifying signatures, which differentiate it from the handful of other, known D_{3h} PAHs.
It is hoped this thesis will encourage the treatment of propellerenes as their own field of study, and will excite its readers, as much as it has excited me.

References

(1) Hückel, E. Quantentheoretische beiträge zum benzolproblem. *Z Phys. A-Hadron Nucl.* **1931,** *70* (3), 204.
(2) Hückel, E. Quanstentheoretische beiträge zum benzolproblem. *Z. Phys.* **1931,** *72* (5-6), 310.
(3) Hückel, E. Quantentheoretische beiträge zum problem der aromatischen und ungesättigten verbindungen. III. *Z. Phys.* **1932,** *76* (9-10), 628.
(4) Veyrat, L.; Jordan, A.; Zimmermann, K.; Gay, F.; Watanabe, K.; Taniguchi, T.; Sellier, H.; Sacépé, B. Low-magnetic-field regime of a gate-defined constriction in high-Mobility Graphene. *Nano Lett.* **2019,** *19* (2), 635.
(5) Kekuié, A. Untersuchungen über aromatische verbindungen ueber die constitution der aromatischen verbindungen. I. Ueber die constitution der aromatischen verbindungen. *Liebigs Ann. Chem.* **1866,** *137* (2), 129.
(6) Kekulé, A. Sur la constitution des substances aromatiques. *Bull. Mens. Soc. Chim. Paris* **1865,** *3*, 98.
(7) Kekulé, F. A. Note sur quelques produits de substitution de la benzine. *Bull. Acad. R. Belg* **1865,** *19*, 551.
(8) Rocke, A. J. It began with a daydream: the 150th anniversary of the Kekulé benzene structure. *Angew. Chem. Int. Ed.* **2015,** *54* (1), 46.
(9) Wotiz, J. H.; Rudofsky, S. Was there a conspiracy when Kekulé's first German benzene-structure paper was frequently listed as published in 1865? *J. Chem. Edu.* **1982,** *59* (1), 23.
(10) Clar, E.; Schoental, R. *Polycyclic hydrocarbons*; Springer, 1964.
(11) Clar, E. Synthesis of ovalene. *Nature* **1948,** *161* (4085), 238.
(12) Harvey, R. G. *Polycyclic aromatic hydrocarbons: chemistry and carcinogenicity*; CUP Archive, 1991.
(13) Simpson, C. D.; Brand, J. D.; Berresheim, A. J.; Przybilla, L.; Räder, H. J.; Müllen, K. Synthesis of a giant 222 carbon graphite sheet. *Chem. Eur. J.* **2002,** *8* (6), 1424.
(14) Boehm, H.-P.; Clauss, A.; Fischer, G. O.; Hofmann, U. Das adsorptionsverhalten sehr dünner kohlenstoff-folien. *Z. Anorg. Allg. Chem.* **1962,** *316* (3-4), 119.
(15) Pott, P. *Chirurgical observations relative to the cataract, the polypus of the nose, the cancer of the scrotum, the different kinds of ruptures, and the mortification of the toes and feet. By Percivall Pott, FRS Surgeon to St. Bartholomew's-Hospital*; Printed by TJ Carnegy, **1775**.
(16) Pott, P. Cancer Scroti. Chirurgical observations relative to the cataract, the polypus of the nose, cancer of the scrotum, different kinds of ruptures, and the mortification of the toes and feet. *Howes, Clarke and Collins, London* **1775**, 63.
(17) Orecchio, S. Polycyclic aromatic hydrocarbons (PAHs) in indoor emission from decorative candles. *Atmos. Environ.* **2011,** *45* (10), 1888.
(18) Rose, M.; Holland, J.; Dowding, A.; Petch, S. R. G.; White, S.; Fernandes, A.; Mortimer, D. Investigation into the formation of PAHs in foods prepared in the home to determine the effects of frying, grilling, barbecuing, toasting and roasting. *Food Chem. Toxicol.* **2015,** *78*, 1.
(19) Lijinsky, W.; Ross, A. E. Production of carcinogenic polynuclear hydrocarbons in the cooking of food. *Food Cosmet. Toxicol.* **1967,** *5*, 343.
(20) Joblin, C.; Tielens, A. G. G. M. PAHs and the universe: A symposium to celebrate the 25th anniversary of the PAH hypothesis. *EAS* **2011,** *46*.
(21) Kwok, S.; Sandford, S. PAHs in astronomy - A review. *Organic Matter in Space (IAU S251)* **2008,** (251), 357.
(22) Salama, F. PAHs in astronomy - a review. *Proc. Int. Astro. Union* **2008,** *4* (S251), 357.
(23) Samorí, P.; Feng, X.; Bonifazi, D. π-Conjugated molecules: from structure to function. *ChemPlusChem* **2019,** *84* (9), 1177.
(24) Neupane, G. P.; Ma, W.; Yildirim, T.; Tang, Y.; Zhang, L.; Lu, Y. 2D organic semiconductors, the future of green nanotechnology. *Nano Mat. Sci.* **2019,** *1* (4), 246.

(25) Ostroverkhova, O. Organic optoelectronic materials: mechanisms and applications. *Chem. Rev.* **2016,** *116* (22), 13279.
(26) Sakamoto, J.; van Heijst, J.; Lukin, O.; Schlüter, A. D. Two-dimensional polymers: just a dream of synthetic chemists? *Angew. Chem. Int. Ed.* **2009,** *48* (6), 1030.
(27) Yang, F.; Cheng, S.; Zhang, X.; Ren, X.; Li, R.; Dong, H.; Hu, W. 2D organic materials for optoelectronic applications. *Adv. Mat.* **2018,** *30* (2), 1702415.
(28) Hirsch, A. The era of carbon allotropes. *Nat. Mat.* **2010,** *9* (11), 868.
(29) Neto, A. H. C.; Guinea, F.; Peres, N. M. R.; Novoselov, K. S.; Geim, A. K. The electronic properties of graphene. *Rev. Mod. Phys.* **2009,** *81* (1), 109.
(30) Balandin, A. A. Low-frequency 1/f noise in graphene devices. *Nat. Nanotech.* **2013,** *8* (8), 549.
(31) Cheng, Z.; Li, Q.; Li, Z.; Zhou, Q.; Fang, Y. Suspended graphene sensors with improved signal and reduced noise. *Nano Lett.* **2010,** *10* (5), 1864.
(32) Gomez De Arco, L.; Zhang, Y.; Schlenker, C. W.; Ryu, K.; Thompson, M. E.; Zhou, C. Continuous, highly flexible, and transparent graphene films by chemical vapor deposition for organic photovoltaics. *ACS nano* **2010,** *4* (5), 2865.
(33) Sattler, K. D. *21st Century Nanoscience–A Handbook: Low-Dimensional Materials and Morphologies (Volume Four)*; CRC Press, 2020.
(34) Backes, C.; Abdelkader, A. M.; Alonso, C.; Andrieux-Ledier, A.; Arenal, R.; Azpeitia, J.; Balakrishnan, N.; Banszerus, L.; Barjon, J.; Bartali, R. Production and processing of graphene and related materials. *2D Mater.* **2020,** *7* (2), 022001.
(35) Hao, Y.; Bharathi, M. S.; Wang, L.; Liu, Y.; Chen, H.; Nie, S.; Wang, X.; Chou, H.; Tan, C.; Fallahazad, B. The role of surface oxygen in the growth of large single-crystal graphene on copper. *Science* **2013,** *342* (6159), 720.
(36) Cook, J. W.; Hewett, C. L.; Hieger, I. 106. The isolation of a cancer-producing hydrocarbon from coal tar. Parts I, II, and III. *J. Chem. Soc. (Resumed)* **1933**, 395.
(37) Clar, E.; Zander, M. 927. Syntheses of coronene and 1:2-7:8-dibenzocoronene. *J. Chem. Soc. (Resumed)* **1957**, 4616.
(38) Wang, X.-Y.; Yao, X.; Müllen, K. Polycyclic aromatic hydrocarbons in the graphene era. *Sci. China Chem.* **2019,** *62* (9), 1099.
(39) Jiang, L.; Niu, T.; Lu, X.; Dong, H.; Chen, W.; Liu, Y.; Hu, W.; Zhu, D. Low-temperature, bottom-up synthesis of graphene via a radical-coupling reaction. *J. Am. Chem. Soc.* **2013,** *135* (24), 9050.
(40) Dutta, S.; Pati, S. K. Novel properties of graphene nanoribbons: a review. *J. Mater. Chem.* **2010,** *20* (38), 8207.
(41) Jolly, A.; Miao, D.; Daigle, M.; Morin, J. F. Emerging Bottom-Up Strategies for the Synthesis of Graphene Nanoribbons and Related Structures. *Angew. Chem. Int. Ed.* **2020,** *59* (12), 4624.
(42) Grimme, S. Do special noncovalent π–π stacking interactions really exist? *Angew. Chem. Int. Ed.* **2008,** *47* (18), 3430.
(43) Antić, M.; Furtula, B.; Radenkovic, S. Aromaticity of nonplanar fully benzenoid hydrocarbons. *J. Phys. Chem. A* **2017,** *121* (18), 3616.
(44) Rickhaus, M.; Mayor, M.; Juríček, M. Strain-induced helical chirality in polyaromatic systems. *Chem. Soc. Rev.* **2016,** *45* (6), 1542.
(45) Rickhaus, M.; Mayor, M.; Juríček, M. Chirality in curved polyaromatic systems. *Chem. Soc. Rev.* **2017,** *46* (6), 1643.
(46) Cahn, R. S.; Ingold, C.; Prelog, V. Specification of molecular chirality. *Angew. Chem. Int. Ed.* **1966,** *5* (4), 385.
(47) Gingras, M. One hundred years of helicene chemistry. Part 1: non-stereoselective syntheses of carbohelicenes. *Chem. Soc. Rev.* **2013,** *42* (3), 968.
(48) Gingras, M.; Félix, G.; Peresutti, R. One hundred years of helicene chemistry. Part 2: stereoselective syntheses and chiral separations of carbohelicenes. *Chem. Soc. Rev.* **2013,** *42* (3), 1007.
(49) Gingras, M. One hundred years of helicene chemistry. Part 3: applications and properties of carbohelicenes. *Chem. Soc. Rev.* **2013,** *42* (3), 1051.
(50) Weissman, S. I. Selectivity in the reduction of enantiomers of hexahelicene in an optically active solvent. *J. Org. Chem.* **1976,** *41* (25), 4040.

(51) Ben Hassine, B.; Gorsane, M.; Geerts-Evrard, F.; Pecher, J.; Martin, R. H.; Castelet, D. Utilisation de la Synthèse Atrolactique Pour L'Évaluation de L'Efficacité D'Inducteurs de Synthèse Asymétrique. *Bull. Soc. Chim. Belges* **1986,** *95* (7), 547.
(52) Kawasaki, T.; Suzuki, K.; Licandro, E.; Bossi, A.; Maiorana, S.; Soai, K. Enantioselective synthesis induced by tetrathia-[7]-helicenes in conjunction with asymmetric autocatalysis. *Tetrahedron: Asymmetry* **2006,** *17* (14), 2050.
(53) Sato, I.; Yamashima, R.; Kadowaki, K.; Yamamoto, J.; Shibata, T.; Soai, K. Asymmetric induction by helical hydrocarbons:[6]-and [5] helicenes. *Angew. Chem.* **2001,** *113* (6), 1130.
(54) Reetz, M. T.; Beuttenmüller, E. W.; Goddard, R. First enantioselective catalysis using a helical diphosphane. *Tet. Lett.* **1997,** *38* (18), 3211.
(55) Hassey, R.; Swain, E. J.; Hammer, N. I.; Venkataraman, D.; Barnes, M. D. Probing the chiroptical response of a single molecule. *Science* **2006,** *314* (5804), 1437.
(56) Hassey, R.; McCarthy, K. D.; Swain, E.; Basak, D.; Venkataraman, D.; Barnes, M. D. Single-molecule chiroptical spectroscopy: Fluorescence excitation of individual helicene molecules in polymer-supported thin-films. *Chirality: The Pharmacological, Biological, and Chemical Consequences of Molecular Asymmetry* **2008,** *20* (9), 1039.
(57) Tang, Y.; Cook, T. A.; Cohen, A. E. Limits on fluorescence detected circular dichroism of single helicene molecules. *J. Phys. Chem. A* **2009,** *113* (22), 6213.
(58) Cohen, A.; Tang, Y. Reply to "Comment on 'Limits on Fluorescence Detected Circular Dichroism of Single Helicene Molecules'". *J. Phys. Chem. A* **2009,** *113* (35), 9759.
(59) Kim, C.; Marks, T. J.; Facchetti, A.; Schiavo, M.; Bossi, A.; Maiorana, S.; Licandro, E.; Todescato, F.; Toffanin, S.; Muccini, M. Synthesis, characterization, and transistor response of tetrathia-[7]-helicene precursors and derivatives. *Org. Electron.* **2009,** *10* (8), 1511.
(60) Shen, Y.; Chen, C.-F. Helicenes: synthesis and applications. *Chem. Rev.* **2012,** *112* (3), 1463.
(61) Robertson, N. Optimierung farbstoffsensibilisierter solarzellen. *Angew. Chem.* **2006,** *118* (15), 2398.
(62) Grätzel, M. Solar water splitting cells. *Nature* **2001,** *414*, 338.
(63) Grätzel, M. In *Materials For Sustainable Energy: A Collection of Peer-Reviewed Research and Review Articles from Nature Publishing Group*; World Scientific, 2011.
(64) Mishra, A.; Fischer, M. K. R.; Bäuerle, P. Metal-free organic dyes for dye-sensitized solar cells: From structure: Property relationships to design rules. *Angew. Chem. Int. Ed.* **2009,** *48* (14), 2474.
(65) Reger, D.; Haines, P.; Heinemann, F. W.; Guldi, D. M.; Jux, N. Oxa [7] superhelicene: A π-extended helical chromophore based on hexa-peri-hexabenzocoronenes. *Angew. Chem. Int. Ed.* **2018,** *57* (20), 5938.
(66) Nakakuki, Y.; Hirose, T.; Sotome, H.; Miyasaka, H.; Matsuda, K. Hexa-peri-hexabenzo [7]helicene: Homogeneously π-extended helicene as a primary substructure of helically twisted chiral graphenes. *J. Am. Chem. Soc.* **2018,** *140* (12), 4317.
(67) Chen, Y.; Lin, C.; Luo, Z.; Yin, Z.; Shi, H.; Zhu, Y.; Wang, J. Double pi-extended undecabenzo[7]helicene. *Angew. Chem. Int. Ed.*
(68) Martin, M. M.; Hampel, F.; Jux, N. A Hexabenzocoronene-based helical nanographene. *Chem.-Eur. J.* **2020,** *26* (45), 10210.
(69) Sitaula, P.; Malone, R.; Longhi, G.; Abbate, S.; Gualtieri, E.; Lucotti, A.; Tommasini, M.; Franzini, R.; Villani, C.; Catalano, V. J. π-extended helical nanographenes: synthesis and photophysical properties of naphtho[1,2-a]pyrenes. **2020**. doi:10.26434/chemrxiv.12931703.v1.
(70) Mori, T. Chiroptical properties of symmetric double, triple, and multiple helicenes. *Chem. Rev* **2021**, *121* (4), 2373-2412.
(71) Kubo, H.; Hirose, T.; Matsuda, K. Control over the emission properties of [5]helicenes based on the symmetry and energy levels of their molecular orbitals. *Org. Lett.* **2017,** *19* (7), 1776.
(72) Kashihara, H.; Asada, T.; Kamikawa, K. Synthesis of a double helicene by a palladium-catalyzed cross-coupling reaction: structure and physical properties. *Chem. Eur. J.* **2015,** *21* (17), 6523.

(73) Note that the structure actually incorporates two [5]helicene, as well as two [4]helicene motifs, and as such one could argue the molecule to be a quadruple helicene instead of a double helicene.
(74) Hosokawa, T.; Takahashi, Y.; Matsushima, T.; Watanabe, S.; Kikkawa, S.; Azumaya, I.; Tsurusaki, A.; Kamikawa, K. Synthesis, structures, and properties of hexapole helicenes: assembling six [5]helicene substructures into highly twisted aromatic systems. *J. Am. Chem. Soc.* **2017,** *139* (51), 18512.
(75) Xue, X.; Scott, L. T. Thermal cyclodehydrogenations to form 6-membered rings: cyclizations of [5] helicenes. *Org. Lett.* **2007,** *9* (20), 3937.
(76) Ayalon, A.; Rabinovitz, M. Reductive ring closure of helicenes. *Tet. Lett.* **1992,** *33* (17), 2395.
(77) Ito, N.; Hirose, T.; Matsuda, K. Facile photochemical synthesis of 5, 10-disubstituted [5]helicenes by removing molecular orbital degeneracy. *Org. Lett.* **2014,** *16* (9), 2502.
(78) Zuzak, R.; Castro-Esteban, J.; Brandimarte, P.; Engelund, M.; Cobas, A.; Piątkowski, P.; Kolmer, M.; Pérez, D.; Guitián, E.; Szymonski, M. Building a 22-ring nanographene by combining in-solution and on-surface syntheses. *Chem. Comm.* **2018,** *54* (73), 10256.
(79) Ansems, R. B. M.; Scott, L. T. Cation–π complexes of a bowl-shaped polycyclic aromatic hydrocarbon. *J. Phys. Org. Chem.* **2004,** *17* (9), 819.
(80) Cho, H. Y.; Ansems, R. B. M.; Scott, L. T. Site-selective covalent functionalization at interior carbon atoms and on the rim of circumtrindene, a C36H12 open geodesic polyarene. *Beilstein J. Org. Chem.* **2014,** *10* (1), 956.
(81) Forkey, D. M.; Attar, S.; Noll, B. C.; Koerner, R.; Olmstead, M. M.; Balch, A. L. Crystallographic characterization of the molecular structure and solid state packing of the fullerene-shaped hydrocarbon C36H12. *J. Am. Chem. Soc.* **1997,** *119* (24), 5766.
(82) Ansems, R. B. M.; Scott, L. T. Circumtrindene: A geodesic dome of molecular dimensions. Rational synthesis of 60 of C60. *J. Am. Chem. Soc.* **2000,** *122* (12), 2719.
(83) Boorum, M. M.; Vasil'ev, Y. V.; Drewello, T.; Scott, L. T. Groundwork for a rational synthesis of C60: cyclodehydrogenation of a C60H30 polyarene. *Science* **2001,** *294* (5543), 828.
(84) Scott, L. T.; Boorum, M. M.; McMahon, B. J.; Hagen, S.; Mack, J.; Blank, J.; Wegner, H.; de Meijere, A. A rational chemical synthesis of C60. *Science* **2002,** *295* (5559), 1500.
(85) Kastler, M.; Schmidt, J.; Pisula, W.; Sebastiani, D.; Müllen, K. From armchair to zigzag peripheries in nanographenes. *J. Am. Chem. Soc.* **2006,** *128* (29), 9526.
(86) Irziquat, B.; Cebrat, A.; Baljozovic, M.; Martin, K.; Parschau, M.; Avarvari, N.; Ernst, K.-H. Stereospecific on-surface cyclodehydrogenation of bishelicenes preservation of handedness from helical to planar chirality. Chem.-Eur. J. **2021**. doi: 10.1002/chem.202106069.

Chapter 2

Synthesis of a Pyrene-based π-extended Triple Helicene

Abstract

The synthesis of large polycyclic aromatic hydrocarbons is a challenging endeavour. On the one hand, it can be difficult to install functional groups on the required positions, and on the other hand, the poor solubility of compounds presents an important bottleneck. This Chapter shows the synthesis of the large, pyrene-based propellerene tripyrenylene, using chemical conversions that circumvent these issues. The synthesis starts with pyrene, which is converted to 4-hydroxypyrene using a ring-contraction/ring-expansion sequence, using optimized purification procedures, which allows access to this material on a gram scale. Then, after conversion to an *ortho*-TMS triflate, using a palladium catalysed aryne trimerization, the desired propellerene is made by stitching three pyrene molecules together in one step. The methodology outlined in this Chapter allows future access to other, large PAHs with trifold symmetry.

Part of the results in this Chapter are published as:
van der Ham A., Filippov D. V., Overkleeft H. S., Schneider G. F. A Three-step Synthesis of 4*H*-Cyclopenta[*def*]phenanthrene from Pyrene. *Eur. J. Org. Chem.* **2021**, 2013 –2017.
van der Ham A., Brouwer A. M., Filippov D. V., Overkleeft H. S., Schneider G. F. Positional effect of π-Extension in Triple Helicenes. **Manuscript in preparation.**

Helicenes, by virtue of their non-planar structure, show interesting physicochemical properties, which has prompted their application in, *e.g.*, chirality sensing,[1-3] asymmetric catalysts,[4-6] and chiro-optical materials. Their implementation is, however, hampered due to their poor photo-stability and low racemization barriers.[7,8] Recent years have therefore seen a shift towards the synthesis of molecules that incorporate helicene motifs, but do not suffer from these shortcomings, primarily by making the molecules more rigid. Approaches to this end include the introduction of heteroatomic functionalities, as well as the fusion of additional benzene rings into so-called π-extended helicenes,[9-13] and the merger of multiple helicene motifs into a single molecule, yielding double,[14-21] triple,[22,23] and even quadruple helicenes (Fig. 2.1).[24] Of these, the triple helicenes, for which the term propellerenes was coined in the previous Chapter, are of particular interest, with hexabenzotriphenylene (HBT; Fig. 2.1), *i.e.*, showing the highest dichroism dissymmetry factor of all known helicenes and helicinoids.[25]

Evidently, the photo-optical properties of aromatic molecules are driven by the size of the conjugated system, and the relationship between these two provides an important guiding principle for the rational design of photo-optical materials.[26-28] The relationship between the size of conjugated systems and photo-optical properties were already investigated by Woodward and Fieser halfway through the last century,[29,30] and have more recently been documented for monohelicenes[31,32] and multiple helicenes.[33] Nonetheless, a systematic study on the effect of π-extension on the properties of helicenes *vis-à-vis* propellerenes appears absent in the literature. Intrigued by the work of Hosokawa *et al.* who synthesized a π-extended hexapole [5]helicene (Fig. 2.1), tripyrenylene **1** was chosen as target molecule, not only to study the effect of π-extension on the properties of propellerenes, but also to investigate whether or not the position of the π-extension is of importance on the photo-optical properties.
This Chapter describes all the work that went into the synthesis of tripyrenylene **1**, the conformational and spectroscopic properties of which will be studied in the following Chapter.

Synthesis outline. Tripyrenylene **1**, is a triphenylene-class propellerene. By far the most popular approach nowadays to synthesize molecules of this class is the palladium(0) catalyzed trimerization of arynes (Scheme 2.1A).[34,35] Given the reactive nature of arynes they have to be generated *in situ*, which can be achieved in an elegant way by treating *ortho*-TMS triflates with a fluoride source, typically CsF or TBAF. The driving forces of this reaction are the formation of a strong Si–F bond, and the cleavage of a triflate group. Although synthesis of the required precursors can be lengthy, this is more than offset by mild reaction conditions, large functional group tolerance, and generally high yields obtainable, all explaining the popularity of this reaction. Indeed, this strategy allows access to structures not attainable *via* any other route. Scheme 2.1B gives a retro-synthetic analysis for the synthesis of tripyrenylene **1**. In short, synthesis of **1** requires *ortho*-TMS triflate precursor **9**, which in turn was to be obtained from 4-hydroxypyrene **4**.

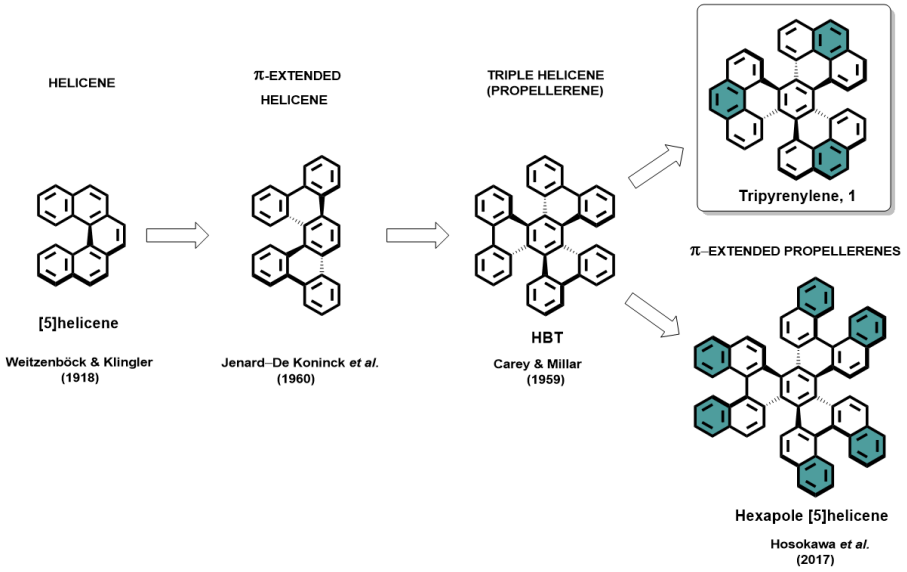
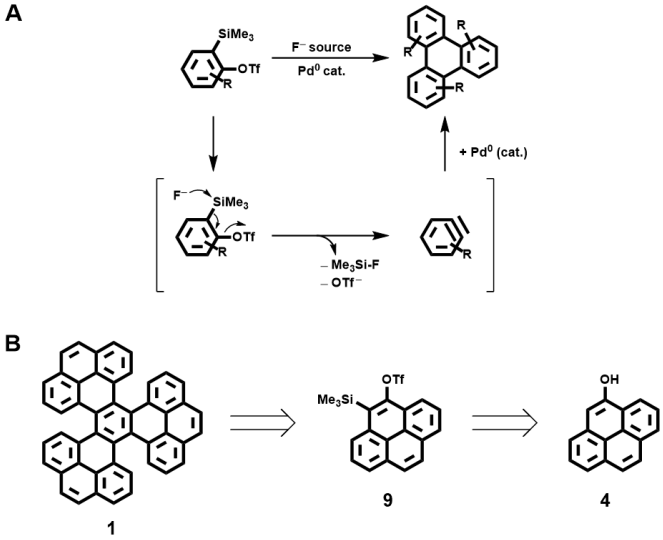
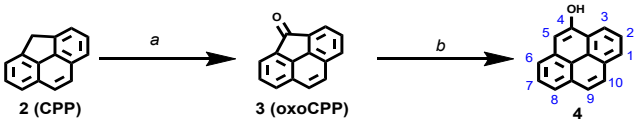


Figure 2.1 Schematic representation of the π-extension of a helicene structure. Names and dates given are related to the first identification of the compound.



Scheme 2.1 (A) General scheme for the palladium(0) catalyzed trimerization of arynes to yield PAHs with a trifold symmetry. A more detailed description is given in Chapter 3. (B) Retro-synthetic analysis for the synthesis of tripyrenylene **1**.

*Synthesis of 4-hydroxypyrene **4***. Synthesis of the required 4-hydroxypyrene **4** was found to be more challenging than expected. Selective derivatization of pyrene on the C-4 position poses a serious synthetic challenge, due to the nature of the molecule, which precludes direct oxidation protocols (For numbering see Scheme 2.2). Electrophilic and radical substitution on pyrene occurs almost exclusively at C-1, after which further derivatization takes place on C-6 or C-8. Exceptions to this rule are the Friedel-Crafts alkylation with tert-butyl chloride, which gives substitution at C-2 followed by C-7 due to steric factors.[36] The only transformations known to date to achieve direct C-4 functionalization are methylation using methyllithium under UV irradiation,[37] and the palladium catalyzed arylation using arylboroxines.[38] Interestingly, a picolinamide directing strategy showed the possibility for selective formation of a C–C bound on the C-4 position of pyrene.[39] Unfortunately, none of these routes are amendable for the introduction of an hydroxyl group at C-4. The most common way of introducing substituents on C-4 is by first reducing pyrene to 1,2,3,6,7,8-hexahydropyrene with sodium metal in refluxing amyl alcohol, followed by substitution and back oxidation with DDQ; an approach developed by Vollmann in the 1930's.[40] A multistep approach to get **4** *via* this route was recently reported and involves the initial introduction of bromine on the desired position, followed by substitution with methoxide and demethylation.[41] Although this, and other procedures,[42-46] yield 4-hydroxypyrene, they all suffer from a large number of steps and unsatisfactory overall yields, making them unattractive for the envisioned large scale synthesis of propellerene **1**. Fortuitously, it was found possible to obtain 4-hydroxypyrene **4** in 50% yield from 4*H*-4-oxocyclopenta[*d,e,f*]phenanthrene (oxoCPP, **3**) by treating it with TMS-azidomethane to affect a Tiffeneau-Demjanov-like rearrangement.[47] The required oxoCPP **3** could be synthesized in 70% yield from CPP **2** by careful oxidation with *t*BuOOH in the presence of a catalytic amount of CrO_3 (Scheme 2.2).[48]

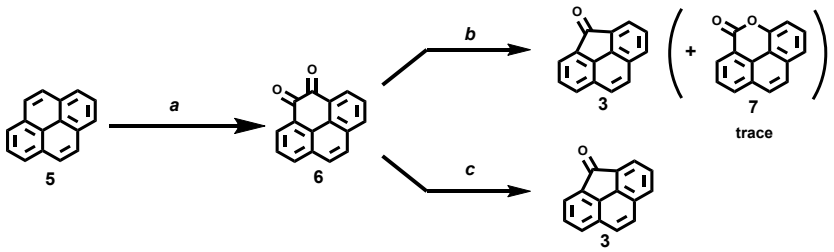


2 (CPP) 3 (oxoCPP) 4

Scheme 2.2 Synthesis of 4-hydroxypyrene **4** from CPP **2**. *Reagents and conditions*: a) *t*BuOOH, CrO_3 (cat.), DCM:H_2O, 70%; b) $TMSCHN_2$, $BF_3{\cdot}Et_2O$, DCM, -78°C → rt, 50%.

Despite the successfulness of this sequence, commercial samples of CPP **2** are relatively expensive, currently on the order of €400 / gram, precluding large-scale synthesis *via* this route. A search through literature shows that, ever since the first extraction of **2** by Kruber from anthracene oil in 1934,[49] much effort has been put into its synthesis, all starting from different parent PAH structures (SI Scheme S2.1).[40,50-57] Unfortunately, all of these are either lengthy, poor yielding, or require the use of hazardous chemicals, making them unamendable for large-scale synthesis.[50-52] A more efficient synthesis route was therefore desired to obtain oxoCPP **3**. This was found possible using a two-step procedure starting from pyrene **5** yielding the desired **4** in 15% overall yield (Scheme 2.3).

*Synthesis of oxoCPP **3***. The first step in the synthesis of oxoCPP **3** was the oxidation of pyrene **5** to the 4,5-dione **6** using a $NaIO_4/RuCl_3$ system. The oxidation of pyrene using this system has been reported several times, including a detailed description of the procedure on a 15 gram scale by Walsh *et al.*[58] One of the drawbacks associated with this reaction is the formation of an intractable residue which is difficult to filter off, seriously hampering the work-up. It was found, however, that by careful addition of the $NaIO_4$ oxidant as an aqueous solution, rather than as a solid, to a solution of **5** and $RuCl_3$ in DCM:THF, and stopping the addition when heating up of the reaction becomes noticeable by touch, a much finer residue is obtained. This residue can then be filtered off using a standard glass fritted filter, significantly expediting the work-up procedure, without negatively affecting the yield (~50%). The product can be purified by column chromatography over silica gel using neat DCM as eluent, which can be recovered and reused to reduce the total amount of solvent needed (Scheme 2.4 and Fig. 2.3A). The next crucial step in the synthesis is then the direct conversion of **6** to mono-ketone **3**.



Scheme 2.3 Synthesis of oxoCPP. *Reagents and conditions*: a) $NaIO_4$, $RuCl_3$, DCM:MeCN:H_2O, rt, 3 hrs (50%); b) PbO, 245 - 260°C, vac., 3 hrs., 4 - 8%; c) 1M NaOH, reflux, 3 d., 30%.

This conversion was initially tried by pyrolysis of **6** at 245 – 260 °C in an evacuated tube in the presence of lead(II) oxide (Scheme 2.3), a procedure described in 1949 by James W. Cook.[59] This resulted in the fractional sublimation of starting material and the desired product as a yellow crystalline sublimate (Fig. 2.2). The latter could, however, only be obtained in poor yields (2 – 8%). When performed on a larger scale, trace amounts of phenanthrene-4,5-lactone **7** were also obtained, whose identity was confirmed by comparison with an authentic sample, prepared by a classic Baeyer–Villiger oxidation of oxoCPP (See Experimental). It was attempted to extant the lead(II) oxide pyrolysis to other substrates, but this ultimately proved unsuccessful (Scheme S2.3). As a final attempt, the benzilic acid rearrangement of **6** was tried, as originally described by the aforementioned Anschütz and Japp in 1878 (Scheme 2.3).[60] Boiling of a suspension of **6** in an aqueous 1M NaOH solution for three days yielded the desired compound **4** in 30% yield as a bright yellow sublimate on the walls of the reaction flask, as well as in the air-cooled condenser fitted to it (Fig. 2.3B and 2.3C). Boiling for a longer period of time did not produce any more material, nor did use of a more concentrated (10M) NaOH solution (10% yield).

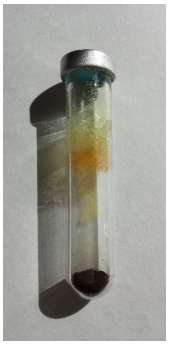


Figure 2.2 Vacuum tube showing fractional sublimation of **3** (yellow) and **6** (orange).

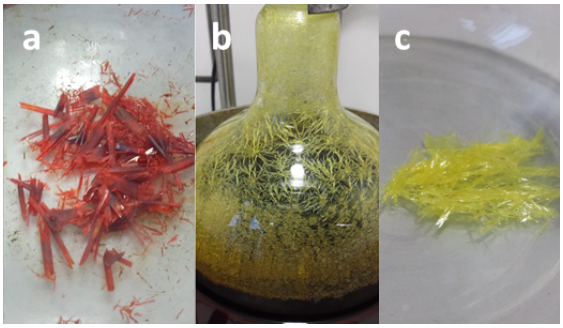
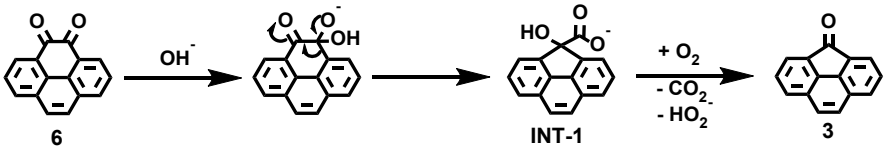


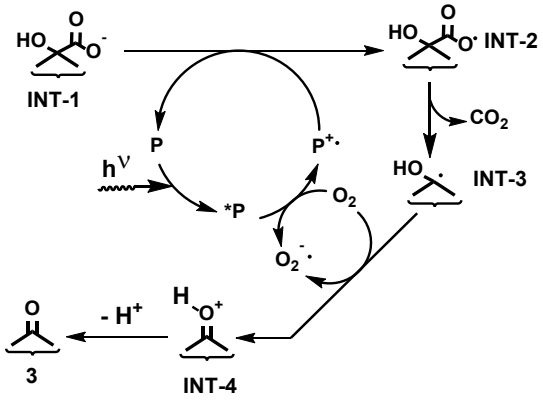
Figure 2.3 Images of the different compounds. a) Crystals of pyrene-4,5-dione **6**; b) deposition of oxoCPP **3** on the wall of a flask; c) recovered, sublimated product **3**.

*Mechanism for the **6** → **3** conversion.* The reaction scheme and proposed mechanism for the conversion of **6** to **3** are given in Scheme 2.4. The reaction starts with the formation of a hydrate, which undergoes a benzilic acid rearrangement to yield an α-hydroxycarboxylic acid intermediate (**INT-1**). This intermediate then undergoes oxidative decarboxylation by oxygen from the air to form **3**. The requirement of oxygen for this conversion was supported by the fact that no product formation was observed when the reaction was performed under an inert atmosphere. In addition, when the reaction was performed in the dark, no product could be isolated. As no dedicated light source was used, it was suspected that the known photo-sensitizability of phenanthrene played a role in this reaction.[61,62] Indeed, examples of self-sensitization of phenanthrene derivatives are known in literature.[63] Based on literary precedent regarding the oxidative decarboxylation of α-hydroxycarboxylates,[64-71] the reaction is presumed to proceed as shown in Scheme 2.4. In short, the reaction is initiated by excitation of molecules containing a phenanthrene moiety **P** (*i.e.* **6** or **3**). The excited species ***P** then undergoes a single electron transfer (SET) to aerial oxygen to produce a superoxide radical and a radical cationic phenanthrene species $\mathbf{P}^{+\cdot}$. The cationic species reacts with carboxylate (**INT-1**) to yield a carboxyl anion radical intermediate (**INT-2**), which is accompanied by re-formation of the ground state phenanthrene species **P**. The radical intermediate (**INT-2**) decomposes with hemolytic C–C bond cleavage, resulting in the formation of CO_2 and a secondary alcohol radical (**INT-3**). Another SET with aerial oxygen generates protonated carbonyl (**INT-4**) and another radical proton. Finally, proton abstraction from **INT-4** gives the ketone product **3**. The superoxide radicals are expected to be quenched in the form of hydrogen peroxide anion. As substituted glycolic acids, like the one supposed to be formed here, are known to be attacked by hydrogen peroxide only slowly, its role is suspected by be insignificant under the present reaction conditions.[72] Moreover, despite exhaustive testing, direct treatment of **6** with different peroxides and superoxides, in different solvents and under various reaction conditions, did not provide any identifiable products. Lastly, addition of $KMnO_4$ as oxidizing agent also did not increase the yield of **3**.

Reaction scheme



Proposed mechanism



Scheme 2.4 Reaction scheme and proposed mechanism for the *in situ* formation and oxidative decarboxylation of benzylic acids.

Custom reaction vessel. To facilitate the easy recovery of the sublimated oxoCPP product, a custom reaction vessel was designed (Fig. 2.4). The vessel consists of a 1 L Duran glass beaker with a flat flange (DN120) fitted with an O-ring, and a raised, flat flange lid with a single ground joint neck, which are affixed using a stainless-steel quick release clamp. The neck is fitted with a glass tube (l = 15 cm) which serves as both a condensing and sublimation tube. After the reaction, the lid is removed and the product washed out with DCM. Simple drying and evaporation of the solvent then provides the pure product, eliminating the need for further purification.

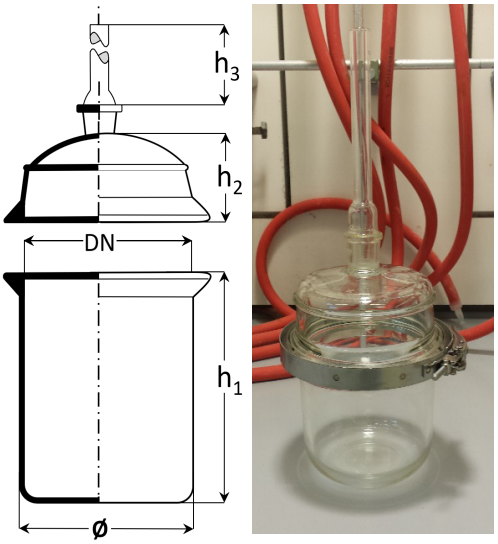
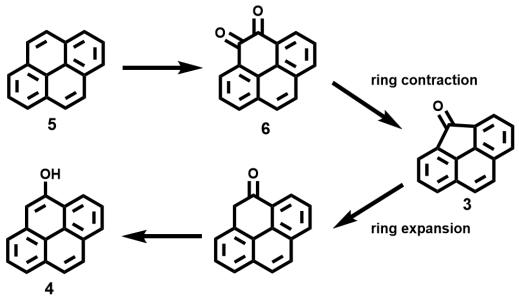


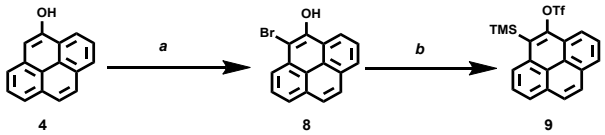
Figure 2.4 Custom reaction vessel for the facile recovery of sublimated material. DN 120, ø = 13 cm, h_1 = 12½ cm, h_2 = 7½ cm, h_3 = 15 cm.

It is interesting to note here that by performing a consecutive ring contraction and ring expansion reaction, a formal reduction of only one of the ketones in pyrene-4,5-dione **6** is achieved, as well as the formal installation of a hydroxide on the C-4 position of pyrene **5** (Scheme 2.5). In addition, with an efficient and economical route to **3** in hand, direct reduction also provided an expedient route to CPP **2** (Scheme S2.2), a valuable precursor in itself.



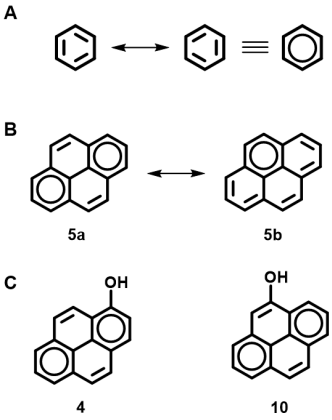
Scheme 2.5 Schematic representation of the conversion of pyrene to 4-hydroxypyrene, illustrating how consecutive ring contraction and ring expansion result in the selective reduction of a single ketone.

Precursor synthesis. With 4-hydroxypyrene **4** in hand, the next step was to selectively *ortho*-brominate it (Scheme 2.6). Bromination, however, proved cumbersome, with overbromination taking place when using most common bromination reagents. This observation was attributed to the enolic character of the hydroxyl group on the C-4 position (See Scheme 2.2 for numbering), which is related to the Clar sextet rule.



Scheme 2.6 Synthesis of propellerene **1** from 4-hydroxypyrene 4. *Reagents and conditions*: a) Br_2, CS_2, -10˚C, 94%; b) i) HMDS, PhMe, reflux, 3 hrs; ii) *n*-BuLi, THF, -78˚C; iii) Tf_2O, -78˚C, 47% over three steps.

Like explained in the introduction, the π electrons in an aromatic system are delocalized, *i.e*. an aromatic ring is said to have more than one resonance structure (Scheme 2.7A). With polycyclic aromatic system, several resonance structures can be drawn in which different rings have localized and delocalized electrons, illustrated for pyrene **5** in Scheme 2.7B. The Clar sextet rule states that: the resonance structure of a polycyclic aromatic system that possesses the greatest number of isolated 6-π electron systems contributes most to the observed chemistry of the overall system.[73] Thus, when both 4-hydroxypyrene **4** and 1-hydroxypyrene **10** are drawn with their Clar sextets it is apparent that in the case of 1-hydroxypyrene **10** the hydroxyl group is attached to a ring which bears a Clar sextet, whereas in the case of 4-hydroxypyrene it is not (Scheme 2.7C). The importance of this seemingly minor difference can be illustrated experimentally using NMR spectroscopy. Thus, when both 1-hydroxy and 4-hydroxypyrene are dissolved in acetone-d_6 in the presence of a small amount of acid, the ^{1}H signal corresponding to the C-5 proton in 4-hydroxypyrene 4 is observed to disappear rapidly ($t_{½}$ ≈ 1 min.). The corresponding C-2 proton in 1-hydroxypyrene **10**, however, showed no exchange even after standing at room temperature for 48 hours (Fig. 2.5A).



Scheme 2.7 Explanation of the Clar sextet rule. (A) The two resonance structures of benzene, with the π-electrons at different locations. The equivalent structure is drawn with a Clar sextet notation. (B) The two resonance structures of pyrene **5**, drawn with Clar sextets. The Clar sextet rule predicts structure **5a**, having two isolated π-sextets, to dominate the observed chemistry of **5**. (C) The structures of 4-hydroxypyrene 5 and 1-hydroxypyrene 12 drawn in their most favorable Clar structure. It is apparent that in **4** the hydroxyl functionality is on a localized π-bond, whereas in **10** it is on an Clar sextet, explaining the lesser reactivity of the latter.

Nonetheless, both compounds show phenolic character, demonstrated by a negative linear relationship between the resonance frequency of the hydroxyl proton and temperature (Fig. 2.5B). Temperature coefficients of -0.04 and -0.01 ppm K^{-1} for 4-hydroxypyrene **4** and 1-hydroxypyrene **10** respectively are typical values for phenols in polar solvents.

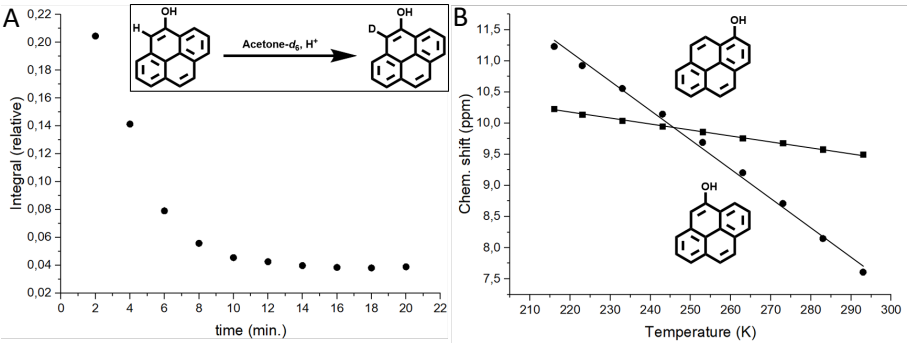
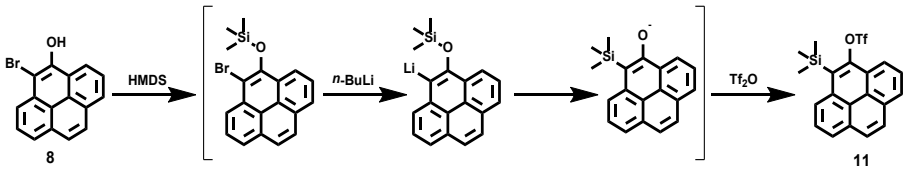


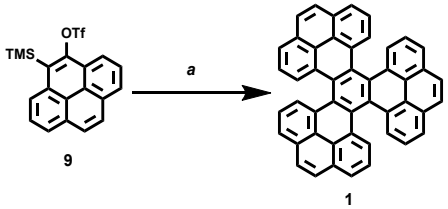
Figure 2.5 (A) Deuteration of 4-hydroxypyrene **4** over time as represented by a decrease of the relative intensity of the ^{1}H resonance corresponding to the C-5 proton (0.55 M in Ace-d_6, approx. 3 eq. of HCl added as a 4.0 M solution in dry dioxane). (B) ^{1}H chemical shift of the hetero-proton on 1-hydroxypyrene **10** (■) and 4-hydroxypyrene **4** (●) at different temperatures (0.55 M in $CDCl_3$). All spectra recorded at a frequency of 500 MHz.

Bromination of **4** was ultimately found possible using elemental bromine in CS_2 at –10°C, given the *ortho*-brominated product **8** in 94% yield. A three-step-one-pot procedure involving *ortho*-lithiation, retro-Brook rearrangement and quenching of the resultant phenolate with triflic anhydride then afford *ortho*-TMS triflate **9** in an overall yield of 47% (Scheme 2.8).



Scheme 2.8 Three-step-one-pot reaction for the conversion of *ortho*-bromophenol **7** to *ortho*-TMS triflate **8.**

Treatment of **9** with CsF in the presence of a palladium(0) catalyst affords tripyrenylene **1**, as a bright yellow solid in 47% yield (Scheme 2.9).



Scheme 2.9 Synthesis of tripyrenylene **1.** *Reagents and conditions*: a) CsF, $Pd_2(dba)_3$, MeCN:Et_2O, rt, o/n, 47%.

To conclude, this Chapter described the optimized synthesis of tripyrenylene from pyrene in six steps with an overall yield of 1.6%. The Chapter started by describing the economical, gram scale synthesis of oxoCPP in two steps from pyrene. By using a single solvent in the chromatography step, the total amount of solvent required was reduced. In addition, by designing a custom reaction vessel, analytically pure product could be obtained, circumventing the need for additional purification. A mechanism was proposed to explain the direct conversion of pyrene-4,5-dione to oxoCPP. The oxoCPP was converted to 4-hydroxypyrene in a ring-expansion reaction, allowing installation of an hydroxyl functionality on an otherwise difficult to access position. From the 4-hydroxypyrene, tripyrenylene could be successfully synthesized, by the merger of three pyrene moieties into a single molecule in one step. The aforementioned oxoCPP was also used to make CPP on a gram-scale in a single reduction step, constituting an improvement over known procedures.

The methodology outlined here, being: i) a consecutive ring-contraction/ring-opening of a vicinal dione, ii) conversion of the resultant phenol to an *ortho*-TMS triflate, and iii) a palladium catalyzed trimerization therewith, constitutes a generally applicable sequence to obtain large PAHs with trifold symmetry on a useful scale. The conformational behavior, physicochemical and spectroscopic properties of tripyrenylene **1** will now be studied in depth in the following Chapter.

References

(1) Hasan, M.; Borovkov, V. Helicene-based chiral auxiliaries and chirogenesis. *Symmetry* **2018,** *10* (1), 10.

(2) Hembury, G. A.; Borovkov, V. V.; Inoue, Y. Chirality-sensing supramolecular systems. *Chem. Rev.* **2008,** *108* (1), 1.

(3) Yang, Y.; Da Costa, R. C.; Fuchter, M. J.; Campbell, A. J. Circularly polarized light detection by a chiral organic semiconductor transistor. *Nat. Photonics* **2013,** *7* (8), 634.

(4) Yamamoto, K.; Shimizu, T.; Igawa, K.; Tomooka, K.; Hirai, G.; Suemune, H.; Usui, K. Rational design and synthesis of [5]helicene-derived phosphine ligands and their application in Pd-catalyzed asymmetric reactions. *Sci. Rep.* **2016,** *6* (1), 1.

(5) Aillard, P.; Voituriez, A.; Marinetti, A. Helicene-like chiral auxiliaries in asymmetric catalysis. *Dalton T.* **2014,** *43* (41), 15263.

(6) Stetsovych, O.; Švec, M.; Vacek, J.; Chocholoušová, J. V.; Jančařík, A.; Rybáček, J.; Kosmider, K.; Stará, I. G.; Jelínek, P.; Starý, I. From helical to planar chirality by on-surface chemistry. *Nat. Chem.* **2017,** *9* (3), 213.

(7) Isla, H.; Crassous, J. Helicene-based chiroptical switches. *Compt. Rend. Chim.* **2016,** *19* (1-2), 39.

(8) Bosson, J.; Gouin, J.; Lacour, J. Cationic triangulenes and helicenes: synthesis, chemical stability, optical properties and extended applications of these unusual dyes. *Chem. Soc. Rev.* **2014,** *43* (8), 2824.

(9) Buchta, M.; Rybáček, J.; Jančařík, A.; Kudale, A. A.; Buděšínský, M.; Chocholoušová, J. V.; Vacek, J.; Bednárová, L.; Císařová, I.; Bodwell, G. J. Chimerical pyrene-based [7]helicenes as twisted polycondensed aromatics. *Chem. Eur. J.* **2015,** *21* (24), 8910.

(10) Nakakuki, Y.; Hirose, T.; Sotome, H.; Miyasaka, H.; Matsuda, K. Hexa-peri-hexabenzo [7]helicene: Homogeneously π-extended helicene as a primary substructure of helically twisted chiral graphenes. *J. Am. Chem. Soc.* **2018,** *140* (12), 4317.

(11) Evans, P. J.; Ouyang, J.; Favereau, L.; Crassous, J.; Fernández, I.; Perles, J.; Martín, N. Synthesis of a helical bilayer nanographene. *Angew. Chem. Int. Ed.* **2018,** *57* (23), 6774.

(12) Cruz, C. M.; Castro-Fernández, S.; Maçôas, E.; Cuerva, J. M.; Campaña, A. G. Undecabenzo [7]superhelicene: a helical nanographene ribbon as a circularly polarized luminescence emitter. *Angew. Chem. Int. Ed.* **2018,** *57* (45), 14782.

(13) Hu, Y.; Paternò, G. M.; Wang, X.-Y.; Wang, X.-C.; Guizzardi, M.; Chen, Q.; Schollmeyer, D.; Cao, X.-Y.; Cerullo, G.; Scotognella, F. π-Extended pyrene-fused double [7]carbohelicene as a chiral polycyclic aromatic hydrocarbon. *J. Am. Chem. Soc.* **2019,** *141* (32), 12797.

(14) Chen, F.; Tanaka, T.; Hong, Y. S.; Mori, T.; Kim, D.; Osuka, A. Closed pentaaza [9]helicene and hexathia [9]/[5]helicene: Oxidative fusion reactions of ortho-phenylene-bridged cyclic hexapyrroles and hexathiophenes. *Angew. Chem.* **2017,** *129* (46), 14880.

(15) Hashimoto, S.; Nakatsuka, S.; Nakamura, M.; Hatakeyama, T. Construction of a highly distorted benzene ring in a double helicene. *Angew. Chem. Int. Ed.* **2014,** *53* (51), 14074.

(16) Sakamaki, D.; Kumano, D.; Yashima, E.; Seki, S. A facile and versatile approach to double N-heterohelicenes: Tandem oxidative C-N couplings of N-heteroacenes via cruciform dimers. *Angew. Chem.* **2015,** *127* (18), 5494.

(17) Ferreira, M.; Naulet, G.; Gallardo, H.; Dechambenoit, P.; Bock, H.; Durola, F. A naphtho-fused double [7]helicene from a maleate-bridged chrysene trimer. *Angew. Chem. Int. Ed.* **2017,** *56* (12), 3379.

(18) Tanaka, H.; Ikenosako, M.; Kato, Y.; Fujiki, M.; Inoue, Y.; Mori, T. Symmetry-based rational design for boosting chiroptical responses. *Commun. Chem.* **2018,** *1* (1), 1.

(19) Liu, X.; Yu, P.; Xu, L.; Yang, J.; Shi, J.; Wang, Z.; Cheng, Y.; Wang, H. Synthesis for the mesomer and racemate of thiophene-based double helicene under irradiation. *J. Org. Chem.* **2013,** *78* (12), 6316.

(20) Wang, X.-Y.; Wang, X.-C.; Narita, A.; Wagner, M.; Cao, X.-Y.; Feng, X.; Müllen, K. Synthesis, structure, and chiroptical properties of a double [7]heterohelicene. *J. Am. Chem. Soc.* **2016,** *138* (39), 12783.
(21) Katayama, T.; Nakatsuka, S.; Hirai, H.; Yasuda, N.; Kumar, J.; Kawai, T.; Hatakeyama, T. Two-step synthesis of boron-fused double helicenes. *J. Am. Chem. Soc.* **2016,** *138* (16), 5210.
(22) Hosokawa, T.; Takahashi, Y.; Matsushima, T.; Watanabe, S.; Kikkawa, S.; Azumaya, I.; Tsurusaki, A.; Kamikawa, K. Synthesis, structures, and properties of hexapole helicenes: assembling six [5]helicene substructures into highly twisted aromatic systems. *J. Am. Chem. Soc.* **2017,** *139* (51), 18512.
(23) Berezhnaia, V.; Roy, M.; Vanthuyne, N.; Villa, M.; Naubron, J.-V. r.; Rodriguez, J.; Coquerel, Y.; Gingras, M. Chiral nanographene propeller embedding six enantiomerically stable [5]helicene units. *J. Am. Chem. Soc.* **2017,** *139* (51), 18508.
(24) Fujikawa, T.; Segawa, Y.; Itami, K. Synthesis and structural features of quadruple helicenes: highly distorted π systems enabled by accumulation of helical repulsions. *J. Am. Chem. Soc.* **2016,** *138* (10), 3587.
(25) Tanaka, H.; Kato, Y.; Fujiki, M.; Inoue, Y.; Mori, T. Combined experimental and theoretical study on circular dichroism and circularly polarized luminescence of configurationally robust D_3-symmetric triple pentahelicene. *J. Phys. Chem. A* **2018,** *122* (37), 7378.
(26) Griffiths, J. *Colour and constitution of organic molecules*; Academic press, **1976**.
(27) Fabian, J.; Hartmann, H. *Light absorption of organic colorants: theoretical treatment and empirical rules*; Springer Science & Business Media, **2013**.
(28) Nishimoto, K. A MO theoretical study of organic dyes I. Effect of chemical softness on the electronic spectra. *Bull. Chem. Soc. Jap.* **1993,** *66* (7), 1876.
(29) Woodward, R. B. Structure and the absorption spectra of α,ß-unsaturated ketones. *J. Am. Chem. Soc.* **1941,** *63* (4), 1123.
(30) Fieser, L. F.; Fieser, M.; Rajagopalan, S. Absorption spectroscopy and the structures of the diosterols. *J. Org. Chem.* **1948,** *13* (6), 800.
(31) Rulíšek, L.; Exner, O.; Cwiklik, L.; Jungwirth, P.; Starý, I.; Pospíšil, L.; Havlas, Z. On the convergence of the physicochemical properties of [n]helicenes. *J. Phys. Chem. C* **2007,** *111* (41), 14948.
(32) Nakai, Y.; Mori, T.; Inoue, Y. Theoretical and experimental studies on circular dichroism of carbo [n] helicenes. *J. Phys. Chem. A* **2012,** *116* (27), 7372.
(33) Mori, T. Chiroptical properties of symmetric double, triple, and multiple helicenes. *Chem. Rev.* **2021,** *121* (4), 2373.
(34) Pozo, I.; Guitián, E.; Pérez, D.; Peña, D. Synthesis of nanographenes, starphenes, and sterically congested polyarenes by aryne cyclotrimerization. *Acc. Chem. Res.* **2019**.
(35) Guitián, E.; Pérez, D.; Peña, D. In *Palladium in Organic Synthesis*; Springer, 2005.
(36) Rodenburg, L.; Brandsma, R.; Tintel, C.; Van Thuijl, J.; Lugtenburg, J.; Cornelisse, J. Synthesis and properties of nitro derivatives of 2-tert-butyl-and 2,7-di-tert-butylpyrene. *Recl. Trav. Chim. Pays-Bas* **1986,** *105* (5), 156.
(37) Peake, D. A.; Oyler, A. R.; Heikkila, K. E.; Liukkonen, R. J.; Engroff, E. C.; Carlson, R. M. Alkyl aromatic synthesis: Nucleophilic alkyl lithium addition. *Synth. Comm.* **1983,** *13* (1), 21.
(38) Mochida, K.; Kawasumi, K.; Segawa, Y.; Itami, K. Direct arylation of polycyclic aromatic hydrocarbons through palladium catalysis. *J. Am. Chem. Soc.* **2011,** *133* (28), 10716.
(39) Odani, R.; Hirano, K.; Satoh, T.; Miura, M. Copper-mediated dehydrogenative biaryl coupling of naphthylamines and 1, 3-azoles. *J. Org. Chem.* **2013,** *78* (21), 11045.
(40) Vollmann, H.; Becker, H.; Corell, M.; Streeck, H. Beiträge zur Kenntnis des Pyrens und seiner Derivate. *Liebigs Ann. Chem.* **1937,** *531* (1), 1.
(41) Sun, W.; Tang, X.; Li, J.; He, M.; Zhang, R.; Han, X. e.; Zhao, Y.; Ni, Z. A novel 4-hydroxypyrene-based "off–on" fluorescent probe with large Stokes shift for detecting cysteine and its application in living cells. *Tet. Lett.* **2020,** *61* (6), 151467.
(42) Newman, M. S. Syntheses in the pyrene field. *J. Org. Chem.* **1951,** *16* (6), 860.

(43) Okamoto, T.; Shudo, K.; Miyata, N.; Kitahara, Y.; Nagata, S. Reactions of K-region oxides of carcinogenic and non-carcinogenic aromatic hydrocarbonds - Comparative studies on reactions with nucleophiles and acid-catalyzed reactions. *Chem. Pharm. Bull.* **1978,** *26* (7), 2014.
(44) Nashed, N. T.; Bax, A.; Loncharich, R. J.; Sayer, J. M.; Jerina, D. M. Methanolysis of K-region arene oxides - Comparison between acid-catalyzed and methodide ion addition-reactions. *J. Am. Chem. Soc.* **1993,** *115* (5), 1711.
(45) Vanduuren, B. L.; Witz, G.; Agarwal, S. C. Synthesis and photorearrangement of 4,5-epoxy-4,5-dihydropyrene. *J. Org. Chem.* **1974,** *39* (8), 1032.
(46) Barton, D. H. R.; Sammes, P. G.; Weingarten, G. G.. Photochemical transformations .29. Steric compression effects in synthesis and reaction of 4-amino-5-methylphenanthrene. *J. Chem. Soc. C* **1971**, (4), 729.
(47) Aoyama, T.; Shioiri, T. New Methods and Reagents in Organic Synthesis. 17. Trimethylsilydiazomethane (TMSCHN2) as a Stable and Safe Substitute for Hazardous Diazomethane. Its Application to the Arndt-Eistert Synthesis. *Chem. Pharm. Bull.* **1981,** *29* (11), 3249.
(48) Harvey, R. G.; Abu-Shqara, E.; Yang, C. X. Synthesis of ketone and alcohol derivatives of methylene-bridged polyarenes, potentially new classes of active metabolites of carcinogenic hydrocarbons. *J. Org. Chem.* **1992,** *57* (23), 6313.
(49) Kruber, O. Über neue Kohlenwasserstoffe aus dem Anthracenöl des Steinkohlenteers. *Chem. Ber.* **1934,** *67* (6), 1000.
(50) Yang, C. X.; Harvey, R. G. Synthesis of 4 H-Cyclopenta[def]phenanthrene. *Polycycl. Arom. Comp.* **1992,** *2* (4), 229.
(51) Minabe, M.; Yoshida, M.; Takayanagi, T. A facile synthesis of 4*H*-cyclopenta[def]phenanthrene. *Bull. Chem. Soc. Jap.* **1988,** *61* (3), 995.
(52) Minaba, M.; Suzuki, K. 4*H*-Cyclopenta[def]phenanthrene. *J. Synth. Org. Chem. Jap.* **1986,** *44* (5), 421.
(53) Kazuo, S. *Technol. Repts. Tohoku Univ.* **1954,** *19*, 63.
(54) Suzuki, K.; Kajigaeshi, S.; Kato, S. Studies on fluorene derivatives .X. Studies on 4, 4', 4"-tribromotribiphenylenepropane and 4'-bromotribiphenylenepropane. *J. Synth. Org. Chem. Jap.* **1958,** *16* (6), 304.
(55) Graebe, C.; Aubin, C. Ueber Diphensäureanhydrid und über o-Diphenylenketoncarbonsäure. *Liebigs Ann. Chem.* **1888,** *247* (3), 257.
(56) Kim, J.; Jin, Y.; Song, S.; Kim, I.; Suh, H. Synthesis of 4H-Cyclopenta[def]phenanthrene from 1-naphthylacetic Acid. *Chem. Lett.* **2009,** *38* (10), 1008.
(57) Medenwald, H. Synthese des 1-Aza-pyrens und des Phenanthrylen-(4.5)-methans. *Chem. Ber.* **1953,** *86* (2), 287.
(58) Walsh, J. C.; Williams, K. L. M.; Lungerich, D.; Bodwell, G. J. Synthesis of Pyrene-4, 5-dione on a 15 g Scale. *Eur. J. Org. Chem.* **2016,** *2016* (36), 5933.
(59) Cook, J. W.; Stephenson, E. F. M. 181. Polycyclic aromatic hydrocarbons. Part XXXIII. Synthesis of naphtho(1′: 2′-1: 2)fluorene and naphtho(2′:1′-2:3)fluorene. *J. Chem. Soc. (Resumed)* **1949**, 842.
(60) Anschütz, R.; Japp, F. R. Ueber die Oxydation des Phenanthrenchinons mittelst Kaliumpermanganat. *Ber. Dtsch. Chem. Ges.* **1878,** *11* (1), 211.
(61) Gijzeman, O. L. J.; Kaufman, F.; Porter, G. Oxygen quenching of aromatic triplet states in solution. Part 1. *J. Chem. Soc. Faraday Trans.* **1973,** *69*, 708.
(62) Horspool, W. M.; Lenci, F. *CRC Handbook of Organic Photochemistry and Photobiology, Volumes 1 & 2*; CRC press, 2003.
(63) Montanaro, S.; Lhiaubet-Vallet, V.; Iesce, M.; Previtera, L.; Miranda, M. A. A mechanistic study on the phototoxicity of atorvastatin: singlet oxygen generation by a phenanthrene-like photoproduct. *Chem. Res. Tox.* **2009,** *22* (1), 173.
(64) Pink, J. M. O., University of British Columbia, **1969**.
(65) He, S.; Chen, X.; Zeng, F.; Lu, P.; Peng, Y.; Qu, L.; Yu, B. Visible-light-promoted oxidative decarboxylation of arylacetic acids in air: Metal-free synthesis of aldehydes and ketones at room temperature. *Chin. Chem. Lett.* **2020,** *31* (7), 1863.

(66) Nakayama, H.; Itoh, A. Aerobic photo-decarboxylation of α-hydroxy carboxylic acid derivatives under visible light irradiation in the presence of catalytic iodine. *Tet. Lett.* **2008,** *49* (17), 2792.
(67) Lemmetyinen, H.; Koskikallio, J.; Lindblad, M.; Kuzmin, M. G. A mechanism involving two photoinduced transients for the photocyanation of phenanthrene in the presence of oxygen and potassium cyanide-18-crown—6 ether in anhydrous acetonitrile. *Acta Chem. Scand. A* **1982,** *36* (5).
(68) Lemmetyinen, H. J. Kinetic analysis of aromatic photocyanation: naphthalene, biphenyl, and phenanthrene. *J. Chem. Soc. Perkin T. 2* **1983,** (8), 1269.
(69) Bhattacherjee, A.; Sneha, M.; Lewis-Borrell, L.; Tau, O.; Clark, I. P.; Orr-Ewing, A. J. Picosecond to millisecond tracking of a photocatalytic decarboxylation reaction provides direct mechanistic insights. *Nat. Comm.* **2019,** *10* (1), 1.
(70) Joshi, P. C.; Pathak, M. A. The role of active oxygen ($^1O_2$ and $O^{\cdot 2-}$) induced by crude coal tar and its ingredients used in photochemotheraphy of skin diseases. *J. Invest. Dermat.* **1984,** *82* (1).
(71) Rahman, M.; Mukherjee, A.; Kovalev, I. S.; Kopchuk, D. S.; Zyryanov, G. V.; Tsurkan, M. V.; Majee, A.; Ranu, B. C.; Charushin, V. N.; Chupakhin, O. N. Recent advances on diverse decarboxylative reactions of amino acids. *Adv. Synth. Cat.* **2019,** *361* (10), 2161.
(72) Witzemann, E. J. The oxidation of alpha-and beta-hydroxybutyric acids with hydrogen peroxide. *J. Am. Chem. Soc.* **1926,** *48* (1), 211.
(73) Clar, E. Aromatic sextet. **1972**.
(74) Kim, J.; Park, S. H.; Cho, S.; Jin, Y.; Kim, J.; Kim, I.; Lee, J. S.; Kim, J. H.; Woo, H. Y.; Lee, K. Low-bandgap poly (4H-cyclopenta[def]phenanthrene) derivatives with 4, 7-dithienyl-2, 1, 3-benzothiadiazole unit for photovoltaic cells. *Polymer* **2010,** *51* (2), 390.
(75) Jin, Y.; Kim, Y.; Kim, S. H.; Song, S.; Woo, H. Y.; Lee, K.; Suh, H. Novel green-light-emitting polymers based on cyclopenta[def]phenanthrene. *Macromol.* **2008,** *41* (15), 5548.
(76) Song, S.; Jin, Y.; Kim, S. H.; Kim, J. H.; Lee, K.; Suh, H. Synthesis and characterization of novel conjugated polymer with 4H-cyclopenta[def]phenanthrene and the sulfanyl group. *Polym. J.* **2009,** *41* (2), 138.
(77) Kim, J.; Park, S. H.; Kim, J.; Cho, S.; Kim, I.; Lee, K.; Suh, H. Syntheses and characterization of new low-band gap polymers containing 4H-cyclopenta[def]phenanthrene unit and 4,7-di(thien-2-yl)-2*H*-benzimidazole-2-spirocyclohexane for photovoltaic device. *Synth. Met.* **2011,** *161* (13-14), 1336.
(78) Shin, Y. R.; Lee, W. H.; Park, J. B.; Kim, J. H.; Lee, S. K.; Shin, W. S.; Hwang, D. H.; Kang, I. N. Synthesis and characterization of new low band-gap polymers containing electron-accepting acenaphtho [1,2-c]thiophene-S,S-dioxide groups. *J. Polym. Sci. Pol. Chem.* **2016,** *54* (4), 498.
(79) Liu, T.; Zhang, H.-X.; Xia, B.-H. Theoretical studies of the electronic structures and optical properties of stable blue-emitting polymer based on 4H-cyclopenta-[def]-phenanthrene. *Polymer* **2008,** *49* (8), 2077.
(80) Shinohara, A.; Pan, C.; Guo, Z.; Zhou, L.; Liu, Z.; Du, L.; Yan, Z.; Stadler, F.; Wang, L.; Nakanishi, T. Viscoelastic Conjugated Polymer Fluids. *Angew. Chem.* **2019**.
(81) Song, S.; Kim, C.; Park, S. H.; Kim, I.; Lee, K.; Jin, Y.; Suh, H. Synthesis and characterization of polycyclopentaphenanthrene with carbazole or oxidiazole pendant units. *Polym. J.* **2012,** *44* (4), 347.
(82) Song, S.; Jin, Y.; Kim, J.; Park, S. H.; Kim, S. H.; Lee, K.; Suh, H. A novel conjugated polymer based on cyclopenta[def]phenanthrene backbone with spiro group. *Polymer* **2008,** *49* (26), 5643.
(83) Song, S.; Jin, Y.; Kim, K.; Kim, S. H.; Shim, Y. B.; Lee, K.; Suh, H. Novel cyclopenta [def] phenanthrene based blue emitting oligomers for OLEDs. *Tet. Lett.* **2008,** *49* (22), 3582.
(84) Suh, H.; Jin, Y.; Park, S. H.; Kim, D.; Kim, J.; Kim, C.; Kim, J. Y.; Lee, K. Stabilized Blue Emission from Organic Light-Emitting Diodes Using Poly (2, 6-(4, 4-bis (2-ethylhexyl)-4*H*-cyclopenta[def]phenanthrene)). *Macromol.* **2005,** *38* (15), 6285.

(85) Kim, J.; Kim, S. H.; Kim, J.; Kim, I.; Jin, Y.; Kim, J. H.; Woo, H. Y.; Lee, K.; Suh, H. Di-aryl substituted poly (cyclopenta[def]phenanthrene) derivatives containing carbazole and triphenylamine units in the main chain for organic light-emitting diodes. *Macromol. Res.* **2011,** *19* (6), 589.

(86) Jin, Y.; Yoo, C.; Kim, K.; Song, S.; Kim, J.; Kim, J.; Suh, H. Novel efficient blue materials with 4*H*-cyclopenta[def]phenanthrene for OLEDs. *Synth. Met.* **2008,** *158* (10), 417.

(87) Jang, S. H.; Tai, T. B.; Park, J. H.; Jeong, H. J.; Chun, E. J.; Kim, Y.-H.; Lee, S.-G.; Singh, O. M.; Yoon, Y. J.; Kwon, S. K. Synthesis and characterization of highly conjugated cyclopenta [def] phenanthrene-based polymers. *Macromol. Res.* **2010,** *18* (2), 185.

(88) Ono, A.; Suzuki, N.; Kamimura, J. Hydrogenolysis of diaryl and aryl alkyl ketones and carbinols by sodium borohydride and anhydrous aluminum (III) chloride. *Synth.* **1987,** *1987* (8), 736.

(89) Gálová M. and Lux L., Aluminum halides in nonaqueous solvents. I. Basic polarographic characteristics. *Chem. Zvesti* **1975**, *29 (3)*, 279.

(90) Hu, J.; Zhang, D.; Harris, F. W. Ruthenium (III) chloride catalyzed oxidation of pyrene and 2, 7-disubstitued pyrenes: An efficient, one-step synthesis of pyrene-4,5-diones and pyrene-4, 5, 9, 10-tetraones. *J. Org. Chem.* **2005,** *70* (2), 707.

(91) Kestens, V.; Auclair, G.; Drozdzewska, K.; Held, A.; Roebben, G.; Linsinger, T. Thermodynamic property values of selected polycyclic aromatic hydrocarbons measured by differential scanning calorimetry. *J. Therm. Anal. Calorim.* **2010,** *99* (1), 245.

(92) Kimura, T.; Minabe, M.; Suzuki, K. Rearrangements and ring expansions of 4*H*-cyclopenta[def]phenanthrene derivatives. *J. Org. Chem.* **1978,** *43* (6), 1247.

(93) Baeyer, A. Mittheilungen aus dem chemischen Laboratorium der Akademie der Wissenschaften in München. *Ber. Dtsch. Chem. Ges.* **1877,** *10* (1), 123.

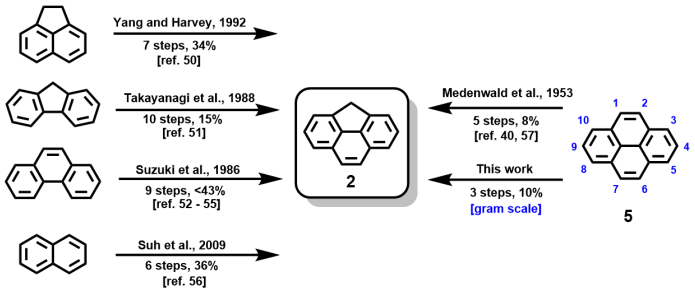
(94) Sieglitz, A.; Schidlo, W. Über Abkömmlinge des 4.5-Methylen-phenanthrens. *Chem. Ber.* **1963,** *96* (4), 1098.

(95) van den Braken—van Leersum, A. M.; Tintel, C.; Van't Zelfde, M.; Cornelisse, J.; Lugtenburg, J. Spectroscopic and photochemical properties of mononitropyrenes. *Recl. Trav. Chim. Pays-Bas* **1987,** *106* (4), 120.

(96) Ott, R.; Zinke, A. Zur Kenntnis des Coronens. *Monatsh. Chem. Verw. Tl.* **1953,** *84* (6), 1132.

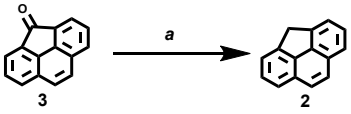
Supplementary results

Reduction of oxoCPP ***3***. The 4*H*-cyclopenta[*def*]phenanthrene (CPP) **2** motive holds interesting properties for the synthesis of photovoltaic[74] and electroluminescent polymers,[75-81] as well as for the production of organic light emitting diodes (OLEDs).[82-87] Interest in this motive stems from the low HOMO-LUMO gap of CPP **2**,[79] allowing its use in high frequency applications. Synthesis of these polymers usually starts from the parent CPP molecule **2**. As such many have attempted to synthesize it, with varying success (Scheme S2.1).[40,50-57] With a successful synthetic route in hand to access large amounts of oxoCPP, it became interesting to see whether it could be directly reduced to CPP **2**.



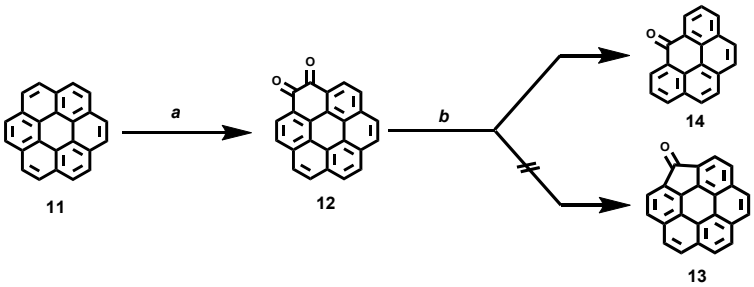
Scheme S2.1 Summary of the literature procedures for the synthesis of CPP and the procedure described in this Chapter for the synthesis of oxoCPP.

A procedure for the direct reduction of **3** to **2** *via* a Wolff-Kishner reaction could be found in literature, with a reported yield of 60%.[57] Given the hazardous nature of hydrazine, conversion was tried using $Al(BH_4)_3$ instead, generated *in situ* by adding a solution of $AlCl_3$ in anhydrous THF to a mixture of $NaBH_4$ and **3** (Scheme 2.8).[88] Gratifyingly, the reduced product could thus be obtained on a one gram scale, with a slightly increased yield of 65% (Scheme S2.2). After work-up, the product could be purified by a standard silica gel column using neat pentane as eluent. As with the purification of **6**, solvent used for the chromatography could be retrieved and reused, reducing the total amount of solvent needed. The yield of the product was found to be highly influenced by the purity of the solution of $AlCl_3$ in THF. When insufficiently dry reagents were used, brown colored solutions were obtained, which resulted in significantly lower yields of the desired product (10 – 30%).[89]



Scheme S2.2 The direct reduction of oxoCPP to CPP. *Reagents and conditions*: a) $NaBH_4$, $AlCl_3$, THF, -78°C → reflux, 3 d., 65%.

Lead(II) oxide mediated pyrolysis. In an attempt to expand the scope of the PbO mediated pyrolysis of germinal diones, coronen-1,2-dione **12** was subjected to the same conditions. Unexpectedly, instead of ring contracted product **13**, decomposed compound **14** was the only identifiable product obtained in low yield (1.9%; Scheme S2.3).

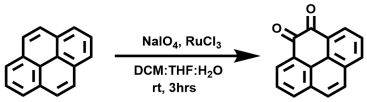


Scheme S2.3 PbO mediated pyrolysis of coronen-1,2-dione. *Reagents and conditions*: a) $Na_2Cr_2O_7$, $PhNO_2$:HOAc, 120°C, 1 hr, 76%; b) PbO, 265°C, vac., 3 hrs, 1.9%.

Experimental

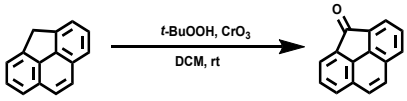
General. All reagents were obtained from commercial sources and were used as received. Solvents used were stored over 4 Å molecular sieves. Reactions were monitored by TLC analysis using Merck 25 DC plastikfolien 60 F254 with detection by using an aqueous solution of $KMnO_4$ (7%) and K_2CO_3 (2%) followed by charring at ~150 °C. Column chromatography was performed on Fluka silica gel (0.04–0.063 mm). High-resolution mass spectra were recorded by direct injection (2 µL of a 2 µM solution in water/acetonitrile; 50:50; v/v and 0.1% formic acid) on a mass spectrometer (Thermo Finnigan LTQ Orbitrap) equipped with an electrospray ion source in positive mode (source voltage 3.5 kV, sheath gas flow 10, capillary temperature 250 °C). The high-resolution mass spectrometer was calibrated prior to measurements with a calibration mixture (Thermo Finnigan). Melting points were recorded on a Stuart scientific SMP3 melting point apparatus and are uncorrected. All NMR experiments were performed on a Bruker AV500 NMR instrument equipped with a BBFO probe head for 5 mm outer diameter tubes. Spectra were recorded at 500 MHz for ^1H, 125 MHz for ^{13}C and 470 MHz for ^{19}F. All deuterated solvents were obtained from a commercial source (Eurisotope) and were used as received. Chemical shifts are given in ppm (δ) relative to TMS (0 ppm), and coupling constants (*J*) are given in Hertz (Hz).

Pyrene-4,5-dione (6)



A solution of $NaIO_4$ (28 g, 130 mmol) in H_2O (500 mL) was added dropwise to a vigorously stirred solution of pyrene (6 g, 30 mmol) and $RuCl_3 \cdot xH_2O$ (600 mg, 3.0 mmol) in DCM (250 mL) and THF (250mL). The addition took approximately 1 hr and was stopped whenever heating of the solution became noticeable by touch. The resultant dark brown suspension was stirred at room temperature for 3 hours and then poured into water (1 L) and the layers separated. The aqueous layer extracted twice with DCM (300 mL) and the organic layer washed twice with water (300 mL). The organic layer was dilute with DCM (400 mL) and filtered through a glass fritted funnel. The residue was rinsed twice with DCM (200 mL) and the combined organic layers were washed with brine (500 mL) and evaporated under reduced pressure to afford a brown-orange residue. The residue was eluted over a silica gel column using neat DCM (R_f = 0.5) as eluent to provide the dione as bright orange crystals. Yield: 3.5 g, 15 mmol, 50%. ^1H NMR (300 MHz, $CDCl_3$) δ 8.48 (dd, J = 7.4, 1.2 Hz, 1H), 8.17 (dd, J = 8.0, 1.2 Hz, 1H), 7.84 (s, 1H), 7.75 (t, J = 7.7 Hz, 1H). HRMS (ESI-TOF) m/z: calc'd for $C_{16}H_9O_2$ [M+H]+: 233.06025 found 233.05950. m.p. 300 °C (dec.), lit. 299 – 302 °C.[90]

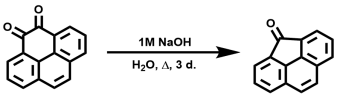
4*H*-cyclopenta[*def*]phenanthren-4-one (4)



4*H*-Cyclopenta[*def*]phenanthrene (500 mg, 2.63 mmol, 1.0 eq) was added to a solution of CrO_3 (13 mg, 0.13 mmol, 0.05 eq.) and aqueous tBuOOH (2.4 mL, 70%, 18.3 mmol, 6.9 eq) in DCM (30 mL). The reaction mixture stirred at room temperature for 3 hrs. The solution was then cooled to 0ºC and added dropwise to a vigorously stirred solution 10% aqueous $Na_2S_2O_5$ solution and stirred for 1 hour. The layers were then separated and the organic layer washed with brine, dried over Na_2SO_4 and evaporated on celite. The product was purified over a silica column using DCM:Pentane (1:3; R_f = 0.3) to provide the product as bright yellow needlesStarting material was also eluted in the first couple of fractions, which was recovered and used for another run of the reaction. Over a total of four cycles, a cumulative yield of 383 mg (1.86 mmol, 71%) of oxoCPP was obtained. ^1H NMR (500MHz, $CDCl_3$) δ 7.78 (d, *J* = 8.0 Hz, 2H), 7.69 (d, *J* = 7.0 Hz,

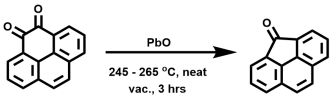
2H), 7.64 (s, 2H), 7.49 (t, *J* = 7.0 Hz, 2H). ^{13}C NMR (125MHz, $CDCl_3$) 193.62, 158.69, 138.95, 132.92, 130.68, 129.08, 127.21, 125.29, 122.35. HRMS (ESI-TOF) m/z: calc'd for $C_{15}H_9O$ [M+H]+: 205.06534 found 205.06473. m.p. 170 – 171 °C, lit. 170 °C.[91]

Benzilic Acid Rearrangement of Pyrene-4,5-dione



In a 2 L round bottom flask, fitted with a ground glass joint tube (l = 15 cm), a suspension of pyrene-4,5-dione (5 g, 21.5 mmol) in aqueous NaOH (1.0 M, 1 L) was refluxed for 3 days with vigorous stirring in contact with air. The flask was allowed to cool to room temperature and the product, which had sublimated as a yellow crystalline solid in the reflux condenser was washed out with DCM to provide an initial yield of 1 g (4.9 mmol, 23%). Material which had collected on the walls of the flask was washed down with DCM, separated from the aqueous reaction mixture, dried over $MgSO_4$, filtered and purified by elution over a silica gel column with 1:10 DCM:Pentane (R_f = 0.3) provided additional product (310 mg, 1.5 mmol, 7%).

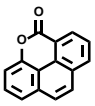
4*H*-cyclopenta[*def*]phenanthren-4-one via Pyrolysis of Pyrene-4,5-dione with PbO



A flame-dried vial charged with an intimate mixture of pyrene-4,5-dione (100 mg, 0.43 mmol) and yellow lead(II) oxide (1 g, 4.5 mmol, 10 eq.) in one portion. The vial was sealed with a shrink cap and evacuated. The vial was then heated on a metal block at 265 °C for 3 hours at which point all starting material had been consumed (as per TLC). After cooling to room temperature the vial was purged with N_2. The bright yellow crystalline sublimate was scraped off, and the residue washed with DCM (3x 10 mL) and filtered. Elution over a silica gel column with EtOAc:pentane (1:30; R_f = 0.5) gave the title compound as the only product. Yield: 7 mg, 0.17 mmol, 8.0%.

Leaving the reaction overnight did not increase the yield. When the reaction was performed on a larger scale (1 g, 4.3 mmol), trace amount of a slightly more polar compound was also obtained, which was putatively assigned as phenanthrene-1,10-lactone (5*H*-naphtho[8,1,2-*cde*]chromen-5-one) based on its ^1H and ^{13}C NMR spectra (Fig. S2.1). The identity was confirmed by comparison of the spectra with those obtained for an authentic sample which was made as follows: oxoCPP (132 mg, 0.65 mmol) was suspended in glacial acetic acid (6 mL) and concentrated sulfuric acid (1.5 mL) slowly added to it. Stirring was continued until all material had dissolved. Then, aqueous hydrogen peroxide (30%, 0.5mL) was added which caused the solution to take on a dark red color. The solution was stirred in contact with air for 10 min. at which point the dark red color had faded and stirring of the pale yellow solution continued for another 3 hours. The resultant suspension was filtered, and the residue taken up in chloroform (~10 mL) which was found to consist of a mixture of starting material and product (TLC, eluent 1:1 DCM:Pentane, R_f = 0.73). The filtrate was poured on ice (~100 mL) and extracted with chloroform (2x 50 mL). The combined organic layers were washed with sat. $NaHCO_3$ (50 mL), dried over Na_2SO_4 and evaporated to dryness. The residue thus obtained was nearly pure lactone. The combined residues were then purified by column chromatography over silica gel using DCM:Pentane (1:3 → 1:1) as eluent to provide the product as a white solid (66 mg, 0.30 mmol, 46%) together with recovery of starting material (19 mg, 0.09 mmol, 14%).

5*H*-naphtho[8,1,2-*cde*]chromen-5-one (7)



^{1}H NMR (300 MHz, Ace-d_6) δ 8.60 (dd, *J* = 7.8, 1.2Hz, 1H), 8.52 (dd, *J* = 7.8, 1.2Hz, 1H), 8.110 (s, 1H), 8.107 (s, 1H), 8.06 (t, *J* = 7.8Hz, 1H), 7.98 (dd, *J* = 7.8, 1.2Hz, 1H), 7.91 (t, *J* = 7.8Hz, 1H), 7.63 (dd, *J* = 7.8, 1.2Hz, 1H). ^{1}H NMR (500 MHz, $CDCl_3$) δ 8.54 (dd, *J* = 7.8, 1.2Hz, 1H), 8.21 (dd, *J* = 7.8, 1.2Hz, 1H), 7.85 (t, *J* = 7.8Hz, 1H), 7.82 (dd, *J* = 11.4, 4.7Hz, 2H), 7.75 (s, 1H), 7.74 (dd, *J* = 7.8, 1.2Hz, 1H), 7.52-7.49 (m, *J* = 7.8Hz, 1H). ^{13}C NMR (125 MHz, $CDCl_3$) δ 161.42, 150.42, 132.80, 131.26, 129.72, 128.71, 128.53, 127.63, 127.56, 127.10, 126.40, 122.63, 119.79, 113.98, 113.04. HRMS (ESI-TOF) m/z: calc'd for $C_{16}H_8O_2$ [M+H]+: 221.05971 found 221.05952. m.p. 194 – 195 °C, lit. 200.5 – 201.5 °C.[92]

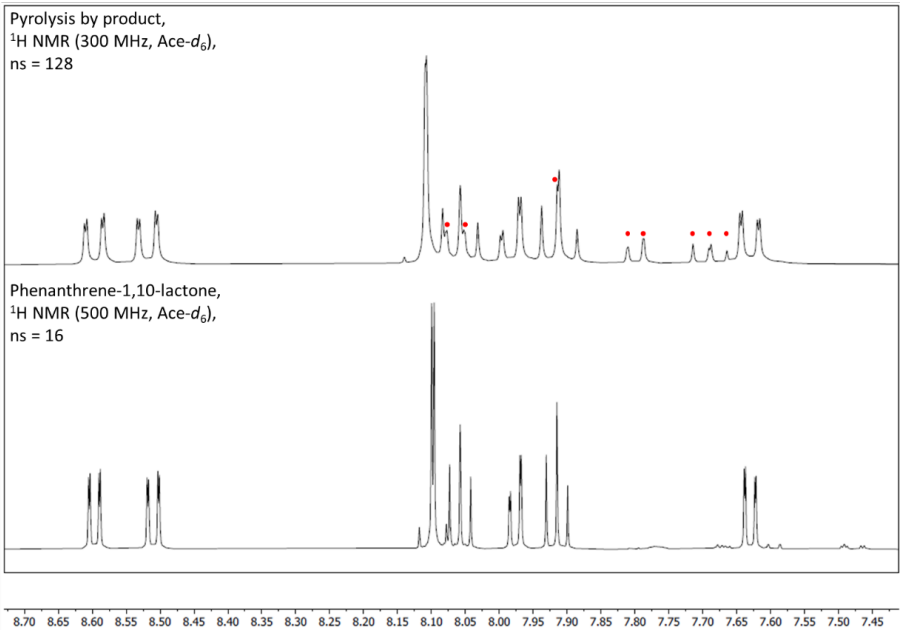
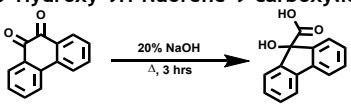


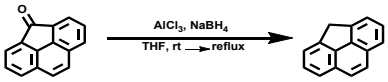
Figure S2.1 ^{1}H spectra of the product isolated in trace amount from the PbO pyrolysis of pyrene-4,5-dione (above) and that obtained for pure phenanthrene-1,10-lactone (below). Signals indicated with red dots in the upper spectrum correspond to residual pyrene-4,5-dione starting material.

9-Hydroxy-9H-fluorene-9-carboxylic acid (15)[93]



A suspension of phenanthrene-9,10-dione (0.96 g, 4.61 mmol) in aqueous NaOH (20% (2 g in 8 ml water), 48 mmol, 10 eq) was heated at 100°C for 3 hrs with vigorous stirring in contact with air. The dark suspension was diluted with an equal portion of water (10 ml), yielding a brown-green suspension. Careful neutralization with concentrated H_2SO_4 caused almost complete dissolution of the precipitate, at which point it was filtered while still warm. Further addition of H_2SO_4 yielded the glycolic acid as a pale yellow precipitate, which was filtered and dried in contact with air. Yield: 0.81 g, 3.60 mmol, 78.0%. ^{1}H NMR (500MHz, 1N NaOD in D_2O) δ 7.55 (dt, J = 7.50, 1.0Hz, 1H), 7.29 (dt, J = 7.50, 1.0Hz, 1H), 7.24 (td, J = 7.50, 1.0Hz, 1H), 7.15 (td, J = 7.50, 1.0Hz, 1H). ^{13}C NMR (125MHz, 1N NaOD in D_2O) δ 179.30, 147.72, 140.45, 129.13, 128.22, 123.20, 120.27, 84.26.

4*H*-Cyclopenta[*def*]phenanthrene (2)

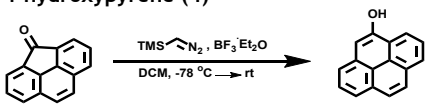


A 250 ml round bottom flask was flame dried under high vacuum, back-purged with argon and allowed to cool to room temperature. The flask was then charged with commercial, sublimated, anhydrous $AlCl_3$ (5g, mmol), cooled on an acetone/liquid nitrogen bath to -80 °C under dry nitrogen provided by a Schlenk line, and anhydrous THF* (75ml) added slowly. Minor gas formation was observed upon addition, which quickly cleared up. The flask was allowed to attain room temperature and the contents dissolved by manually swirling the flask. This yielded a near colorless 0.5 M solution of $AlCl_3$ in THF, which was used immediately in the reaction.*
A flame dried two-necked flask, fitted with a reflux condenser and closed off with rubber septa was purged with argon, cooled on an ice bath and charged with oxoCPP (1.6 g, 8.09 mmol) and granulated $NaBH_4$ (1.43 g, 38 mmol, 4.8eq).* To this was added the solution as prepared above (43.3 ml, 21.3 mmol, 2.6 eq), which was accompanied by minor evanescence. The flask was then put under a positive pressure of N_2 provided by a Schlenk line and the contents stirred. After approximately 10 minutes the yellow color had faded and the solution attained a grey color. The ice bath was thereupon replaced with an oil bath and heated to reflux (70 °C) for 3 days. The solution was then poured unto ice (~100 ml), extracted with DCM, the organic fractions washed with $NaHCO_3$ and brine, dried over Na_2SO_4, filtered and eluted over a silica gel column using neat pentane to provide CPP as a colorless, crystalline plates (1.0 g, 5.26 mmol, 65%). ^{1}H NMR (400MHz, Ace-d_6) δ 7.89 (s, 2H), 7.86 (d, *J* = 8.00 Hz, 2H), 7.74 (d, *J* = 8.00 Hz, 2H), 7.66 (t, *J* = 8.00 Hz, 2H), 4.37 (s, 2H). HRMS (ESI-TOF) m/z: calc'd for C16H10 [M+H]+: 191.08608 found 191.08549. m.p. 113 – 114 °C, lit. 113.5 – 114.5 °C.[94]

* Anhydrous, ≥99.9%, inhibitor-free THF was obtained from Sigma Aldrich with a reported water content < 0.005%.

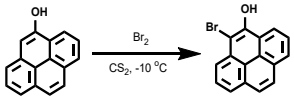
* Use of granulated $NaBH_4$ is preferred as much heavier evanescence is observed when using powdered $NaBH_4$. A slightly lower yield (60%) was observed when reducing 9-fluorenone with powered $NaBH_4$.

4-hydroxypyrene (4)



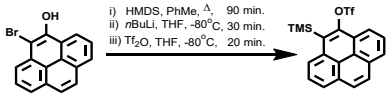
To a stirred mixture of 4*H*-cyclopenta[*d,e,f*]phenanthren-4-one (162 mg, 0.78 mmol) and $BF_3{\cdot}Et_2O$ (150 ul, 1.2 mmol, 1.5 eq) in DCM (10ml) was added trimethylsilyldiazomethane (2M in hexanes, 600 uL, 1.2 mmol, 1.5 eq) in DCM (15 mL) at -78°C over 20 minutes. The mixture was allowed to slowly attain room temperature overnight and then, poured into ice cold water (30 mL). The organic layer was separated and the aqueous layer extracted with chloroform (1x 30 mL). The combined organic layers were washed with brine, dried over $MgSO_4$ and charged on celite. The compound was eluted over a silica gel column using 1:50 EtOAC:pentane as eluent, to yield the title compound as a pale yellow solid which turns brown upon standing in contact with air. An analytical sample was obtained by recrystallization of the product from pentane:Et_2O. Yield: 86 mg, 0.39 mmol, 50.5%. m.p. 203-206 °C (dec.) ^{1}H NMR (500MHz, Acetone-d_6) δ 9.46 (brs, 1H), 8.64 (dd, J = 8.0, 1.0Hz, 1H), 8.29 (dd, J = 7.5, 1.0Hz, 1H), 8.11 (ABq, 2H, $\Delta\delta_{AB}$ = 0.025, J_{AB} = 9.0Hz), 8.09—8.04 (m, 2H), 7.94 (t, J = 7.5Hz, 1H), 7.51 (s, 1H). ^{13}C NMR (125MHz, Acetone-d_6) δ 152.94, 133.44, 132.02, 131.02, 131.90, 128.31, 127.89, 127.14, 126.56, 126.35, 126.31, 126.30, 123.90, 123.10, 121.50, 120.63. HRMS (ESI-TOF) m/z: calc'd for $C_{16}H_{11}O$ $[M+H]^+$: 219.08044, found 219.08025. m.p. 181 °C (dec.).

4-bromo-5-hydroxypyrene (8)



To a solution of 4-hydroxypyrene (360 mg, 1.7 mmol) in CS_2 (35 ml) at -10 °C was added dropwise a solution of Br_2 in CS_2 (0.3M, 5.5 ml, 1.7 mmol, 1 eq) and the solution stirred under an argon atmosphere for 6 hours. The solution was then quenched by the dropwise addition of sat. $Na_2S_2O_4$ (10 ml) at -10 °C. The organic phase was then separated, washed with brine and charged on celite. The compound was eluted over a silica gel column using EtOAc:Pentane (1:20) as eluent, to provide the title compound in the form of fine, pale yellow needles. Yield: 464 mg, 1.56 mmol, 94%. ^{1}H NMR (500 MHz, Ace-d_6) δ 8.79 (s, 1H), 8.63 (dd, J = 1.0, 8.0Hz, 1H), 8.33 (dd, J = 1.0, 7.5 Hz, 1H), 8.24 (dd, J = 1.0, 7.5 Hz, 1H), 8.07 (dd, J = 1.0, 7.5 Hz, 1H), 8.041 (s, 1H), 8.039 (s, 1H), 8.037 (t, J = 8.0Hz, 1H), 7.999 (t, J = 8.0 Hz, 1H). ^{13}C NMR (125 MHz, Ace-d_6) δ 150.09, 132.35, 132.28, 131.42, 128.67, 128.43, 128.11, 127.69, 127.34, 126.31, 125.13, 125.12, 124.38, 122.42, 121.62, 104.73. The compound was found to be unstable upon standing in contact with air and was used without further characterization.

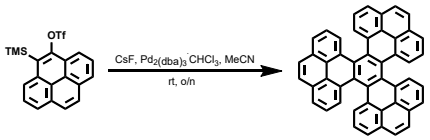
5-(trimethylsilyl)pyren-4-yl trifluoromethanesulfonate (9)



A solution of 4-bromo-5-hydroxypyrene (0.220 g, 0.74 mmol) and HMDS (0.17 mL, 0.43 mmol) in THF (5 mL) was refluxed for 90 minutes. The solvent and excess reagent were then removed under reduced pressure to yield a colorless oil. [^{1}H NMR (300MHz, $CDCl_3$) δ 8.62 (dd, J = 1.2, 7.8Hz, 1H), 8.48 (dd, J = 1.8, 7.8Hz, 1H), 8.22 (dd, J = 0.9, 7.5Hz, 1H), 8.13 (dd, J = 1.2, 7.5Hz, 1H), 8.09-8.01 (m, 4H), 0.54 (s, 9H)]. The residue was dissolved in THF (5 mL) and the solution cooled to -80 °C using an Ace:liquid N_2 bath. Then, *n*-BuLi in hexanes (0.77 mL, 2.46 M, 1.90 mmol, 2.6 eq.) added in one portion, stirring continued for 30 minutes and Tf_2O (0.16 mL, 0.93 mmol) then added. Stirring was continued for another 20 min. and the reaction then quenched by the addition of cold sat. $NaHCO_3$ (~5 mL). The layers were separated, the aqueous layer

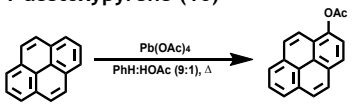
extracted with Et_2O (2x 10 mL), and the combined organic layers dried over Na_2SO_4, filtered and concentrated under reduced pressure. Column chromatography over silica gel (Et_2O:hexane, 1:500) afforded the product as a white solid. Yield: 143 mg, 0.35 mmol, 47%. ^1H NMR (500 MHz, $CDCl_3$) δ 8.54 (dd, *J* = 7.95, 0.90 Hz, 1H), 8.42 (d, *J* = 7.90 Hz, 1H), 8.26 (dd, *J* = 7.65, 0.85 Hz, 1H), 8.09 (t, *J* = 7.85 Hz, 1H), 8.06 (s, 1H), 8.05 (s, 1H), 8.03 (t, *J* = 7.65 Hz, 1H), 0.73 (s, 9H). ^{13}C NMR (125 MHz, $CHCl_3$) δ 148.76, 133.91, 131.63, 131.54, 131.07, 128.11, 127.66, 127.13, 126.94, 126.52, 126.33, 126.22, 125.86, 125.15, 124.02, 119.67, 119.00 (q, $^1J_{CF}$ = 320.68 Hz). ^{19}F NMR (470 MHz, $CDCl_3$) δ 72.52. HRMS (ESI-TOF) m/z: calc'd for $C_{20}H_{18}F_3O_3SSi$ $[M+H]^+$: 423.06925, found 423.06906.

Tripyrenylene (1)-*C*$_2$



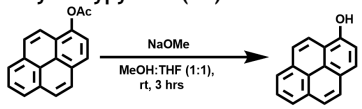
The compound obtained above (143 mg, 0.35 mmol) was dissolved in a mixture of dry MeCN (7 mL) and dry Et_2O (2 mL) together with $Pd_2(dba)_3{\cdot}CHCl_3$ (20 mg, 0.018 mmol). Then, finely powdered anhydrous CsF (170 mg, 1.1 mmol) was added in one portion and the mixture stirred at room temperature overnight under a N_2 atmosphere. The resulting suspension was allowed to settle, the supernatant withdrawn and the residue successively washed with MeCN (2x 5 mL) and Et_2O (1x 10 mL). The residue was then taken up in DCM (~10 mL), evaporated onto celite using a rotary evaporator at room temperature, and eluted over a short silica gel column using DCM:Pentane (1:10 → 1:3). Fractions containing the product (TLC, DCM:Pentane (1:10), R_f = 0.3) were evaporated at room temperature using a rotary evaporator to provide the title compound as a dark orange solid. Yield: 33 mg, 54.9 μmol, 47.1%. ^1H NMR (500 MHz, Tol-d_8) δ 8.43 (d, *J* = 8.0 Hz, 1H), 7.87 (dd, *J* = 7.5, 1.0 Hz, 1H), 7.85 (s, 1H), 7.40 (t, *J* = 7.5 Hz, 1H). ^{13}C NMR (125 MHz, DCM-d_2) δ 131.83, 130.33, 128.78, 128.36, 127.35, 126.17, 125.35, 124.61. HRMS (ESI-TOF) m/z: calc'd for $C_{48}H_{25}$ $[M+H]^+$: 601.19563, found 601.19508.

1-acetoxypyrene (16)[95]



A solution of pyrene (3.0 g, 14.8 mmol) and $Pb(OAc)_4$ (7.3 g, 16.5 mmol) in glacial AcOH (12 mL) and anhydrous benzene (100 mL) was stirred under reflux for 3 h. The mixture was cooled, diluted with toluene (250 mL) and washed with H_2O (3 × 250 mL). The organic layer was charged on celite and eluted over a silica gel column using neat toluene as eluent to afford the 1-acetoxypyrene as a white solid (1.62g, 6.22mmol, 37.7%).^1H NMR (300MHz, $CDCl_3$) δ 8.00 – 7.97 (m, 3H), 7.93 (ABq , ΔδAB = 0.03, J_{AB} = 9.0Hz, 2H), 7.83 – 7.90 (m, 3H), 7.68 (d, *J* = 13.5, 1H), 2.42 (s, 3H). ^{13}C NMR (126MHz, $CDCl_3$) δ 169.84, 144.25, 131.03, 130.86, 129.26, 128.09, 127.01, 126.96, 126.20, 125.50, 125.14, 124.96, 124.43, 123.03, 120.13, 119.68, 77.41, 77.16, 76.90, 21.06.

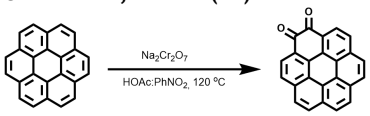
1-hydroxypyrene (10)



To a solution of 1-acetoxypyrene (646 mg, 2.48 mmol) in MeOH:THF (5:5) was added NaOMe (135 mg, 2.5 mmol) and the resultant bright yellow suspension stirred for 3 hrs. The reaction was quenched by the addition of 1M HCl (10 ml) and extracted with EtOAc. The organic phase

was dried over MgSO4, filtered, evaporated to driedness to provide 1-hydroxypyrene in quantitative yield. ^{1}H NMR (300MHz, $CDCl_3$) δ 9.46 (s, 1H), 8.53 (d, *J* = 9.3Hz, 1H), 8.09-8.03 (m, 4H), 7.91 (ABq , ΔδAB = 0.108, J_{AB} = 9.0Hz, 2H), 7.91 (t, *J* = 7.8Hz, 1H) 7.67 (d, *J* = 8.4 Hz, 1H). ^{13}C NMR (75MHz, $CDCl_3$) δ 152.76, 132.74, 132.72, 128.20, 126.95, 126.88, 126.74, 126.59, 125.92, 125.53, 125.02, 124.83, 124.59, 122.27, 119.60, 113.90.

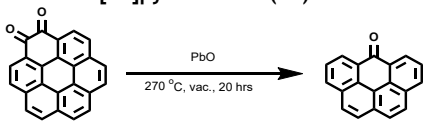
Coronene-1,2-dione (12)[96]

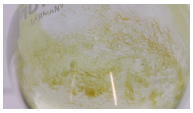


Over the course of 1 h a solution of $Na_2Cr_2O_7$ (4 g, 13.4 mmol) in glacial acetic acid (30 mL) was added dropwise to a boiling solution (~120 °C) of coronene (1 g, 3.3 mmol) in nitrobenzene (30 mL) and glacial acetic acid (5 ml). Another 30ml of glacial acetic acid were added and the solution allowed to cool to room temperature, and then further cooled on ice. The precipitate was collected by vacuum filtration and the residue washed with acetic acid, dilute H_2SO_4 and cold water. Yield of fine, dark-purple crystals 834 mg, 2.52 mmol, 76.5%. Of all solvents tried, only DMSO provided enough dissolution to allow for NMR measurements (Fig. S2.2 – S2.6).* ^{1}H NMR (850 MHz, DMSO-d6) 8.50 (s, 2H), 8.40 (d, *J* = 0.85, 8.0Hz, 2H), 8.33 (d, *J* = 8.5Hz, 2H), 8.28 (d, *J* = 8.0Hz, 2H), 8.15 (d, *J* = 8.5Hz, 2H). ^{13}C NMR (213MHz, DMSO-d_6) 178.86, 130.98, 129.91, 129.89, 128.18, 127.91, 127.76, 127.21, 126.08, 123.97, 122.64. Residual coronene signals were also observed: ^{1}H NMR (850 MHz, DMSO-d_6) 9.06 (s, 2H). ^{13}C NMR (213MHz, DMSO-d_6) 128.33, 126.38, 121.57. MALDI-TOF calc'd 330.068, found 329.760.

* The compound also dissolves in acetic acid with a brown color, in trifluoroacetic acid with a purple color and sulfuric acid with a dark-green color.

6*H*-Benzo[*cd*]pyren-6-one (14)





An intimate mixture of coronene-1,2-dione (700 mg, 2.12 mmol) and lead(II) oxide (7.7 g, 34.5 mmol, 16.3 eq.) was divided over four vials which had previously been flame dried under vacuum. The vials were shrink capped and evacuated to high vacuum prior to being heated on an aluminum heating block at 270 °C for 20 hours. Fine yellow crystals sublimated on the walls of the tubes above the metal block. The vials were allowed to attain room temperature, purged with argon and the contents extracted with chloroform. The extracts were evaporated on celite on a rotary evaporator and flushed over a silica gel column using neat DCM as eluent. The product eluting at R_f = 0.5 was isolated in the form of fine, yellow needles and identified as 6*H*-benzo[*cd*]pyren-6-one by 1D and 2D NMR (Fig. S2.7 and S2.8). Yield: 12.1 mg, 0.04 mmol, 1.9%. ^{1}H NMR (850 MHz, DMSO-d_6) 8.76 (d, *J* = 8.5Hz, 2H), 8.59 (d, *J* = 8.5Hz, 2H), 8.36 (d, *J* = 8.5Hz, 2H), 8.24 (d, *J* = 8.5Hz, 2H), 8.03 (t, *J* = 8.5Hz, 2H). ^{13}C NMR (HSQC, HMBC, 213MHz, DMSO-d_6) 182.93, 134.76, 131.83, 130.77, 128.40, 128.84, 128.71, 127.02, 126.97, 126.93, 119.86.

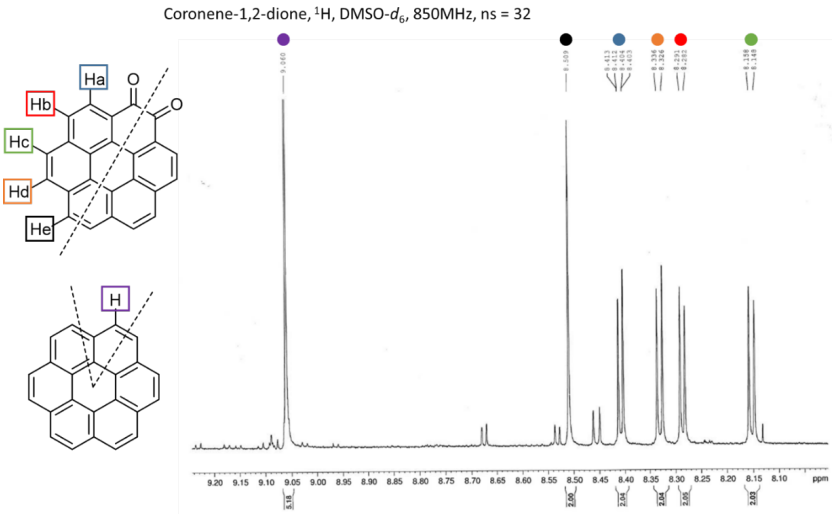


Figure S2.2 ^{1}H spectrum of coronene-1,2-dione **12** with protons indicated. Also observed is the signal of residual coronene starting material.

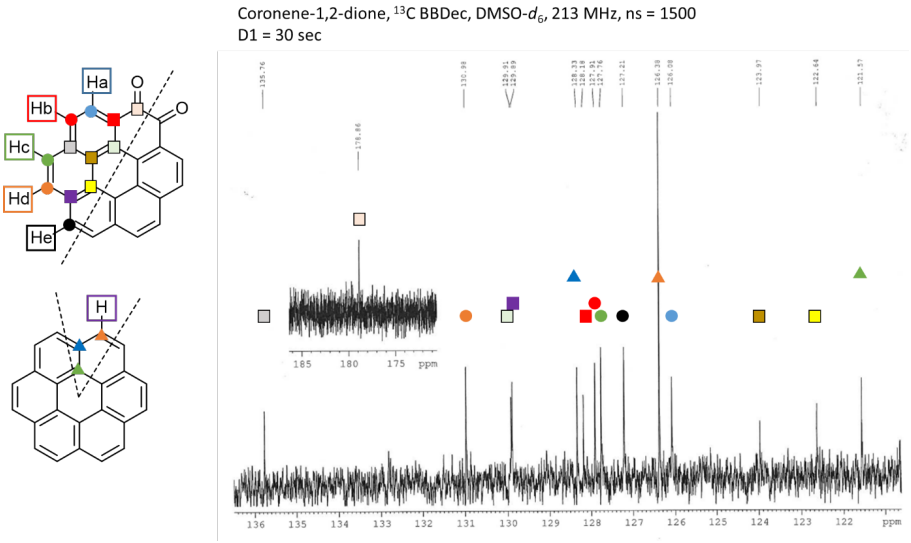


Figure S2.3 ^{13}C{^{1}H} spectrum of coronene-1,2-dione **12** with individual carbon signals labelled. Also observed are signals of residual coronene starting material.

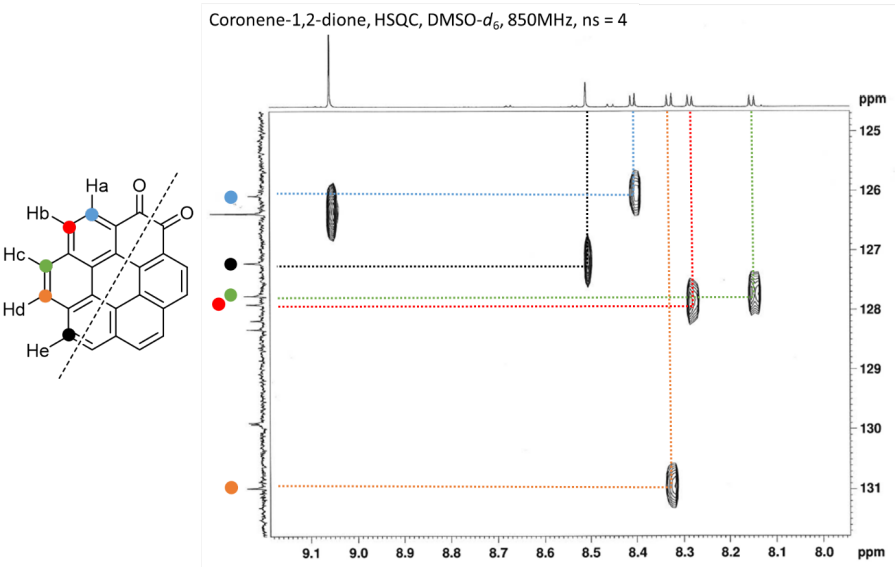


Figure S2.4 Part of the HSQC spectrum of coronene-1,2-dione **12** showing $^{1}J_{CH}$ couplings.

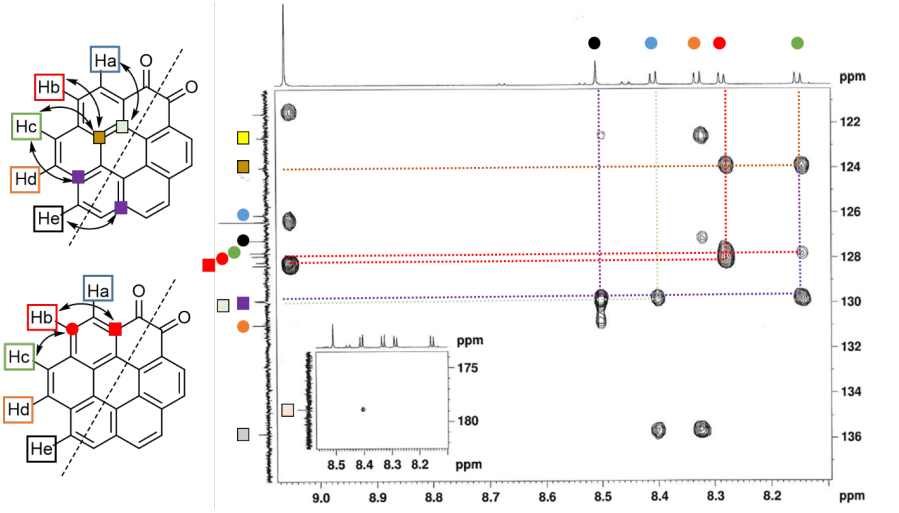


Figure S2.5 Part of the HMBC spectrum of coronene-1,2-dione **12** showing selected $^{3}J_{CH}$ couplings.

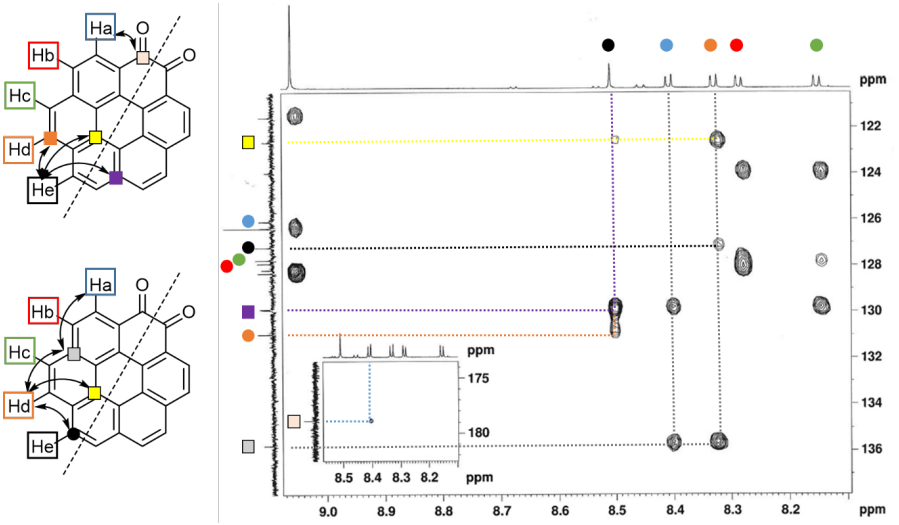


Figure S2.6 Part of the HMBC spectrum of coronene-1,2-dione **12** showing selected $^{3}J_{CH}$ couplings.



Figure S2.7 ^{1}H spectrum of 6*H*-benzo[cd]pyrenone **14**. Also observed are signals of unidentified side-product.

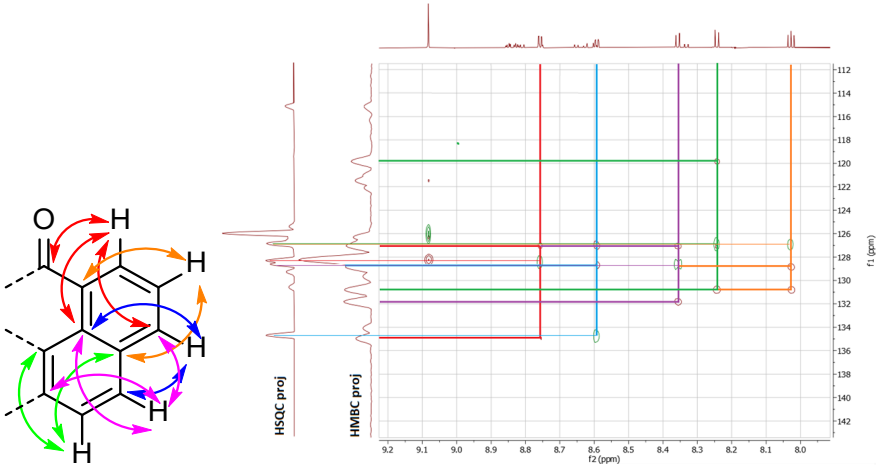


Figure S2.8 Overlay of the HSQC and HMBC spectra of 6*H*-benz[*cd*]pyrenone **14** showing $^{1}J_{CH}$ and $^{3}J_{CH}$ correlations as red and green cross peaks respectively. Note that there is cross peak overlap for the proton resonance at 8.24 ppm, due to $^{3}J_{CH}$ correlation across the symmetry plane (green lines).

Chapter 3

Conformational Behavior and Spectroscopic Properties of a Pyrene-based π-extended Triple Helicene

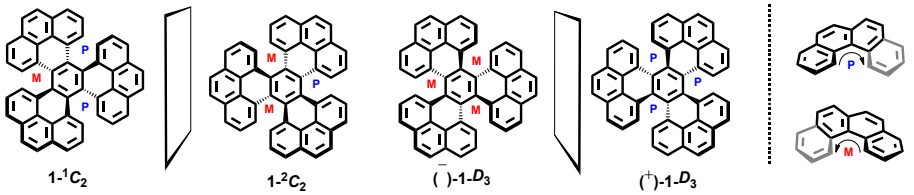
Abstract

The previous Chapter described the synthesis of tripyrenylene. This Chapter will start by analysing its conformational behaviour using variable temperature NMR. The different conformational isomers of the propellerene are then separated and their spectroscopic properties studied and compared to other helicenes and propellerenes. The effect an increase in the π-conjugated system has on the physico-chemical properties of helicene molecules is studied and, in particular, whether the location of π-extension is of importance or not. It is shown that tripyrenylene exhibits behaviour very similar to other (π-extended) propellerenes, suggesting the location of the π-extension to be of lesser importance than the π-extension itself. It also indicates that the properties of multiple helicenes are dictated by the helical motif itself. Using DFT computations, the similarities between the different helicenes and propellerenes are traced back to the molecular orbital level.

Parts of this Chapter are published as:
van der Ham A., Hansen T., Brouwer A. M., Overkleeft H. S., Hamlin T., Filippov D. V., Schneider G. F. **Manuscript in preparation.** Pre-print available (doi: 10.26434/chemrxiv-2021-kn2qg)

One striking characteristic property of aromatic molecules is their ability to absorb and emit light in the ultraviolet (UV) and visible range (~200 – 800 nm). Absorption of light takes place when the light shone onto a molecule is able to excite an electron from an occupied orbital to an unoccupied orbital; emission takes place when the excited electron falls back to its original, ground state. Because π electrons are less tightly bound than sigma electrons, they are more easily excited (π → π*), requiring less energy to do so, and thus absorption takes place at longer wavelengths. When π electrons are delocalized in a conjugated system, this energy gap becomes even smaller, resulting in absorption taking place at ever longer wavelengths. Because the optical properties of aromatic molecules are thus driven by the size of their conjugated system, the relationship between these two factors provides an important guiding principle for the design of PAH-based photo-optical materials.[2-4] Yet, although such relationships have been well documented for monohelicenes[7,8] and multiple helicenes,[10] a systematic study on the effects of π-extension on the physicochemical properties of helicenes *vis-à-vis* propellerenes appears absent in the literature.

An initial comparison of the reported UV-Vis spectra of [5]helicene (**5H**),[1] dibenzo[*f,j*]picene (**DBP**),[5] hexabenzotriphenylene-C_2 (**HBT-C_2**) and Kamikawa *et al.*'s hexapole [5]helicene-C_2 (**HH-C_2**) shows that an increase in the size of the aromatic system is associated with an, expected, bathochromic broadening of the absorption curve, with the absorption onset shifting from ~370 to 500 nm (Fig. 3.1). A number of conserved absorption features can be discerned in all spectra. A global absorption maximum close to 250 nm is observed, with **5H** and **DBP** showing two local maxima centered around 300 nm (dotted line), which are red shifted for **HBT-C_2** and **HH-C_2** to 350 and 390 nm respectively. All spectra also show a distinctive shoulder in the absorption onset, which broadens and shifts from 330 nm for **5H** to 450 nm for **HH-C_2**. Before tripyrenylene **1**, prepared in the preceding Chapter, can be compared to this list, its exact structure first needs to be defined. As explained in Chapter 1, what differentiates propellerenes from other helicene derivatives, is that they can adopt two distinct conformations: a C_2 and D_3 conformation, depending on the relative orientation of the wings, and the resultant molecular symmetry. Apart from these two conformations, each conformation exists as a pair of enantiomers, which are non-superimposable mirror images of one another (Scheme 3.1). In the previous chapter, analysis of the conformation in which **1** was isolated was purposefully foregone. This issue will therefore be addressed here first.



1-$^1C_2$ **1-$^2C_2$** **(⁻)-1-D_3** **(⁺)-1-D_3**

Scheme 3.1 Structures of the two enantiomers of **1**-C_2 and **1**-D_3, with the chirality of the helical motifs labelled.

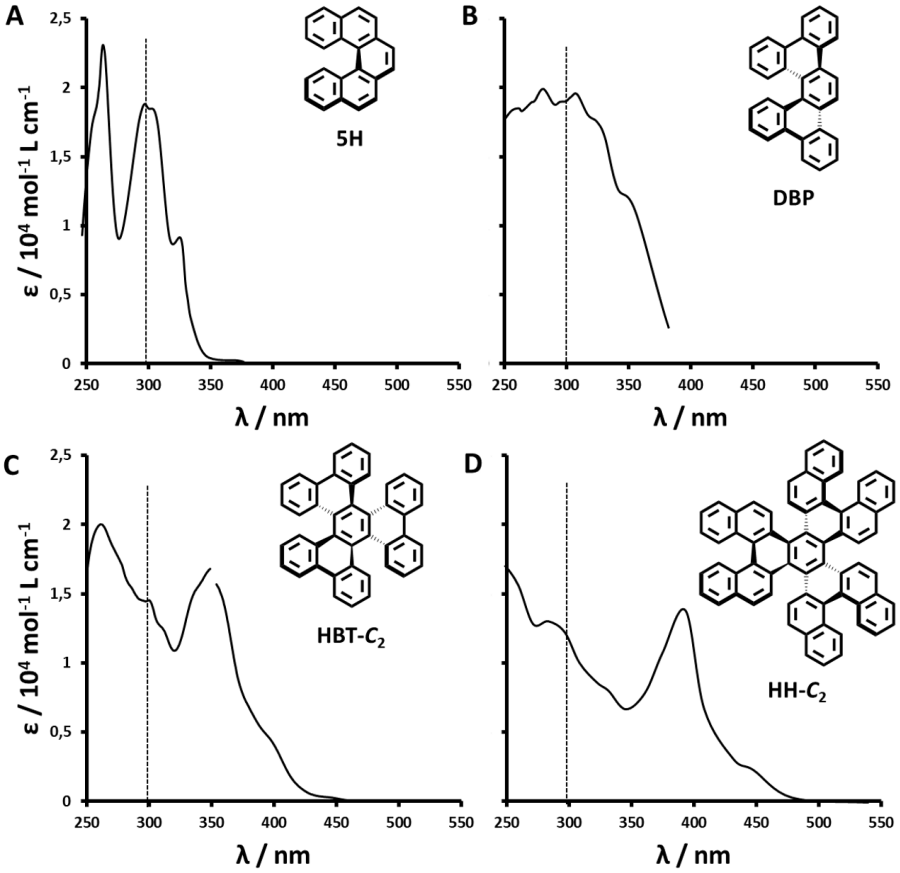


Figure 3.1 Experimental UV-Vis spectra of (A) [5]helicene,[1] (B) dibenzopicene[5] and (C) HH-C_2[6], recreated from those originally reported.[9] Spectrum of HBT-C_2 (D) was recorded in this work. Absorptions are arbitrarily scaled. Dotted line added at 300 nm for ease of reference.

VT NMR. One of the most straightforward methods of determining the conformation in which a propellerene resides is by variable temperature (VT) NMR spectroscopy (Fig. 3.3A). At room temperature, the ^{1}H spectrum of **1** only shows four resonances due to rapid interconversion between the two C_2 conformations (Fig. 3.2 and Fig. 3.4). When cooled to –100°C, however, interconversion is no longer possible and a dramatic change in the spectrum is observed, with the emergence of additional resonances corresponding to individual protons on **1**-C_2 (note that the two conformers are both chemically and magnetically equivalent and thus their resonances coincide). The coalescence temperature for the interconversion between the two C_2 conformers was found to be approximately –90 °C, corresponding to a barrier height to interconversion of 10.0 kcal mol^{-1}, which is close to the computed value of 9.9 kcal mol^{-1} (Fig. 3.3B). Heating of the solution to 80 °C resulted in conversion to the D_3 conformation. This was evidenced by the disappearance of the C_2 resonances, with a half time of approximately 20 mins., corresponding to a barrier height of $\Delta G^{\ddagger}$ = 26.0 kcal mol^{-1}, and which is in excellent agreement with the computed value of 26.4 kcal mol^{-1}. When the solution was again cooled to –80 °C, only an insignificant change in chemical shift was observed but no change in the number or multiplicity of the resonances. This confirmed **1** to now reside in the D_3 conformation, which was further verified by recording VT NMR spectra of the isolated conformers in different solvents (Fig. 3.4).

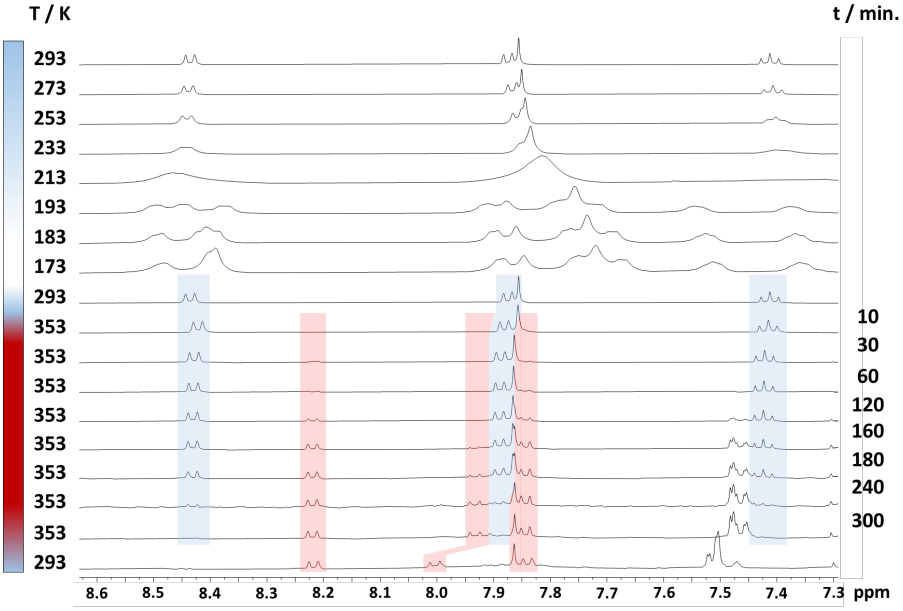


Figure 3.2 ^{1}H VT-NMR spectra of **1** in Tol-d_8. Spectra are arbitrarily scaled for clarity. Multiplets around 7.5 ppm originate from the solvent. Resonances shaded in blue and red belong to the C_2 and D_3 conformer respectively. Observed is a dramatic change in resonances upon cooling of **1** in the C_2 conformer, and a gradual disappearance of the C_2 resonances and appearance of resonances of the D_3 conformer when the solution is heated to 100 °C.

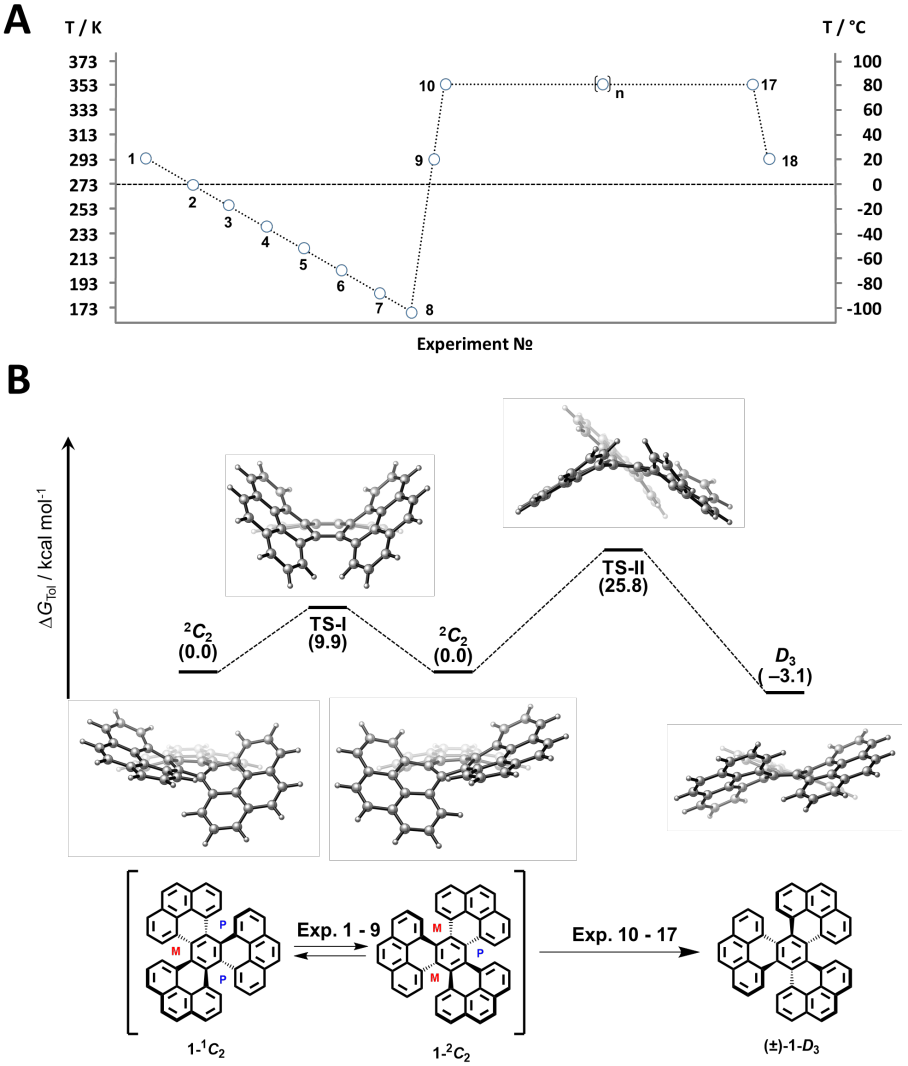


Figure 3.3 (A) Temperature profile of the VT-NMR experiment shown in Fig. 3.2. (B) Potential energy surface for the interconversion of **1** between its C_2 and D_3 conformations. Gibbs free energies (in kcal mol^{-1}) were computed at the SMD(Toluene)-PBE-D3(BJ)/6-31G(d,p) level. Indicated are which processes take place at which points during the VT NMR experiment.

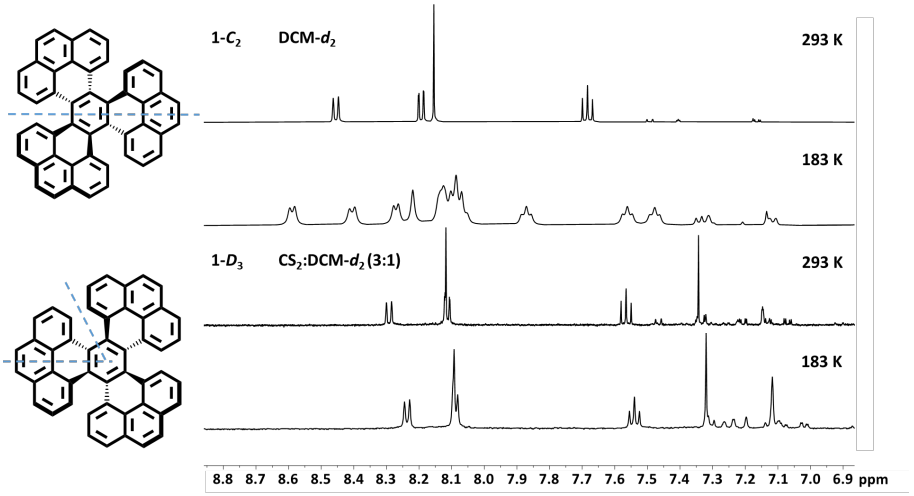


Figure 3.4 Reference ^{1}H VT-NMR spectra of the C_2 and D_3 conformer of **1** in DCM-d_2 and CS_2:DCM-d_2 (3:1) respectively. Signals in the spectrum of **1**-D_3 upfield of 7.5 ppm originate from impurities in the solvent. Blue dashed lines indicate the symmetry axes of the propellerenes.

It is of interest to note that, during the $C_2 \rightarrow D_3$ conversion at 80 °C, the compound was found to precipitate out of solution. This indicates that the D_3 conformer of tripyrenylene is significantly less soluble than the C_2 conformer. Computationally, the dimerization energies of the C_2 and D_3 conformer were indeed found to be –21.9 and –24.4 kcal mol^{-1} respectively, corroborating this observation. This observation can be attributed to a much better stacking of the D_3 conformer, due to its lesser degree of contortion from planarity compared to the C_2 conformer. Indeed, the intermolecular distances were found to be 4.50 and 4.40 Å for the C_2 and D_3 dimer respectively (Fig. 3.5).

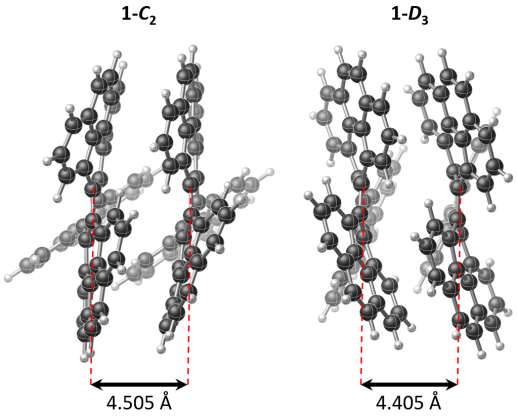
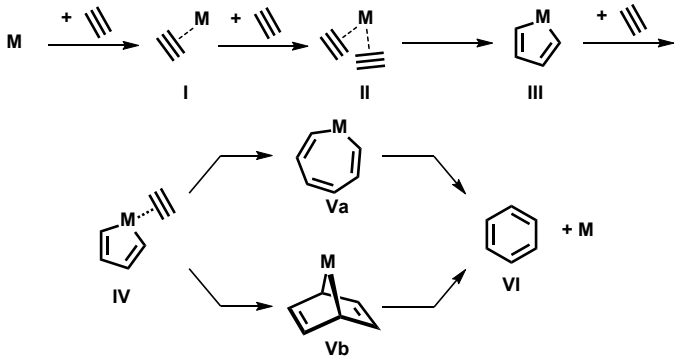


Figure 3.5 Computed gas-phase geometries of the **1**-C_2 and **1**-D_3 dimer, showing the intercore distance. The shortest intermolecular C — C distance was approximately 3.37 Å for both structures.

Palladium catalyzed [2+2+2] aryne cyclotrimerization. What the NMR experiments show is that tripyrenylene **1** was synthesized as the C_2 conformer, even though the DFT computations indicated that this conformer is thermodynamically less favorable than the D_3 conformer (Fig. 3.3A). Although surprising at first, this is actually in agreement with the fact that the palladium(0) catalyzed [2+2+2] cycloaddition of arynes is known to proceed under kinetic control.[11-13]



Scheme 3.2 General reaction scheme for the [2 + 2 + 2] cycloaddition of three alkynes, catalyzed by a transition metal **M**. Substituents on the alkynes and (solvent) ligands on the metal center were omitted for clarity. Adopted from: ,,Mechanistic Studies of Transition-Metal-Catalyzed [2 + 2 + 2] Cycloaddition Reactions" (Ref. 9).

The general reaction scheme for the [2 + 2 + 2] cycloaddition of three alkynes is given in Scheme 3.2. In short, the reaction starts with the barrierless coordination of two alkyne units to the metal center (**I** and **II**), which then combine to give diene **III**. Note that this reaction is only barrierless when disregarding solvents or ligands coordinating to the metal center. Gibbs free energies of association and dissociation of solvent molecules and ligands are typically on the order of 1 – 2 kcal mol^{-1} and –10 – +20 kcal mol^{-1}, respectively.[14,15] Coordination of a third alkyne then gives metallocomplex **IV**. Insertion of the third alkyne typically proceeds *via* one of two possible mechanisms: in a two-step fashion *via* a seven-membered intermediate (**Va**), known as the Schore mechanism;[16] or in a concerted [4 + 2] cycloaddition fashion, *i.e.* a canonical Diels-Alder reaction (**Vb**).[17] Reductive elimination of the metal then regenerates the catalyst, and yields the final, aromatic product **VI**. Yet, despite the plethora of computational studies related to the transition metal catalyzed coupling of alkynes, the corresponding reaction of arynes is much less studied.[18] To understand at which point in the reaction kinetic control over the reaction is exerted, and whether this control is substrate dependent or independent, the entire potential energy surface (PES) of this reaction was computed.

In view of the computational cost associated with large systems, the PES of the [2+2+2] cycloaddition of benzyne, which yields the planar triphenylene, was computed first (Fig. 3.6A). This was then extended to the phenanthren-4,5-yne system which yields hexabenzotriphenylene (HBT; Fig. 3.6B), for which the steric control of this reaction was first reported. PESs were computed at the SMD($CHCl_3$)-PBE-D3(BJ)/6-31G(d,p) level, and both the benzyne and phananthryne reactions were found to proceed in a similar fashion, starting with the step-wise coordination of two aryne units to a single palladium(0) atom. A palladacyclic intermediate **B3**/**P3** is then formed *via* a transition state **TS-I**. In the case of benzyne, the intermediate **B3** has a planar C_{2v} symmetry,[19] whereas steric clash between the spatially proximal rings in palladacycle **P3** results in the adaptation of a non-planar geometry. Coordination of a third aryne to the palladium center in diene **B3**/**P3** results in a further lowering in free Gibbs energy, yielding reaction intermediates **B4**/**P4**. It is of interest to note that this final aryne unit is oriented orthogonal to the diene plane. This geometrical feature is observed only when dispersion is accounted for (*i.e.* when using ωB97X-D or PBE-D3(BJ) as functionals). When no dispersion correction is applied (*i.e.* uncorrected B3LYP) the aryne ring is centered on the Pd atom, *i.e.* yielding a D_2 symmetry in the case of benzyne (Fig. S3.1). Although not directly comparable, a similar non-symmetrical structure was found both experimentally and computationally for the $V^+(C_4H_4)\cdots(C_2H_2)$ complex.[20] For both **B4** and **P4**, transition states could only be located for insertion of the final aryne *via* a Schore mechanism (**TS-II**). As reported before by others,[6] it was not possible to locate a TS that describes a concerted [4 + 2] cycloaddition, *i.e.* a canonical Diels-Alder addition. To prove that such a concerted mechanism is much less favorable, a constrained PES can be constructed in which bond forming C···C distances are artificially constrained to be synchronously concerted (Fig. S3.2). Although the initial products of both PESs are different, the energetic maximum of the concerted synchronous reaction is approximately 25 kcal mol^{-1} more endergonic with respect to the TS of the step-wise addition (*i.e.* **TS-II**). This is attributable to a much less favorable orbital alignment, steric clash and the requirement for an unfavorable dearomatization of the palladacyclic complex. The C_2 symmetry of **B5** and **P5** is introduced at this point along the reaction coordinate and is retained after ring closure *via* a low energy barrier (**TS-III**). Based on this finding, it can be concluded that the kinetic control of this reaction is substrate independent.

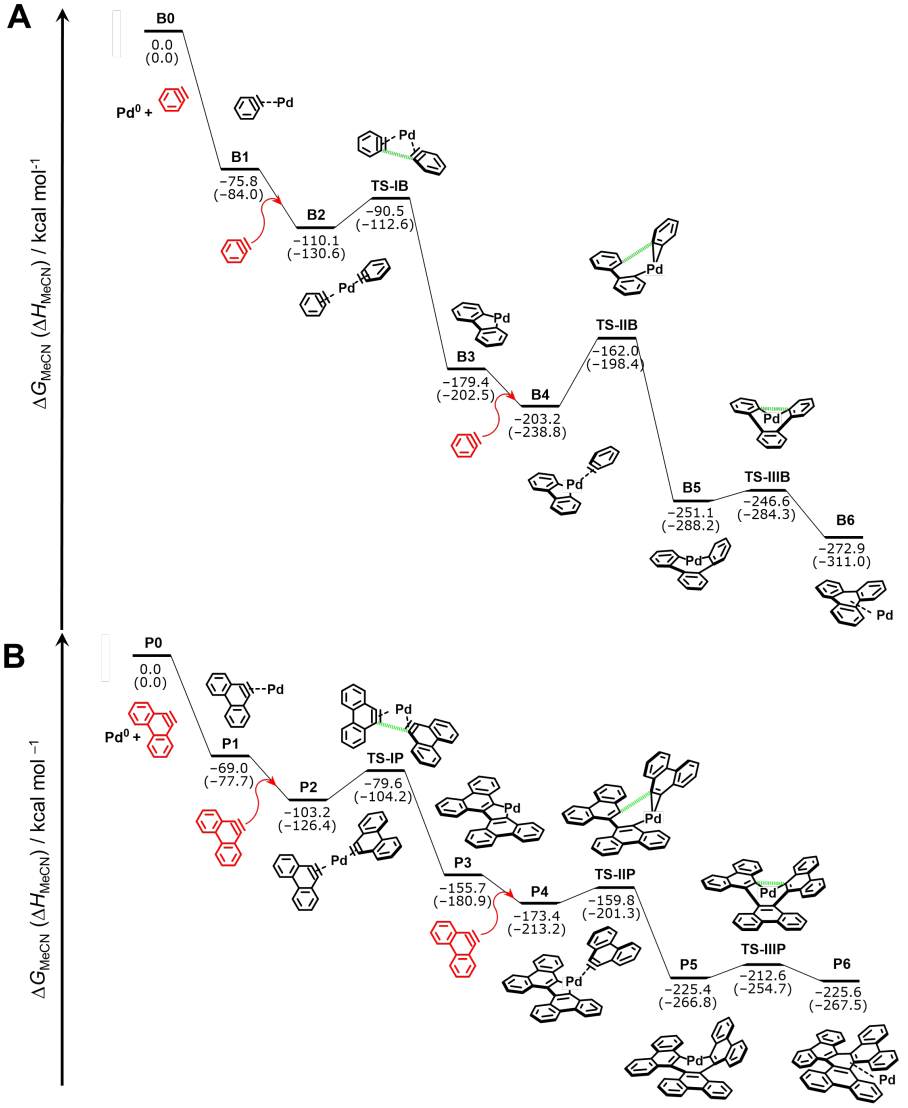


Figure 3.6 The potential energy surface of the palladium(0) catalyzed trimerization of benzyne (A) and phenanthren-9,10-yne (B). Gibbs free energies and enthalpies are computed at the SMD(MeCN)-PBE-D3(BJ)/6-31G(d,p) level of theory are given in kcal mol^{-1}.

UV-Vis Spectroscopy. Because interconversion of the C_2 conformer to the D_3 conformer is sufficiently slow at room temperature, combined with the fact that the D_3 conformer is thermodynamically preferred to a significant degree (Fig. 3.3), the isomers can be separated and their photo-optical properties studied separately.[21]

The UV-Vis spectrum of a solution of **1**-C_2 in chloroform shows an absorption onset at 504 nm, corresponding to an optical band gap of 2.46 eV (Fig. 3.7). Weak shoulders are observed at 439 nm and 416 nm, which were computed using time dependent (TD) DFT at B3LYP/6-311+G(2d,p)//B3LYP-D3(BJ)/6-31G(d,p) to correspond to the HOMO → LUMO transition, and a mixture of different frontier orbital transitions (λ_{calc} = 451 nm, f = 0.0606; λ_{calc} = 424 nm, f = 0.0097) (Table S3.2). Two local maxima are found at 385 nm and 365 nm, with a global maximum located at 295 nm ($\varepsilon_{max,C2}$ = 3.05 x 10^4 mol^{-1} L cm^{-1}). The spectrum of **1**-D_3 is distinctly different to that of **1**-C_2. The absorption onset is slightly red shifted compared to that of **1**-C_2 at 522 nm, corresponding to an optical band gap of 2.37 eV. Absorption bands are found at 506 nm and 473 nm, corresponding respectively to the HOMO → LUMO +1 (λ_{calc} = 482 nm, f = 0.0000) and a mixed HOMO → LUMO / HOMO –1 → LUMO +1 (λ_{calc} = 445 nm, f = 0.0264) transition. A single local maximum is found at 394 nm with the global maximum located at 282 nm ($\varepsilon_{max,D3}$ = 2.83 x 10^4 mol^{-1} L cm^{-1}). Comparison of the UV-Vis spectra of **1** to that of **HBT** (Fig. 3.7) and **HH** (Fig. 3.1) in the same solvent shows, apart from a bathochromic shift and broadening, a near identical band pattern.[6] This provides an initial hint that, although increased conjugation results in a change in photo-optical properties, the exact location at which this increased conjugation is introduced is only of nominal importance.

Recording of the emission spectrum of **1**-D_3, when excited at the 394 nm band revealed, apart from the expected mirror image of the absorption spectrum, a minor emission band around 400 nm, ahead of a main emission band around 515 nm (Fig. 3.8A). Recording of a 2D excitation/emission spectrum revealed the origin of the 400 nm emission to originate from an absorption feature at 350 nm (Fig. S3.4). It was initially speculated that this feature was indicative of excimer formation.

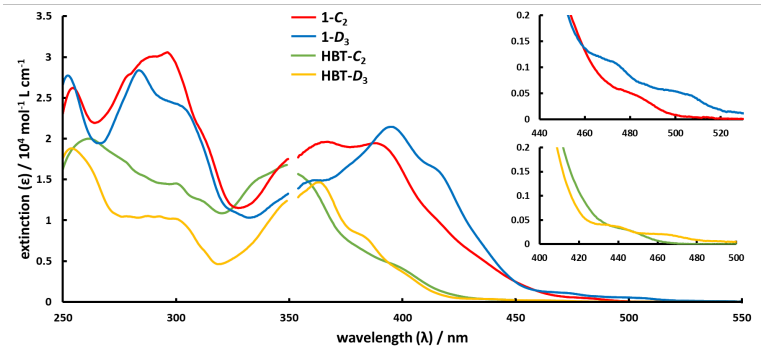


Figure 3.7 UV-Vis spectra of **HBT** and **1** recorded as solutions in chloroform at room temperature. The gap around 350 nm is due to switching of the lamp. Insets show the separate absorption onsets of the tripyrenylenes (top) and HBT (bottom).

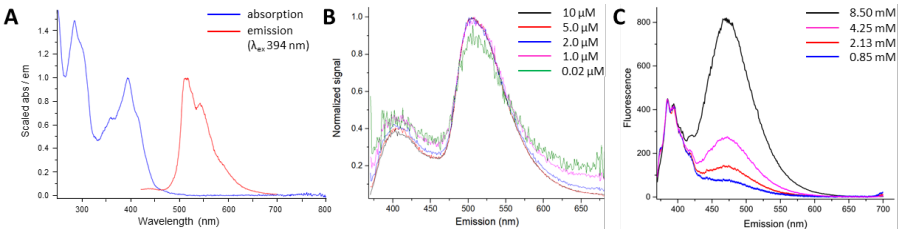


Figure 3.8 (A) Absorption/emission spectrum of **1**-D_3 (*n*-heptane:$CHCl_3$, $c \approx 1 \cdot 10^{-5}$ M). (B) Dilution array fluorescence spectra of **1**-D_3 in *n*-heptane, excited at 350 nm. Emission normalized to the feature around 520 nm. (C) Dilution array fluorescence spectrum of pyrene in *n*-heptane excited at 350 nm. Normalized to the emission around 400 nm. Note the change in relative intensity of the maxima around 400 and 475, which is not observed for the features in **1**-D_3.

The concept of excimer formation is best illustrated using the parent pyrene molecule. Pyrene itself is well-known to form excimers in solution, giving rise to a broad, featureless emission at around 500 nm (also see Fig. 3.8C).[22-25] Excimers (E) are formed when a ground state (S_0) monomeric molecule (M) is excited to a higher energy exited state (S_1, M*) and then associates with another, ground state, molecule (Fig. 3.9A).[26-28] The pyrene excimer complex is geometrically distinct from the ground state pyrene dimer (D) and its excited counterpart (D*). Namely, whereas the excimer complex adopts a sandwich configuration, the ground state and excited pyrene dimer adopt slipped-parallel configurations.[27] Thus, upon relaxation of the excimer complex, a state will be reached which is higher in energy than the ground state dimer (D), and indeed does not constitute a stationary point on the PEL (Fig. 3.9A). The stabilization of the excimer has traditionally been attributed to exciton resonance, whereby the excitation energy is delocalized over both components of the excimer complex, and light will therefore be emitted from the excimer at a longer wavelength than from the monomer; *i.e.* $h\nu^{e}_{em} < h\nu^{m}_{ex/em}$ (Fig. 3.8A).[22]

The presence of dimeric excimer formation can be experimentally verified by recording the excitation/emission spectrum at different substrate concentrations. At lower concentrations, less dimer formation and thus excimer formation is expected, and which is shown for pyrene in Figure 3.8C. For **1**, however, the relative intensity of the emissions at 400 and 520 nm remains invariant with concentration, suggesting the formation of an *intramolecular excimer*. In other words, irradiation of **1** can lead to formation of an excited **1^{1}*** species which emits light at a particular wavelength ($h\nu^{1*}_{em}$, $\lambda \approx 400$ nm). However, within **1**, the enforced close proximity of the pyrene units also allows adjacent wings to couple to one another, *i.e.* form an intramolecular excimer, which emits light of lower energy ($h\nu^{2*}_{em}$, $\lambda \approx 520$ nm; Fig. 3.9B). Examples of intramolecular excimer formation are known for several PAHs in the literature.[29-32] To prove this hypothesis, time-resolved fluorescence experiments can be performed. As formation of the excimer requires diffusion an excited molecule to a ground state molecule, one would expect a delayed emission after the excitation event. If indeed found, these results would constitute the first, indirect, experimental proof that the

central ring of (benzoid) propellerenes are not conjugated (*i.e.* do not constitute a classical Clar sextet), which has thus far only been inferred computationally.[33-37] These experiments are currently underway. Other possible explanations for the observed emission pattern are the presence of minor, but strongly emitting, impurities or; preferential excitation of higher energy states (*i.e.* a violation of Kasha's rule).

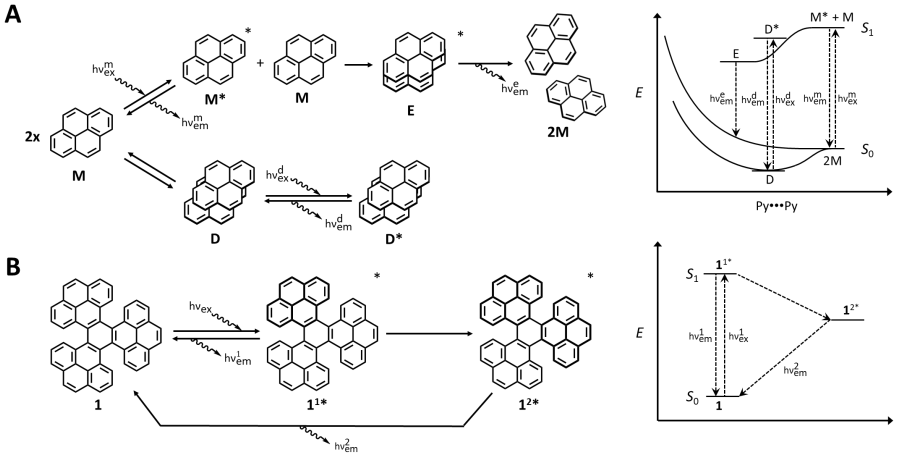


Figure 3.9 Schematic overview of the formation of pyrene eximers (A) and intramolecular eximer formation in **1** (B). Schematic potential energy diagrams for both processes are given to the right. For pyrene the PES is plotted as a function of the intermolecular distance.

Frontier Orbitals. The similarity in absorption-emission spectra between the different propellerenes suggests that the underlying molecular orbital structure is also similar. The frontier molecular orbitals (FMOs) of both conformers of **1** and **HBT** were therefore computed using TD-DFT at B3LYP/6-311+G(2d,p)//B3LYP-D3(BJ)/6-31G(d,p), (which was first verified on **5H** (Table S3.1)), and compared to those reported for **HH**.[6] The HOMOs and LUMOs of **1** in both conformations are largely of an expected π and π*-type, respectively. The HOMO/HOMO –1 and LUMO/LUMO +1 pairs are distinguishable by the pattern of the MOs on the wings of the propellerenes (Fig. 3.10). This feature allows tracking of the frontier orbitals during the $C_2 \rightarrow D_3$ conversion. It is observed that, during this transition, the HOMO of **1**-C_2 becomes more stabilized, whereas the LUMO becomes more destabilized, yielding the HOMO –1 and LUMO +1 in **1**-D_3 respectively. Concomitantly, the HOMO –1 and LUMO +1 of **1**-C_2 become more and less destabilized respectively, yielding the HOMO and LUMO of **1**-D_3. The net result is a widening of the band gap from –3.12 eV to –3.20 eV. This effect has also been reported for **HH,**[6] and computing of the frontier orbitals of **HBT** revealed a near identical effect (Fig. 3.10, Table S3.2), suggesting this "frontier orbital cross-over effect" to be a general feature of benzoid triphenylenes. It has been proposed this effect is the result of a greater planarity of propellerenes in their D_3 conformation.

For full comparison, computation of the FMOs of **5H** and **DBP** revealed a clear correlation between π-extension and size of the HOMO – LUMO gap, with an increase

and decrease in the HOMO and LUMO energy respectively, when going from **5H** to **1** and **HH** (Fig. S3.3); supporting the bathochromic shift observed in their UV-Vis spectra (Fig. 3.1).[38] Conversely, the near identical HOMO – LUMO gap of **1** *vis-à-vis* **HH** further confirms the notion that the position of π-extension is of lesser relevance than the fact of π-extension itself.

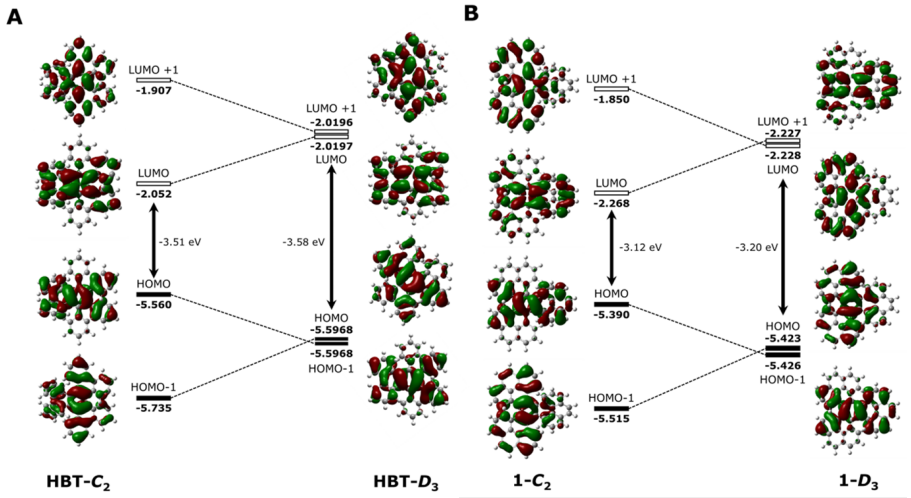


Figure 3.10 Energy diagrams of the frontier orbitals of both enantiomers of **HBT** (A) and **1** (B) as computed at TDDFT-B3LYP/6-311+G(2d,p)//B3LYP-D3(BJ)/6-31G(d,p). Phases arbitrarily colored.

To conclude, it was shown that tripyrenylene **1** was isolated in a C_2 conformation. Computationally, this conformer was found to be thermodynamically less favorable, compared to the D_3 conformer. By computing the entire PES of the palladium catalyzed aryne trimerization used to synthesize it, it was shown that this reaction proceeds under kinetic control. This kinetic control could be pinpointed to the final aryne insertion step, which proceeds in a step-wise manner, rather than in a canonical Diels-Alder fashion. Using variable temperature NMR the conversion to the more stable isomer could be monitored. The spectroscopic properties of the separate isomers were then studied. Comparison of these properties to those of known helicenes, combined with a detailed FMO analysis, revealed that the position at which extension of the π-conjugated system is introduced is insignifcant, suggesting the helical motifs in these molecules to be dominant in dictating their photo-optical properties. Some initial evidence was found suggesting that the central ring of propellerenes may not be conjugated, something which has often be postulated based on computational models. Experiments are currently underway to validate these results.

References

(1) Kubo, H.; Hirose, T.; Matsuda, K. Control over the Emission Properties of [5]Helicenes Based on the Symmetry and Energy Levels of Their Molecular Orbitals. *Org. Lett.* **2017,** *19* (7), 1776.

(2) Griffiths, J. *Colour and constitution of organic molecules*; Academic press, **1976**.

(3) Fabian, J.; Hartmann, H. *Light absorption of organic colorants: theoretical treatment and empirical rules*; Springer Science & Business Media, 2013.

(4) Nishimoto, K. A MO theoretical study of organic dyes I. Effect of chemical softness on the electronic spectra. *Bull. Chem. Soc. Jap.* **1993,** *66* (7), 1876.

(5) Jenard-de Koninck, A.; Defay, N.; de Ridder, R. Synthèses dans le domaine des composés polycycliques aromatiques. XX. synthèses du 1,2-3,4-5,6-7,8-tétrabenzophénanthrène (ou tétrabenzo[a,c,g,i]phénanthrène) et du 1,12-2,3-10,11-tribenzopérylène (ou tribenzo[b,n,p,q,r]pérylène). *Bull. Soc. Chim. Belges* **1960,** *69* (11-12), 558.

(6) Hosokawa, T.; Takahashi, Y.; Matsushima, T.; Watanabe, S.; Kikkawa, S.; Azumaya, I.; Tsurusaki, A.; Kamikawa, K. Synthesis, structures, and properties of hexapole helicenes: Assembling six [5]helicene substructures into highly twisted aromatic systems. *J. Am. Chem. Soc.* **2017,** *139* (51), 18512.

(7) Rulíšek, L.; Exner, O.; Cwiklik, L.; Jungwirth, P.; Starý, I.; Pospíšil, L.; Havlas, Z. On the convergence of the physicochemical properties of [n] helicenes. *J. Phys. Chem. C* **2007,** *111* (41), 14948.

(8) Nakai, Y.; Mori, T.; Inoue, Y. Theoretical and experimental studies on circular dichroism of carbo [n] helicenes. *J. Phys. Chem. A* **2012,** *116* (27), 7372.

(9) The UV-Vis spectrum of dibenzo[f,j]picene was recorded in dioxane, all others in chloroform. However, inspection of the spectra suggests solvent effects to be negligible.

(10) Mori, T. Chiroptical properties of symmetric double, triple, and multiple helicenes. *Chem. Rev.* **2021,** *121* (4), 2373.

(11) Peña, D.; Cobas, A.; Pérez, D.; Guitián, E.; Castedo, L. Kinetic control in the palladium-catalyzed synthesis of C_2-symmetric hexabenzotriphenylene. A conformational study. *Org. Lett.* **2000,** *2* (11), 1629.

(12) Pozo, I.; Guitián, E.; Pérez, D.; Peña, D. Synthesis of nanographenes, starphenes, and sterically congested polyarenes by aryne cyclotrimerization. *Acc. Chem. Res.* **2019,** *52*(9), 2472-2481.

(13) Guitián, E.; Pérez, D.; Peña, D. In *Palladium in Organic Synthesis*; Springer, **2005**.

(14) Kluwer, A. M.; Elsevier, C. J.; Bühl, M.; Lutz, M.; Spek, A. L. Zero-valent palladium complexes with monodentate nitrogen σ-donor ligands. *Angew. Chem. Int. Ed.* **2003,** *42* (30), 3501.

(15) Hosokawa, T.; Asada, T.; Kamikawa, K. Theoretical examination of the plausible reaction process for stereoselective synthesis of hexapole helicene *via* a palladium-catalyzed [2+2+2] cyclotrimerization of [5]helicenyl aryne. *J. Phys. Chem. A* **2020,** *124* (4), 652.

(16) Schore, N. E. Transition metal-mediated cycloaddition reactions of alkynes in organic synthesis. *Chem. Rev.* **1988,** *88* (7), 1081.

(17) Examples of trimerization reactions which do not follow these two typical pathways are given in the preceding reference.

(18) Roglans, A.; Pla-Quintana, A.; Solà, M. Mechanistic studies of transition-metal-catalyzed [2+2+2] cycloaddition reactions. *Chem. Rev.* **2020**, *121*(3), 1894-1979.

(19) Retbøll, M.; Edwards, A. J.; Rae, A. D.; Willis, A. C.; Bennett, M. A.; Wenger, E. Preparation of benzyne complexes of group 10 Metals by intramolecular Suzuki coupling of *ortho*-metalated phenylboronic esters: Molecular structure of the first benzyne-palladium(0) complex. *J. Am. Chem. Soc.* **2002,** *124* (28), 8348.

(20) Marks, J. H.; Ward, T. B.; Brathwaite, A. D.; Ferguson, S.; Duncan, M. A. Cyclotrimerization of acetylene in gas phase $V^+(C_2H_2)_n$ complexes: Detection of intermediates and products with infrared spectroscopy. *J. Phys. Chem. A* **2019,** *123* (31), 6733.

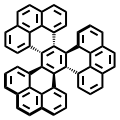
(21) Given the sufficiently large barrier to interconversion of the two D_3 enantiomers their separation using chiral HPLC chromatography should be possible. Unfortunately, despite many attempts in this direction, such a separation was not found possible for **1**-D_3.
(22) Förster, T.; Kasper, K. Ein konzentrationsumschlag der fluoreszenz des pyrens. *Z. Elektrochem.* **1955,** *59* (10), 976.
(23) Stevens, B. Evidence for the photo-association of aromatic hydrocarbons in fluid media. *Nature* **1961,** *192* (4804), 725.
(24) Birks, J. B.; Christophorou, L. G. Excimer fluorescence spectra of pyrene derivatives. *Spectrochimica Acta* **1963,** *19* (2), 401.
(25) Hanlon, A. D.; Milosavljevic, B. H. Appropriate excitation wavelength removes obfuscations from pyrene excimer kinetics and mechanism studies. *Photochemical & Photobiological Sciences* **2013,** *12* (5), 787.
(26) Birks, J. B. Excimers. *Rep. Prog. Phys.* **1975,** *38* (8), 903.
(27) Winnik, F. M. Photophysics of preassociated pyrenes in aqueous polymer solutions and in other organized media. *Chem. Rev.* **1993,** *93* (2), 587.
(28) Förster, T. Excimers and exciplexes. *The Exciplex. Academic, New York* **1975**, 1.
(29) Okamoto, Y.; Nakamura, M.; And, M. S.; Takamuku, S. Formation of intramolecular excimer in aryl phosphates and their reactivities. *Photochem. Photobiol.* **1992,** *56* (3), 403.
(30) Turro, N. J. *Modern molecular photochemistry*; University science books, 1991.
(31) Birks, J. B.; Christophorou, L. G. Excimer fluorescence of aromatic hydrocarbons in solution. *Nature* **1962,** *194* (4827), 442.
(32) Hirayama, F. Intramolecular excimer formation. I. Diphenyl and triphenyl alkanes. *J. Chem. Phys.* **1965,** *42* (9), 3163.
(33) Fernandez, I.; Frenking, G. Direct estimate of conjugation and aromaticity in cyclic compounds with the EDA method. *Faraday Discuss.* **2007,** *135*, 403.
(34) Pierrefixe, S. C. A. H.; Bickelhaupt, F. M. Aromaticity: molecular-orbital picture of an intuitive concept. *Chem. Eur. J.* **2007,** *13* (22), 6321.
(35) Roy, M.; Berezhnaia, V.; Villa, M.; Vanthuyne, N.; Giorgi, M.; Naubron, J. V.; Poyer, S.; Monnier, V.; Charles, L.; Carissan, Y. Stereoselective syntheses, structures, and properties of extremely distorted chiral nanographenes embedding hextuple helicenes. *Angew. Chem. Int. Ed.* **2020,** *59* (8), 3264.
(36) Antić, M.; Furtula, B.; Radenkovic, S. Aromaticity of nonplanar fully benzenoid hydrocarbons. *J. Phys. Chem. A* **2017,** *121* (18), 3616.
(37) Hosokawa, T.; Tsurusaki, A.; Kamikawa, K. Assembly of [5]helicene subunits by palladium-catalyzed reactions: Synthesis, structures, properties, and theoretical study of multiple helicenes. *J. Synth. Org. Chem. Jap.* **2020,** *78* (11), 1013.
(38) Wade, L. G. Conjugated systems, orbital symmetry, and ultraviolet spectroscopy. *Organic chemistry. Englewood Cliffs, NJ: Prentice Hall* **1991**, 667.
(39) Pena, D.; Pérez, D.; Guitián, E.; Castedo, L. Synthesis of hexabenzotriphenylene and other strained polycyclic aromatic hydrocarbons by palladium-catalyzed cyclotrimerization of arynes. *Org. Lett.* **1999,** *1* (10), 1555.
(40) Adachi, K.; Hirose, S.; Ueda, Y.; Uekusa, H.; Hamura, T. Thermodynamically stable *o*-quinodimethane: Synthesis, structure, and reactivity. *Chem. Eur. J.* **2020**, *27* (11), 3665-3669.
(41) Frisch, M. J.; Trucks, G. W.; Schlegel, H. B.; Scuseria, G. E.; Robb, M. A.; Cheeseman, J. R.; Scalmani, G.; Barone, V.; Mennucci, B.; Petersson, G. A. Gaussian 09 Revision D. 01, 2009. *Gaussian Inc. Wallingford CT* **2009**.
(42) PBE was used as both exchange and correlation functional, and was called using the pbepbe keyword in the Gaussian 09 software. At the DFT-D3(BJ) level of theory the s6 and s8 values are set to 1 and 0.7875 respectively, whereas the ABJ1 and ABJ2 values are set respectively to 0.4289 and 4.4407.
(43) Grimme, S.; Antony, J.; Ehrlich, S.; Krieg, H. A consistent and accurate ab initio parametrization of density functional dispersion correction (DFT-D) for the 94 elements H-Pu. *J. Chem. Phys.* **2010,** *132* (15), 154104.

(44) Grimme, S.; Ehrlich, S.; Goerigk, L. Effect of the damping function in dispersion corrected density functional theory. *J. Comp. Chem.* **2011,** *32* (7), 1456.
(45) Hay, P. J.; Wadt, W. R. Ab initio effective core potentials for molecular calculations. Potentials for K to Au including the outermost core orbitals. *J. Chem. Phys.* **1985,** *82* (1), 299.
(46) Marenich, A. V.; Cramer, C. J.; Truhlar, D. G. Universal solvation model based on solute electron density and on a continuum model of the solvent defined by the bulk dielectric constant and atomic surface tensions. *J. Phys. Chem. B* **2009,** *113* (18), 6378.
(47) Bootsma, A. N.; Wheeler, S. E. Popular integration grids can result in large errors in DFT-computed free energies. *ChemRxiv. Preprint* **2019**.
(48) Ribeiro, R. F.; Marenich, A. V.; Cramer, C. J.; Truhlar, D. G. Use of solution-phase vibrational frequencies in continuum models for the free energy of solvation. *J. Phys. Chem. B* **2011,** *115* (49), 14556.
(49) Funes-Ardoiz, I.; Paton, R. S. (2016). GoodVibes: GoodVibes v1.0.2. http://doi.org/10.5281/zenodo.595246.
(50) Legault, C. Y. *CYLview, 1.0 b, Université de Sherbrooke, 2009*, 2013.
(51) Vacek, J.; Hrbáč, J.; Strašák, T.; Církva, V.; Sýkora, J.; Fekete, L.; Pokorný, J.; Bulíř, J.; Hromadová, M.; Crassous, J. Anodic deposition of enantiopure hexahelicene layers. *ChemElectroChem* **2018,** *5* (15), 2080.
(52) Kashihara, H.; Asada, T.; Kamikawa, K. Synthesis of a double helicene by a palladium-catalyzed cross-coupling reaction: Structure and physical properties. *Chem. Eur. J.* **2015,** *21* (17), 6523.
(53) Bédard, A. C.; Vlassova, A.; Hernandez-Perez, A. C.; Bessette, A.; Hanan, G. S.; Heuft, M. A.; Collins, S. K. Synthesis, crystal structure and photophysical properties of pyrene–helicene hybrids. *Chem. Eur. J.* **2013,** *19* (48), 16295.
(54) Saito, H.; Uchida, A.; Watanabe, S. Synthesis of a three-bladed propeller-shaped triple [5]Helicene. *J. Org. Chem.* **2017,** *82* (11), 5663.
(55) Sakai, H.; Kubota, T.; Yuasa, J.; Araki, Y.; Sakanoue, T.; Takenobu, T.; Wada, T.; Kawai, T.; Hasobe, T. Synthetic control of photophysical process and circularly polarized luminescence of [5]carbohelicene derivatives substituted by maleimide units. *J. Phys. Chem. C* **2016,** *120* (14), 7860.

Experimental

General. All reagents were obtained from commercial sources and were used as received. Hexabenzotriphenylene was synthesized according to known procedures.[11,39] Solvents used were stored over 4 Å molecular sieves. Reactions were monitored by TLC analysis using Merck 25 DC plastikfolien 60 F254 with detection by using an aqueous solution of $KMnO_4$ (7%) and K_2CO_3 (2%) followed by charring at ~150 °C. Column chromatography was performed on Fluka silica gel (0.04–0.063 mm). High-resolution mass spectra were recorded by direct injection (2 µL of a 2 µM solution in water/acetonitrile; 50:50; v/v and 0.1% formic acid) on a mass spectrometer (Thermo Finnigan LTQ Orbitrap) equipped with an electrospray ion source in positive mode (source voltage 3.5 kV, sheath gas flow 10, capillary temperature 250 °C). The high-resolution mass spectrometer was calibrated prior to measurements with a calibration mixture (Thermo Finnigan). All NMR experiments were performed on a Bruker AV500 NMR instrument equipped with a BBFO probe head for 5 mm outer diameter tubes. Spectra were recorded at 500 MHz for ^{1}H, 125 MHz for ^{13}C and 470 MHz for ^{19}F. All deuterated solvents were obtained from a commercial source (Eurisotop) and were used as received. Chemical shifts are given in ppm (δ) relative to TMS (0 ppm), and coupling constants (*J*) are given in Hertz (Hz).

Tripyrenylene 1-*C*$_2$



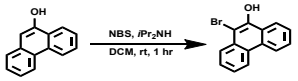
^{1}H NMR (500 MHz, Tol-d_8) δ 8.43 (d, *J* = 8.0 Hz, 1H), 7.87 (dd, *J* = 7.5, 1.0 Hz, 1H), 7.85 (s, 1H), 7.40 (t, *J* = 7.5 Hz, 1H).

Tripyrenylene 1-*D*$_3$



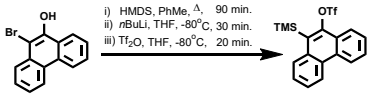
A solution of **1-*C*$_2$** in toluene was heated to 80 °C for 5 hours, resulting in the formation of a bright yellow precipitate. The solvent was removed under reduced pressure to yield the desired product. ^{1}H NMR (500 MHz, CS_2:DCM-d_2) δ 8.29 (d, *J* = 8.0 Hz, 1H), 8.11 (dd, *J* = 7.5, 1.0 Hz, 1H), 8.12 (s, 1H), 7.57 (t, *J* = 7.5 Hz, 1H).

10-Bromo-9-phenanthrol (2)[40]



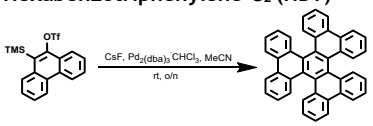
Commercial 9-phenanthrol was purified by column chromatography over silica gel using EtOAc:Pentane (1:25) as eluent and used immediately. The 9-phenanthrol (1.57 g, 8.1mmol) was dissolved in DCM (50 mL) together with *i*Pr$_2$NH (0.1 mL, 0.7 mmol). A solution of NBS (1.44 g, 8.1mmol) in DCM (50 mL) was then added dropwise over 30 min on ice. After addition was complete, the mixture was stirred for another 3 hours. The reaction mixture was then poured onto H_2O (100 mL), and acidified to pH 1 by the addition of a few drops of concentrated H_2SO_4. The resulting mixture was extracted with DCM, and the combined organic layers were dried over anhydrous Na_2SO_4, filtered, and concentrated under reduced pressure. Column chromatography of the residue (1:20 EtOAc:Pentane) afforded the desired compound as a pale-yellow solid (1.79 g, 6.55 mmol, 81.1%). ^{1}H NMR (500Mz, $CDCl_3$) 8.67-8.61 (m, 2), 8.39 (dd, *J* = 1.5, 13.0 Hz, 1H), 8.14 (dd, *J* = 1.5, 13.5 Hz, 1H), 7.75-7.69 (m, 1H), 7.68-7.63 (m, 1H), 7.59-7.56 (m, 1H), 6.30 (s, 1H).

10-(trimethylsilyl)phenanthren-9-yl trifluoromethanesulfonate (3)



A solution of 10-bromo-9-phenanthrol (0.476 g, 1.74 mmol) and HMDS (0.4 mL, 1.92 mmol) in THF (6 mL) was refluxed for 90 minutes. The solvent and excess reagent were then removed under reduced pressure, the residue redissolved in THF (12 mL) and the solution cooled to -80°C using an Ace:liquid N_2 bath. Then, *n*-BuLi in hexanes (1.83 mL, 2.46 M, 1.83 mmol) was added dropwise and stirring continued for 30 minutes before Tf_2O (0.37 mL, 2.18 mmol) was added in one portion. Stirring was continued for 20 min. and the reaction then quenched by the addition of cold sat. $NaHCO_3$. The layers were separated, the aqueous layer extracted with Et_2O, and the combined organic layers dried over Na_2SO_4, filtered and concentrated under reduced pressure. Column chromatography over silica gel (Et_2O–hexane, 1:99) afforded the product (0.2 g, 30%) as a colourless oil. ^{1}H NMR (500MHz, $CDCl_3$) δ 8.70-8.66 (m, 2H), 8.27 (dd, 8.00, 1.5 Hz, 1H), 8.19 (dd, 8.00, 1.5 Hz, 1H), 7.75-7.66 (m, 4H), 0.67 (s, 9H). ^{13}C NMR (125MHz, $CHCl_3$) δ 134.78, 132.91, 130.65, 130.12, 129.86, 128.51, 127.44, 127.33, 126.77, 125.94, 123.47, 122.88, 122.36, 118.92 (q, $^1J_{CF}$ = 320.7Hz), 2.38. ^{19}F NMR (470MHz, $CDCl_3$) δ -72.61.

Hexabenzotriphenylene-*C*$_2$ (HBT)



The oil obtained above was dissolved in dry MeCN (10 mL) together with $Pd_2(dba)_3{\cdot}CHCl_3$ (28 mg, 0.026 mmol). Then, finely powdered anhydrous CsF (244 mg, 1.6 mmol) was added and the mixture stirred at room temperature overnight under a dry N_2 atmosphere. The suspension was filtered, and the residue washed with MeCN (5 mL) and Et_2O (1 mL) and dried under vacuum to afford the title compound as a yellow solid. Yield: 7 mg, 21%. ^{1}H NMR (500 MHz, DCM-d_2) δ 8.65 (d, *J* = 8.0 Hz, 6H), 8.20 (d, *J* = 8.5 Hz, 6H), 7.64 (ddd, J = 8.2, 6.9, 1.2 Hz, 6H), 7.29 (m, 6H). The C_2 conformer was converted to the D_3 conformer as described for **1**. ^{1}H NMR (500 MHz, $CDCl_3$) δ 8.54 (d, *J* = 7.5 Hz, 6H), 8.16 (d, *J* = 8.0 Hz, 6H), 7.57 – 7.52 (m, 6H), 7.23 – 7.19 (m, 6H).

VT NMR experiments. All variable temperature experiments NMR experiments were performed on a Bruker AV500 NMR instrument equipped with a BBFO probe head for 5 mm outer diameter tubes. Spectra were recorded at 500 MHz for ^{1}H. To determine the $C_2 \rightarrow D_3$ interconversion barrier height, a solution of pyrene propeller-C_2 in toluene-d_8 was heated to 80 °C and kept at this temperature. The decrease in signal intensity of resonances corresponding to the C_2 conformer, relative to that of residual solvent signal, was monitored over time. Barrier heights were then derived from the signal decrease half time $t_{½}$ using the Eyring equation:

$$k = \frac{k_b T}{h} e^{-\frac{\Delta G^{\ddagger}}{RT}};\ t_{1/2} = \frac{\ln(2)}{k}$$

where k is the rate constant in sec^{-1}, k_b is Boltzmann's constant, T is the absolute temperature, h is Planck's constant, R is the universal gas constant and the transmission coefficient has been set to 1 and has thus been omitted. For the $^1C_2 \leftrightarrow {}^2C_2$ interconversion barrier heights solutions of pyrene propeller C_2 in toluene-d_8 were cooled and the barrier height derived from the coalescence temperature (T_c) as:

$$\Delta G^{\ddagger} = RT_c \left[23 + \frac{T_c}{\Delta \nu}\right]$$

where $\Delta\nu$ is the coupling constant in Hertz.

Computational. Equilibrium geometries of all structures were computed at the DFT level of theory using the Gaussian 09 Rev. D.01 program,[41] using the PBE functional[42] and 6-31G(d,p) basis set and D3(BJ) dispersion correction.[43,44] For structures containing Pd atoms the LANL2DZ (with effective core potential) basis set was used on Pd and a 6-31G(d,p) basis set on all other atoms.[45]Geometries were optimized in the gas-phase and subsequently re-optimized in combination with the SMD model to include solvent effects, using acetonitrile as the solvent parameter.[46] For the time-dependent (TD) DFT computations, geometries were first optimized in the gas-phase using the B3LYP functional, 6-31G(d,p) basis set and D3(BJ) dispersion correction, and TD computations then performed using the same functional but using the larger 6-311+G(2d,p) basis set. For all computations the convergence criteria were set to tight (Opt = tight; Max. Force = $1.5 \cdot 10^{-7}$, Max. Displacement = $6.0 \cdot 10^{-7}$), and an internally defined super-fine grid size was used (SCF = tight, Int = VeryFineGrid), which is a pruned 175,974 grid for first-row atoms and a 250,974 grid for all other atoms.[47] These parameters were chosen because of the significant dependence of computed frequencies on the molecular orientation when using smaller grid sizes. This effect was particularly pronounced for transition metals and transition state structures.[47]

Denoted free Gibbs energies were computed using Equation S1, in which ΔE_{gas} is the gas-phase energy (electronic energy), $\Delta G^{T}_{gas,QH}$ (T = 293.15 K, p = 1 atm., C = 1 M) is the sum of corrections from the electronic energy to the free Gibbs energy in the quasi-harmonic oscillator approximation, including zero-point-vibrational energy, and ΔG_{solv} is their corresponding free solvation Gibbs energy. The $\Delta G^{T}_{gas,QH}$ were computed using the quasi-harmonic approximation in the gas phase according to the work of Truhlar - the quasi-harmonic approximation is the same as the harmonic oscillator approximation except that vibrational frequencies lower than 100 cm^{-1} were raised to 100 cm^{-1} as a way to correct for the breakdown of the harmonic oscillator model for the free energies of low-frequency vibrational modes.[48,49] All stationary points found were checked for either no imaginary frequencies for local minima or one imaginary frequency for transition state structures.

$$\begin{aligned} \Delta G^{T}_{solv} &= \Delta E_{gas} + \Delta G^{T}_{gas,QH} + \Delta G_{solv} \\ &= \Delta G^{T}_{gas} + \Delta G_{solv} \end{aligned} \qquad \text{(Eq. S1)}$$

Transition states for the propellerene interconversion were obtained by first performing a dihedral angle scan in the Gaussian software to provide guess structures for a QST3 search.

Transition states in the palladium(0) catalyzed reactions were obtained using a QST2 search. The obtained guess structures were optimized to a transition state using the Berny algorithm and confirmed by an intrinsic reaction coordinate calculation. Frontier orbitals were computed using TDDFT at the B3LYP/6-311+G(2d,p) level, using geometries optimized at the SMD($CHCl_3$)-B3LYP-D3(BJ)/6-31G(d,p) level of theory. Molecular structures were illustrated using CYLview.[50]

Supplementary Figures and Tables

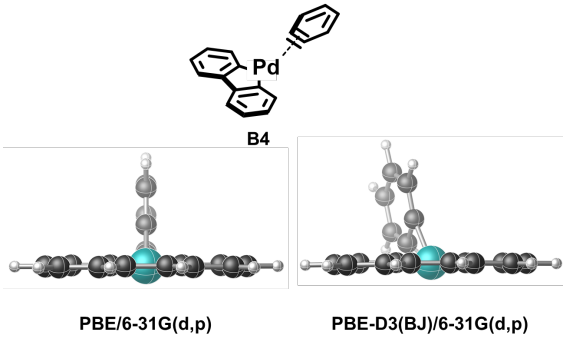


Figure S3.1. Computed gas-phase geometries of the **B4** complex, optimized without and with D3(BJ) dispersion correction.

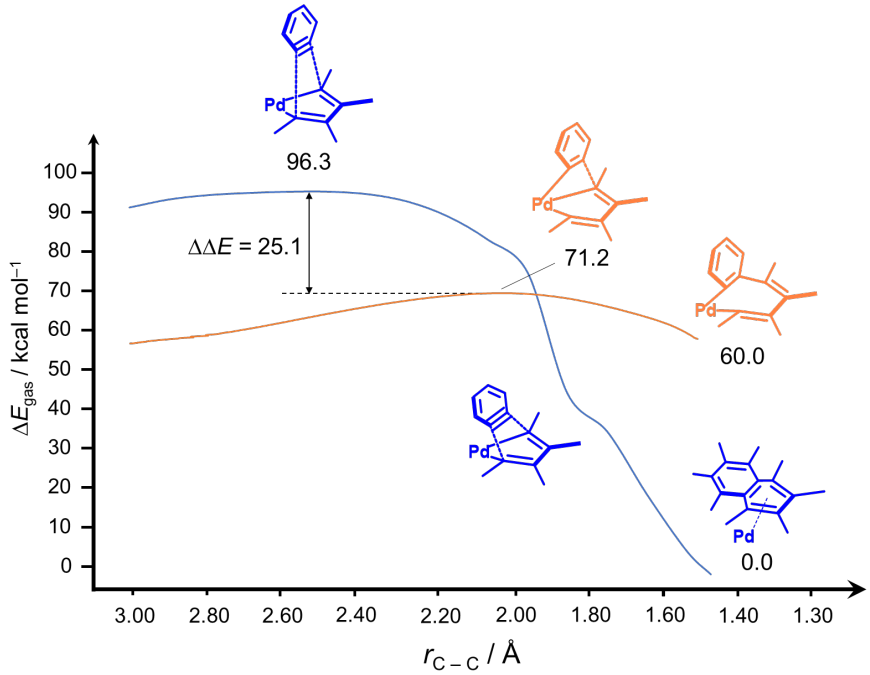


Figure S3.2 Potential energy surfaces for the step-wise addition (orange) and concerted synchronous addition (blue) of **P3**···phenanthr-4,5-yne complexes. Reported are gas-phase electronic energies (kcal mol^{-1}) projected unto the bond forming C – C distances (dashed lines in structures) at PBE-D3(BJ)/6-31G(d,p). Structures are drawn in abbreviated form for clarity.

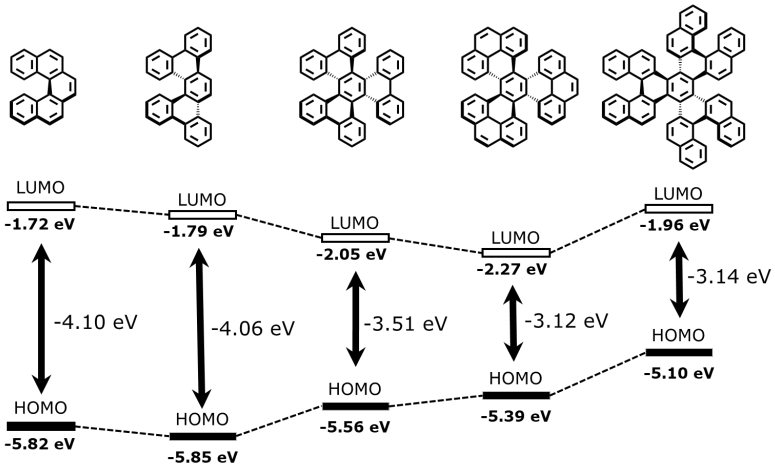


Figure S3.3 Energy diagram of the FMOs of helicenes and propellerenes computed at the B3LYP-D3(BJ)/6-311+G(2d,p)//B3LYP-D3(BJ)/6-31G(d,p) level of theory.

Table S3.1 Computed HOMO – LUMO energies of [5]helicene at different levels of theory, and the experimental HOMO energy level, in eV.

	1	**2**	**3**	**4**	**5**	**6**
LUMO		-1.72	-1.85	-2.08	-1.34	-1.29
HOMO	-5.81	-5.82	-5.97	-5.49	-5.53	-5.49
gap		-4.10	-4.12	-3.41	-4.19	-4.20

1 Experimental value[51]
2 B3LYP/6-311+G(2d,p)//B3LYP-D3(BJ)/6-31G(d,p) [This Work]
3 PCM(ACN)B3LYP/6-311++G(d,p)[51]
4 M06-2X/6-31+G(d,p)//PCM(Acetone)B3LYP/6-31G(d,p)[52]
5 IEFPCM(DCM)B3LYP/6-31G(d)[53]
6 B3LYP/6-31G(d)[54,55]

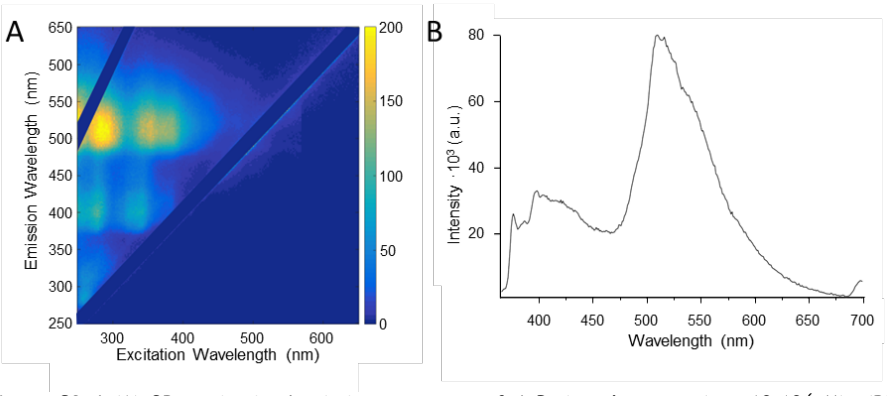


Figure S3.4 (A) 2D excitation/emission spectrum of **1**-D_3 in *n*-heptane (c = $10 \cdot 10^{-6}$ M). (B) Emission spectrum of **1**-D_3 in *n*-heptane:$CHCl_3$, excited at 350 nm.

Table S3.2 Transition energies, wavelengths, and oscillator strengths (*f*) of benzoid triphenylenes as computed at the TDDFT/B3LYP/6-311+G(2d,p)//SMD($CHCl_3$)-B3LYP-D3(BJ)/6-31G(d,p) level of theory. HOMO → LUMO transitions are shaded in grey.

HBT-C2

HOMO = 138; LUMO = 139

Excited State 1:		Singlet-A
2.9039 eV	426.95 nm	f=0.0002
137 -> 139		0.51513
138 -> 140		0.47924
Excited State 2:		Singlet-A
3.0329 eV	408.79 nm	f=0.0666
137 -> 140		-0.22871
138 -> 139		0.66124
Excited State 3:		Singlet-A
3.3879 eV	365.96 nm	f=0.2998
137 -> 140		0.62936
138 -> 139		0.21034
138 -> 141		0.18027

HBT-D3

HOMO = 138; LUMO = 139

Excited State 1:		Singlet-A
2.8021 eV	442.47 nm	f=0.0000
137 -> 139		0.46261
137 -> 140		-0.18357
138 -> 139		0.18361
138 -> 140		0.46256
Excited State 2:		Singlet-A
3.0157 eV	411.13 nm	f=0.0284
137 -> 139		-0.18273
137 -> 140		-0.46008
138 -> 139		0.46046
138 -> 140		-0.18261
Excited State 3:		Singlet-A
3.2555 eV	380.85 nm	f=0.4477
137 -> 139		-0.45234
137 -> 140		-0.18099
138 -> 139		-0.18094
138 -> 140		0.45236

1-C2

HOMO = 156; LUMO = 157

Excited State 1:		Singlet-A
2.6500 eV	467.87 nm	f=0.0001
155 -> 157		0.53026
156 -> 158		-0.45459
Excited State 2:		Singlet-A
2.7487 eV	451.06 nm	f=0.0606
154 -> 157		-0.21271
156 -> 157		0.66093
Excited State 3:		Singlet-A
2.9217 eV	424.36 nm	f=0.0097
154 -> 157		0.58276
155 -> 158		0.33993
156 -> 157		0.14427

1-D3

HOMO = 156; LUMO = 157

Excited State 1:		Singlet-A
2.5687 eV	482.68 nm	f=0.0000
155 -> 157		-0.49269
156 -> 158		0.49624
Excited State 2:		Singlet-A
2.7860 eV	445.03 nm	f=0.0264
155 -> 158		0.47977
156 -> 157		0.49734
Excited State 3:		Singlet-A
2.8694 eV	432.09 nm	f=0.1988
154 -> 157		-0.33192
155 -> 157		0.43049
156 -> 158		0.42769
156 -> 159		0.13314

Chapter 4

Understanding the Conformational Preference of Propeller-shaped Polycyclic Aromatic Hydrocarbons

Abstract

In the previous Chapter the conformational preference of tripyrenylene was discussed in depth. A thermodynamic preference for a D_3 conformer was found, even though its synthesis was found to proceed under kinetic control to yield a C_2 product. This preference for a D_3 conformation is, however, not universal for all propellerenes, and the conformational behavior of propellerenes, in general, has been a standing question in the field. Because the physicochemical and photo-optical properties of propellerenes are highly dependent on their conformation, understanding the origin of the conformational preference of propellerenes is of paramount importance, if one wishes to rationally design propellerenes with specific physicochemical properties.

Parts of this Chapter are published as:

- van der Ham A., Hansen T., Overkleeft H. S., Filippov D. V., Hamlin T. A., Schneider G. F. Understanding the Conformational Preference of Propeller-shaped Polycyclic Aromatic Hydrocarbons. **Manuscript submitted.**
- van der Ham, A., Schneider, G. F., Lutz, Martin. CCDC 2056845: Experimental Crystal Structure Determination. **2021**, DOI: 10.5517/ccdc.csd.cc2719vg

Arguably the first propellerene to be synthesized was perfluorotriphenylene, whose crystal structure unequivocally showed it to reside in a counterintuitive C_2 symmetrical conformation.[1] Some 27 years later, Pascal *et al.* would successfully synthesize the elusive perchlorotriphenylene,[2,3] by the *in vacuo* pyrolysis of perchlorophthalic anhydride.[4] Crystallographically it, too, was found to reside in a highly twisted C_2 conformation. One year later the same group published a paper addressing this conformational conundrum for the first time.[5] Using semi-empirical and Hartree-Fock based computations they found that in the C_2 conformation the central ring of propellerenes adopts a puckered twist-boat configuration, whereas in the D_3 conformation the central ring adopts a more planar, chair-like configuration (Fig. 4.1). Conversely they observed the wings to be more planar in the C_2 conformation versus the D_3 conformation.[6] Based on these observations, in this initial report, they therefore concluded that the minimization of distortion from planarity of the wings in the C_2 conformation, at the expense of that of the central ring, was the key driving factor as to why a propellerene molecule would preferentially adopt a C_2 conformation.[6] This is additionally based on the notion that the wings and central ring are expected to behave as aromatic systems, *i.e.* distortion from planarity is resisted by the disruption of the π-conjugated system this would entail.

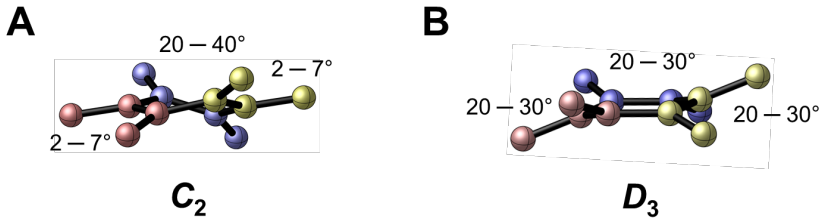


Figure 4.1 Representative geometries of the core fragment and radial bonds in the C_2 and D_3 conformation with key dihedral angles color-coded (pink, blue, yellow), with the range of angles found in **1-8**. This also illustrates the different ways in which the wings are adjoined to the core in the different conformations.

Although this theory seems to hold when considering only *ortho*-substituted triphenylenes, including *e.g.* hexamethyltriphenylene[7,8] and hexaiodotriphenylene,[9] it fails when π–extended, or benzoid, triphenylenes are considered, which all prefer a D_3 conformation. Realizing this problem, Pascal *et al.* published another, largely computational study in 1999, where they meticulously studied the geometry of a range of propellerenes in their different conformations.[10] There they argued that „*the C_2/D_3 dichotomy is a purely electronic effect*", as opposed to a steric one. Using a number of real and hypothetical molecules they stated the ability of bond alternation in the central ring to be key, asserting that „*The central ring geometry is not a product of the conformation, but a determining factor*". They additionally proposed a rule-of-thumb which states that when the circumference of the central ring is smaller than 8.5 Å a D_3 symmetry is preferred, whereas a C_2 symmetry is preferred when the circumference is larger than 8.6 Å. Interestingly, they proposed a molecule, colloquially known as „Pascal's super propellerene", which would invalidate this rule (See Chapter 6).

Many others have since tackled the question on the conformational behavior of propellerenes, both from a computational and experimental point of view, concluding a combination of aromatic, steric, and electrostatic factors to be at play in driving the conformational preference of propellerenes.[5,10-14] Recent advances in computational chemistry and expansion of the propellerene library prompted a revisit of this topic. Based on newly gained insights regarding the conformational behavior of propellerenes, it was hypothesized that the origin of the conformational preference of propellerenes could be rationalized from a balance in the individual preference of the central ring of the propellerene molecule and the wings attached thereto. To this end, a combined experimental and computational study was undertaken to elucidate and comprehensively describe the thermodynamic and kinetic factors that drive the conformational preference of propellerene molecules.

Model set and method validation. Notwithstanding the wide range of propellerenes known, to make the present study manageable, this Chapter focusses on a select set of triphenylene class of propellerenes (**1** – **8**), which constitutes the most studied class. Before continuing, it is important to define the two integral parts of propellerenes: the six central carbon atoms, called the *core*, and the rings and substituents attached thereto, collectively called the *wings* (highlighted in red and green, respectively, in Figure 4.2). Propellerenes can be further divided into two families based on the composition of the wings: those with substituents only on the *ortho*-position are denoted *ortho*-substituted (Fig. 4.2; **1** – **4**), whereas those with additional fused benzene rings are denoted as benzoid (Fig. 4.2; **5** – **8**), whereas those bearing. Experimentally, benzoid triphenylenes are reported to prefer a D_3 conformation, whereas *ortho*-substituted triphenylenes always prefer a C_2 conformation.

The geometries of this select set of triphenylene class propellerenes (**1** – **8**) were optimized at PBE-D3(BJ)/6-31G(d,p) in their C_2 and D_3 conformation (Fig. 4.2). Computed free Gibbs energies for the different conformers are in agreement with observed experimental preference of the propellerenes, both in gas phase (Fig. 4.2) and solution phase (Table S4.1), with all *ortho*-substituted triphenylenes (**1** – **4**) preferring a C_2 conformation,[8,9,12,15-18] and all benzoid triphenylenes (**5** – **8**) preferring a D_3 conformation (Fig. 4.2).[19-23] The ability of propellereness to interconvert between their two conformations at room temperature in solution was investigated. Computing of the corresponding transitions states gratifyingly gave values in good agreement with experimental values (Table S4.1). In short, with the exception of **1**, the barrier height to interconversion for all propellerenes, relative to the C_2 conformer (see Eq. 3), is sufficiently high ($\Delta G^{\ddagger}$ > 24 kcal mol^{-1}) to prevent spontaneous isomerization at room temperature (Table S4.1).

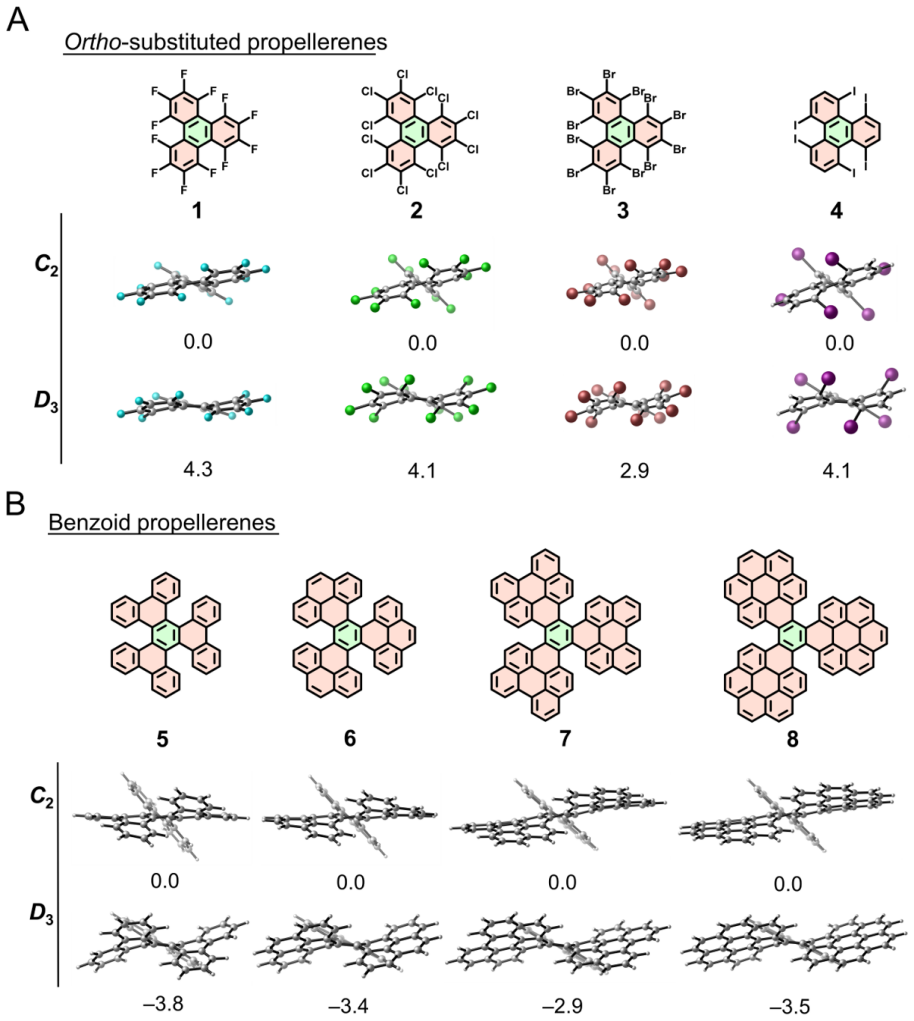


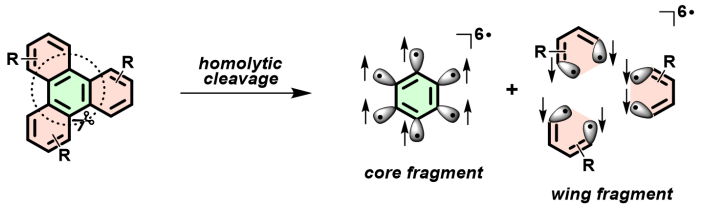
Figure 4.2 Structures and computed geometries of propellerenes **1-8** in the C_2 and D_3 conformation. The propellerenes have been grouped into the benzoid family (**1-4**; A) and the *ortho*-substituted family (**5-8**; B). The central rings have all been colored green and all wings have been colored red. Values provided below the structures are the Gibbs free energies (ΔG; kcal mol^{-1}) computed at PBE-D3(BJ)/6-31G(d,p), expressed relative to the energy of the C_2 conformer. For computational details see the Experimental.

Activation Strain Model. Having validated the computational method and having mapped the thermodynamic preference of the different propellerenes subclasses, attention is now directed at finding the origins of this preference. It was hypothesized that the balance between the intrinsic preferences of the core and the wings of a propellerene determines its most favorable conformation. To test this hypothesis, the activation strain model (ASM) was employed.[24] This computational model considers the rigidity of defined molecular fragments in a chemical system, as well as the ability of these fragments to interact with one another. Thus, in this model, the total energy of a system (ΔE_{tot}) is decomposed into a total strain term of all the molecular fragments (ΔE_{strain}), and an interaction energy term (ΔE_{int}):

$$\Delta E_{tot} = \Delta E_{strain} + \Delta E_{int} \qquad \text{(Eq. 1)}$$

Here, the strain energy, ΔE_{strain}, encompasses the penalty that needs to be paid in order to deform the molecular fragments from an initial state (here the C_2 conformation) to another state (here the D_3 conformation). The interaction energy term, ΔE_{int}, accounts for all the interactions that occur between these two molecular fragments in their different states (including both covalent and non-covalent interactions).

In the original ASM model, the different states of the molecular fragments are projected unto a reaction coordinate, typically describing bimolecular reactions,[25,26] (examples of dyotropic and cyclization reactions of unimolecular systems are also known in the literature).[27,28] However, for the present study, the ASM has to be extended to allow tracking of the changes in the ΔE_{strain} and ΔE_{int} terms experienced by *different parts of the same molecule*, in their two distinct conformations (Scheme 4.1). Therefore, to apply the ASM method in an insightful manner, the core and wings as defined above are designated as separate fragments. These are then cleaved homolytically to yield (uncharged) fragments with spins of +6 and –6 on the core and wings, respectively (Scheme 2). The analysis is then performed on the spin-restricted fragments in their spin-unrestricted electronic configuration. This approach is similar to that used by Krenske *et al.*[29-31] and others,[32] but differs in that in the present model, radicals are not capped and fragment geometries are not relaxed.



Scheme 4.1 Schematic representation of the homolytic cleavage of propellerenes to yield hexaradical core and wing fragments.

In the present model, the total energy of the propellerene system is further expressed as the sum of the strain experienced by the core ($\Delta E_{\text{strain}}^{\text{core}}$) and the wings fragments ($\Delta E_{\text{strain}}^{\text{wing}}$), and the interaction between them (ΔE_{int}; here primarily existing in the form of covalent C─C bonds). Equation 1 can thus be re-written as:

$$\Delta E_{\text{tot}} = \left(\Delta E_{\text{strain}}^{\text{core}} + \Delta E_{\text{strain}}^{\text{wing}}\right) + \Delta E_{\text{int}} \qquad \text{(Eq. 2)}$$

In the present study, all the energy terms are expressed with respect to the C_2 conformation (Eq. 3). As such, positive values of $\Delta\Delta E$ (as well as $\Delta\Delta G$ and $\Delta\Delta V$) indicate a preference for the C_2 conformation, whereas negative values represent a preference for the D_3 conformation.

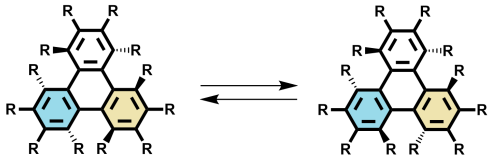
$$\Delta\Delta E = \Delta E_{\text{tot}}^{D_3} - \Delta E_{\text{tot}}^{C_2} \qquad \text{(Eq. 3)}$$

Table 4.1 summarizes the results of the activation strain analysis (ASA). A sharp contrast is found between the total strain ($\Delta E_{\text{strain}}^{\text{total}}$), which is always more stabilizing in the C_2 conformation (with exception of entry **1** discussed later), and the interaction energy term (ΔE_{int}) which is always less destabilizing in the C_2 conformation. Decomposition of the total strain energy terms into the strain energies of the individual fragments (Eq. 2), reveals the core to always be less destabilizing in the C_2 conformation, whereas the wings are generally more destabilizing in this conformation. Exception to this is, again, perfluorotriphenylene **1**, whose wing strain shows a minor preference for the D_3 conformation.

Before further explaining these observations, it is important to reiterate that the wings in a propellerene molecule can only adopt two, geometrically possible arrangements, resulting in either a C_2 or D_3 symmetry of the propellerene molecule. The core, which is formed from the joining together of these wings, is therefore forced to adopt either a twist-boat or chair-like geometry, respectively (see Fig. 4.1 and 4.2). In other words, *the arrangement of the wings dictates the shape of the core*.

The wings. The aromatic wings of propellerenes have an intrinsic preference to be flat, yet their merger into a single molecule forces them to geometrically concede. Indeed, as highlighted in Figure 4.3, in the D_3 conformation, the wings are by and large planar, and thus unstrained, whereas steric congestion of the wings in the C_2 conformation necessitates a significant distortion from planarity. This desire of the wings to be flat is quantitatively reflected in their general preference for a D_3 conformation (Table 4.2). For the *ortho*-substituted propellerenes (**1** – **4**) a trend in $\Delta E_{\text{strain}}^{\text{wing}}$ is additionally found whereby an increase in the size of the substituents gives rise to an increase in destabilizing wing strain as F < Cl < Br < I, whereas for benzoid propellerenes no clear trend is observed. Propellerene **1** does not follow the general observation that the wings of propellerenes prefer a D_3 conformation of the molecule. It is observed that in **1** the rings directly attached to the propellerene core are more planar in the C_2 conformation than in the D_3 conformation, whereas the

Table 4.1 Activation strain and energy decomposition analysis of propellerenes **1-8**. All energies (kcal mol^{-1}) are computed at ZORA-PBE-D3(BJ)/TZ2P//PBE-D3(BJ)/6-31G(d,p) and are reported with respect to the C_2 conformation.



	$\Delta\Delta E$	$\Delta\Delta E^{\text{total}}_{\text{strain}}$	$\Delta\Delta E^{\text{core}}_{\text{strain}}$	$\Delta\Delta E^{\text{wing}}_{\text{strain}}$	$\Delta\Delta E_{\text{int}}$	$\Delta\Delta E_{\text{Pauli}}$	$\Delta\Delta V_{\text{elstat}}$	$\Delta\Delta E_{\text{oi}}$
1	5.0	1.2	0.9	0.4	3.8	–53.5	21.7	35.5
2	4.3	–2.3	1.9	–4.2	6.5	–74.9	34.3	47.1
3	3.1	–3.1	2.5	–5.6	6.3	–58.0	30.1	34.0
4	4.2	–3.2	3.3	–6.4	7.3	–135.6	45.0	97.8
5	–3.9	–6.9	1.5	–8.4	3.0	–52.2	22.8	32.4
6	–3.1	–5.0	1.3	–6.3	1.9	–48.2	19.5	30.6
7	–2.9	–4.8	2.1	–6.9	1.9	–49.6	18.6	32.8
8	–3.4	–5.1	1.0	–6.1	1.7	–59.8	21.8	39.7

substituents attached thereto (*i.e.* F) are bend more out-of-plane, than they are in the D_3 conformer. The balance between these two factors results in a preference for the C_2 conformation. It is important to note that *this balancing game is only possible for ortho-substituted wings, due to the relative flexibility of the unitary benzene ring, whereas benzoid extended wings are too rigid, and these will therefore always show a D_3 preference.*

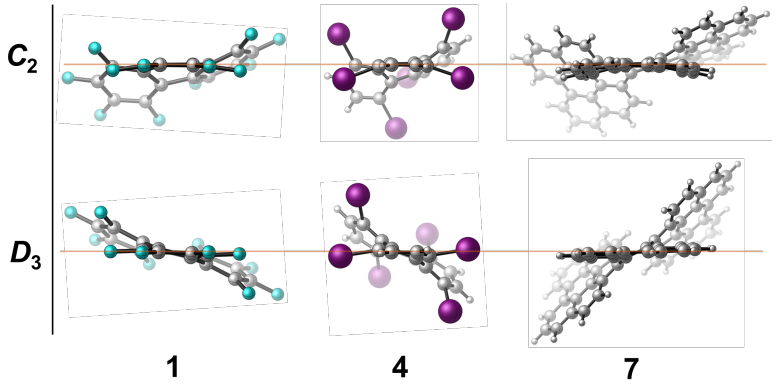


Figure 4.3 Side-view of propellerene **1**, **4** and **7**. Brown lines highlight the different extents of deformation (*i.e.* out-of-plane bending of the wings) in the C_2 conformation, compared to their relative planarity in the D_3 conformation.

The radial bonds. Within the ASM, the interaction energy term (ΔE_{int}) describes the interaction between two defined molecular fragments. In the present propellerene model, this constitutes the interaction between the core and wing fragments, and thus primarily concerns the covalent C─C bonds connecting the two fragments together. To better understand the interaction energy term, it can be decomposed into physically meaningful energy terms using a canonical energy decomposition analysis (EDA), to allow its analysis within the Kohn-Sham molecular orbital theory (KS-MO).[33-35] The EDA decomposes the ΔE_{int} into the following four physically meaningful energy terms:

$$\Delta E_{int} = \Delta V_{elstat} + \Delta E_{Pauli} + \Delta E_{oi} + \Delta E_{disp} \quad \text{(Eq. 4)}$$

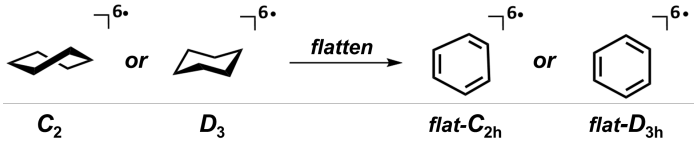
Herein, ΔV_{elstat} is the electrostatic interaction between the unperturbed charge distributions of the (deformed) reactants and is usually attractive, ΔE_{Pauli} encompasses the destabilizing the Pauli repulsion between occupied closed-shell orbitals of both fragment, ΔE_{oi}, accounts for orbital interactions in the form of polarization and charge transfer between the fragments (*i.e.* HOMO–LUMO interactions) and ΔE_{disp} represents classical dispersion interactions between the fragments.

Looking at the radial bonds which connect the propellerene wings to the core, it is observed that they are shorter in the C_2 conformation than in the D_3 conformation, on the order of 0.01 Å. To verify whether observed trends in interaction energy between the wings and core (Table 4.1) originate from bond lengths alone, or whether the geometry of the bond attachment is of also importance, consistent geometry computations were performed. The radial bonds of propellerenes in their D_3 conformer were thus artificially shortened to be of the same length as in their corresponding C_2 conformer. This expectedly gave more stabilizing interaction energy as a result of more stabilizing ΔV_{elstat} and ΔE_{oi} terms, despite also giving more destabilizing ΔE_{Pauli}. Importantly, although absolute differences in ΔE_{int} between the two conformations became smaller, identical trends were still observed, indicating that the trends in ΔE_{int} (Table 4.1) are dictated by the way in which the radial bonds are attached, rather than by their lengths. Namely, in the C_2 conformation, the twist-boat geometry of the core allows two of the wings to join in an almost coplanar fashion, whereas in the D_3 conformation the chair-like geometry of the ring dictates a more skewed attachment of the wings (Fig. 4.1; highlighted pink and yellow). As a result, the orbital overlap is less favorable in the more skewed D_3 conformation, compared to the C_2 conformation.

It was additionally noted that, as the radial bonds were shortened to that of the C_2 conformer, the total strain of the propellerenes became more destabilizing, located solely on the wings. This is due to the fact that, as the radial bonds are shortened, the wings approach each other at closer distances, and despite the differences in radial bond length being only minute, an increase in destabilizing strain of up to 19.5 kcal mol^{-1} was found in the case of 6. When radial bonds in C_2 conformers were artificially lengthened, an opposite effect was found.

The core. Conversely with the radial bonds, the C—C bonds within the core of propellerenes are always longer in the C_2 conformation than in the D_3 conformation; *i.e.* the core of the C_2 conformer is larger than that of the D_3 conformer. To understand whether the preference of the core for a C_2 conformation is due to these differences in bond length or whether it stems from an intrinsic preference for the geometry of a twist-boat conformation, a numerical experiment was performed. Bond lengths of propellerene core fragments in their C_2 and D_3 conformation were constrained and all dihedral angles were artificially set to 0°, forcing the rings to become flat. Surprisingly, absolute differences in total energy diminished, and even shifted in favor of the D_3 conformation (Table 4.2). As an exemplary experiment, when the bare core was allowed to relax further, without constrains, bond lengths became even shorter and a planar, benzene-like molecule was obtained. Thus, the core of a propellerene molecule ideally wants to have shorter C—C bonds, however, in the context of a propellerene is geometrically prohibited from doing so by the presence of the wings. These findings reinforce the notion that that the conformation of the core is enforced by the wings, rather than the other way around, and corrects the previous assertion of Pascal *et al.* that "*the core geometry is not a product of the conformation*".[10,36-41]

Table 4.2 Numerical experiments on the core fragments of propellerenes **1-8**. $\Delta\Delta E_{int}$ denotes the difference in single point energy of the core after planarization with fixed bond lengths, compared to that computed in their original C_2 and D_3 conformation. All energies computed at ZORA-PBE-D3(BJ)/TZ2P//PBE-D3(BJ)/6-31G(d,p) (kcal mol^{-1}), reported with respect to the $C_2 \rightarrow D_3$ conversion.

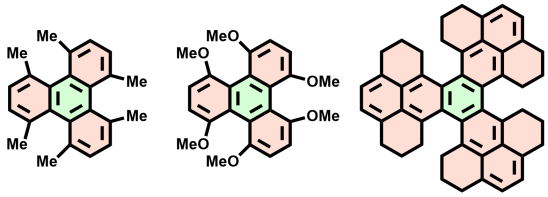


	$\Delta\Delta E_{int}$
1	–0.9
2	–1.3
3	–3.6
4	–1.5
5	–0.3
6	–0.3
7	–0.8
8	–4.9

Combining the ASM and EDA analyses, it can be concluded that propellerenes have two choices: (i) either have shorter radial bonds between the wings and the core, resulting in more stabilizing interaction energy between the wings and core, however also more congested wings (more destabilizing steric repulsion between the wings), or (ii) have longer radial bonds, giving rise to less stabilizing ΔE_{int}, while also giving less congested wings (less destabilizing steric repulsion between the wings). In other words, the balance at play is not so much between the core and the wings, but between the wings and the bonds connecting them to the core. Furthermore, when wings of the propellerene are rigid (*i.e.* benzoid triphenylenes), a D_3 conformation will always be preferred, as this conformation minimizes steric repulsion between the wings, which is able to overcome the intrinsic C_2 preference of the core and radial bonds. In contrast, the relative flexibility of *ortho*-substituted wings results in a lesser degree of D_3 preference or even a C_2 preference, and which allows the core and radial bonds to dictate the adaptation of a C_2 conformation. It is this dichotomy that uniquely sets benzoid propellerenes apart from the ortho-substituted family. This interplay is graphically illustrated in Figure S4.3.

Model validation. To validate this hypothesis, additional molecules (**9** – **11**) were selected and analysed using the present model (Table 4.3). These molecules all have alkyl substituents on the *ortho* position. It is observed that compound 9 follows the general trend observed for the halogenated propellerenes (Table 4.2), i.e. the wings prefer a D_3 conformation, whereas the core and radial bonds prefer a C_2 conformation, the latter term of which is able to overcompensate the total strain term. Compounds **9** and **11**, however behave more like perfluorotriphenylene **1** in which all terms, including the wings, prefer a C_2 conformation. This is accounted for by the present model, as the preference of *ortho* substituted propellerenes for a C_2 conformation is related to the ability of the substituents to bend. Compound **11** is a particularly interesting case, being the hydrogenated variant of **2**, which prefers a D_3 conformation. In other words, upon hydrogenation of **2**, the *ortho*-carbons of the wings change from sp^2 to sp^3, making them more flexible, causing a shift in preference from D_3 to C_2. To further illustrate this point, the structure of an extreme example, hexa-adamantyltriphenylene **12** was also computed (Figure S4.4). It was found that, despite belonging to the *ortho*-substituted family of propellerenes, **12** still prefers a D_3 conformation. This is because the extreme steric bulk of the adamantyl moieties prevents them from bending out-of-plane.

Table 4.2 Activation strain and energy decomposition analysis of propellerenes **9** – **11**. All energies (kcal mol^{-1}) are computed at ZORA-PBE-D3(BJ)/TZ2P//PBE-D3(BJ)/6-31G(d,p) and are reported with respect to the C_2 conformation.



9 **10** **11**

	$\Delta\Delta E$	$\Delta\Delta E^{\text{total}}_{\text{strain}}$	$\Delta\Delta E^{\text{core}}_{\text{strain}}$	$\Delta\Delta E^{\text{wing}}_{\text{strain}}$	$\Delta\Delta E_{\text{int}}$	$\Delta\Delta E_{\text{Pauli}}$	$\Delta\Delta V_{\text{elstat}}$	$\Delta\Delta E_{\text{oi}}$
9	4.9	3.3	3.3	0.0	1.6	–133.3	52.6	88.2
10	3.3	–4.3	2.7	–7.0	7.6	168.2	–35.4	–125.0
11	4.2	2.8	2.4	0.4	1.4	61.9	–22.0	–38.9

Combined, based on the ASA, it is found that the integral propellerene parts all share the same characteristics in both propellerene families. Importantly, it is the magnitude of the interaction energy between the core and the wings that varies most between the two families, and ultimately lays at the heart of the sharp contrast in conformational preference between *ortho*- and benzoid-substituted propellerenes. The magnitude of the interaction energy is, in turn, dictated by the flexibility of the propellerene wings. When wings are relatively flexible (*i.e*. *ortho*-substituted propellerenes) they are able to adopt a more distorted C_2 conformation, allowing for shorter radial bonds between the core and the wings, with concomitantly more a stabilizing interaction energy. In contrast, more rigid wings cannot deform sufficiently (*i.e*. benzoid-substituted propellerenes), and thus necessitate longer radial bonds to avoid steric clash between the wings, and incurring less stabilizing interaction energy (Fig. 4.4). This interplay between the flexibility of the wings and length of the radial bonds is graphically illustrated in Figure 4.5. There it is apparent that for *ortho*-substituted propellerenes, conversion from the C_2 conformation to the D_3 conformation is associated with flatter wings (favorable) but also longer radial bonds (unfavorable), whereas for the benzoid-substituted propellerenes there is hardly any change in radial bond length during interconversion, and the preference for a D_3 conformation is thus purely dictated by the relative planarity of the wings in the two conformations.

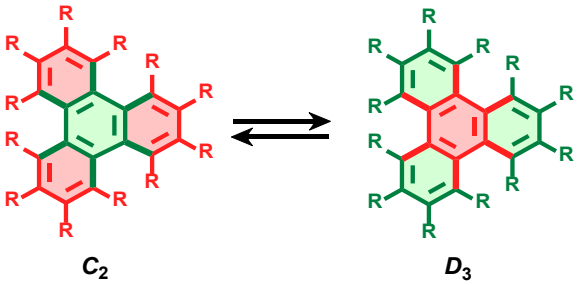


Figure 4.4. Schematic overview of the $C_2 \rightleftarrows D_3$ interconversion of propellerenes to graphically illustrate that the wings of propellerenes prefer to adopt the D_3 conformation, whereas the radial bonds and core want to reside in a more distorted C_2 conformation. The green color indicates that the fragment prefers the specific conformation, while the opposite is true for the red color. Radial bonds drawn in bold.

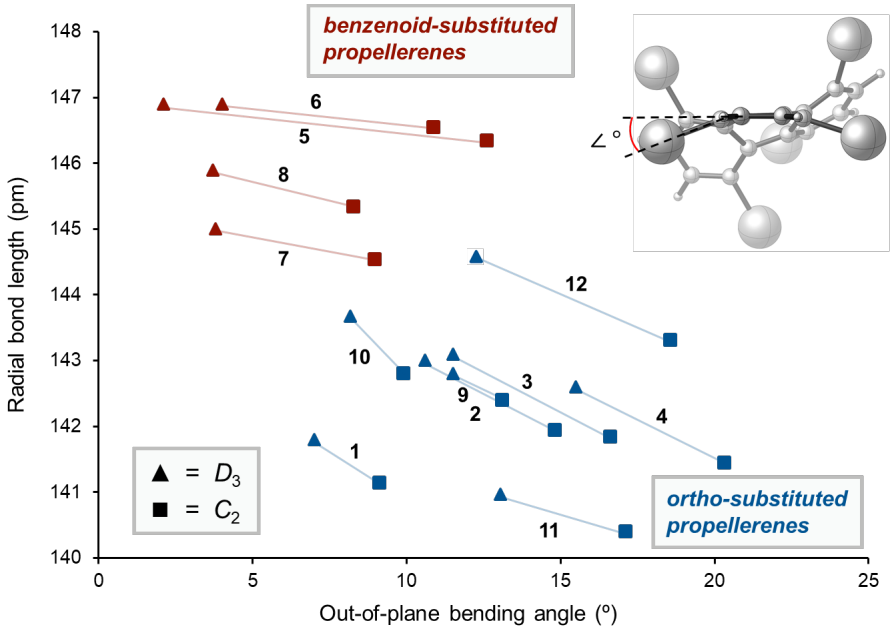


Figure 4.5. Plot of the average radial bond length as a function of the average bending angle of wings of propellerenes **1**-**8** in the C_2 and D_3 conformation. Compounds and conformations are groups as: benzoid-C_2 (brown squares), benzoid-D_3 (brown triangles), *ortho*-C_2 (blue squares) and *ortho*-D_3 (blue triangles). The definition of the out-of-plane bending angle is illustrated in the top right corner.

To conclude, the conformational preference of propeller-shaped polycyclic aromatic hydrocarbons has been the topic of heavy debate. Triphenylene-class propellerenes with substituents on the *ortho*-position prefer to adopt a conformation with a C_2 conformation, whereas those with benzoid substituents prefer to adopt a D_3 conformation. Herein, a comprehensible framework is provided that rationalizes the driving forces behind the conformational preference of a range of structurally diverse propellerenes.

The origin of the thermodynamic preference of propellerenes could be quantified using a novel adaptation of the activation strain model (ASM). By strategically fragmenting propellerene molecules, it is found that both the core and wings of propellerenes desire to be flat, however, their merger necessitates significant deformation, away from their ideal geometry, to minimize steric interactions between the wings. The desire of the wings for the D_3 conformation to always be greater than the desire of the core for a C_2 conformation. Attention is therefore shifted to the radial bonds, which connect the core and wings together. These were also found to always prefer a C_2 conformation and, in the case of *ortho*-substituted propellerenes, are even able to overrule the preference of the wings. It was ultimately concluded that the balance at play in propellerenes is between *the extent to which the wings can bend and the radial bonds can contract*. When wings are flexible, a C_2 conformation will be preferred, when wings are rigid, a D_3 conformation will always be preferred.

These findings will equip experimentalists with the insight to understand and rationalize the trends in conformational behavior of propellerenes and allow the tailor-made design of novel sterically congested structures. Although applied here only to propellerenes, the present methodology is broadly applicable and will open up new avenues not only in the field of PAH research but in the field of physical chemistry at large, and should prove useful in the rational design of novel functional constructs.

References

(1) Hursthouse, M. B.; Smith, V. B.; Massey, A. G. The crystal and molecular structure of dodecafluorotriphenylene, C18F12. *J. Fluor. Chem.* **1977,** *10* (2), 145.

(2) Campbell, M. C.; Humphries, R. E.; Munn, N. M. Perchlorotriphenylene: a compound with severe molecular twisting? *J. Org. Chem.* **1992,** *57* (2), 641.

(3) Gall, J. H.; MacNicol, D. D.; Mallinson, P. R.; Welsh, P. A. Discovery and crystal structure of a novel chlorocarbon host: perchlorofluorene-9-spirocyclohexa-2′,5′-diene. *Tet. Lett.* **1985,** *26* (33), 4005.

(4) Shibata, K.; Kulkarni, A. A.; Ho, D. M.; Pascal Jr, R. A. Perchlorotriphenylene. *J. Am. Chem. Soc.* **1994,** *116* (13), 5983.

(5) Shibata, K.; Kulkarni, A. A.; Ho, D. M.; Pascal Jr, R. A. The Pursuit of Perchlorotriphenylene. *J. Org. Chem.* **1995,** *60* (2), 428.

(6) In their study, Pascal *et al.* considered only the carbon framework when commenting on the relative planarity of the wings. In the present study, the out-of-plane bending of the ortho substituents is also included.

(7) Chen, L.; Zhang, C.; Wen, C.; Zhang, K.; Liu, W.; Chen, Q. Gold-catalyzed cyclotrimerization of arynes for the synthesis of triphenylenes. *Catal. Commun.* **2015,** *65*, 81.

(8) Wang, Y.; Stretton, A. D.; McConnell, M. C.; Wood, P. A.; Parsons, S.; Henry, J. B.; Mount, A. R.; Galow, T. H. 1,4,5,8,9,12-hexamethyltriphenylene. A molecule with a flipping twist. *J. Am. Chem. Soc.* **2007,** *129* (43), 13193.

(9) Tan, Q.; Zhou, D.; Zhang, T.; Liu, B.; Xu, B. Iodine-doped sumanene and its application for the synthesis of chalcogenasumanenes and silasumanenes. *Chem. Comm.* **2017,** *53* (74), 10279.

(10) Barnett, L.; Ho, D. M.; Baldridge, K. K.; Pascal, R. A. The Structure of Hexabenzotriphenylene and the Problem of Overcrowded "D3h" Polycyclic Aromatic Compounds. *J. Am. Chem. Soc.* **1999,** *121* (4), 727.

(11) Balaban, A. T.; Randić, M. *Structural approach to aromaticity and local aromaticity in conjugated polycyclic systems*; Springer, 2011.

(12) Smith, V. B.; Massey, A. G. Perfluorophenyl derivatives of the elements—XXII: Perfluorotriphenylene. *Tetrahedron* **1969,** *25* (22), 5495.

(13) Coe, P. L.; Stephens, R.; Tatlow, J. C. 622. Aromatic polyfluoro-compounds. Part XI. Pentafluoro-phenyl-lithium and derived compounds. *J. Chem. Soc. (Resumed)* **1962**, 3227.

(14) Falk, R. A. Hexafluorobenzene and related fluoroaromatic compounds (Thermal and radiation stability of aromatic fluorocarbons makes them useful as plastics, lubricants, hydraulic and gyroscopic fluids and heat transfer fluids for nuclear powerplants). *Sperry Eng. Rev.* **1963,** *16*, 24.

(15) Naritomi, M.; Murofushi, H.; Nakashima, N. Dopants for a perfluorinated graded index polymer optical fiber. *Bull. Chem. Soc. Jap.* **2004,** *77* (11), 2121.

(16) Frampton, C. S.; MacNicol, D. D.; Rowan, S. J. Synthesis and structural properties of the first dodecakis (aryloxy) triphenylenes. *J. Mol. Struct.* **1997,** *405* (2-3), 169.

(17) Nishinaga, T.; Inoue, R.; Matsuura, A.; Komatsu, K. Formation of a novel arenium ion from the radical cation of a twisted triphenylene fully annelated with bicyclo [2.2. 2] octene units. *Org. Lett.* **2002,** *4* (9), 1435.

(18) Li, Z.; Zhi, L.; Lucas, N. T.; Wang, Z. Triangle-shaped polycyclic aromatics based on tribenzocoronene: facile synthesis and physical properties. *Tetrahedron* **2009,** *65* (17), 3417.

(19) Hosokawa, T.; Takahashi, Y.; Matsushima, T.; Watanabe, S.; Kikkawa, S.; Azumaya, I.; Tsurusaki, A.; Kamikawa, K. Synthesis, structures, and properties of hexapole helicenes: Assembling six [5]helicene substructures into highly twisted aromatic systems. *J. Am. Chem. Soc.* **2017,** *139* (51), 18512.

(20) Berezhnaia, V.; Roy, M.; Vanthuyne, N.; Villa, M.; Naubron, J.-V. r.; Rodriguez, J.; Coquerel, Y.; Gingras, M. Chiral nanographene propeller embedding six enantiomerically stable [5]helicene units. *J. Am. Chem. Soc.* **2017,** *139* (51), 18508.

(21) Zuzak, R.; Castro-Esteban, J.; Brandimarte, P.; Engelund, M.; Cobas, A.; Piątkowski, P.; Kolmer, M.; Pérez, D.; Guitián, E.; Szymonski, M. Building a 22-ring nanographene by combining in-solution and on-surface syntheses. *Chem. Comm.* **2018,** *54* (73), 10256.

(22) Peña, D.; Cobas, A.; Pérez, D.; Guitián, E.; Castedo, L. Kinetic control in the palladium-catalyzed synthesis of C_2-symmetric hexabenzotriphenylene. A conformational study. *Org. Lett.* **2000,** *2* (11), 1629.

(23) Pradhan, A.; Dechambenoit, P.; Bock, H.; Durola, F. Twisted polycyclic arenes by intramolecular Scholl reactions of C_3-symmetric precursors. *J. Org. Chem.* **2013,** *78* (6), 2266.

(24) For a step-by-step protocol, see: a) P. Vermeeren, S. C. C. van der Lubbe, C. Fonseca Guerra, F. M. Bickelhaupt, T. A. Hamlin, *Nat. Protoc.* **2020**, *15*, 649; for reviews, see: b) F. M. Bickelhaupt, *J. Comp. Chem.* **1999**, *20*, 114; c) W.-J. van Zeist, F. M. Bickelhaupt, *Org. Biomol. Chem.* **2010**, *8*, 3118; d) I. Fernández, F. M. Bickelhaupt, *Chem. Soc. Rev.* **2014**, *43*, 4953; e) L. P. Wolters, F. M. Bickelhaupt, *WIRES Comput. Mol. Sci.* **2015**, 5, 324; f) F. M. Bickelhaupt, K. N. Houk, *Angew. Chem.* **2017**, *129*, 10204; *Angew. Chem. Int. Ed.* **2017**, *56*, 10070.

(25) Vermeeren, P.; Hansen, T.; Grasser, M.; Silva, D. R.; Hamlin, T. A.; Bickelhaupt, F. M. SN2 versus E2 competition of F– and PH2– revisited. *J. Org. Chem.* **2020,** *85* (21), 14087.

(26) Vermeeren, P.; Hansen, T.; Jansen, P.; Swart, M.; Hamlin, T. A.; Bickelhaupt, F. M. A unified framework for understanding nucleophilicity and protophilicity in the SN2/E2 competition. *Chem.-Eur. J.* **2020,** *26* (67), 15538.

(27) Fernández, I.; Bickelhaupt, F. M.; Cossío, F. P. Ene-ene-yne reactions: Activation strain analysis and the role of aromaticity. *Chem. Eur. J.* **2014,** *20* (34), 10791.

(28) Fernández, I.; Bickelhaupt, F. M.; Cossío, F. P. Type-I dyotropic reactions: understanding trends in barriers. *Chem. Eur. J.* **2012,** *18* (39), 12395.

(29) Krenske, E. H.; Houk, K. N.; Holmes, A. B.; Thompson, J. Entropy versus tether strain effects on rates of intramolecular 1,3-dipolar cycloadditions of *N*-alkenylnitrones. *Tet. Lett.* **2011,** *52* (17), 2181.

(30) Krenske, E. H.; Davison, E. C.; Forbes, I. T.; Warner, J. A.; Smith, A. L.; Holmes, A. B.; Houk, K. N. Reverse cope elimination of hydroxylamines and alkenes or alkynes: theoretical investigation of tether length and substituent effects. *J. Am. Chem. Soc.* **2012,** *134* (4), 2434.

(31) Krenske, E. H.; Perry, E. W.; Jerome, S. V.; Maimone, T. J.; Baran, P. S.; Houk, K. N. Why a Proximity-Induced Diels–Alder Reaction is So Fast. *Org. Lett.* **2012,** *14* (12), 3016.

(32) Gold, B.; Shevchenko, N. E.; Bonus, N.; Dudley, G. B.; Alabugin, I. V. Selective transition state stabilization via hyperconjugative and conjugative assistance: stereoelectronic concept for copper-free click chemistry. *J. Org. Chem.* **2011,** *77* (1), 75.

(33) Bickelhaupt, F. M.; Baerends, E. J.; John Wiley and Sons New York, NY, USA, 2000; Vol. 15.

(34) Van Meer, R.; Gritsenko, O. V.; Baerends, E. J. Physical meaning of virtual Kohn–Sham orbitals and orbital energies: an ideal basis for the description of molecular excitations. *J. Chem. Theo. Comp.* **2014,** *10* (10), 4432.

(35) a) Zhao, L.; von Hopffgarten, M.; Andrada, D. M. *WIRES Comput. Mol. Sci.* **2018**, *8*, e1345; b) G. Frenking, FM Bickelhaupt. *The EDA Perspective of Chemical Bonding in The Chemical Bond. Fundamental Aspects of Chemical Bonding* **2014,** *4*, 121.

(36) Although the exact reason for the preference of the core for a C_2 conformation could not be elucidated, these findings corroborate those made by others which found the central ring of propellerenes to be poorly or even non-aromatic; *i.e.* aromaticity and thus a drive to planarity are not significant factors in determining the conformational preference of the core in the context of a propellerene molecule. See the following references.

(37) Fernandez, I.; Frenking, G. Direct estimate of conjugation and aromaticity in cyclic compounds with the EDA method. *Faraday Discuss.* **2007,** *135*, 403.

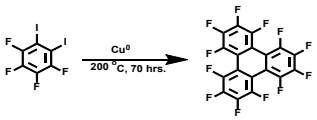
(38) Pierrefixe, S. C. A. H.; Bickelhaupt, F. M. Aromaticity: molecular-orbital picture of an intuitive concept. *Chem. Eur. J.* **2007,** *13* (22), 6321.
(39) Roy, M.; Berezhnaia, V.; Villa, M.; Vanthuyne, N.; Giorgi, M.; Naubron, J. V.; Poyer, S.; Monnier, V.; Charles, L.; Carissan, Y. Stereoselective syntheses, structures, and properties of extremely distorted chiral nanographenes embedding hextuple helicenes. *Angew. Chem. Int. Ed.* **2020,** *59* (8), 3264.
(40) Antić, M.; Furtula, B.; Radenkovic, S. Aromaticity of nonplanar fully benzenoid hydrocarbons. *J. Phys. Chem. A* **2017,** *121* (18), 3616.
(41) Hosokawa, T.; Tsurusaki, A.; Kamikawa, K. Assembly of [5]helicene subunits by palladium-catalyzed reactions: Synthesis, structures, properties, and theoretical study of multiple helicenes. *J. Synth. Org. Chem. Jap.* **2020,** *78* (11), 1013.
(42) Chang, N.-h.; Chen, X.-c.; Nonobe, H.; Okuda, Y.; Mori, H.; Nakajima, K.; Nishihara, Y. Synthesis of substituted picenes through Pd-catalyzed cross-coupling reaction/annulation sequences and their physicochemical properties. *Org. Lett.* **2013,** *15* (14), 3558.
(43) Macrae, C. F.; Sovago, I.; Cottrell, S. J.; Galek, P. T. A.; McCabe, P.; Pidcock, E.; Platings, M.; Shields, G. P.; Stevens, J. S.; Towler, M. Mercury 4.0: From visualization to analysis, design and prediction. *J. Appl. Crystallogr.* **2020,** *53* (1), 226.
(44) Shao, Y.; Molnar, L. F.; Jung, Y.; Kussmann, J.; Ochsenfeld, C.; Brown, S. T.; Gilbert, A. T. B.; Slipchenko, L. V.; Levchenko, S. V.; O'Neill, D. P. Advances in methods and algorithms in a modern quantum chemistry program package. *Phys. Chem. Chem. Phys.* **2006,** *8* (27), 3172.
(45) Frisch, M. J.; Trucks, G. W.; Schlegel, H. B.; Scuseria, G. E.; Robb, M. A.; Cheeseman, J. R.; Scalmani, G.; Barone, V.; Mennucci, B.; Petersson, G. A. Gaussian 09 Revision D. 01, 2009. *Gaussian Inc. Wallingford CT* **2009**.
(46) PBE was used as both exchange and correlation functional, and was called using the pbepbe keyword in the Gaussian 09 software. At the DFT-D3(BJ) level of theory the s6 and s8 values are set to 1 and 0.7875 respectively, whereas the ABJ1 and ABJ2 values are set respectively to 0.4289 and 4.4407.
(47) Grimme, S.; Antony, J.; Ehrlich, S.; Krieg, H. A consistent and accurate ab initio parametrization of density functional dispersion correction (DFT-D) for the 94 elements H-Pu. *J. Chem. Phys.* **2010,** *132* (15), 154104.
(48) Grimme, S.; Ehrlich, S.; Goerigk, L. Effect of the damping function in dispersion corrected density functional theory. *J. Comp. Chem.* **2011,** *32* (7), 1456.
(49) Hay, P. J.; Wadt, W. R. Ab initio effective core potentials for molecular calculations. Potentials for K to Au including the outermost core orbitals. *J. Chem. Phys.* **1985,** *82* (1), 299.
(50) Karton, A. How reliable is DFT in predicting relative energies of polycyclic aromatic hydrocarbon isomers? comparison of functionals from different rungs of jacob's ladder. *J. Comp. Chem.* **2017,** *38* (6), 370.
(51) Minenkov, Y.; Singstad, Å.; Occhipinti, G.; Jensen, V. R. The accuracy of DFT-optimized geometries of functional transition metal compounds: a validation study of catalysts for olefin metathesis and other reactions in the homogeneous phase. *Dalton T.* **2012,** *41* (18), 5526.
(52) Sperger, T.; Fisher, H. C.; Schoenebeck, F. Computationally deciphering palladium-catalyzed reaction mechanisms. *WIRES Comp. Mol. Sci.* **2016,** *6* (3), 226.
(53) Josa, D.; Rodríguez-Otero, J.; Cabaleiro-Lago, E. M.; Rellán-Piñeiro, M. Analysis of the performance of DFT-D, M05-2X and M06-2X functionals for studying π···π interactions. *Chem. Phys. Lett.* **2013,** *557*, 170.
(54) Marenich, A. V.; Cramer, C. J.; Truhlar, D. G. Universal solvation model based on solute electron density and on a continuum model of the solvent defined by the bulk dielectric constant and atomic surface tensions. *J. Phys. Chem. B* **2009,** *113* (18), 6378.
(55) Bootsma, A. N.; Wheeler, S. E. Popular Integration Grids Can Result in Large Errors in DFT-Computed Free Energies. *ChemRxiv. Preprint* **2019**.

(56) Ribeiro, R. F.; Marenich, A. V.; Cramer, C. J.; Truhlar, D. G. Use of solution-phase vibrational frequencies in continuum models for the free energy of solvation. *J. Phys. Chem. B* **2011,** *115* (49), 14556.
(57) Funes-Ardoiz, I.; Paton, R. S. **2016**. GoodVibes: GoodVibes v1.0.2. http://doi.org/10.5281/zenodo.595246.
(58) Legault, C. Y. *CYLview, 1.0 b, Université de Sherbrooke, 2009*, 2013.
(59) ADF2017.103, SCM Theoretical Chemistry, Vrije Universiteit : Amsterdam (Netherlands), **2010**. http://www.scm.com.
(60) te Velde, G.; Bickelhaupt, F. M.; Baerends, E. J.; Fonseca Guerra, C.; Van Gisbergen, S. J. A.; Snijders, J. G.; Ziegler, T. Chemistry with ADF. *J. Comp. Chem.* **2001,** *22* (9), 931.
(61) Fonseca Guerra, C.; Snijders, J. G.; te Velde, G.; Baerends, E. J. Towards an order-N DFT method. *Theo. Chem. Acc.* **1998,** *99* (6), 391.
(62) Cosmo, R.; Sternhell, S. Steric effects. Inversion of 4,5-disubstituted 9,10-dihydrophenanthrenes. *Austr. J. Chem.* **1987,** *40* (1), 35.
(63) Cosmo, R.; Hambley, T. W.; Sternhell, S. Skeletal deformation in 4,5-disubstituted 9, 10-dihydrophenanthrenes and 4, 5-disubstituted phenanthrenes. *J. Org. Chem.* **1987,** *52* (14), 3119.
(64) Based on the absence of observable interconversion after 20 hrs at 70 °C.

Experimental

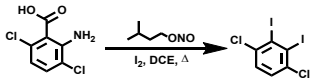
Synthesis. All reagents were obtained from commercial sources and were used as received. Solvents used were stored over 4 Å molecular sieves. Reactions were monitored by TLC analysis using Merck 25 DC plastikfolien 60 F254 with detection by using an aqueous solution of $KMnO_4$ (7%) and K_2CO_3 (2%) followed by charring at ~150 °C. Column chromatography was performed on Fluka silica gel (0.04–0.063 mm). High-resolution mass spectra were recorded by direct injection (2 µL of a 2 µM solution in water/acetonitrile; 50:50; v/v and 0.1% formic acid) on a mass spectrometer (Thermo Finnigan LTQ Orbitrap) equipped with an electrospray ion source in positive mode (source voltage 3.5 kV, sheath gas flow 10, capillary temperature 250 °C). The high-resolution mass spectrometer was calibrated prior to measurements with a calibration mixture (Thermo Finnigan). All NMR experiments were performed on a Bruker AV500 NMR instrument equipped with a BBFO probe head for 5 mm outer diameter tubes. Spectra were recorded at 500 MHz for ^{1}H, 125 MHz for ^{13}C and 470 MHz for ^{19}F. All deuterated solvents were obtained from a commercial source (Eurisotop) and were used as received. Chemical shifts are given in ppm (δ) relative to TMS (0 ppm), and coupling constants (*J*) are given in hertz (Hz). For synthetic procedures and NMR data related to HBT (**5**) and tripyrenylene (**6**) see the previous Chapter.

Perfluorotriphenylene (1)[12]



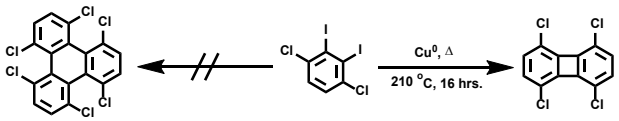
A crimp top vial, which had been flame dried under vacuum, was charged with an intimate mixture of 1,2-diiodotetrafluorobenzene (3 g, 2.5 mmol) and copper powder (3 g). The tube was sealed, evacuated to high vacuum (< 1 mbar) and then heated on a metal block to 200°C for 70 hrs. After cooling down to room temperature, the tube was backfilled with argon and opened. The sublimate of colorless to pale pink crystals was removed and identified as nearly pure perfluorotriphenylene (217 mg, 0.49 mmol, 19.6%). ^{13}C NMR (125 MHz, THF-d_8) δ 143.8 (dt, $^1J_{CF}$ = 260 Hz, $^3J_{CF}$ = 13 Hz), 140.9 (dd, $^1J_{CF}$ = 264 Hz, $^3J_{CF}$ = 11 Hz), 121.1 (br t, $^2J_{CF}$ = 9.5 Hz); ^{19}F NMR (471 MHz, THF-d_8) δ -141.7 (d, $^3J_{FF}$ = 13 Hz), -152.2 (d, $^3J_{FF}$ = 13 Hz). MALDI-TOF calc'd 444.1788 m/z, found 444.659 m/z.

1,4-Dichloro-2,3-diiodobenzene (13)[42]



A solution of isoamyl nitrite (1.6 mL, 1.40 g, 6 mmol) and iodine (4.54 g, 5 mmol) in 1,2-dichloroethane (200 mL) was heated to reflux and a solution of 2,5-dichloroanthranilic acid (1.03 g, 2.5 mmol) in dioxane (25 mL) added over a period of 20 min. The mixture was refluxed for 1h, then cooled and filtered. The filtrate was washed with aqueous 5% $Na_2S_2O_4$ (2x 50ml), 1M HCl (1x 25 mL) and brine (1x 25 mL). The organic layer was dried over $MgSO_4$, filtered and evaporated to dryness. The residue was purified by column chromatography over silica gel using neat pentane as eluent to provide 1,4-dichloro-2,3-diiodobenzene as a white crystalline solid. Yield: 1.0 g, 2.5 mmol, quant. ^{1}H NMR (500MHz, $CDCl_3$) δ 7.42 (s, 2H). ^{13}C NMR (125MHZ, $CDCl_3$) δ 137.03, 129.28, 114.97.

1,4,5,8,9,12-Hexachlorotriphenylene (14) // 1,4,5,8-tetrachlorobiphenylene (15)



The 1,4-dichloro-2,3-diiodobenzene (0.5 g) was intimately mixed with copper powder (2 g) and charged in a shrink cap vial which had previously been flame dried under high vacuum and back-purged with dry argon gas. The vial was sealed, evacuated to high vacuum and heated on a heating block to 210°C for a total of 16 hrs. A pale yellow crystalline sublimate was careful removed from the upper part of the vial (Fig. S4.1A). ^{1}H NMR (850MHz, $CDCl_3$) δ 6.70 (s, 4H). ^{13}C NMR (212MHz, $CDCl_3$) δ 145.45, 132.20, 122.16. The remainder of material was dissolved in DCM, filtered twice over glass wool, and the resultant dark orange solution evaporated under reduced pressure. NMR spectroscopy indicated an unidentifiably complex mixture of aromatic molecules. The aforementioned crystals were cystallographically identified as 1,4,5,8-tetrachlorobiphenylene (Fig. S4.2B-D). **Space Group**: P 2_1/n (14), **Cell**: *a* 3.8455(5)Å *b* 14.531(3)Å *c* 9.8534(15)Å, *α* 90° *β* 92.535(13)° *γ* 90. [CCDC 2056845: Experimental Crystal Structure Determination: 1,4,5,8-tetrachlorobiphenylene]

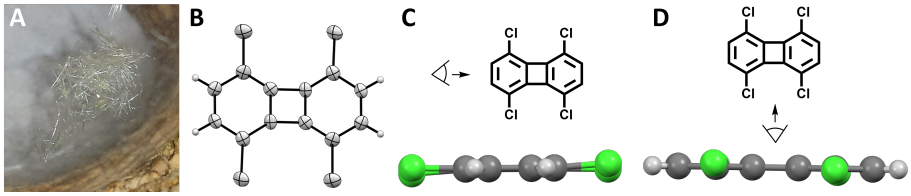


Figure S4.1 Crystals (A), ORTEP-styled drawing with ellipsoids at 50% probability (B), and two side views (C and D) of the crystal structure of 1,4,5,8-tetrachlorobiphenylene. Note that the aromatic structure is planar, whereas the chlorine atoms are bend out-of-plane in a "paired trans" fashion. Structures illustrated in B, C and D were generated with the Mercury 4.2.0 software suite.[43]

Computational. Equilibrium geometries of all structures were initially computed in the Spartan 10 program.[44] Computations were performed in the gas phase at the DFT level of theory using the ωB97X-D functional and 6-31G(d,p) basis set. The resulting structures were further refined using the Gaussian 09 Rev. D.01[45] program using the PBE functional[46] and 6-31G(d,p) basis set and using the D3(BJ) dispersion correction.[47,48] For structures containing I atoms the LANL2DZ (with effective core potential) basis set was used on I and a 6-31G(d,p) basis set on all other atoms.[49] Both the ωB97X-D and PBE functional are amongst the best performing in describing PAH structures.[50-53] Geometries were optimized in the gas-phase and subsequently re-optimized in combination with the SMD model to include solvent effects, using the appropriate solvent parameter.[54] The geometry convergence criteria were set to tight (Opt=tight; Max. Force = $1.5{\cdot}10^{-7}$, Max. Displacement = $6.0{\cdot}10^{-7}$), and an internally defined super-fine grid size was used (SCF=tight, Int= VeryFineGrid), which is a pruned 175,974 grid for first-row atoms and a 250,974 grid for all other atoms. These parameters were chosen because of the significant dependence of computed frequencies on the molecular orientation when using smaller grid sizes. This effect was particularly pronounced for transition metals and transition state structures.[55]

The denoted free Gibbs energy was calculated using Equation S1, in which ΔE_{gas} is the gas-phase energy (electronic energy), $\Delta G^{T}_{gas,QH}$ (T = 293.15 K, p = 1 atm., C = 1 M) is the sum of corrections from the electronic energy to the free Gibbs energy in the quasi-harmonic oscillator approximation, including zero-point-vibrational energy, and ΔG_{solv} is their corresponding free solvation Gibbs energy. The $\Delta G^{T}_{gas,QH}$ were computed using the quasi-harmonic approximation in the gas phase according to the work of Truhlar - the quasi-harmonic approximation is the same

as the harmonic oscillator approximation except that vibrational frequencies lower than 100 cm^{-1} were raised to 100 cm^{-1} as a way to correct for the breakdown of the harmonic oscillator model for the free energies of low-frequency vibrational modes.[56,57] All stationary points found were checked for either no imaginary frequencies for local minima or one imaginary frequency for transition state structures.

$$\Delta G^{T}_{solv} = \Delta E_{gas} + \Delta G^{T}_{gas,QH} + \Delta G_{solv} = \Delta G^{T}_{gas} + \Delta G_{solv} \quad \text{(Eq. S1)}$$

Transition states for the propellerene interconversion were obtained by first performing a dihedral angle scan in the Gaussian software to provide guess structures for a QST3 search. Transition states in the palladium(0) catalyzed reactions were obtained using a QST2 search. The obtained guess structures were optimized to a transition state using the Berny algorithm and confirmed by an intrinsic reaction coordinate calculation. The electronic energy fragments generated as described in the main text were computed at the same level of theory as the original propellerene molecules. Molecular structures were illustrated using CYLview.[58]

The activation strain model (ASM) analysis[24] and energy decomposition analysis (EDA)[33-35] were performed using the Amsterdam Density Functional (ADF2019.302)[59-61] software package based on the gas-phase structures obtained by Gaussian 09. The fragment-based approach was also performed using these optimized gas-phase geometries. Computations were performed using the PBE functional with D3(BJ) dispersion correction. The basis set used, denoted TZ2P, is of triple-ζ quality for all atoms and has been improved by two sets of polarization functions. The accuracies of the fit scheme (Zlm fit) and the integration grid (Becke grid) were, for all calculations, set to VERYGOOD. Relativistic effects were accounted for by using the zeroth-order regular approximation (ZORA). All computations were performed in the gas-phase.

Propellerene barrier heights to interconversion. To determine whether propellerenes are able to freely interconvert between their two conformations the barrier height for interconversion (*i.e.*, between the C_2 and D_3) was computed. This showed that for most the barrier heights are sufficiently height ($\Delta G^{\ddagger}_{C_2 \rightarrow D_3}$ > 24 kcal mol^{-1}) to prevent the spontaneous isomerization at room temperature (Table S4.1). On the other hand, for propellerene **1** the barrier height of interconversion is prohibitively low, so as to preclude isolation of the individual isomers ($\Delta G^{\ddagger}_{C_2 \rightarrow D_3}$ = 5.8 kcal mol^{-1}). Experimentally, the barrier heights for interconversion have been reported for a number of propellerenes and are in close agreement with computational results. Synthesis of propellerene **6** (tripyrenylene) was described in the previous Chapters. Variable temperature NMR experiments gave a barrier height to interconversion for **6** of 26.0 kcal mol^{-1}, which is in excellent agreement with the computed value of 25.8 kcal mol^{-1} (Fig. 3.2). For the unknown propellerene **7** computed values were compared to that of the known hexapole helicene from Kamikawa *et al.*, which were found to be in close agreement ($\Delta G^{\ddagger}_{C_2 \rightarrow D_3}$ = 7.6 *versus* 10.4 kcal mol^{-1}). Perfluorotriphenylene 1 was synthesized according to a known procedure,[12] and its ^{19}F NMR spectrum did not show any deconvolution or coalescence of the resonances at the technical limit of 173 K, indicating a barrier height below 8.8 kcal mol^{-1} (Fig. S4.2). Due to the unsuitability of perchlorotriphenylene **6** for variable temperature NMR experiments, hexachlorotriphenylene **14** was selected as model compound instead. Attempts to synthesize it were, however, unsuccessful (*vide supra*), yielding only the hitherto unknown 1,4,5,8-tetrachlorobiphenylene **15**, whose identity could be unequivocally stabilized from its crystal structure (See synthesis section above). Computed values for **6** were therefore compared to those reported for the known 4,5-dichloro-9,10-dihydrophenanthrene, which again shows close agreement ($\Delta G^{\ddagger}_{C_2 \rightarrow D_3}$ = 22.6 *versus* 24.2 kcal mol^{-1}).

Supplementary Figures and Tables

Table S4.1 Computed and experimental barrier heights for the conformer interconversion of benzoid and *ortho*-substituted propellerenes. All energies are reported with respect to the $C_2 \rightarrow D_3$ transition, and are expressed in kcal mol^{-1}. Computed at the SMD-PBE-D3(BJ)/6-31G(d,p) level of theory. Solvent parameter corresponds with experimental conditions.

	Preference (exp.)	$\Delta\Delta G_{solv.}$ (comp.)	$\Delta G^{\ddagger}_{C_2 \leftrightarrow D_3}$ (exp.)	$\Delta G^{\ddagger}_{C_2 \leftrightarrow D_3}$ (comp.)
1	C_2	4.2	<8.8	5.8
2	C_2	4.0	22.6[62,63]	28.8
3	C_2	2.9	---	34.9
4	C_2	4.5	>28.0[9,64]	31.0
5	D_3	–3.6	26.2[22]	25.1
6	D_3	–3.4	26.0	25.8
7	D_3	–3.0	---[19]	23.3
8	D_3	–3.4	---	28.7

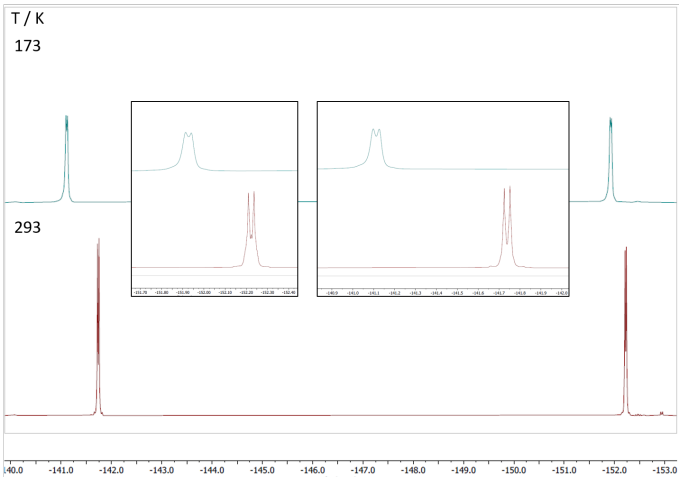
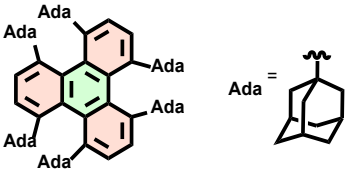


Figure S4.2 ^{19}F VT-NMR spectra of perfluorotriphenylene **1** in THF-d_8.



12

Figure S4.4 Structure of compound **12**.

Chapter 5

Freestanding Non-covalent Thin Films of the Propeller-shaped Polycyclic Aromatic Hydrocarbon Decacyclene

Abstract

Whereas the previous Chapters were concerned with the synthesis and conformational behavior of propellerenes, this chapter will focus on their supramolecular behavior. Although van der Waals forces are often responsible for the poor solubility of aromatic molecules, it will be shown here that these interactions can in fact be exploited to form mechanically stable, nanometer thin films, capable of being freestanding over micrometer distances. Using a combination of computational chemistry and microscopic imaging techniques, these thin films will be studied on the molecular and macroscale. The mechanical strength of these films will be probed and quantified using state-of-the-art AFM nano-indentation experiments. Self-assembled thin films, which are mechanically stable upon formation, without the requirement for further crosslinking, constitute the ultimate goal of reticular chemistry and the results reported here constitute a first step towards this goal.

Parts of this Chapter are published as:
van der Ham A., Liu X., Calvani D., Melcrova A., Kozdra M., Buda F., Overkleeft H. S., Roos W., Filippov D.V., Schneider G.F. **Manuscript accepted for publication in Nat. Comm.**

Nanometer thin, porous membranes hold promise for a wide range of applications, ranging from hydrogen fuel cells and desalination, to biomedical applications and nanoelectronics.[1-7] The particular interest in nanometer thin membranes stems from the fact that such membranes constitute the best trade-off between permeability and selectivity.[8,9] This is in part due to a significantly diminished hydrodynamic resistance towards water molecules, and by being less prone to fouling and clogging of pores.[10] When designing novel membranes, control over the functionality of the membrane, in terms of chemical composition, thickness, pore size and pore charge is therefore crucial. One particularly successful approach to make nanometer thin membranes is through molecular self-assembly (MSA),[11-13] which allows membrane properties to be tuned by incorporation of specific functional groups into the molecular building blocks used to make the membrane. However, a major hurdle in the development of such bottom-up membranes is the requirement to crosslink the individual building blocks, to achieve mechanical stability. This is typically achieved either *via* the incorporation of reactive functional groups into the monomeric building blocks, by thermal annealing,[14,15] photon[16] or electron irradiation.[17] These techniques often lead to loss of chemical definition, resulting in poor sample-to-sample reproducibility. Bottom-up membrane formation, without the need for annealing but with good mechanical stability thus constitutes the ultimate goal. Within the field of reticular chemistry, several types of 2D non-covalent organic frameworks (non-COFs), like supramolecular organic frameworks (SOHs) and hydrogen-bonded organic frameworks (HOFs) are at the forefront of development in this direction.[18-21] Although a supramolecular framework based purely on π- π stacking interactions was recently reported, this existed in the form of a crystalline solid.[22] Entirely 2D thin films based solely on non-covalent interactions between aromatic small molecules, like the one reported here, are not known in the literature to date.

Langmuir-Blodgett (LB) thin films composed of the small propellerene, decacyclene, have previously being developed for use in light-emitting devices.[23,24] The stacking behavior of this molecule and the mechanical properties of these thin films were, however, unexplored. The present study therefore starts with simulation assemblies of decacyclene molecules on a water surface using Molecular Dynamics (MD) simulations, in conjunction with DFT computations, to get a molecular picture of the packing of decacyclene at the air-water interface. Thin films are then produced, and a range of high-resolution microscopic techniques (AFM, SEM and TEM) used to get a microscopic image of the thin films. The van der Waals forces, which hold the molecules in these thin films together, were found to be strong enough to allow them to be free-standing over micrometer distances. State-of-the-art AFM nanoindentation then quantify the mechanical strength of these unique thin films.

Decacyclene thin films constitute the first PAH-based, non-covalent thin films, with a mechanical strength on par with that of known non-covalent membranes. These results therefore serve as an important step towards the fabrication of mechanically stable membranes, not requiring annealing.

Decacyclene[25] thin films were prepared in a KSV minithrough, using Millipore® ultrapure water as subphase. Thin films were subjected to several compression-decompression cycles and the surface pressure monitored throughout (Fig. 5.1A and B). A strong hysteresis was observed, showing smaller mean molecular areas with each cycle, going from an initial onset of 40 Å^2 / molecule to only 22 Å^2 / molecule.[26] This indicates that the decacyclene monolayer is unstable at the air-water interface, and molecular rearrangements take place during the compression process. These molecular rearrangements entail the adaptation of a thermodynamically more favorable orientation of the molecules in the monolayer, which is known to be the direct result of factors such as intermolecular interactions, phase transitions and lateral diffusion.[27]

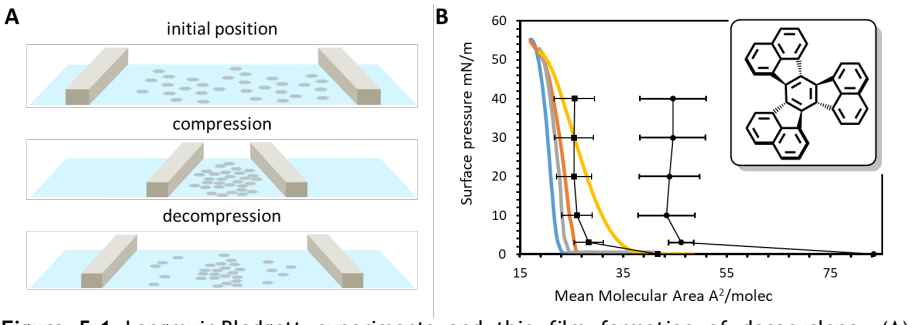


Figure 5.1 Langmuir-Blodgett experiments and thin film formation of decacyclene. (A) Schematic representation of the compression-decompression of decacyclene molecules at the air-water interface in a Langmuir-Blodgett through. (B) Representative experimental Langmuir-Blodgett isotherms for two consecutive compression/decompression cycles on a single sample, showing surface pressure as a function of mean molecular area. Black lines are isotherms computed using MD simulations, for systems containing 30 (●) and 60 (■) molecules, respectively. Reported values are averaged over 3 separate MD simulations with error bars indicating standard deviations. Insert shows the molecular structure of decacyclene.

Molecular Dynamics Simulations. To study the molecular processes taking place at the air-water interface during the compression, Molecular Dynamics (MD) simulations were performed. The model system used consisted of a box of water molecules, with a total of 30 or 60 decacyclene molecules on each side (Fig. 5.2A and 5.2B). Input geometries for decacyclene were obtained from DFT computations at PBE/6-31G(d,p). Optimized geometries with a D_3 symmetry were computed to be thermodynamically preferred over those with a C_2 symmetry (ΔG_{gas} = –0.3 kcal mol^{-1}; Fig. S5.2), in line with crystallographic data.[28] After pre-equilibration of the system at 300 K, the average intermolecular distance between decacyclene molecules was found to be ~3.6 Å (Fig. 5.2C), which is in good agreement with that computed with DFT for a decacyclene dimer (3.68 Å), (Fig. 5.1C)[29] and crystallographically (3.9 Å).[30]

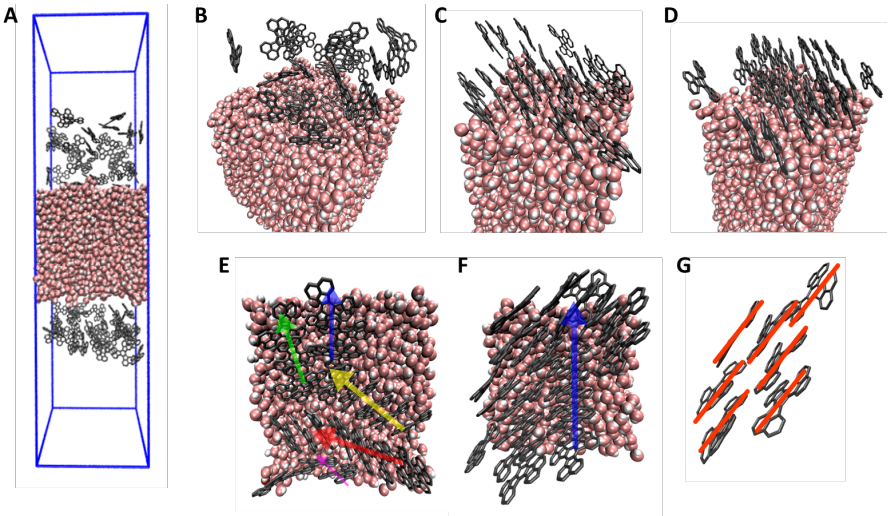


Figure 5.2 Molecular Dynamics (MD) simulation on decacyclene thin films. (A), MD simulation box (5.0 x 5.0 x 20.0 nm^3) containing water molecules represented by a space filling model, and the random, pre-equilibration position of decacyclene molecules (30) on both sides thereof represented by a liquorice model in grey. Protons explicitly drawn on water but omitted from decacyclene. (B) Top view of A. (C) Same system as B, after equilibration at 300 K. (D) Same system as C, after compression to a surface pressure of 30 mN m^{-1}. (E) Top view of D after equilibration at 300 K. Differently colored arrows added to highlight different stacking domains. (F) Same system as in E after compression to a surface pressure of 30 mN m^{-1}. (G) Highlight of molecules found in F showing the onset of roof-tiling.

In all cases, a parallel stacking mode was found most favorable. In the MD simulations, the stacked molecules were found to align themselves perpendicularly to the water surface, forming distinct domains with different relative orientations (Fig. 5.2D–F). Intuitively, such an arrangement decreases the total surface area of the hydrophobic, decacyclene molecules with the water surface. These findings thus served as an initial validation that the MD model is able to accurately describe the intermolecular interactions in this system. Note that decacyclene was previously found experimentally to have an intrinsic preference to absorb parallel to the surface of copper(100) foil.[31,32]

After pre-equilibration of the system, the surface area of the simulation box was reduced in the x-y plane, corresponding to an increase in surface pressure in the Langmuir-Blodgett compression technique. Plotting of the surface pressure as a function of the Mean Molecular Area (MMA) thus yields an isotherm, which can be compared to those obtained experimentally (Fig. 5.1B). Systems containing 30 and 60 decacyclene molecules were modelled. In former case, a monolayer of molecules was found with an average MMA of approximately 44 $Å^2$/molecule; in the latter case, a bimolecular layer is obtained, with an MMA of roughly 26 $Å^2$/molecule. The computed isotherm for the bimolecular layer system was found to be in reasonable agreement with experimental data. In both cases, upon compression, molecules in their distinct domains were found to intercalate with neighboring domains to adopt a slipped

stacking mode, a process called "roof-tiling" (Fig. 5.2G).[33] When using a racemic mixture of D_3 conformers, *i.e.* containing equal numbers of (+) and (–) rotating molecules, distinct domains are still formed, containing a random mixture of isomers. Such systems give isotherms identical to optically pure systems (SI Fig. S5.5). Apart from domain reformations, a change in the orientation of the molecules relative to the water surface is also observed upon compression. Quantification of the tilt angle (*i.e.* the angle of the plane of a decacylene molecule to the surface of water), revealed that, upon compression, the preferred tilt angle shifts from 50 to almost 90 degrees, driven by a desire to minimize the contact area with the water surface (Fig. 5.3).

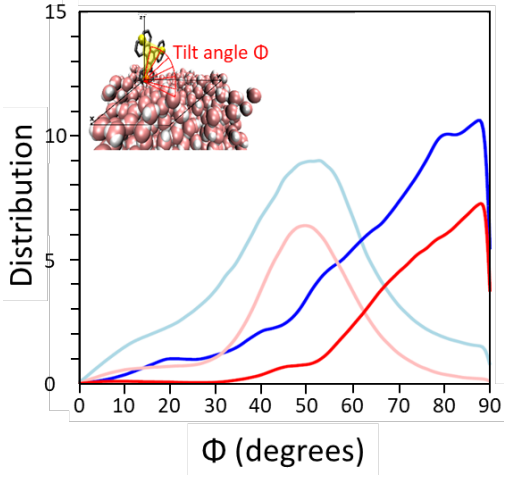


Figure 5.3 Distribution of the tilt angle (Φ) per decacylene molecule as derived from the MD simulations. The definition of the tilt angle (Φ) as the arc between the plane of a decacylene molecule (yellow) and the x-y plane of the water surface, is illustrated in the top left. Shown are the distributions of the tilt angles for systems consisting of 60 (blue) and 30 (red) decacylene molecules, before (light) and after (dark) compression to a surface pressure of 30 mN m^{-1}. Distribution curves were obtained *via* Gaussian broadening with default standard deviation and normalized per amount of decacylene molecules, using a Kernel Density Estimation to produce this plot with N_{bins} = 1897.

To characterize the thin films on a microscopic scale, samples were transferred unto a Si/SiO_2 wafer by horizontal lifting at constant pressure (25 mN m^{-1}) and imaged using atomic force microscopy (AFM) (Fig. 5.4A). This showed a uniform coverage of the substrate by the thin film, with a thickness of 2.49 ± 1.25 nm (Fig. 5.4B), corresponding roughly to a bimolecular layer. This average thickness corresponds nicely with the bimolecular layer obtained from the MD simulations (*vide supra*). No crystallinity of the thin film was found with transmission electron microscopy (TEM; data not shown). To test the mechanical stability of the thin film, samples were transferred onto a copper TEM grid, covered with holey Quantifoil®.[34] Using scanning electron microscopy (SEM), thin films were found capable of being free-standing over 0.6 and 1.0 µm diameter apertures with only minimal defects (Fig. 5.4C). Transfer onto a 2 µm holey grid showed thin films could be free-standing even over these larger distances (Fig. 5.4D), yet with less reproducibility.

As the thin films are able to be free-standing, without having required any form of annealing, it became interesting to quantify their mechanical strength. This was done using AFM nanoindentation experiments,[35,36] using samples transferred onto a golden TEM grid covered with holey UltrAufoil®.[37] Initial images of the free-standing thin films showed a small height increase depicted as a lighter color around the perimeter of the aperture (Fig. 5.4D, Fig. S5.6, Fig. S5.7, ø = 1 µm). The thin films themselves were found to recede slightly into the apertures as a result of the van der Waals attraction between the thin film and the TEM substrate (Fig. S5.7B). The same effect was previously observed for graphene,[36,38] as well as for nanoparticle-based free-standing membranes.[39]

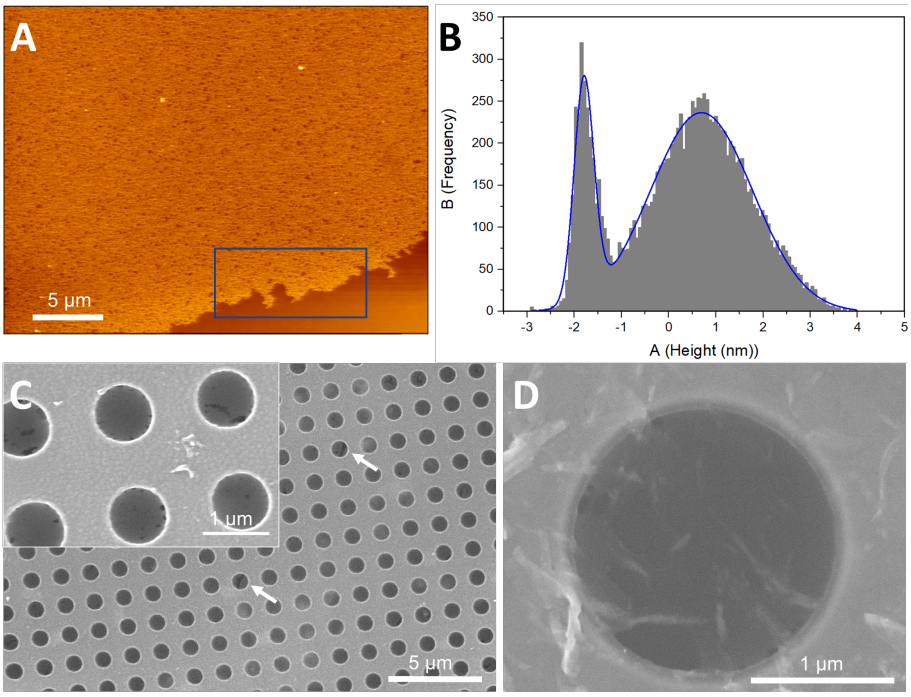


Figure 5.4 (A) AFM image of a decacyclene film transfered unto a Si/SiO_2 wafer. (B) Height profile of the area marked in blue in A, showing a film thickness of 2.49 ± 0.71 nm. (C) SEM image of a decacyclene film free-standing over 0.6 µm diameter apertures. Ruptured films are indicated by arrows. Insert shows a zoom on the same grid, illustrating minor film defects as dark regions. (D) SEM image of a near-defect free decacyclene film free-standing over a 2 µm aperture.

The freestanding thin films were indented in the center of the circular apertures with an AFM tip (nominal radius 2 nm) until failure of the decacyclene film occurred (Fig. 5.5A-B, Fig. S5.6). For every indentation, the depth of the indentation by the AFM tip was plotted as a function of the applied force (Fig. 5.5C). The resulting force-indentation curves were analyzed using an elastic model for a 2D material in the form

of a circular disk clamped along its circumference.[36] According to this model, the dependency of the applied force *F* on the vertical tip position δ can be written as linear addition of pretension σ^{2D} and the elastic modulus in 2D material E^{2D}:

$$F = \sigma^{2D}(\pi R)\left(\frac{\delta}{R}\right) + E^{2D}(q^3 R)\left(\frac{\delta}{R}\right)^3 \quad \text{(Eq. 1)}$$

Here, *R* is the radius of the clamped thin film and $q = (1.05 - 0.15\nu - 0.16\nu^2)^{-1}$ is a dimensionless constant depending on the Poisson's ratio of the material. Considering the forces holding the film together are dominantly of a Van der Waals character, a Poisson's ratio ν = 0.33 was assumed, as previously used for freestanding nanoparticle membranes,[39,40] and protein monolayers grown on water,[41] which are all held together solely by Van der Waals interactions. The 2D approximation is only valid for systems where the film thickness *h* is considerably smaller than its diameter *R*, *i.e.* $R/h > 1$. In this case *R* = 1 μm and *h* = 2.5 nm, and thus the approximation holds for this system.

After the first contact with the decacyclene film, the tip induces elastic deformation fitting to the theory (Fig 5.5C, red curve). The fit is valid up to the point of non-elastic changes in the material, which appear as a change in the slope or a small drop in the force (Fig. 5.5C, red arrow; Fig. S5.8). These non-elastic changes were previously observed for graphene flakes as well as a consequence of cracks induced in the membrane.[42] Such points are hence not considered as full rupture of the decacyclene film, which is here defined as an event when the applied force decreases considerably (> 2 nN; Fig. 5C, green arrow). The distribution of penetration forces and the force inducing non-elastic deformations are shown in Figures 5.5D and 5.5E (see also Fig. S5.9A and B). On average, the thin film fails at an applied force of 26 ± 9 nN (N = 26) with cracks being induced at a force of 8 ± 4 nN (N = 27). Note that sharper AFM tips require smaller forces to induce failure of a material.[36,43] To objectively assess the material's properties, intrinsic parameters were needed.

The model described by Eq. 1 is a linear addition of the pretension and 2D elastic modulus. The fit approaches the prestress-independent limit when indented deep enough to produce nonlinear behavior. This condition is met here as, at deeper indentation, a successful fit is obtained that yields a 2D elastic modulus E^{2D}. An effective Young's modulus *E* can therefore be derived for the decacyclene film, by dividing the 2D elastic modulus with the film thickness as $E = E^{2D}/h$. An histogram of the effective Young's moduli thus derived shows a narrow distribution with the mean value at 6 ± 4 GPa (N = 27) (Fig. 5.5F, Fig. S5.9D). The resulting Young's modulus depends on the chosen Poisson's ratio of the material, which was chosen based on literary precedent (ν = 0.33). The data was also fitted with a Poisson's ratio for a graphene monolayer ν = 0.165, in which case the Young's modulus values increase by ~14%, indicating only a moderate influence of Poisson's ratio on the results. The elastic strength of the present decacyclene film is thus comparable with 2D MOFs (~5 GPa)[44], one order of magnitude less than 2D COFs (~26 GPa),[45] and three orders of magnitude less than pristine graphene (~1 TPa).[36]

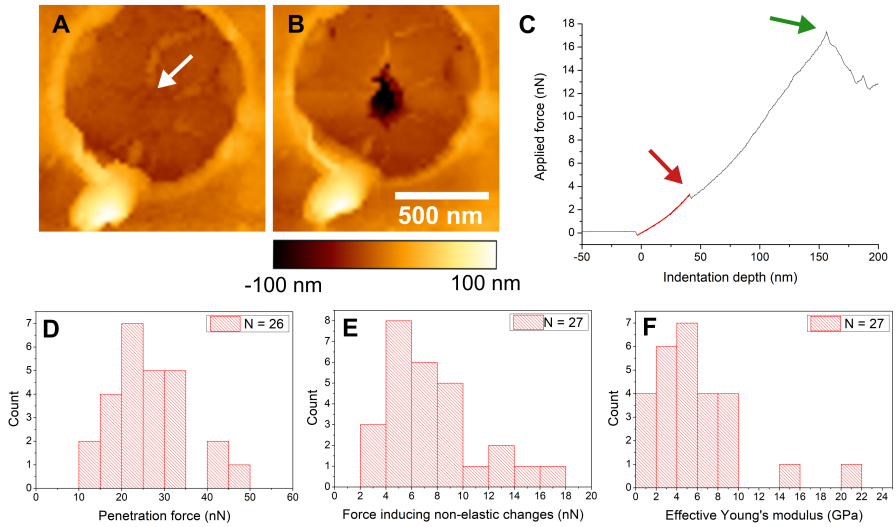


Figure 5.5 AFM nanoindentation of decacyclene films spanning over a 1 μm circular aperture. Representative AFM images before (A) and after (B) nanoindentation. White arrow in panel (A) indicates the point of the indentation with the AFM tip. (C) Representative force-indentation curve. Red curve shows the fit in the elastic regime. Red arrow points to a small drop in the slope of the curve. Above this point the fit of the elastic properties is no longer valid. The green arrow shows the breaking event when the thin film fully ruptures. (D) Histogram of the penetration force needed to rupture the thin film. (E) Histogram of the force inducing non-elastic changes in the thin films. (F) Effective Young's modulus of decacyclene film.

To conclude, it was shown that the small propellerene decacyclene is able to form stable, free-standing thin films, held together solely by collective van der Waals forces, and without the requirement of crosslinking or annealing. Computational modeling of the experimental conditions revealed the molecular reorientations and stacking interactions that take place at the air-water interface during Langmuir-Blodgett compression. Despite being held together by van der Waals forces, thin films were found stable enough to be free-standing over micrometer distances, which allowed quantification of their mechanical strength using AFM nanoindentation experiments. Thin films are found capable of withstanding point loads of 26 ± 9 nN, with a corresponding Young's modules of 6 ± 4 GPa, which is on par with reported 2D membranes. Although the present thin films are not yet capable for use in a device setting, these results constitute the starting point for further development of PAH-based, non-covalent thin films.

References

(1) Cohen-Tanugi, D.; Grossman, J. C. Nanoporous graphene as a reverse osmosis membrane: recent insights from theory and simulation. *Desalination* **2015,** *366*, 59.

(2) Wang, Z.; Wu, A.; Colombi Ciacchi, L.; Wei, G. Recent advances in nanoporous membranes for water purification. *Nanomaterials* **2018,** *8* (2), 65.

(3) Kim, W.-g.; Nair, S. Membranes from nanoporous 1D and 2D materials: A review of opportunities, developments, and challenges. *Chem. Eng. Sci.* **2013,** *104*, 908.

(4) Wang, L.; Boutilier, M. S. H.; Kidambi, P. R.; Jang, D.; Hadjiconstantinou, N. G.; Karnik, R. Fundamental transport mechanisms, fabrication and potential applications of nanoporous atomically thin membranes. *Nat. Nanotech.* **2017,** *12* (6), 509.

(5) Adiga, S. P.; Jin, C.; Curtiss, L. A.; Monteiro-Riviere, N. A.; Narayan, R. J. Nanoporous membranes for medical and biological applications. *WIRES Nanomed. Nanobiotech.* **2009,** *1* (5), 568.

(6) Song, N.; Gao, X.; Ma, Z.; Wang, X.; Wei, Y.; Gao, C. A review of graphene-based separation membrane: Materials, characteristics, preparation and applications. *Desalination* **2018,** *437*, 59.

(7) Makra, I.; Gyurcsányi, R. E. Electrochemical sensing with nanopores: A mini review. *Electrochem. Comm.* **2014,** *43*, 55.

(8) Park, H. B.; Kamcev, J.; Robeson, L. M.; Elimelech, M.; Freeman, B. D. Maximizing the right stuff: The trade-off between membrane permeability and selectivity. *Science* **2017,** *356* (6343).

(9) Nunes, S. P.; Culfaz-Emecen, P. Z.; Ramon, G. Z.; Visser, T.; Koops, G. H.; Jin, W.; Ulbricht, M. Thinking the future of membranes: Perspectives for advanced and new membrane materials and manufacturing processes. *J. Membrane Sci.* **2020,** *598*, 117761.

(10) Wei, G.; Quan, X.; Li, C.; Chen, S.; Yu, H. Direct growth of ultra-permeable molecularly thin porous graphene membranes for water treatment. *Environmental Science: Nano* **2018,** *5* (12), 3004.

(11) Cheng, W.; Campolongo, M. J.; Tan, S. J.; Luo, D. Freestanding ultrathin nano-membranes via self-assembly. *Nano Today* **2009,** *4* (6), 482.

(12) Biswas, A.; Bayer, I. S.; Biris, A. S.; Wang, T.; Dervishi, E.; Faupel, F. Advances in top–down and bottom–up surface nanofabrication: Techniques, applications & future prospects. *Adv. Colloid Interfac.* **2012,** *170* (1-2), 2.

(13) Thiruvengadathan, R.; Korampally, V.; Ghosh, A.; Chanda, N.; Gangopadhyay, K.; Gangopadhyay, S. Nanomaterial processing using self-assembly-bottom-up chemical and biological approaches. *Rep. Prog. Phys.* **2013,** *76* (6), 066501.

(14) Liu, X.; He, M.; Calvani, D.; Qi, H.; Gupta, K. B. S. S.; de Groot, H. J. M.; Sevink, G. J. A.; Buda, F.; Kaiser, U.; Schneider, G. F. Power generation by reverse electrodialysis in a single-layer nanoporous membrane made from core–rim polycyclic aromatic hydrocarbons. *Nat. Nanotech.* **2020,** *15* (4), 307.

(15) Wu, R.; Yue, W.; Li, Y.; Huang, A. Ultra-thin and high hydrogen permeable carbon molecular sieve membrane prepared by using polydopamine as carbon precursor. *Materials Letters* **2021,** *295*, 129863.

(16) Feng, X.; Schlüter, A. D. Towards macroscopic crystalline 2D polymers. *Angew. Chem. Int. Ed.* **2018,** *57* (42), 13748.

(17) Angelova, P.; Vieker, H.; Weber, N.-E.; Matei, D.; Reimer, O.; Meier, I.; Kurasch, S.; Biskupek, J.; Lorbach, D.; Wunderlich, K. A universal scheme to convert aromatic molecular monolayers into functional carbon nanomembranes. *ACS nano* **2013,** *7* (8), 6489.

(18) Pfeffermann, M.; Dong, R.; Graf, R.; Zajaczkowski, W.; Gorelik, T.; Pisula, W.; Narita, A.; Müllen, K.; Feng, X. Free-standing monolayer two-dimensional supramolecular organic framework with good internal order. *J. Am. Chem. Soc.* **2015,** *137* (45), 14525.

(19) Hisaki, I. Hydrogen-bonded porous frameworks constructed by rigid π-conjugated molecules with carboxy groups. *J. Incl. Phenom. Macro.* **2020,** *96* (3), 215.

(20) Lin, R.-B.; He, Y.; Li, P.; Wang, H.; Zhou, W.; Chen, B. Multifunctional porous hydrogen-bonded organic framework materials. *Chem. Soc. Rev.* **2019,** *48* (5), 1362.
(21) Suzuki, Y.; Tohnai, N.; Saeki, A.; Hisaki, I. Hydrogen-bonded organic frameworks of twisted polycyclic aromatic hydrocarbon. *Chem. Comm.* **2020,** *56* (87), 13369.
(22) Deng, J.-H.; Luo, J.; Mao, Y.-L.; Lai, S.; Gong, Y.-N.; Zhong, D.-C.; Lu, T.-B. π-π stacking interactions: Non-negligible forces for stabilizing porous supramolecular frameworks. *Science advances* **2020,** *6* (2), eaax9976.
(23) Das, S.; Chowdhury, A.; Pal, A. J. Alternating-current and direct-current responses of light-emitting devices based on decacyclene langmuir-blodgett films. *Phys. Status Solidi A* **2001,** *185* (2), 383.
(24) Acharya, S.; Parichha, T. K.; Talapatra, G. B. Spectroscopic properties of decacyclene assembled in Langmuir Blodgett film mixed with stearic acid. *Mol. Cryst. Liq. Cryst. Sci. Technol. Sect. C-Mol. Mat.* **2000,** *12* (1), 91.
(25) Amick, A. W.; Scott, L. T. Trisannulated benzene derivatives by acid catalyzed aldol cyclotrimerizations of cyclic ketones. Methodology development and mechanistic insight. *J. Org. Chem.* **2007,** *72* (9), 3412.
(26) Nishikata, Y.; Konishi, T.; Morikawa, A.; Kakimoto, M.-a.; Imai, Y. Preparation and monolayer thickness of Langmuir–Blodgett films of polyimides having various chemical structures. *Polym. J.* **1988,** *20* (3), 269.
(27) Vollhardt, D.; Fainerman, V. B. Progress in characterization of Langmuir monolayers by consideration of compressibility. *Adv. Colloid Interfac.* **2006,** *127* (2), 83.
(28) Ho, D. M.; Pascal Jr, R. A. Decacyclene: a molecular propeller with helical crystals. *Chem. Mater.* **1993,** *5* (9), 1358.
(29) The binding energy of the dimer was found to be 23.1 kcal mol^{-1} in terms of Gibbs free energy at PBE-D3(BJ)/6-31G(d,p)l.
(30) Wang, H.; Xu, X.; Li, L.; Yang, C.; Ji, H.-F. Optoelectronic property and sensing applications of crystalline nano/microwires of decacyclene. *Micro Nano Lett.* **2011,** *6* (9), 763.
(31) Schunack, M.; Lægsgaard, E.; Stensgaard, I.; Besenbacher, F. Bonding and ordering of decacyclene molecules on Cu (110) studied by scanning tunneling microscopy. *J. Chem. Phys.* **2002,** *117* (18), 8493.
(32) Schunack, M.; Linderoth, T. R.; Rosei, F.; Lægsgaard, E.; Stensgaard, I.; Besenbacher, F. Long jumps in the surface diffusion of large molecules. *Phys. Rev. Lett.* **2002,** *88* (15), 156102.
(33) Yao, Z.-F.; Wang, J.-Y.; Pei, J. Control of π–π stacking via crystal engineering in organic conjugated small molecule crystals. *Cryst. Growth Des.* **2018,** *18* (1), 7.
(34) Ermantraut, E.; Wohlfart, K.; Tichelaar, W. Perforated support foils with pre-defined hole size, shape and arrangement. *Ultramicroscopy* **1998,** *74* (1-2), 75.
(35) Roos, W. H.; Bruinsma, R.; Wuite, G. J. L. Physical virology. *Nature physics* **2010,** *6* (10), 733.
(36) Lee, C.; Wei, X.; Kysar, J. W.; Hone, J. Measurement of the elastic properties and intrinsic strength of monolayer graphene. *science* **2008,** *321* (5887), 385.
(37) Russo, C. J.; Passmore, L. A. Ultrastable gold substrates for electron cryomicroscopy. *Science* **2014,** *346* (6215), 1377.
(38) Bunch, J. S.; Verbridge, S. S.; Alden, J. S.; van der Zande, A. M.; Parpia, J. M.; Craighead, H. G.; McEuen, P. L. Impermeable atomic membranes from graphene sheets. *Nano Lett.* **2008,** *8* (8), 2458.
(39) He, J.; Kanjanaboos, P.; Frazer, N. L.; Weis, A.; Lin, X. M.; Jaeger, H. M. Fabrication and mechanical properties of large-scale freestanding nanoparticle membranes. *Small* **2010,** *6* (13), 1449.
(40) Kanjanaboos, P.; Joshi-Imre, A.; Lin, X.-M.; Jaeger, H. M. Strain patterning and direct measurement of Poisson's ratio in nanoparticle monolayer sheets. *Nano Lett.* **2011,** *11* (6), 2567.
(41) Singh, A.; Konovalov, O. Measuring elastic properties of a protein monolayer at water surface by lateral compression. *Soft Matter* **2013,** *9* (10), 2845.

(42) Lee, G.-H.; Cooper, R. C.; An, S. J.; Lee, S.; van der Zande, A.; Petrone, N.; Hammerberg, A. G.; Lee, C.; Crawford, B.; Oliver, W. High-strength chemical-vapor–deposited graphene and grain boundaries. *Science* **2013,** *340* (6136), 1073.
(43) Denning, D.; Bennett, S.; Mullen, T.; Moyer, C.; Vorselen, D.; Wuite, G. J. L.; Nemerow, G.; Roos, W. H. Maturation of adenovirus primes the protein nano-shell for successful endosomal escape. *Nanoscale* **2019,** *11* (9), 4015.
(44) Hermosa, C.; Horrocks, B. R.; Martínez, J. I.; Liscio, F.; Gómez-Herrero, J.; Zamora, F. Mechanical and optical properties of ultralarge flakes of a metal–organic framework with molecular thickness. *Chem. Sci.* **2015,** *6* (4), 2553.
(45) Hao, Q.; Zhao, C.; Sun, B.; Lu, C.; Liu, J.; Liu, M.; Wan, L.-J.; Wang, D. Confined synthesis of two-dimensional covalent organic framework thin films within superspreading water layer. *J. Am. Chem. Soc.* **2018,** *140* (38), 12152.
(46) Pantelic, R. S.; Suk, J. W.; Magnuson, C. W.; Meyer, J. C.; Wachsmuth, P.; Kaiser, U.; Ruoff, R. S.; Stahlberg, H. Graphene: Substrate preparation and introduction. *J. Struct. Biol.* **2011,** *174* (1), 234.
(47) Frisch, M. J.; Trucks, G. W.; Schlegel, H. B.; Scuseria, G. E.; Robb, M. A.; Cheeseman, J. R.; Scalmani, G.; Barone, V.; Mennucci, B.; Petersson, G. A. Gaussian 09 Revision D. 01, 2009. *Gaussian Inc. Wallingford CT* **2009**.
(48) Grimme, S.; Antony, J.; Ehrlich, S.; Krieg, H. A consistent and accurate ab initio parametrization of density functional dispersion correction (DFT-D) for the 94 elements H-Pu. *J. Chem. Phys.* **2010,** *132* (15), 154104.
(49) Grimme, S.; Ehrlich, S.; Goerigk, L. Effect of the damping function in dispersion corrected density functional theory. *J. Comp. Chem.* **2011,** *32* (7), 1456.
(50) Ribeiro, R. F.; Marenich, A. V.; Cramer, C. J.; Truhlar, D. G. Use of solution-phase vibrational frequencies in continuum models for the free energy of solvation. *J. Phys. Chem. B* **2011,** *115* (49), 14556.
(51) Funes-Ardoiz, I.; Paton, R. S. **2016**. GoodVibes: GoodVibes v1.0.2. http://doi.org/10.5281/zenodo.595246.
(52) Legault, C. Y. *CYLview, 1.0 b, Université de Sherbrooke,* ***2009***, 2013.
(53) Berendsen, H. J. C.; van der Spoel, D.; van Drunen, R. GROMACS: a message-passing parallel molecular dynamics implementation. *Comput. Phys. Commun.* **1995,** *91* (1-3), 43.
(54) Lindahl, E.; Hess, B.; Van Der Spoel, D. GROMACS 3.0: a package for molecular simulation and trajectory analysis. *Mol. Mod. Ann.* **2001,** *7* (8), 306.
(55) Van Der Spoel, D.; Lindahl, E.; Hess, B.; Groenhof, G.; Mark, A. E.; Berendsen, H. J. C. GROMACS: fast, flexible, and free. *J. Comp. Chem.* **2005,** *26* (16), 1701.
(56) Hess, B.; Kutzner, C.; Van Der Spoel, D.; Lindahl, E. GROMACS 4: algorithms for highly efficient, load-balanced, and scalable molecular simulation. *J. Chem. Theo. Comp.* **2008,** *4* (3), 435.
(57) Pronk, S.; Páll, S.; Schulz, R.; Larsson, P.; Bjelkmar, P.; Apostolov, R.; Shirts, M. R.; Smith, J. C.; Kasson, P. M.; van der Spoel, D. GROMACS 4.5: a high-throughput and highly parallel open source molecular simulation toolkit. *Bioinformatics* **2013,** *29* (7), 845.
(58) Abraham, M. J.; Murtola, T.; Schulz, R.; Páll, S.; Smith, J. C.; Hess, B.; Lindahl, E. GROMACS: High performance molecular simulations through multi-level parallelism from laptops to supercomputers. *SoftwareX* **2015,** *1*, 19.
(59) Páll, S.; Abraham, M. J.; Kutzner, C.; Hess, B.; Lindahl, E.; **2014**, Tackling exascale software challenges in molecular dynamics simulations with GROMACS.
(60) York, D. M.; Darden, T. A.; Pedersen, L. G. The effect of long-range electrostatic interactions in simulations of macromolecular crystals: A comparison of the Ewald and truncated list methods. *J. Chem. Phys.* **1993,** *99* (10), 8345.
(61) Bussi, G.; Donadio, D.; Parrinello, M. Canonical sampling through velocity rescaling. *J. Chem. Phys.* **2007,** *126* (1), 014101.
(62) Horn, H. W.; Swope, W. C.; Pitera, J. W.; Madura, J. D.; Dick, T. J.; Hura, G. L.; Head-Gordon, T. Development of an improved four-site water model for biomolecular simulations: TIP4P-Ew. *J. Chem. Phys.* **2004,** *120* (20), 9665.

(63) Harris, J. G. Liquid-vapor interfaces of alkane oligomers: structure and thermodynamics from molecular dynamics simulations of chemically realistic models. *J. Phys. Chem.* **1992,** *96* (12), 5077.
(64) Vega, C.; De Miguel, E. Surface tension of the most popular models of water by using the test-area simulation method. *J. Chem. Phys.* **2007,** *126* (15), 154707.
(65) Chen, F.; Smith, P. E. Simulated surface tensions of common water models. *J. Chem. Phys.* **2007,** *126*, 221101.
(66) Jorgensen, W. L.; Maxwell, D. S.; Tirado-Rives, J. Development and testing of the OPLS all-atom force field on conformational energetics and properties of organic liquids. *J. Am. Chem. Soc.* **1996,** *118* (45), 11225.
(67) Kaminski, G. A.; Friesner, R. A.; Tirado-Rives, J.; Jorgensen, W. L. Evaluation and reparametrization of the OPLS-AA force field for proteins via comparison with accurate quantum chemical calculations on peptides. *J. Phys. Chem. B* **2001,** *105* (28), 6474.
(68) Martin, M. G. Comparison of the AMBER, CHARMM, COMPASS, GROMOS, OPLS, TraPPE and UFF force fields for prediction of vapor–liquid coexistence curves and liquid densities. *Fluid Phase Equilibr.* **2006,** *248* (1), 50.
(69) Dodda, L. S.; Cabeza de Vaca, I.; Tirado-Rives, J.; Jorgensen, W. L. LigParGen web server: an automatic OPLS-AA parameter generator for organic ligands. *Nucleic Acid Res.* **2017,** *45* (W1), W331.
(70) Marenich, A. V.; Jerome, S. V.; Cramer, C. J.; Truhlar, D. G. Charge model 5: An extension of Hirshfeld population analysis for the accurate description of molecular interactions in gaseous and condensed phases. *J. Chem. Theo. Comp.* **2012,** *8* (2), 527.
(71) Frisch, M. J.; Trucks, G. W.; Schlegel, H. B.; Scuseria, G. E.; Robb, M. A.; Cheeseman, J. R.; Scalmani, G.; Barone, V.; Petersson, G. A.; Nakatsuji, H.; Gaussian, Inc., Wallingford CT, 2016.
(72) Martínez, J. M.; Martínez, L. Packing optimization for automated generation of complex system's initial configurations for molecular dynamics and docking. *J. Comp. Chem.* **2003,** *24* (7), 819.
(73) Martínez, L.; Andrade, R.; Birgin, E. G.; Martínez, J. M. PACKMOL: a package for building initial configurations for molecular dynamics simulations. *J. Comp. Chem.* **2009,** *30* (13), 2157.
(74) Van der Spoel, D.; Lindahl, E.; Hess, B.; Van Buuren, A. R.; Apol, E.; Meulenhoff, P. J.; Tieleman, D. P.; Sijbers, A.; Feenstra, K. A.; Van Drunen, R. *Gromacs User Manual version 4.5.6*, **2010**.
(75) Fine, R. A.; Millero, F. J. Compressibility of water as a function of temperature and pressure. *J. Chem. Phys.* **1973,** *59* (10), 5529.
(76) Humphrey, W.; Dalke, A.; Schulten, K. VMD: visual molecular dynamics. *J. Mol. Graphics* **1996,** *14* (1), 33.
(77) Roos, W. H. In *Single Molecule Analysis*; Springer, **2011**.
(78) Ribeiro, A. A. S. T.; Horta, B. A. C.; Alencastro, R. B. D. MKTOP: a program for automatic construction of molecular topologies. *J. Brazil. Chem. Soc.* **2008,** *19* (7), 1433.
(79) Jorgensen, W. L.; Severance, D. L. Aromatic-aromatic interactions: free energy profiles for the benzene dimer in water, chloroform, and liquid benzene. *J. Am. Chem. Soc.* **1990,** *112* (12), 4768.
(80) Gowers, R. J.; Linke, M.; Barnoud, J.; Reddy, T. J. E.; Melo, M. N.; Seyler, S. L.; Domanski, J.; Dotson, D. L.; Buchoux, S.; Kenney, I. M. *MDAnalysis: a Python package for the rapid analysis of molecular dynamics simulations*; Los Alamos National Lab.(LANL), Los Alamos, NM (United States), 2019.

Experimental

Sample preparation. Decacyclene was synthesized according to the procedure of Amick and Scott.[25] Identity and purity of the material were checked using ^{1}H NMR spectroscopy on a Bruker AV500 NMR instrument equipped with a BBFO probe head for 5 mm outer diameter tubes. Spectra were recorded at 500 MHz for ^{1}H using deuterated chloroform obtained from a commercial source (EurIsoTop®). Thin film samples were prepared on a Langmuir–Blodgett trough (KSV NIMA, Finland) filled with Millipore® Ultrapure water (18 MΩ cm^{-1}). The surface pressure was measured with a Wilhelmy balance. A solution of decacyclene in chloroform (75 µl, 1.1 mM) was carefully spread on the water surface using a micropipette. After 30 min, the surface was compressed by two barriers with a fixed speed of 2 mm min^{-1} to reach a certain surface. Thin film samples were transferred onto silicon wafers at constant pressure by the Langmuir–Schäfer method. Samples were transferred onto copper or gold TEM grids following standard procedures.[46] Copper substrate for IR experiments was obtained from Puratonic® and had a thickness of 0.025 mm and a 99.999% purity.

Thin film characterization. AFM images of the thin films on Si/SiO_2 wafers were recorded on a JPK Nano Wizard Ultra Speed machine with a silicon 254 probe (AC 160 TS, Asylum Research) with 300 kHz nominal resonance frequency. The images were scanned in intermittent contact mode in air at room temperature. The SEM images were recorded by using an FEI NOVA nano SEM 200 scanning electron microscope.

Density Functional Theory. Equilibrium geometries were computed at the PBE/6-31G(d,p) level of theory using the Gaussian 09 Rev. D.01 program suite,[47] using the D3(BJ) dispersion correction.[48,49] The geometry convergence criteria were set to tight (Opt = tight; Max. Force = $1.5{\cdot}10^{-7}$, Max. Displacement = $6.0{\cdot}10^{-7}$), and an internally defined super-fine grid size was used (SCF=tight, Int=VeryFineGrid), which is a pruned 175,974 grid for first-row atoms and a 250,974 grid for all other atoms. Free Gibbs energies were computed using Equation S1, in which ΔE_{gas} is the gas-phase energy (electronic energy) and $\Delta G^{T}_{gas,QH}$ (T = 293.15 K, p = 1 atm., C = 1 M) is the sum of corrections from the electronic energy to the free Gibbs energy in the quasi-harmonic oscillator approximation, including zero-point-vibrational energy. The $\Delta G^{T}_{gas,QH}$ were computed using the quasi-harmonic approximation in the gas phase according to the work of Truhlar in which vibrational frequencies lower than 100 cm^{-1} were raised to 100 cm^{-1} to correct for the breakdown of the harmonic oscillator model for the free energies of low-frequency vibrational modes.[50,51] Stationary points were checked to have no imaginary frequencies for local minima, and one imaginary frequency for the transition state structure. All DFT structures were illustrated using CYLview.[52]

$$\Delta G^{T}_{gas} = \Delta E_{gas} + \Delta G^{T}_{gas,QH} \qquad \text{(Eq. S1)}$$

*Molecular Dynamics***.** All MD simulations were carried out using the GROMACS 2016 software suite.[53-59] The Particle Mesh Ewald (PME) method was employed to accurately account for electrostatic interactions.[60] The cut-off for Coulomb and Lennard-Jones interactions was set to 10 Å. During the NVT simulation the temperature was kept fixed with the V-rescale coupling method.[61]

Simulation setup. The model for a body of water, comprised of 4139 water molecules, was simulated in a periodic box (5.0 x 5.0 x 20.0 nm^3) using the TIP4P-Ew/2004 force field.[62] The water surface tension was used as defined within the GROMACS software suite (Equation S2):

$$\gamma_{water} = \frac{1}{2} L_z [P_{zz} - \frac{1}{2}(P_{xx} + P_{yy})] \qquad \text{(Eq. S2)}$$

where L_z is the box length in the *z* direction, P_{xx}, P_{yy} and P_{zz} are the respective xx, yy and zz element of the pressure tensor,[63] and the ½ originates from the presence of two x-y plane surfaces in the system. The system was first energetically minimized and then equilibrated for 8 ns with NVT at 300 K to obtain an average surface tension of γ_{water} = 58.46 mN m^{-1}. This value is in good agreement with previous studies.[64,65] The water model was further validated using a radial distribution function and density analysis (Fig. S5.4).

Simulation setting for the water-propellerene interfaces. Decacyclene molecules were simulated using the OPLS-AA force field (see Table S1)[66-68] and LigParGen[69] parameterization with charges calculated with the CM5 model[70] using the Gaussian 16 Rev. C.01 program suite.[71] Input geometries for decacyclene were obtained from DFT (*vide supra*).

Simulation run. Random input positions of 30 or 60 decacyclene molecules on both water surfaces were generated using the PACKMOL18 program.[72,73] Having two independent water-decacyclene interfaces provides a more symmetric MD simulation box and increases the statistics of the results by averaging on both interfaces. Moreover, the presence of the decacyclene molecule on both sides avoids the diffusion of water molecules through the periodic boundary condition along the z-axis. The two interfaces can be considered independent due to the thickness (5 nm) of the water box and the vacuum space (at least 5 nm on each side) above each interface along the z-axis. For each simulation, the system was first equilibrated with NVT at 70 K for 5 ns, and the temperature then raised to 300 K for another 5 ns. After these pre-equilibration simulations, the production run consists in NVT simulations were ran at 300 K for 10 ns. The final configuration extracted from the production run was used as a starting point for the subsequent NPT surface tension simulations. These series of simulations are repeated independently three times starting from a different random packing, in order to check the effect of initial conditions on the final results.

Series of simulations were repeated independently three times, starting from different random packings, in order to counteract the effect of initial conditions on the final results.

Surface Tension calculations

Surface tension coupling for surfaces parallel to the xy-plane was used, using normal pressure coupling for the z-direction, while the surface tension is coupled to the x/y dimensions of the box. The surface pressure was then increased stepwise, to generate pressure-area isotherms. At each chosen surface pressure (0, 3, 10, 20, 30, 40, 50 mN m^{-1}), the surface tension coupling molecular dynamics were performed while monitoring the change of the area in the x-y plane. In order to execute the constant surface tension simulations, the Berendsen pressure coupling was used.[74] For this coupling method to be effective, a value for the compressibility is required, which is close to the real compressibility of the system, namely 4.5 x 10^{-5} bar^{-1}. [75] Simulations were stopped after 10 ns, at which point an equilibrium state was reached. Data presented in the manuscript was obtained averaging the values on the last 10 ns of each corresponding simulation. The x-y area values are equilibrated enough with an error around ±0.05 Å. (Fig. S5.3). These series of simulations were repeated independently starting from each last equilibration simulation described in the previous paragraph, in order to increase the reproducibility of the results.

All MD results were illustrated using Visual Molecular Dynamics (VMD).[76]

AFM nanoindentation experiments

AFM imaging and nanoindentation of the TEM grid supported freestanding thin films was performed with an JPK Nano Wizard Ultra Speed AFM.[35,36] The TEM grid (with apertures of 1 µm in diameter) was immobilized by tape on top of a glass slide and imaged in QI™ mode. The experiments were performed in air at room temperature (22°C) using SNL-10A cantilevers (Bruker) with a calibrated spring constant of 0.432 ± 0.003 Nm^{-1} and a silicon nitride tip with nominal radius of 2 nm. The imaging force was ~400–600 pN. After imaging the free-standing thin films, the intact thin films were indented in the center by a force up to 50 nN with an indentation velocity of 300 nm sec^{-1}. Force-distance curves were recorded during indentation. After indentation, the same spot was imaged again.

AFM image analysis

Both the AFM images and the force curves were processed using JPK Data Processing software. Representative images before and after indentation are shown at Fig. S5.6. The height profile of a thin film spanning over a circular aperture is plotted in Fig. S5.7. The profile exhibits a dip in height in the middle, as also previously reported for suspended graphene membranes,[36] and a small elevation of the thin film height around the circumference of the aperture.

AFM force-indentation curves analysis

In brief, the nanoindentation experiment yield the deflection of the cantilever as a function of the Z-piezo displacement. This dependency was converted to the applied force versus the vertical distance between the tip and the sample surface by subtracting the deflection of the cantilever itself.[77] The contact point between the tip and the thin film was defined as a point, when the force-indentation curve starts exhibiting non-zero force. The initial increase in the force-indentation response up to the first apparent change in the slope or a small drop in the force (< 2 nN) was fitted using Eq. 1 according to the model for elastic properties of a 2D material described in Ref [36]. Two parameters were derived from the fit: prestress in 2D and elastic modulus in 2D. By dividing the 2D elastic modulus by the film thickness h = 2.5 nm, the effective Young's modulus of the decacyclene film is obtained. The analysis was done independently on two sets of data, the curves with the small drop in the force increase (Fig. S5.8A; N = 7), and the curves with apparent change in the slope (Fig. S5.8B; N = 20). Figure S5.9 shows the histograms of the pre-tension in 2D, the effective Young's modulus, the force inducing non-elastic changes in the thin film (when a small drop or slope change occurs), and the force needed to fully rupture the thin film. The latter is being defined as a force drop > 2 nN. The histograms show comparable distributions for the two subsets of data and hence the data from both subsets were combined and included into overall statistical analysis of the mechanical properties of the decacyclene films.

Supplementary Figure and Tables

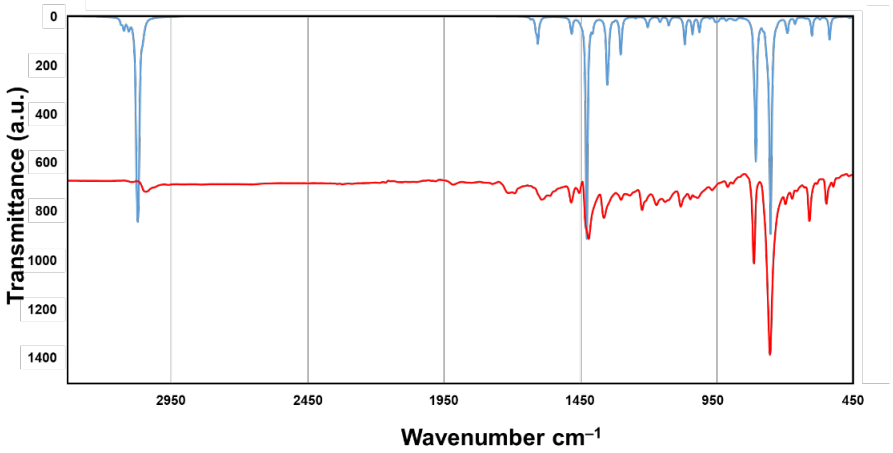


Figure S5.1 Infrared spectra of decacyclene as computed for the dimer at the PBE/6-31G(d,p) level (blue), and experimentally recorded for the powder (red).

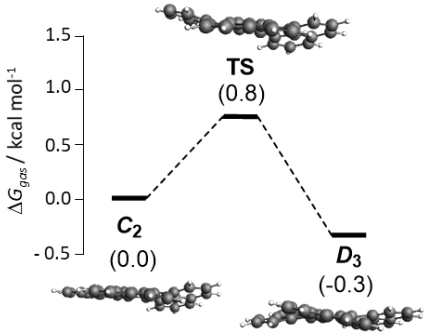


Figure S5.2 Potential energy surface for the interconversion of decacyclene between its C_2 and D_3 conformer. Energies are expressed as Gibbs free energies in kcal mol^{-1}, as computed at PBE-D3(BJ)/6-31G(d,p).

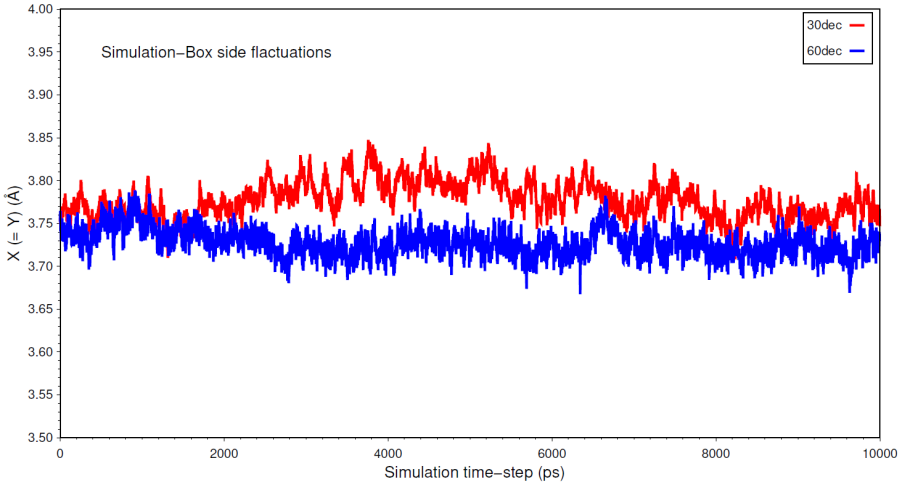


Figure S5.3 Fluctuations of the simulation box side X (= Y) during the Surface Tension MD at 30 mN m^{-1} for 30 and 60 decacyclene systems, respectively in red and blue color. The simulation time-steps are reported in ps.

Table S5.1 Assigned force field types for decacyclene molecule list for reproduce the simulation.[78]

OPLS-AA atom type	Description
opls_145	Benzene C - 12 site.[79] Use #145B for biphenyl
opls_146	Benzene H - 12 site.
opls_145B	Biphenyl C1

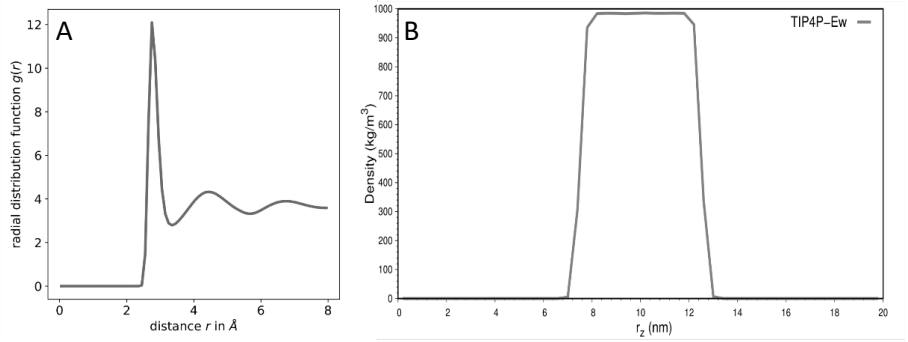


Figure S5.4 (A) O-O radial distribution function *g*(r) for water, calculated using the MDAnalysis tool.[80] (B) Density curve (kg m^{-3}) of the water molecules along the *z*-coordinate r_z (nm) of the water box.

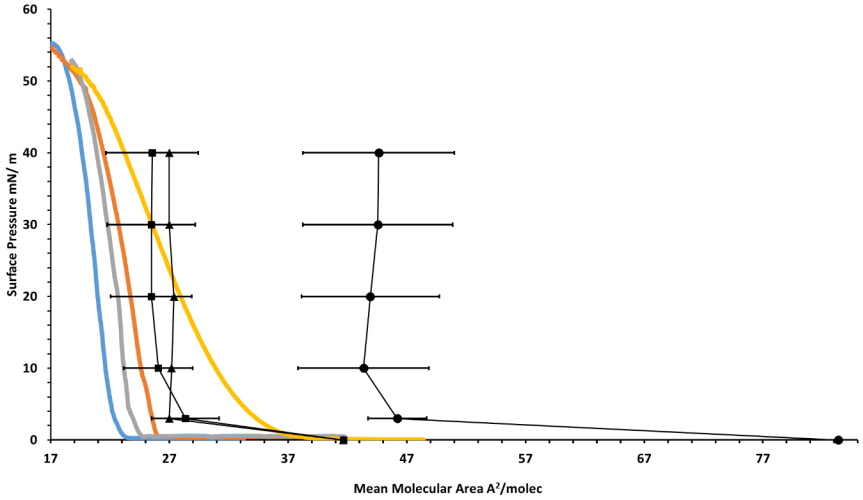


Figure S5.5 Representative experimental Langmuir-Blodgett isotherms for two consecutive compression/decompression cycles on a single sample, showing surface pressure as a function of mean molecular area. Black lines are isotherms computed using MD simulations for a system containing 60 (+) rotating decacyclene molecules (■), 60 (-) rotating molecules (●), and a system with a mixture of 30 (+) and 30 (-) rotating decacyclene molecules (▲).

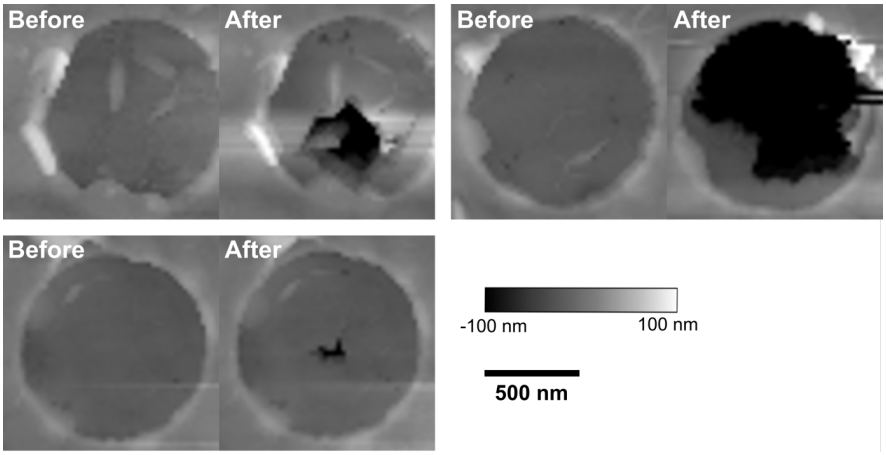


Figure S5.6 Representative AFM images of the decacyclene film spanning over the circular apertures before and after the nanoindentation with a force load of 50 nN.

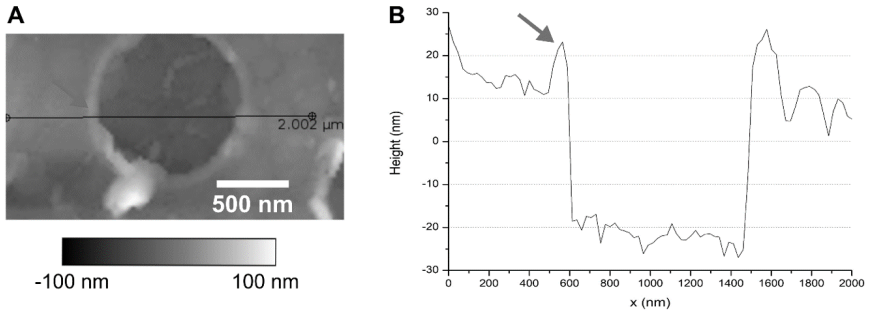


Figure S5.7 (A) AFM image of a thin film spanning over the circular aperture with a cross-section line highlighted. (B) Corresponding height profile along the cross-section line. Arrows in both panels point to the increase in height at the rim of the aperture, visible as a lighter color in the AFM image.

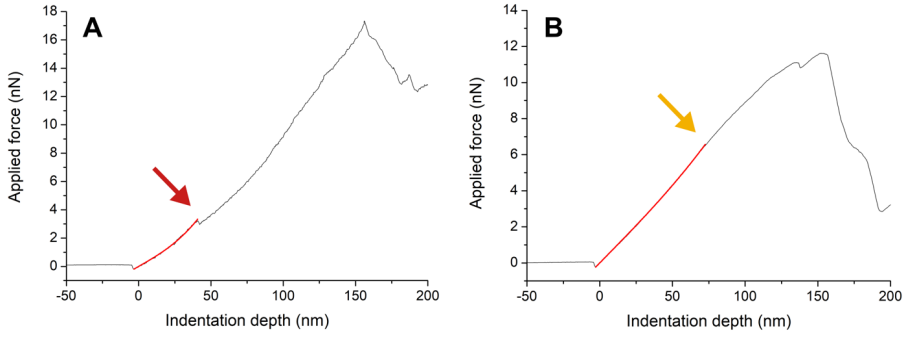


Figure S5.8 Representative force-indentation curves. Curves displaying (A) small drop in the applied force (arrow), and (B) change in the slope (arrow). Red lines represent fits of the experimental data according to Eq. 1.[36]

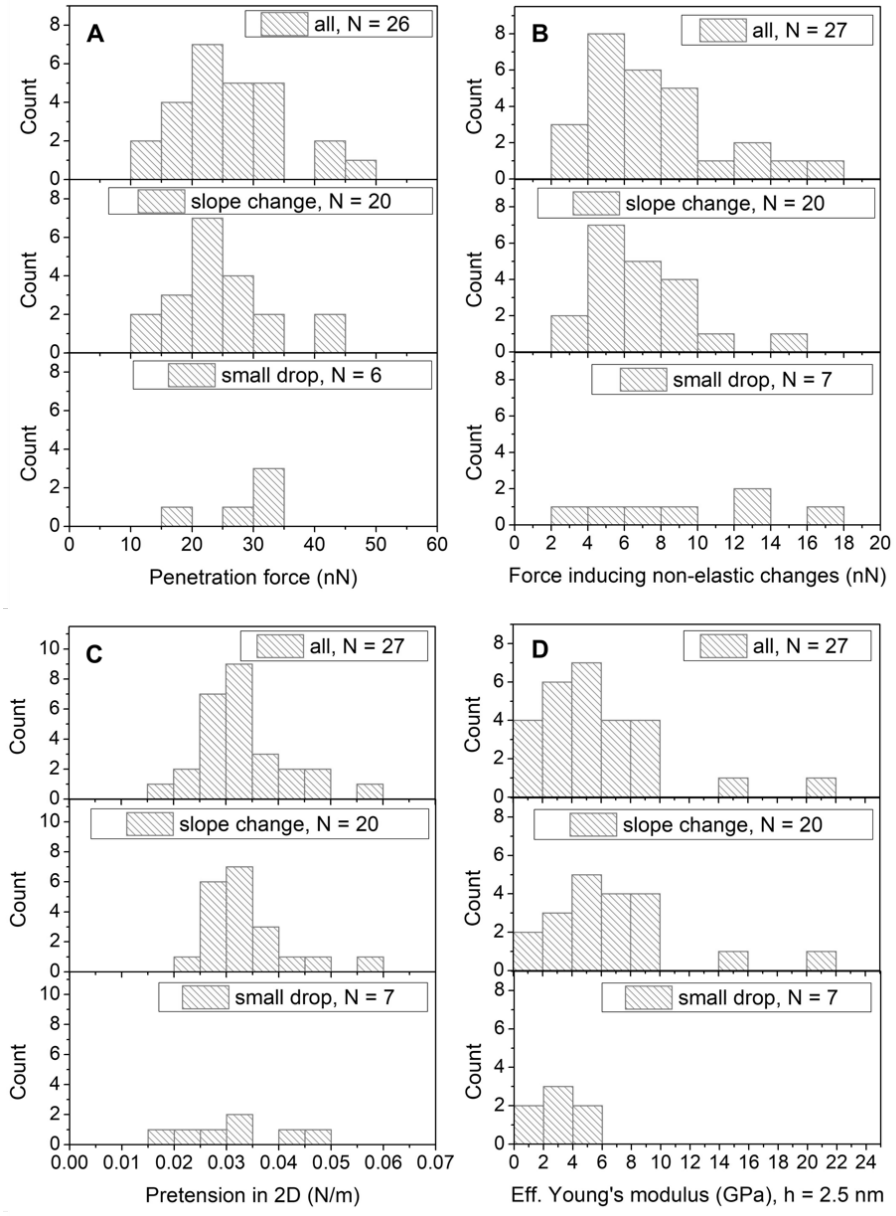


Figure S5.9 Mechanical parameters from the AFM nanoindentation experiments. Histograms of the parameters from all the acquired force-indentation curves, from the subset of the curves with an apparent change in the slope, and from the subset with the small drop in the force are shown. (A) Penetration force needed to fully rupture the thin film (demonstrated as a drop in the applied force > 2 nN). (B) Force inducing non-elastic changes. *i.e.* the force when the first small drop or the slope change occurs. (C) Pretension in 2D material as defined in Ref. [36]. (D) Effective Young's modulus of decacyclene film.

Chapter 6

Summary and prospects

Summary

The presence of a cyclic, π-conjugated, *i.e.* aromatic, system in organic molecules has a drastic impact on their physicochemical behavior. On the one hand, aromaticity is responsible for the many useful properties of these molecules, ranging from having vibrant colors, to their use in nano-electronic devices. On the other hand, aromaticity can be a burden, as it can make the synthesis and handling of these molecules a difficult endeavor. The problems with polycyclic aromatic hydrocarbons (PAHs) become larger with the size of the molecule. Due to their planar structure, molecules can approach each other at short distances, resulting in amplification of the van der Waals forces, also known as π-π stacking interactions, acting between them, thus seriously limiting their solubility. To circumvent this problem, several strategies, outlined in **Chapter 1**, have been devised.

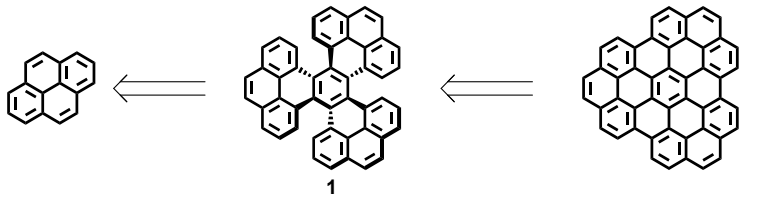


Figure 6.1 Retrosynthetic analysis of the synthesis of circum(30)triphenylene from pyrene *via* a non-planar, propellerene, intermediate.

In the present Thesis, a „non-planar precursor strategy'' was used, with the aim to synthesize the large, planar, PAH circum(30)triphenylene (Fig. 6.1). Synthesis of this molecule was deemed most efficient by ring closure of the non-planar precursor, tripyrenylene **1**. As evidenced throughout this thesis, synthesis of trifold symmetric, propeller-shaped PAHs, *i.e.* propellerenes, can be achieved in different ways (Fig. 6.2). In **Chapter 4**, perfluorotriphenylene, the first ever propellerene, was synthesized by the Ullman coupling of a 1,2-diiodo precursor, whereas in **Chapter 5**, decacyclene was synthesized by the condensation reaction of acenaphthenone. To obtain tripyrenylene **1**, however, more exotic conditions were needed.

In this case, **1** was obtained *via* the palladium catalyzed trimerization of *in situ* generated alkyne. This route is described in detail in **Chapter 2**, and in brief here.

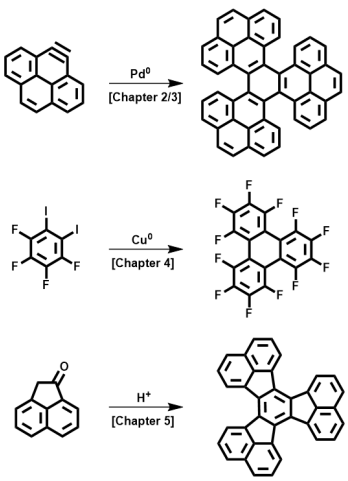


Figure 6.2 Schematic illustration of different ways in which trimeric PAHs can be obtained, as used in different Chapters in this Thesis. From top to bottom: tripyrenylene **1** (Ch. 2/3), perfluorotriphenylene (Ch. 4), and decacyclene (Ch. 5).

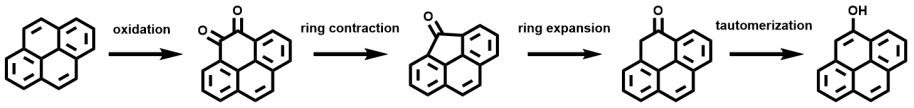


Figure 6.3 Schematic representation of the conversion of pyrene to 4-hydroxypyrene *via* a ring contraction/ring expansion sequence.

One of the initial hurdles in the synthesis of the non-planar precursor was the inaccessibility of 4-hydroxypyrene. As direct oxidation protocols on pyrene are unable to yield 4-hydroxypyrene, a novel two-step procedure, involving ring contraction and ring expansion, was developed (Fig. 6.3). Bromination and subsequent conversion into an *ortho*-TMS triflate in a three-step-one-pot reaction gave the required intermediate. A palladium catalyzed trimerization then gave the desired propellerene **1** (Fig. 6.4).

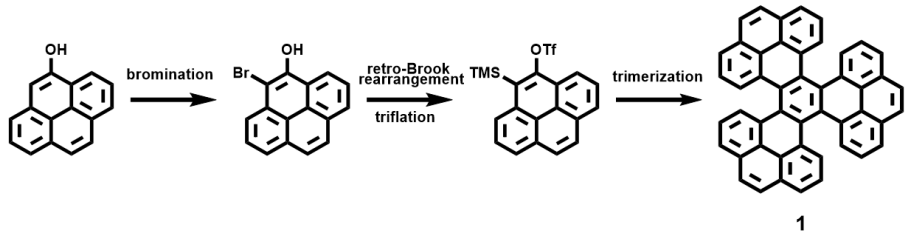


Figure 6.4 Schematic representation of the conversion of 4-hydroxypyrene to propellerene **1** *via* an *ortho*-TMS triflate.

Although on first inspection tripyrenylene **1** might seem to be flat, steric hindrance actually forces the so-called „wings'' of the molecule to bend out-of-plane, causing the molecule to adopt a non-planar shape. Because of their non-planarity, combined with their trifold symmetry, propellerenes can adopt two possible geometrical configurations. These are the C_2 and D_3 conformation, each of which have their mirror images (Fig. 6.5).

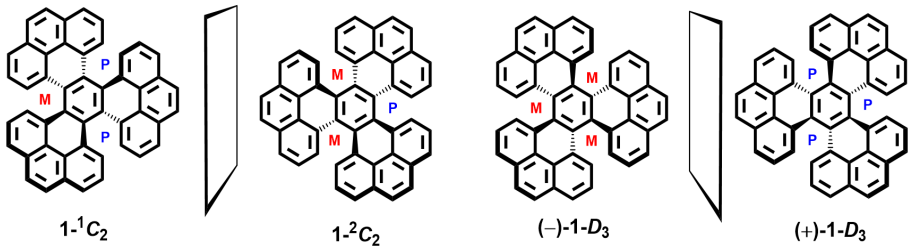


Figure 6.5 The different conformations of propellerene **1**. Structures are given of the C_2 and D_3 conformation, together with their two enantiomers. Chirality of the helical motifs in the molecules are labelled.

The physicochemical properties of propellerenes are dictated by their conformation. A proper understanding of the relationship between the two is thus imperative if they are to be used in a device setting, for example in solar cells. **Chapter 3** details the spectroscopic properties of the different conformations of propellerene **1** as well as the (positional) effect of extension of the π-conjugated system. It shows that the presence of helical motifs is the dictating factor when it comes to the physicochemical properties. Moreover, although extension of the π-conjugated system has a significant impact, the exact position of this extension is of lesser importance.

The conformation propellerenes adopt is, however, no trivial matter, with some propellerenes preferring a C_2 conformation, and others preferring a D_3 conformation. It was Pascal *et al.* who first proposed rules of thumb, aimed at explaining the dichotomy observed between *ortho*-substituted propellerenes and benzoid propellerenes, which prefer a C_2 and D_3 conformation, respectively.[1] These rules are:

- *The conformational preference is related to the central ring circumference.*
- *The conformation of the central ring is not a product of the wings.*
- *The C_2/D_3 dichotomy is a purely electronic (and not steric) effect.*

What is interesting is that they proposed a molecule, colloquially known as ,,Pascal's super propellerene'', which defies these rules, by having a circumference greater than 8.6 Å (Fig. 6.6), yet which was computationally predicted to still preferentially adopt a D_3 conformation.

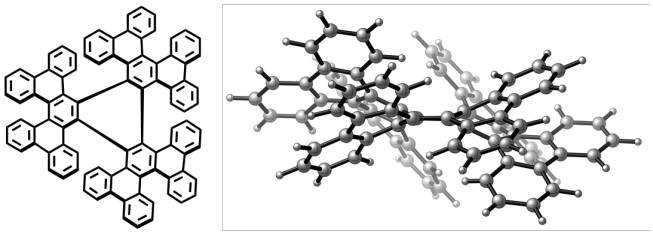


Figure 6.6 Schematic and molecular structure of Pascal's super propellerene.

Despite its daunting structure, it should be feasible to synthesize this molecule using the methodology outlined in this Thesis (Figure 6.7). The key step is the ring expansion of the known 17*H*-tetrabenzo[a,c,g,i]fluoren-17-one with TMS-azidomethane, to yield a phenol, which can be turned into an *ortho*-TMS triflate. Palladium-catalyzed aryne trimerization then yields the super propellerene.

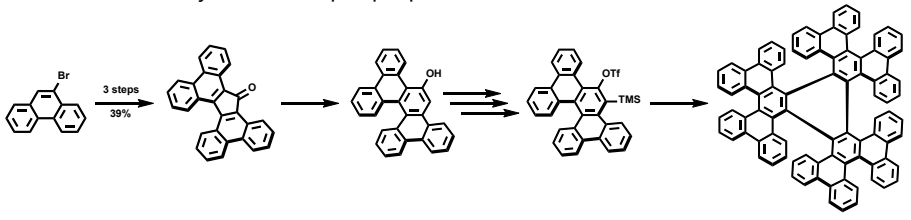


Figure 6.7 Synthetic scheme for the synthesis of Pascal's super propellerene.

Despite the efforts of Pascal *et al.* and others, no comprehensive model exists to date that can explain the origins of the conformation preference of propellerenes. **Chapter 4** of this Thesis changes this. By computationally dissecting propellerene molecules the preference of their constituent parts was unravelled. It was found that the wings of propellerenes prefer a D_3 conformation, yet their size and rigidity dictate the degree of this preference: the more flexible the wings, the weaker the preference. Combined with a preference of the core and radials bonds for a C_2 conformation, the overall result is *ortho*-substituted propellerenes preferentially adopting a C_2 conformation, and benzoid propellerenes adopting a D_3 conformation. Combined, **Chapters 3** and **4** thus describe the origin of the conformational preference of propellerenes and the effect this preference has on the spectroscopic properties of these molecules, which will ultimately enable the rational design of propellerenes with desired properties.

The strong π-π stacking interactions aromatic molecules can engage in was classified above as a cumbersome property, because of the poor solubility it engenders. **Chapter 5**, however, makes use of this property, showing the formation of a molecularly thin film from the small propellerene decacyclene. The collective action of van der Waals forces acting between the decacyclene molecules allows the formation of a mechanically stable thin film, able to be free-standing over micrometer distances, despite being only 2.5 nm thick. The strength of these thin films could be quantified using state-of-the-art atomic force microscopy (AFM) nano-indentation experiments, showing it to be on par with known 2D membranes. Although no applications of these particular thin films were shown yet, they constitute a first of their kind, showing that covalent cross-linking under harsh conditions is not a prerequisite to form stable membranes from aromatic molecules.

Perspective – PAHs in Astrochemistry

The target molecule of this Thesis was circum(30)triphenylene, a large, planar PAH with D_{3h} symmetry. The electronic nature of the PAH periphery, as well as the symmetry and shape of an aromatic molecule all influence its properties,[2-5] and within the family of planar PAHs, those possessing a D_{3h} symmetry constitute a particularly elusive sub-family. To date, only a handful of homocyclic, unsubstituted PAHs belonging to this sub-family have been synthesized.[6-8] They are especially stable with tribenzo(a,g,m)coronene, *e.g.*, having a reported T_1 life time of over 10 seconds.[8] Similarly, the Raman signal intensity of $C_{96}H_{30}$ was predicted to be greater when the atoms are arranged in a D_{3h} fashion *versus* a D_{6h} one.[9]

The spectroscopic properties of PAHs are of critical importance in the astrochemistry field. The first observations of broad emission bands in the mid-IR range of many emitting stellar regions posed a mystery as to their origins, earning them the title of unidentified infrared emission bands (UIRs).[10-16] Where the first spectra were recorded with ground-based and airborne studies, later studies with the Infrared Space Observatory (ISO; 1995-8) and the Spitzer Space Telescope (SST; 2003-20) much improved the resolution (Fig. 6.8A and B), and showed their ubiquitous presence in the interstellar medium (ISM). The hypothesis that PAHs could be the carriers of these UIRs was first put forward by Allamandola, Tielens and Baker in 1985.[17-20] Some 35 years later, the presence of PAHs in the ISM is now well-established. However, the actual composition, *i.e.* the specific molecules, making up these bands, remains uncertain, and only in 2018 was strong evidence provided for the presence of one specific aromatic molecule (benzonitrile) in the ISM.[21]

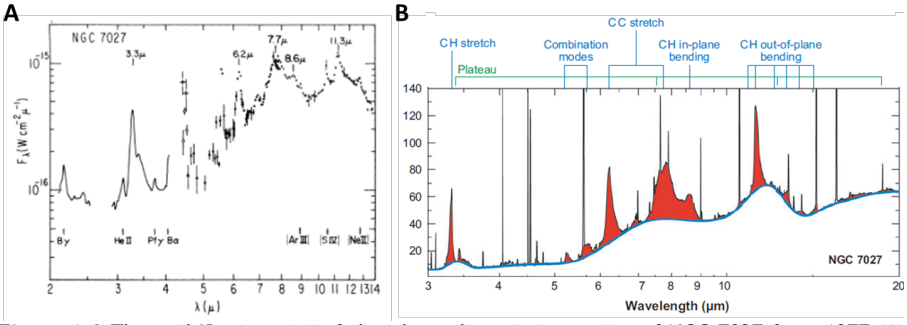


Figure 6.8 The mid-IR spectrum of the photo-dissociation region of NGC 7027 from 1977 (A) and 2002 (B) (Reproduced and adapted from refs. [16] and [22] respectively).

A further refinement of the PAH hypothesis was made by Alexander Tielens in 2013. From analysis of the energetics involved in the IR emissions, as well as numerous computed reference spectra, a size range of 50 – 150 carbon atoms was estabilished.[22-25] The lower limit of C_{50} was additionally supported from the fact that PAHs smaller than this are unstable in the UV field, due to their poor heat capacity.[26] This necessity of PAHs to be big in order to serve as emitters of the IR bands is known as the *grand-PAH hypothesis*,[27] and much recent research has been divulged in this direction.

The missing link. One question that is central to the grand-PAH hypothesis is: how are they formed? The present axiom is that larger PAHs are formed from smaller ones *via* so-called Hydrogen-Abstraction/Acetylene Addition (HACA) and Hydrogen Abstraction/Vinylacetylene Addition (HAVA) reactions (Fig. 6.9). In this way, C_2H_2 and C_4H_4 fragments can be introduced. In PAH terminology, these represent *K*-region installation and benzene fusion, respectively. It was recently proposed, by Wnuk et al., that the D_{3h} PAHs tribenzo(a,g,m)coronene and circum(30)triphenylene could serve as intermediates in the formation of the stable C_{54} PAH circum(30)coronene in the interstellar medium (ISM).[28,29] These molecules can be regarded as symmetrical expansions upon a central triphenylene core and their formation is thought off as starting from triphenylene and proceeding *via* a series of consecutive HACA's and HAVA's (Fig. 6.9). Combined with their aforementioned stability and dependence of the vibrational modes on their size, shape and symmetry, the relative scarcity of D_{3h} PAHs makes them ideal candidates for detection in the ISM. A study as to their spectroscopic peculiarities is thus much warranted.

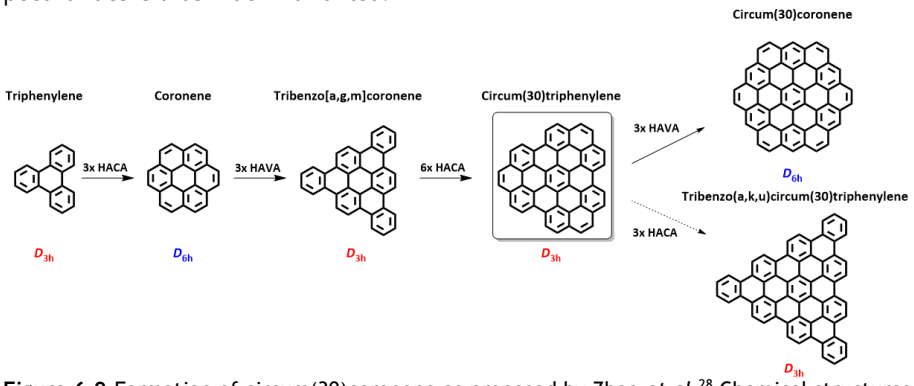


Figure 6.9 Formation of circum(30)coronene as proposed by Zhao *et al*.[28] Chemical structures of PAHs are drawn in their Clar structure with the symmetry group they belong to given below. HACA = Hydrogen-Abstraction/Acetylene Addition; HAVA = Hydrogen Abstraction/Vinylacetylene Addition. HACA results in the net introduction of a C_2H_2 unit, HAVA results in the net introduction of a C_4H_4 unit.

With 48 carbon atoms, circum(30)triphenylene lies at the lower limit of the definition of a grand-PAH. Of the D_{3h} PAHs shown in Fig. 6.9, only of circum(30)triphenylene the IR spectrum remains unknown. In light of its potential implications in the hypothesis outlined above, it is desirable to study the IR properties of circum(30)triphenylene both experimentally and computationally.

Apart from constructive PAH transformations, destructive transformations are equally of interest. When excited PAHs are unable to relax *via* IR emission, they undergo photo-fragmentation, mainly *via* the sequential loss of H_2 and C_2H_2 fragments from the molecule. For neutral PAHs larger than $C_{33}H_n$, IR radiative relaxation is predicted to be the dominant mode. For cationic PAHs, formed upon photoionization, relaxation *via* IR emission is dominant regardless of size of the molecule.[30] In order to understand the dynamics of PAH(-cation) dissociation, dedicated studies are used that can identify

characteristic fragmentation patterns upon photo-excitation, and the dependence of different fragmentation pathways on, *e.g.*, wavelength and photon intensity. Intuitively, the *K*-regions in circum(30)triphenylene are the most labile part of the molecule,[31] and one would therefore expect, upon irradiation, sequential loss of C_2H_2 fragments to yield hexabenzocoronene, which then fragments further (Figure 6.10). This hypothesis can be neatly tested, as the fragmentation pathways of the latter are now well documented.[32-35]

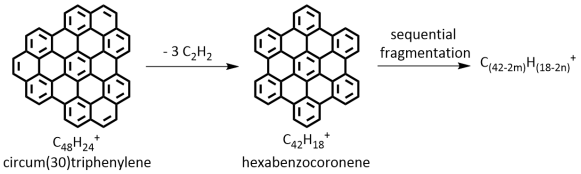


Figure 6.10 Hypothesized fragmentation of circum(30)triphenylene to hexabenzocoronene and beyond. Note that PAHs are drawn as their cationic species, rather than neutral. This aspect will not be considered further here.

Synthesis. The synthesis of circum(30)triphenylene has not been reported before, although its existence was suspected as a high molecular weight pyrolysis product in the combustion of methane.[36] A number of substituted[7,37] and a perchlorinated[38] derivative of circum(30)triphenylene have been reported and characterized before, yet the synthetic routes employed there are not amendable for synthesis of the parent structure. Interestingly, circum(30)triphenylene has also been used as a model compound, to computationally study the first-order hydrogenation of graphene.[39] It was tried to synthesize circum(30)triphenylene *via* ring closure of tripyrenylene **1** synthesized in **Chapter 2** (Figure 6.11).[2,40] Several methods to achieve such aromatic ring closures are known, which are collectively known as the Scholl reaction, after Roland Scholl, who reported the synthesis of perylene from naphthalene upon treatment with $AlCl_3$. Since then, many different conditions have been developed to affect ring closure of aromatic molecules,[41] these include irradiation with UV-light in the presence of iodine, treatment with inorganic oxidizers (*e.g.* $AlCl_3$, $FeCl_3$, $MoCl_5$),[42] organic oxidizers (*e.g.* DDQ),[43] and acids (*e.g.* PIFA).[42] Of these, only photo-irradiation of **1** as a dilute solution in DCM with a low-pressure mercury vapor lamp was tried, which unfortunately did not yield the desired circum(30)triphenylene. Other reaction conditions remain to be tested.

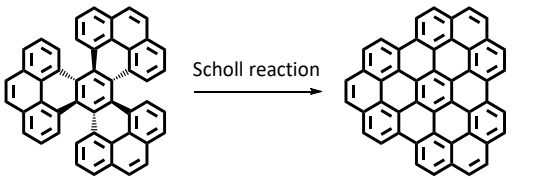


Figure 6.11 Synthesis of circum(30)triphenylene by the Scholl reaction of tripyrenylene **1**.

Infrared. The IR spectra of D_{3h} PAHs can be roughly divided into three regions: i) 700 – 900 cm^{-1}, ii) 1200 – 1600 cm^{-1} and, iii) 3100 – 3300 cm^{-1} (Fig. 6.12A).[1] Absorptions below 700 cm 1 originate from vibrations related to ring deformations which will not be discussed here. Region i) contains out-of-plane C – H waging modes, and can be further refined to solo (900 – 850 cm^{-1}), duo (850 – 800 cm^{-1}) or trio/quarto (800 – 700 cm^{-1}) vibrations.[44] Region ii) contains C – H waging modes, and region iii) contains C – H stretching modes. To identify the vibrations associated with difference absorption lines, spectra were computed using DFT computations at the B3LYP/4-31G level of theory, using geometries optimized at the same level. Although seemingly a rather low level of theory, spectra obtained at this level benefit from requiring only a single scaling factor of 0.958 to bring the computed harmonic frequencies into good agreement with experimental fundamentals. It is for this reason its use has become standard in the astro-chemistry field,[45-47] and all spectra in the NASA Ames PAH spectral database are computed at this level.[48] The major absorptions and vibrations in the different regions will now be discussed separately for the different PAHs.

i) The low wavelength IR region for the fully benzoid PAHs **1** – **3** each has a major absorption corresponding to a collective in-phase, out-of-plane C – H waging vibration ①, situated at 776, 785 and 794 cm^{-1}, respectively. For circum(30)triphenylene **4**, the frequency of the corresponding vibration is significantly upshifted to 888 cm^{-1}. Compounds **2** and **3** additionally show an absorption corresponding to a collective duo C – H waging mode at 842 cm^{-1} ②. In triphenylene **1** and **4** such a mode is, obviously, absent, although there are several anti-phase duo waging modes.

ii) In the middle wavelength region, the number of absorptions increases greatly with the size of the molecule. Absorptions in this region correspond to different collections of duo C – H rocking ③ and scissoring ④ vibrations. Circum(30)triphenylene **4** shows an additional absorption at 1675 cm^{-1}, corresponding to an anomalous scissoring mode (Fig. S6.1).

iii) In the high wavelength region two main absorptions are found, each corresponding to different collective anti-phase ⑤ and in-phase ⑥ C – H stretching modes. Interestingly, for the fully benzoid PAHs **1** – **3** the frequency of these absorptions are found to increase only nominally with an increase in size of the molecule. For the larger PAHs **2** – **4** a particular kind of duo ''through ring'' asymmetric C – H stretching vibration is found ⑦, with circum(30)triphenylene **4**, in turn, uniquely showing a major absorption at 3188 cm^{-1}, corresponding to a mono "through ring" C – H asymmetric stretching vibration ⑧.

[1] In astrochemistry this region is more commonly discussed in terms of 3 – 14 μm (*cf*. Fig. 6.2).

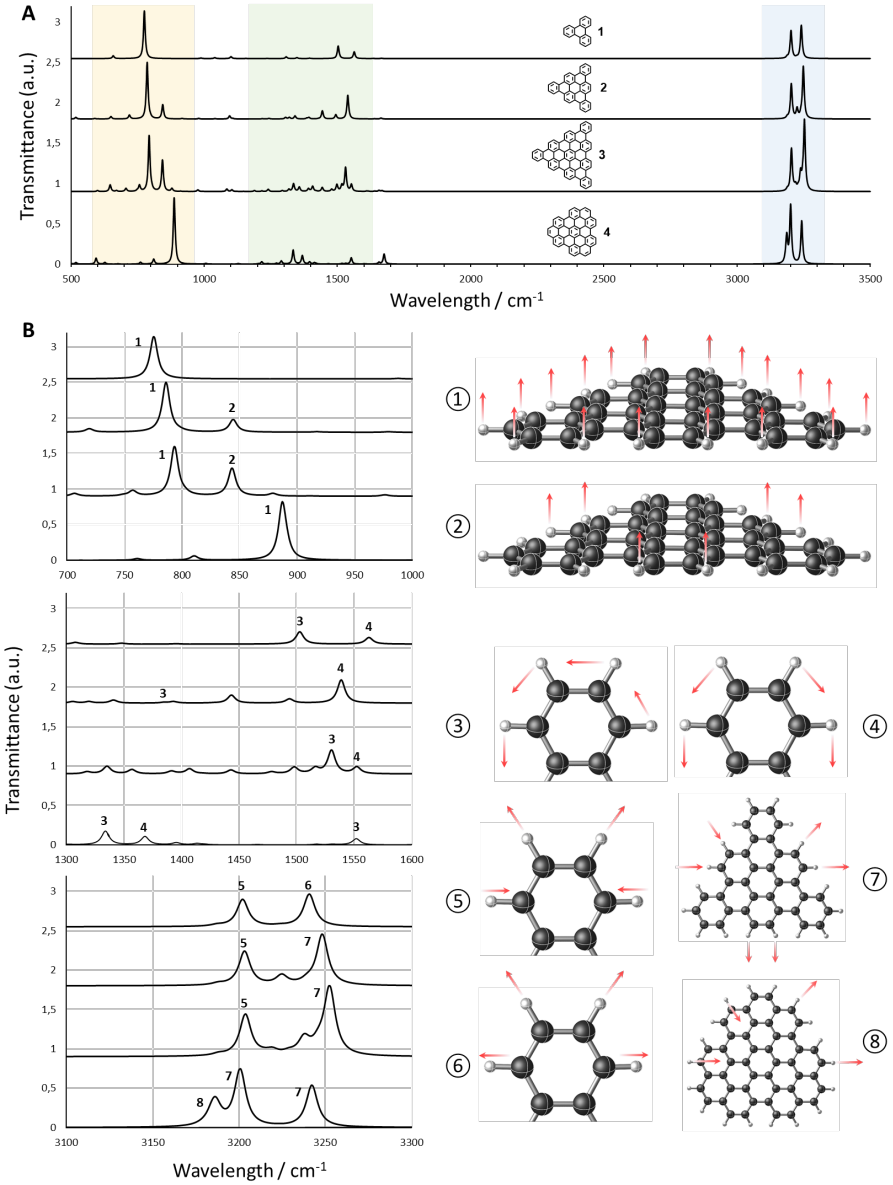


Figure 6.12 (A) Computed IR spectra (at B3LYP/4-31G) of D_{3h} PAHs **1** – **4** (top-to-bottom). (B) Selected regions of the computed IR spectra shown in (A) with the main absorptions in each region labelled. All spectra are to the same scale and arbitrarily offset. Images on the right show the vibrations associated with the corresponding absorption. Vectors not drawn to scale and with arbitrary absolute phase.

From the computational IR study it can be concluded that, although there are broad similarities between the IR spectra of D_{3h} PAHs, the non-fully benzoid circum(30)triphenylene deviates from the general fingerprint, showing distinct features at 888, 1552 and 1675 cm^{-1}. The 888 cm^{-1} vibration in particular (mode ① in Fig. 6.8B) is significantly shifted compared to the corresponding mode in the other PAHs, coinciding with a bright feature in the IRIS nebula (Fig. 6.13). This 11.2 μm band is one of the so-called "unidentified infrared bands" (UIB), and which is currently assumed to be composed of a number of closely packed vibrational modes.[49]

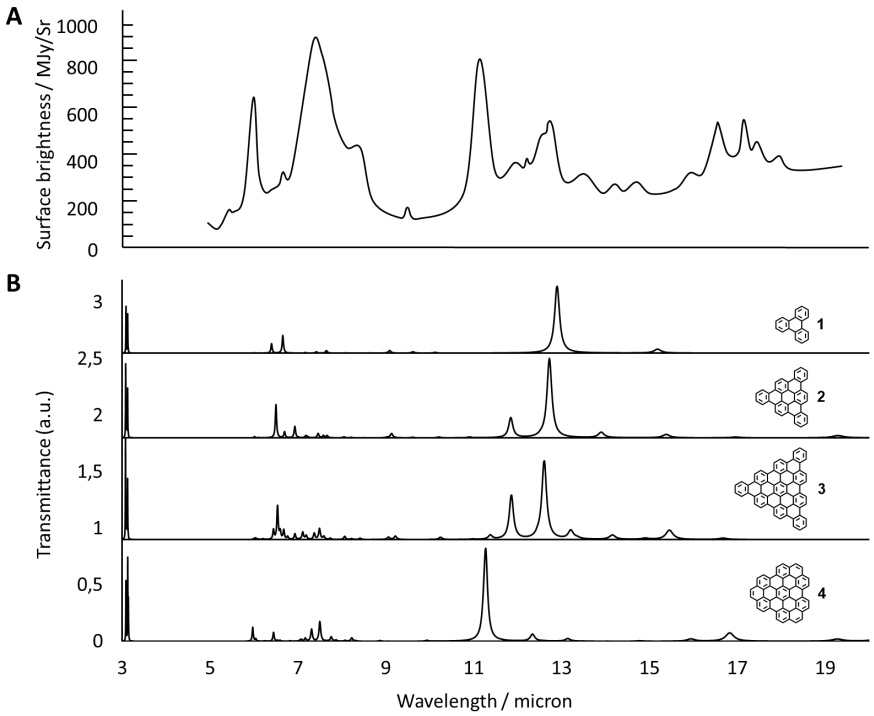


Figure 6.13 Comparison between (A) the experimentally recorded IR spectrum of the dense medium of the northwest photon dominated region of NGC7023; reproduced from ref. [50], and (B) computed IR spectra of selected D_{3h} PAHs. Note the coincidence of the 11.2 μm feature in the experimental spectrum, with that computed for circum(30)triphenylene. Note that MJy/Sr in (A) stands for megaJansky per steradian, which is a unit for spectral flux density.

To conclude, with these preliminary results in hand, the next step will be to synthesize circum(30)triphenylene and record its IR spectrum and photo-dissociation spectrum in astronomically similar conditions, in order to confirm or disprove its astrochemical relevance.

References

(1) Barnett, L.; Ho, D. M.; Baldridge, K. K.; Pascal, R. A. The structure of hexabenzotriphenylene and the problem of overcrowded "D_{3h}" polycyclic aromatic Compounds. *J. Am. Chem. Soc.* **1999,** *121* (4), 727.

(2) Dias, J. R. Perimeter topology of benzenoid polycyclic hydrocarbons. *J. Chem. Info. Mod.* **2005,** *45* (3), 562.

(3) Dias, J. R. Phenyl substituted benzenoid hydrocarbons—relationships of the leapfrog algorithm in regard to Clar's sextet rule, strain-free, and perimeter topology concepts. *Polycycl. Arom. Comp.* **2005,** *25* (2), 113.

(4) Efros, L. S. The aromatic bond and some problems of the structure of aromatic compounds. *Russ. Chem. Rev.* **1960,** *29* (2), 66.

(5) Reddy, K. V. *Symmetry and Spectroscopy of Molecules*; New Age International, **1998**.

(6) Zuzak, R.; Castro-Esteban, J.; Brandimarte, P.; Engelund, M.; Cobas, A.; Piątkowski, P.; Kolmer, M.; Pérez, D.; Guitián, E.; Szymonski, M. Building a 22-ring nanographene by combining in-solution and on-surface syntheses. *Chem. Comm.* **2018,** *54* (73), 10256.

(7) Feng, X.; Wu, J.; Ai, M.; Pisula, W.; Zhi, L.; Rabe, J. P.; Müllen, K. Triangle-Shaped Polycyclic Aromatic Hydrocarbons. *Angew. Chem.* **2007,** *119* (17), 3093.

(8) Obenland, S.; Schmidt, W. In *Polycyclic Aromatic Hydrocarbons and Astrophysics*; Springer, **1987**.

(9) Castiglioni, C.; Negri, F.; Rigolio, M.; Zerbi, G. Raman activation in disordered graphites of the $A_{1'}$ symmetry forbidden k≠ 0 phonon: the origin of the D line. *J. Chem. Phys.* **2001,** *115* (8), 3769.

(10) Gillett, F. C.; Forrest, W. J. Spectra of the Becklin-Neugebauer point source and the Kleinmann-Low nebula from 2.8 to 13.5 microns. *The Astrophysical Journal* **1973,** *179*, 483.

(11) Gillett, F.; Forrest, W.; Merrill, K. 8-13-micron spectra of NGC 7027, BD+ 30 3639, and NGC 6572. *The Astrophysical Journal* **1973,** *183*, 87.

(12) Gillett, F. C.; Kleinmann, D. E.; Wright, E. L.; Capps, R. W. Observations of M82 and NGC 253 at 8-13 microns. *The Astrophysical Journal* **1975,** *198*, L65.

(13) Cohen, M.; Anderson, C. M.; CowLey, A.; Coyne, G. V.; Fawley, W.; Gull, T. R.; Harlan, E. A.; Herbig, G. H.; Holden, F.; Hudson, H. S. The Peculiar Object HD 44179 (" The Red Rectangle"). *The Astrophysical Journal* **1975,** *196*, 179.

(14) Merrill, K. M.; Soifer, B. T.; Russell, R. W. The 2-4 micron spectrum of NGC 7027. *The Astrophysical Journal* **1975,** *200*, L37.

(15) Grasdalen, G. L.; Joyce, R. R. Additional observations of the unidentified infrared features at 3.28 and 3.4 microns. *The Astrophysical Journal* **1976,** *205*, L11.

(16) Russell, R. W.; Soifer, B. T.; Willner, S. The 4 to 8 micron spectrum of NGC 7027. *The Astrophysical Journal* **1977,** *217*, L149.

(17) Allamandola, L. J.; Tielens, A.; Barker, J. Polycyclic aromatic hydrocarbons and the unidentified infrared emission bands-Auto exhaust along the Milky Way. *The Astrophysical Journal* **1985,** *290*, L25.

(18) Leger, A.; Puget, J. Identification of the 'unidentified' IR emission features of interstellar dust? *Astron. Astrophys.* **1984,** *137*, L5.

(19) Puget, J. L.; Léger, A. A new component of the interstellar matter: Small grains and large aromatic molecules. *Annu. Rev. Astron. Astr.* **1989,** *27* (1), 161.

(20) Allamandola, L. J.; Tielens, A.; Barker, J. R. Interstellar polycyclic aromatic hydrocarbons-The infrared emission bands, the excitation/emission mechanism, and the astrophysical implications. *The Astrophysical Journal Supplement Series* **1989,** *71*, 733.

(21) McGuire, B. A.; Burkhardt, A. M.; Kalenskii, S.; Shingledecker, C. N.; Remijan, A. J.; Herbst, E.; McCarthy, M. C. Detection of the aromatic molecule benzonitrile (c-C6H5CN) in the interstellar medium. *Science* **2018,** *359* (6372), 202.

(22) Tielens, A. The molecular universe. *Rev. Mod. Phys.* **2013,** *85* (3), 1021.

(23) Peeters, E.; Hony, S.; Van Kerckhoven, C.; Tielens, A.; Allamandola, L. J.; Hudgins, D. M.; Bauschlicher, C. W. The rich 6 to 9 m spectrum of interstellar PAHs. *Astron. Astrophys.* **2002,** *390* (3), 1089.
(24) Sellgren, K. The near-infrared continuum emission of visual reflection nebulae. *The Astrophysical Journal* **1984,** *277*, 623.
(25) Ricca, A.; Bauschlicher Jr, C. W.; Boersma, C.; Tielens, A. G. G. M.; Allamandola, L. J. The infrared spectroscopy of compact polycyclic aromatic hydrocarbons containing up to 384 carbons. *The Astrophysical Journal* **2012,** *754* (1), 75.
(26) Le Page, V.; Snow, T. P.; Bierbaum, V. M. Hydrogenation and charge states of polycyclic aromatic hydrocarbons in diffuse clouds. II. Results. *The Astrophysical Journal* **2003,** *584* (1), 316.
(27) Andrews, H.; Boersma, C.; Werner, M. W.; Livingston, J.; Allamandola, L. J.; Tielens, A. PAH emission at the bright locations of PDRs: the grandpah hypothesis. *The Astrophysical Journal* **2015,** *807* (1), 99.
(28) Zhao, L.; Xu, B.; Ablikim, U.; Lu, W.; Ahmed, M.; Evseev, M. M.; Bashkirov, E. K.; Azyazov, V. N.; Howlader, A. H.; Wnuk, S. F. Gas-Phase Synthesis of Triphenylene (C18H12). *Chem. Phys. Chem.* **2019,** *20* (6), 791.
(29) Stein, S. On the high temperature chemical equilibria of polycyclic aromatic hydrocarbons. *J. Phys. Chem.* **1978,** *82* (5), 566.
(30) Jochims, H. W.; Ruhl, E.; Baumgartel, H.; Tobita, S.; Leach, S. Size effects on dissociation rates of polycyclic aromatic hydrocarbon cations: Laboratory studies and astophysical implications. *The Astrophysical Journal* **1994,** *420*, 307.
(31) Jochims, H. W.; Baumgärtel, H.; Leach, S. Structure-dependent photostability of polycyclic aromatic hydrocarbon cations: Laboratory studies and astrophysical implications. *The Astrophysical Journal* **1999,** *512* (1), 500.
(32) Zhen, J.; Castellanos, P.; Bouwman, J.; Linnartz, H.; Tielens, A. G. G. M. Infrared spectra of hexa-peri-hexabenzocoronene cations: HBC+ and HBC2+. *The Astrophysical Journal* **2017,** *836* (1), 28.
(33) Palotás, J.; Martens, J.; Berden, G.; Oomens, J. Laboratory IR spectroscopy of protonated hexa-peri-hexabenzocoronene and dicoronylene. *J. Mol. Spectrosc.* **2021,** *378*, 111474.
(34) Zhen, J.; Paardekooper, D. M.; Candian, A.; Linnartz, H.; Tielens, A. Quadrupole ion trap/time-of-flight photo-fragmentation spectrometry of the hexa-peri-hexabenzocoronene (HBC) cation. *Chem. Phys. Lett.* **2014,** *592*, 211.
(35) Zhen, J.; Castellanos, P.; Linnartz, H.; Tielens, A. G. G. M. Photo-fragmentation behavior of methyl-and methoxy-substituted derivatives of hexa-peri-hexabenzocoronene (HBC) cations. *Mol. Astrophys.* **2016,** *5*, 1.
(36) Siegmann, K.; Sattler, K. Formation mechanism for polycyclic aromatic hydrocarbons in methane flames. *J. Chem. Phys.* **2000,** *112* (2), 698.
(37) Kastler, M.; Schmidt, J.; Pisula, W.; Sebastiani, D.; Müllen, K. From armchair to zigzag peripheries in nanographenes. *J. Am. Chem. Soc.* **2006,** *128* (29), 9526.
(38) Tan, Y.-Z.; Yang, B.; Parvez, K.; Narita, A.; Osella, S.; Beljonne, D.; Feng, X.; Müllen, K. Atomically precise edge chlorination of nanographenes and its application in graphene nanoribbons. *Nat. Comm.* **2013,** *4*, 2646.
(39) Boukhvalov, D. W.; Feng, X.; Müllen, K. First-principles modeling of the polycyclic aromatic hydrocarbons reduction. *J. Phys. Chem. C* **2011,** *115* (32), 16001.
(40) Dias, J. R. The most stable class of benzenoid hydrocarbons− new topological correlations of strain-free total resonant sextet benzenoids. *J. Chem. Info. Comp. Sci.* **2004,** *44* (4), 1210.
(41) Grzybowski, M.; Sadowski, B.; Butenschön, H.; Gryko, D. T. Synthetic applications of oxidative aromatic coupling—from biphenols to nanographenes. *Angew. Chem. Int. Ed.* **2020,** *59* (8), 2998.
(42) King, B. T.; Kroulík, J.; Robertson, C. R.; Rempala, P.; Hilton, C. L.; Korinek, J. D.; Gortari, L. M. Controlling the Scholl reaction. *J. Org. Chem.* **2007,** *72* (7), 2279.
(43) Zhai, L.; Shukla, R.; Rathore, R. Oxidative C− C bond formation (Scholl reaction) with DDQ as an efficient and easily recyclable oxidant. *Org. Lett.* **2009,** *11* (15), 3474.

(44) Tommasini, M.; Lucotti, A.; Alfè, M.; Ciajolo, A.; Zerbi, G. Fingerprints of polycyclic aromatic hydrocarbons (PAHs) in infrared absorption spectroscopy. *Spectrochim. Acta A* **2016,** *152*, 134.
(45) Bauschlicher, C. W.; Langhoff, S. R. The calculation of accurate harmonic frequencies of large molecules: the polycyclic aromatic hydrocarbons, a case study. *Spectrochim. Acta A* **1997,** *53* (8), 1225.
(46) Bauschlicher Jr, C. W.; Bakes, E. L. O. Infrared spectra of polycyclic aromatic hydrocarbons (PAHs). *Chem. Phys.* **2000,** *262* (2-3), 285.
(47) Peeters, E.; Bauschlicher Jr, C. W.; Allamandola, L. J.; Tielens, A. G. G. M.; Ricca, A.; Wolfire, M. G. The PAH emission characteristics of the reflection nebula NGC 2023. *The Astrophysical Journal* **2017,** *836* (2), 198.
(48) Bauschlicher Jr, C. W.; Ricca, A.; Boersma, C.; Allamandola, L. J. The NASA Ames PAH IR spectroscopic database: Computational version 3.00 with updated content and the introduction of multiple scaling factors. *The Astrophysical Journal Supplement Series* **2018,** *234* (2), 32.
(49) Boersma, C.; Bregman, J.; Allamandola, L. J. Properties of polycyclic aromatic hydrocarbons in the northwest photon dominated region of NGC 7023. II. Traditional PAH analysis using k-means as a visualization tool. *The Astrophysical Journal* **2014,** *795* (2), 110.
(50) Boersma, C.; Bregman, J. D.; Allamandola, L. J. Properties of polycyclic aromatic hydrocarbons in the northwest photon dominated region of NGC 7023. I. PAH size, charge, composition, and structure distribution. *The Astrophysical Journal* **2013,** *769* (2), 117.
(51) Frisch, M. J.; Trucks, G. W.; Schlegel, H. B.; Scuseria, G. E.; Robb, M. A.; Cheeseman, J. R.; Scalmani, G.; Barone, V.; Mennucci, B.; Petersson, G. A. Gaussian 09 Revision D. 01, 2009. *Gaussian Inc. Wallingford CT* **2009**.
(52) Bootsma, A. N.; Wheeler, S. E. Popular Integration Grids Can Result in Large Errors in DFT-Computed Free Energies. *ChemRxiv. Preprint* **2019**.

Experimental

Computations. Equilibrium geometries of all structures were computed at the DFT level of theory using the Gaussian 09 Rev. D.01 program,[51] using the B3LYP functional and 4-31G basis set. For all computations the convergence criteria were set to tight (Opt = tight; Max. Force = $1.5 \cdot 10^{-7}$, Max. Displacement = $6.0 \cdot 10^{-7}$), and an internally defined super-fine grid size was used (SCF = tight, Int = VeryFineGrid), which is a pruned 175,974 grid for first-row atoms and a 250,974 grid for all other atoms.[52] All stationary points found were checked to constitute true local minima, by the absence of negative frequencies.

Supplementary Figure

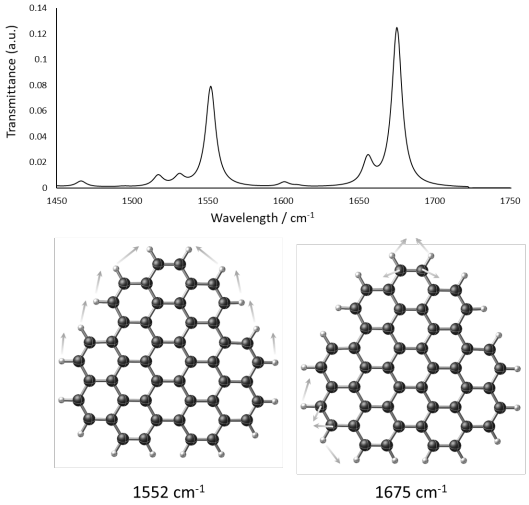


Figure S6.1 Computed anomalous vibrations observed for circum(30)triphenylene.

Samenvatting in het Nederlands

Polycyclische aromatische koolwaterstoffen (PAKs) zijn chemische verbindingen, bestaande koolstof- en wateratomen, welke zo verbonden zijn, dat een cyclische verbinding ontstaat. Deze verbindingen noemt men aromatisch als zij voldoen aan een aantal vereisten: naast het vormen van een cyclisch geheel, dienen de zogeheten pi-elektronen in het system zich vrij te kunnen verplaatsen tussen naastgelegen koolstofatomen, dient het aantal pi-elektronen gelijk te zijn aan $4n + 2$ (de zogeheten regel van Hückel), en dient het molecuul (relatief) vlak te zijn. Als aan al deze vereisten is voldaan verkrijgt het molecuul eigenschappen waarmee het zich ten zeerste onderscheidt van andere chemische verbindingen, te denken bijvoorbeeld aan suikers en eiwitten. Voorbeelden van deze eigenschappen zijn het kunnen aannemen van uiteenlopen kleuren, het elektrisch geleidend zijn, maar ook de carcinogeniteit van deze verbindingen is een direct gevolg van de bovengenoemde delocalisatie van de pi-elektronen in het molecuul.

Het doelmolecuul van dit proefschrift was circum(30)trifenyleen; een PAK met de brutoformule $C_{48}H_{18}$. Dit grote molecuul wordt geïmpliceerd als zijnde een cruciaal intermediair in de formatie en deformatie van PAKs in het zogeheten interstellaire medium: de ruimte en energie tussen sterren in een sterrenstelsel. Hierover hieronder meer. De synthese van grote PAK-verbindingen is echter een uitdagende onderneming, niet in de minste plaats door hun slechte oplosbaarheid, als gevolg van hun vlakke vorm. Derhalve is Hoofdstuk 2 in zijn geheel gewijd aan de synthese van het voorlopermolecuul, tripyrenyleen. De grondgedachte hierachter is dat, doordat tripyrenyleen een niet-vlakke, propellervormige structuur heeft, zij nog enige oplosbaarheid bezit. Deze niet-vlakke vorm is het gevolg van de sterische hinder die delen van het molecuul ondervinden, namelijk daar waar atomen ruimtelijk in elkaars buurt zitten. Als, echter, in een volgende synthesestap deze sterische hinder wordt weggenomen in een ringsluitingsreactie, verliest het molecuul haar oplosbaarheid en slaat neer uit het reactiemengsel. Deze „oplosbare voorloper strategie'' is derhalve uiterst geschikt om de synthese van grote PAK-moleculen te vergemakkelijken.

Door haar niet-vlakke structuur bezit tripyrenyleen een aantal interestante eigenschappen. In het bijzonder is zij een „drievoudige heliceen'', door de aanwezigheid van drie spiraalvormige motieven in haar structuur. Helicenen worden voor tal van toepassingen gebruikt, van organische synthese tot fotocellen, en welke nader beschreven staan in Hoofdstuk 1. Door de aanwezigheid van meerdere spiraalvormige motieven kan tripyrenyleen meerdere ruimtelijke conformaties aannemen. Deze „conformationele ruimte'' wordt in Hoofdstuk 3 uiteengezet, en de invloed van de vorm van het molecuul op haar fysisch-chemische eigenschappen nader bestudeerd. Uit de aldaar beschreven studie blijkt dat de spiraalvormige motieven doorslaggevend zijn in welke spectroscopische eigenschappen propellereenmoleculen vertonen. Tevens vindt het dat *de mate van pi-conjugatie* belangrijk is, maar niet de *locatie* van deze conjugatie, voor de fysisch-chemische eigenschappen van het molecuul.

Het daaropvolgende Hoofdstuk 4 probeert een verklaring te vinden voor de experimenteel waargenomen conformationele voorkeur van propellerenen. Deze is namelijk niet eenduidig, daar sommige propellerenen bij voorkeur een conformatie met C_2 symmetrie aannemen, en sommigen een conformatie met D_3 symmetrie verkiezen. Door propellereenmoleculen met behulp van computermodellen strategisch in stukken te knippen, kunnen de voorkeuren van individuele delen van de propellerenen opgehelderd worden. Uit het model blijkt dat verschillende delen, verschillende voorkeuren hebben, en dat de grootte en de balans in deze voorkeuren uiteindelijk doorslaggevend zijn in welke conformatie het gehele propellereenmolecuul aanneemt. Door het begrip dat in dit hoofdstuk verkregen is, kunnen toekomstige propellereenmolecuul rationeel worden ontworpen al naar gelang hun beoogde toepassing.

Waar de eerdere hoofdstukken kijken naar de synthese en eigenschappen van individuele moleculen, kijkt Hoofdstuk 5 naar de interactie tussen propellereenmoleculen; dat heet, het supramoleculaire gedrag. In het bijzonder laat Hoofdstuk 5 zien dat de vereende interactie van vele duizenden decacycleenmoleculen

de productie mogelijk maakt van een membranen van nanometer dikte. Schoon deze smalle dikte, zijn deze membranen nochtans in staat om micrometer lange afstanden te overbruggen zonder de noodzaak voor ondersteuning, noch voor de covalente verbinding van de individuele moleculen. Louter de zogeheten van der Waals interacties volstaan. De mechanische sterkte van deze membranen kon worden gekwantificeerd met behulp van atoomkrachtmicroscopie. De sterkte van deze membranen was in de zelfde ordegrootte als die van andere 2D membranen. Doordat geen hoge temperaturen of andere extreme behandeling van de membranen nodig was om mechanische sterkte te bewerkstelligen, zou de hier gerapporteerde methode gebruikt kunnen worden om chemisch wel-gedefinieerde membranen te maken. Mogelijke toepassingen van zulke membranen zijn gebruik in brandstofcellen, ontzouting, biomedische applicaties en nano-elektronica.

Als laatste geeft Hoofdstuk 6 een samenvatting van het in dit Proefschrift beschreven werk en gaat zij nader in op het doelmolecuul, circum(30)trifenyleen. Zoals al eerder genoemd is dit molecuul mogelijk aanwezig in de ruimte, en wel specifiek in de interstellaire ruimte. Deze aanname is gepostuleerd op basis van infrarood spectra die genomen zijn van sterrenstelsels. Doordat het niet mogelijk is om naar deze sterrenstelsels af te reizen en monsters te verzamelen, is men tegenwoordig bezig om de extreme condities van de interstellaire ruimte op aarde na te bootsen en het (spectroscopische) gedrag van moleculen onder deze condities te onderzoeken. Door de ruimtelijke en aardse spectra met elkaar te vergelijken, samen met computationeel verkregen spectra, kunnen hypotheses vervolgens bekrachtigd of ontkracht worden. Het wordt momenteel aangenomen dat enkel hele grote en hele kleine PAK moleculen aanwezig zijn in de interstellaire ruimte en dat deze in elkaar over kunnen gaan door de additie en abstractie van kleine koolwaterstoffragmenten. In dit geheel is circum(30)trifenyleen geïmpliceerd als zijnde een cruciale, intermediaire verbinding die deze kleine en grote PAKs met elkaar verbindt. Toekomstig onderzoek zal dan ook gericht zijn op het bestuderen van de experimentele en computationele spectroscopische eigenschappen van circum(30)trifenyleen.

List of Publications

1. van der Ham, A.,* Hansen, T.,* Lodder, G., Codée, J. D., Hamlin, T. A., & Filippov, D. V. (2019). Computational and NMR Studies on the Complexation of Lithium Ion to 8-Crown-4. *ChemPhysChem*, *20*(16), 2103-2109.

2. van der Ham, A., Schneider, G. F., & Lutz, M. (2021) CCDC 2056845: Experimental Crystal Structure Determination. doi: 10.5517/ccdc.csd.cc2719vg

3. van der Ham, A., Overkleeft, H. S., Schneider, G. F., & Filippov, D. V. (2021). A Three-step Synthesis of 4H-Cyclopenta[def]phenanthrene from Pyrene. *Eur. J. Org. Chem.*, 13, 2013-2017.

4. Arjmandi-Tash H., Bellunato, A., van der Ham, A., & Schneider, G. F. (2021). Inert Mask Lithography of Edge Narrowed Graphene Nanoribbons Directly Contacted to Metallic Electrodes. *Adv. Mater. Interfaces. 8*(20), 20100293.

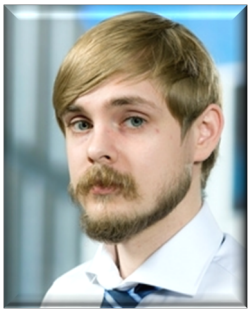
5. van der Ham, A.,* Liu, X.,* Calvani, D., Melcrová, A., Kozdra, M., Buda, F., Roos, W. H., Overkleeft, H. S., Filippov, D. V., & Schneider, G. F. (2021). Freestanding Non-covalent Thin Films of the Propeller-shaped Polycyclic Aromatic Hydrocarbon Decacyclene. *Manuscript accepted for publication in Nat. Comm.*

6. van der Ham, A.,* Hansen T.,* Filippov, D. V., Hamlin, T. A., & Scheider, G. F. (2021). Understanding the Conformational Preference of Propeller-shaped Polycyclic Aromatic Hydrocarbons Conformations. *Manuscript submitted. Available as pre-print at ChemRxiv* (doi: 10.26434/chemrxiv-2021-gfd9q)

7. van der Ham, A., Hansen, T., Brouwer A. M., Overkleeft, H. S., Hamlin, T. A., Filippov, D. V. & Schneider, G. F. (2021). Positional Effect of π-extension in Triple Helicenes. *Manuscript in preparation. Available as pre-print at ChemRxiv* (doi: 10.26434/chemrxiv-2021-kn2qg)

8. Crone, N. S. A., van Hilten, N., van der Ham, A., Boyle, A. L., Kros, A. Azobenzene-based amino acids for photocontrol of coiled coil peptides. *Manuscript in preparation.*

Curriculum vitae



Alex van der Ham was born on the 13th of March, 1993 in The Hague, The Netherlands. From 2005 until 2011 he attended the Adelbert College in Wassenaar where he obtained his secondary education diploma, with a specialization in the exact sciences (VWO). In his final year he participated in the 32nd National Chemistry Olympiad, becoming a top-10 finalist. Having both an interest in chemistry and cellular biology, in 2011 he started his Biopharmaceutical Sciences bachelor at the University of Leiden. As part of his Bachelors program he performed an internship at the Analytical Biosciences Department, under the supervision of dr. Peter Lindenburg. This research concerned the miniaturization of capillary electrophoresis (CE). He acquired his Bachelors' degree *cum laude* (ave. score > 85%) in 2014.

Having realized that chemistry was the greater of his passions, that same year he continued with a Masters' program in Medicinal chemistry, also at Leiden University. The first internship of one year was in the group of prof. dr. Mario van der Stelt, where he developed an *in vivo* active, nanomolar potent inhibitor for ABHD16a, an enzyme whose function at the time was still poorly understood. Where the desire was clear to continue a career in academia, for his second internship, he decided to develop his own research project. Under the supervision of dr. Dmitri Filippov, he synthesized the small crown ether 8C4, and investigated its binding to lithium ions using both NMR spectroscopy, as well as computationally, in collaboration with Thomas Hansen. This research would result in a paper, published in the journal ChemPhysChem. The Masters' degree, too, was obtained *cum laude*, in 2016.

After that he joined the group of dr. Grégory Schneider, with joined supervision by dr. Dmitri Filippov, with the goal of synthesizing and studying polycyclic aromatic hydrocarbons. In the five years that followed he would synthesize various aromatic molecules, including on a multigram scale, the results of which are concentrated in Chapter 2 of this Thesis. He studied these molecules with a wide range of analytical techniques, ranging from spectroscopic techniques like IR, Raman, UV-Vis and NMR, to microscopic techniques like SEM, TEM and AFM, the fruits of which are found in Chapters 3 and 5. Moreover, the computational work that started at the end of his Masters would prove to be the starting point for a fond interest in computational chemistry, the results of which are scattered throughout this Thesis, but are primarily located in Chapter 4.

Parts of the work reported in this thesis were presented in the form of a poster both on national (CHAINS 2016 – 2020; Reedijk Symposium 2017 – 2019) and

international conferences (Chem2DMat 2017 (Strassbourg) and 2019 (Dresden); Nobel Prize Conference 2018 (Groningen)). A poster prize was obtained at the Reedijk Symposium in 2019. He also gave an oral presentation on his work at CHAINS 2020.

His broad interests, already evidenced in his early years, made him now pursue a post-doctoral position in NMR spectroscopy in the United Kingdom, particularly in the groups of prof. dr. Gareth A. Morris in Manchester, and that of prof. dr. Simon B. Duckett at the University of York.

Acknowledgments

A PhD is never a lone man's journey. Faces come, faces go, and each encounter shapes you. As such, I would like to start by thanking my two co-promotors, Grégory and Dima, who helped me in becoming the scientist I am today.

I would like to thank Thomas, not only for being a mentor and guide into the field of computational chemistry, but also a respected colleague and kind friend. The same goes for Xue, who has been my office mate for almost the entire duration of my PhD and whose expertise in the material science field has been invaluable when it comes to experimental work and publications. The second long term office mate to especially mention is Pauline, with whom I shared many a banter moment, on both scientific as well as (well, mostly) non-scientific topics.

In this regard I will also fondly remember Roderick and Kassandra who were always able to lighten the mood when experiments were not going the way they were supposed to, and for providing much needed distraction. A wholehearted thankyou also goes to Liuba for all the fun times, both inside and outside the lab. And of course a big thankyou to all the other graphenians, Lin, Xiaoyan, Wangyan, Amedeo, Lia, Batuhan, Andy, Max, Weizhe and Thomas for their incessant support throughout this journey.

A special thankyou goes out to the EE.4 lab mates, Jacob, Mark, Dennis, Coralie, Jerre, Koen-1 and Koen-2 with whom the lab was never a boring place to be! A separate mention of course goes to Tim, klootviool, for being a friend, comrade, and fellow mad scientist!

This list would not be complete without also thanking Fons and Karthick for the many hours invested in making the crazy NMR experiments I kept throwing at them actually happen, and helping me prepare for my future in NMR spectroscopy. Similarly, I would like to thank Dario for the nice and fruitful collaborations. And a final thankyou goes to all the others from Biosyn and SBC, with whom I collaborated, or who were simply able to put a smile on my face.

I would like to conclude by thanking Anna, without whom my PhD, indeed my life, would not have been the same!

Alex